An Investigation of Mild Mitochondrial Uncouplers and Their Potential to Treat Obesity

Ethan Pacchini

Thesis submitted in fulfilment of the requirements for the degree of

Doctor of Philosophy

under the supervision of
A/Prof Tristan Rawling and Prof Andrew McDonagh

Statement of Originality

I, Ethan Pacchini, declare that this thesis is submitted in fulfilment of the requirements for the award of Doctor of Philosophy in the School of Mathematical and Physical Sciences at the University of Technology Sydney.

This thesis is wholly my own work unless otherwise referenced or acknowledged. In addition, I certify that all information sources and literature used are indicated in the thesis. This document has not been submitted for qualifications at any other academic institution.

Production Note:
Signature removed prior to publication.

Ethan Pacchini   28th February 2025

COVID-19 Impact Statement

The experimental work in this thesis began in 2021 and was impacted greatly by the COVID-19 pandemic particularly in 2021-2022. Research progress was affected and delayed during due to several factors including:

1. Delivery times for consumable orders such as biological assay consumables and chemical reagents were extended from weeks to months.

2. Access to laboratories and experimental facilities at UTS were limited for a 4-month duration in accordance with New South Wales COVID-19 policies.

This research was unable to be transitioned into a completely online format due to the nature of laboratory-based activities required. In response to this, the project's scope was adjusted to ensure these core aims could be addressed despite the extended timeline.

Table of Contents

List of Figures

treated with aryl amides **6-17** and DNP for 1 hour at concentrations between 0.1 µM to 100 µM using a JC-1 assay. CCCP tested at concentrations of 0.01-100 µM Data represents mean ± SEM of three independent experiments.

List of Tables

List of Schemes

List of Abbreviations

4-HNE	4-hydroxynnonenal
ADP	adenosine diphosphate
ANT	adenine nucleotide translocase
ATP	adenosine triphosphate
BSA	bovine serum albumin
CC	control chow
CCCP	carbonylcyanide-3-chlorophenylhydrazone
$CDCl_3$	deuterated chloroform
CLogP	calculated logP
CTCL	cutaneous T-cell lymphoma
DCC	dicyclohexylcarbodiimide
DCM	dichloromethane
DCVC	dry column vacuum chromatography
DMSO-d_6	deuterated dimethyl sulfoxide
DMF	dimethylformamide
DNP	2,4-dinitrophenol
$\Delta\Psi m$	mitochondrial membrane potential
Emax	maximum level of depolarization
EC50	half maximal activity concentration
ECAR	extracellular acidification rate
EDCI	1-ethyl-3-(3-dimethylaminopropyl) carbodiimide
ETC	electron transport chain
EtOH	ethanol

Et₃N	triethylamine
FAD	flavin adenine dinucleotide
FCCP	carbonyl cyanide p-trifluoro-methoxyphenyl hydrazone
FFDCA	Federal Food, Drug and Cosmetic Act
HBA	hydrogen bond acceptors
HBD	hydrogen bond donors
HCl	hydrochloric acid
HFD	high fat diet
HPA	human plasma albumin
IC50	half maximal inhibitory concentration
K₂CO₃	potassium carbonate
k_i	initial proton transport rate
LDH	lactate dehydrogenase
MIM	mitochondrial inner membrane
MW	molecular weight
NAD	nicotinamide adenine dinucleotide
NaOH	sodium hydroxide
NMR	nuclear magnetic resonance
OCR	oxygen consumption rate
OXPHOS	oxidative phosphorylation
PER	proton efflux rate
PMF	protonmotive force
POPC	1-palmitoyl-2-oleoyl-sn-glycero-3-phosphocholine
qNMR	quantitative nuclear magnetic resonance
RB	rotatable bonds

ROS	reactive oxygen species
SAR	structure-activity relationship
SEM	standard error mean
TBAOAc	tert-butyl ammonium acetate
TBAOH	tert-butyl ammonium hydroxide
TFA	trifluoroacetic acid
TGA	Therapeutic Goods Administration
TLC	thin layer chromatography
TPP	triphenylphosphonium
UCP	uncoupling protein

Equations

$$I_f = \frac{R_t - R_0}{R_d - R_0}$$

$$y = y_0 + (y_{max} - y_0)\frac{x^n}{k^n + x^n}$$

$$EC_{50} = k(\frac{0.5}{y_1 - y_0})^{1/n}$$

$$p_i = \frac{1}{Q} \exp\left(-\frac{\varepsilon_i}{kT}\right) = \frac{\exp\left(-\frac{\varepsilon_i}{kT}\right)}{\sum_{j=1}^{M} \exp\left(-\frac{\varepsilon_j}{kT}\right)}$$

$$\theta_{average} = (\theta_1 \times p_1) + (\theta_2 \times p_2)$$

Publications

(Not related to this thesis)

Roy R., York E., **Pacchini E.**, Rawling T. 2023. Effects of cationic head group structure on cytotoxicity and mitochondrial actions of amphiphilic ionic liquids. *Food and Chemical Toxicology.* 183(21):114202

MacDermott-Opeskin H., Clarke C., Roseblade A., York E., **Pacchini E.**, Roy Ritik., Cranfield C., Gale P.,O'Mara M., Murray M., Rawling T. 2022. Protonophoric and Mitochondrial Activity of Aryl-Carbamate Substituted Fatty Acids. *Organic & Biomolecular Chemistry*. 21(1).

Acknowledgements

Firstly, I would like to thank my supervisor Associate Professor Tristan Rawling for his help and guidance throughout this project. Over the past seven years of being your intern, honours and now PhD student, I have learnt so much from you and will forever appreciate the banter, challenges and opportunities you gave me which helped me grow into the researcher I am today. I would like to thank my co-supervisor Professor Andrew McDonagh for all of his help and guidance over the past seven years as well.

Secondly, I would like to thank my collaborators. Massive thank you to Dr Daniel McNaughton for working with Tristan and I in pushing the boundaries of this project to levels we didn't know where possible. Thank you to my other collaborators; Dr Katie Wilson and Aaron Pye for your computational chemistry expertise, and Dr Richard Kim and Dr Chantal Donovan for testing one of my synthesised compounds in mouse models.

Huge shoutout to the Rawling research group, both past and present; Meryem-Nur Duman, Ritik Roy, Edward York, Freddy Ha, Phoenix Chick and Mirielle Kalayji for joining me along for the highs and lows of research and being such an open and welcoming group to work with.

Lastly, I would like to thank my friends and family for their encouragement and moral support over the course of this project. To my fiancé Vanessa, I would not have made it through my PhD without your unconditional love and care. Thank for being there for me even in moments where I had to prioritise my work and inspiring me to push forward when times get rough. I hope I have made you all proud with this accomplishment.

Abstract

Mitochondria play essential roles in cell health, including production of the energy carrying molecule adenosine triphosphate (ATP) via oxidative phosphorylation (OXPHOS). OXPHOS is a coupled process where the energy derived from nutrient oxidation is used to generate a proton gradient across the mitochondrial inner membrane (MIM) that is used to power the enzyme ATP-synthase. Mitochondrial uncouplers are typically weak acid protonophores that shuttle protons across the MIM to collapse the proton gradient, leading to futile cycles of nutrient oxidation without ATP synthesis. In response, cells ramp up nutrient and oxygen consumption and production of reactive oxygen species (ROS) is affected. Mitochondrial uncouplers have shown potential as treatments for neurodegenerative diseases, cancer and obesity, however their clinical progress is hindered by major toxicity concerns. For example, the uncoupler 2,4-dinitrophenol (DNP) was used in the 1930's as a weight loss drug but was later prohibited for human consumption due to significant adverse side effects which included several fatalities. Recent attention has been directed to the development of mild mitochondrial uncouplers, which partially collapse the proton gradient across the MIM without affecting ATP production or causing mitochondrial toxicity. Previous attempts to develop mild uncouplers have focused on lipophilic cations as self-limiting uncouplers and yielded mixed results. This thesis explores, for the first time, the influence of proton transport rate in the development of mild uncouplers.

In 2020, aryl-urea substituted fatty acids were reported as a new class of protonophoric mitochondrial uncoupler that displayed anticancer activity *in vitro* and *in vivo*. These agents act as full mitochondrial uncouplers, however in contrast to classical protonophores like DNP, aryl-urea substituted fatty acids utilise a urea-based anion transport group to facilitate the critical step in their protonophoric cycle; permeation of the deprotonated anionic form of the

uncoupler across the MIM. Here, the aryl-ureas self-assemble into membrane permeable dimers via intermolecular hydrogen bonds between carboxylate and urea groups.

This thesis introduces "aryl amides" a new class of fatty acid protonophores derived from aryl-urea substituted fatty acids, where the urea group is replaced with an amide group. In Chapter 2, the first library of aryl amides were designed and synthesised as close derivatives of their aryl urea counterparts. Thus, these aryl amides possessed C18 fatty acid chains capped with chloro- and/or trifluoromethyl-substituted phenylamides in 3,4- and 3,5-substitution patterns. In cell-based studies, it emerged that all aryl amides were active uncouplers that diminished the proton gradient across the MIM and stimulated respiration. However, in contrast to the 3,5-substituted analogues, the 3,4-substituted aryl amides produced only partial proton gradient collapse, and did not affect ATP production and therefore have an activity profile consistent with mild mitochondrial uncoupling. In vesicle-based assays used to study proton transport, the 3,4-substituted aryl amides transported protons across model lipid bilayers at slower rates than full uncouplers in the series, indicating that proton transport rate may be a determinant of mild mitochondrial uncoupling. Upon further investigation, their slower rate of transport can be attributed to their diminished capacity to dimerise, which is a key factor in their protonophoric cycle. Computational studies suggested that 3,4-substitution caused a misalignment of the dipole angle relative to the amide hydrogen bond axis, which in turn hinders dimerisation and lowers proton transport rate, therefore leading to mild uncoupling. This is the first study to draw a link between proton transport rate and mild mitochondrial uncoupling.

The aryl amides presented in Chapter 2 have cLogP values between 6.94-7.27, therefore they are not 'drug-like' molecules due to their high lipophilicity (>5) and rotatable bond count (>10) as per Lipinski and Verber's rules of oral bioavailability. These sub-optimal physicochemical properties are likely to result in poor pharmacokinetic properties *in vivo*

which arises from the C18 fatty acid chain. Therefore, in Chapter 3 chain contraction of the aryl amides was explored with the aim of developing drug-like mild uncouplers. 3,4-Substituted aryl amides with C16, C12 and C8 fatty acid chains were synthesised and their protonophoric and uncoupling activity was first assessed *in vitro*. Despite their 3,4-substitution, most C16 aryl amides acted as full uncouplers, and produced similar effects as DNP. In contrast, most of the C12 aryl amides acted as mild uncouplers while all C8 aryl amides were largely inactive. This pattern in activity was also observed in vesicle-based proton transport assays and was attributed to reductions in the lipophilicity of the aryl amides as the alkyl chain was shortened. From these studies the C12 aryl amide **10** emerged as the most potent and drug-like mild uncoupler in the series and was studied in mouse models with high fat diet (HFD)-induced obesity. Although mice administered with **10** (10 mg/kg) through oral gavage exhibited no adverse effects, the aryl amide failed to induce statistically significant reductions in body weight compared to control mice. Further investigations on the pharmacokinetics of **10** could prove whether fatty acid protonophores can have feasible physiochemical properties to be used as a potential option for treating obesity.

Overall, this project provides the first experimental evidence linking mild mitochondrial uncoupling to proton transport rate, and that proton transport rate of the aryl amides can be manipulated by substitution pattern and lipophilicity. Further studies should aim to substantiate these findings by investigating the proton transport rates of a wide variety of known full and mild uncouplers. These studies may also identify new mild uncouplers with superior physicochemical properties than the aryl amides that may show improved efficacy in animal models of obesity.

CHAPTER 1

Introduction

1.1 Mitochondria: Structure, Function and Mitochondrial Uncoupling as a Therapeutic Strategy

Mitochondria are small organelles within mammalian cells which have the primary function of converting energy stored in nutrients (e.g. fats and sugars) into adenosine triphosphate (ATP), the energy currency of cells used to power many cellular processes[1-2]. The metabolic pathway of converting energy from nutrients into ATP is known as oxidative phosphorylation (OXPHOS). Due to their vital role in nutrient metabolism, the mitochondria has been a prominent therapeutic drug target for decades.

1.1.1 Mitochondria: Structure and Function

The mitochondria consists of an outer membrane, inner membrane and matrix which play different roles in cellular function. The outer membrane is permeable to small molecules and contains channels which allow for the transport of larger molecules through it[3]. The matrix is the site for OXPHOS and contains vital enzymes involved in the citric acid cycle[2]. The mitochondrial inner membrane (MIM) is widely impermeable, surrounds the matrix and is a common therapeutic target[3]. Within the matrix, nutrients are metabolised through the citric acid cycle and the energy from this process is transferred in the form of electrons onto carriers such as flavin adenine dinucleotide (FAD) and nicotinamide adenine dinucleotide (NAD$^+$). As a result, reducing them into FADH$_2$ and NADH and allowing them to carry electrons to the electron transport chain (ETC), which contains a series of enzymes embedded in the MIM[4]. These enzymes are known as "Complexes", where Complexes I, III and IV are proton pumps which shuttle protons from the matrix into the intermembrane space, forming a proton gradient across the MIM[5]. Protons that travel in the direction of the induced gradient pass through the MIM through ATP synthase, an enzyme consisting of two molecular motors which couples protonmotive force and mitochondrial inner membrane potential ($\Delta\Psi_m$) to ATP production[6-7].

The protons being channelled across the MIM power conformational changes within ATP synthase's molecular motors, in turn facilitating the conversion of adenosine diphosphate (ADP) into ATP. This describes OXPHOS (**Figure 1**), the metabolic pathway of converting energy from nutrients into ATP, where nutrient oxidation is coupled to ATP synthesis through the MIM proton gradient. Thus, the mitochondria is a prominent therapeutic drug target due to its regulation of energy metabolism.
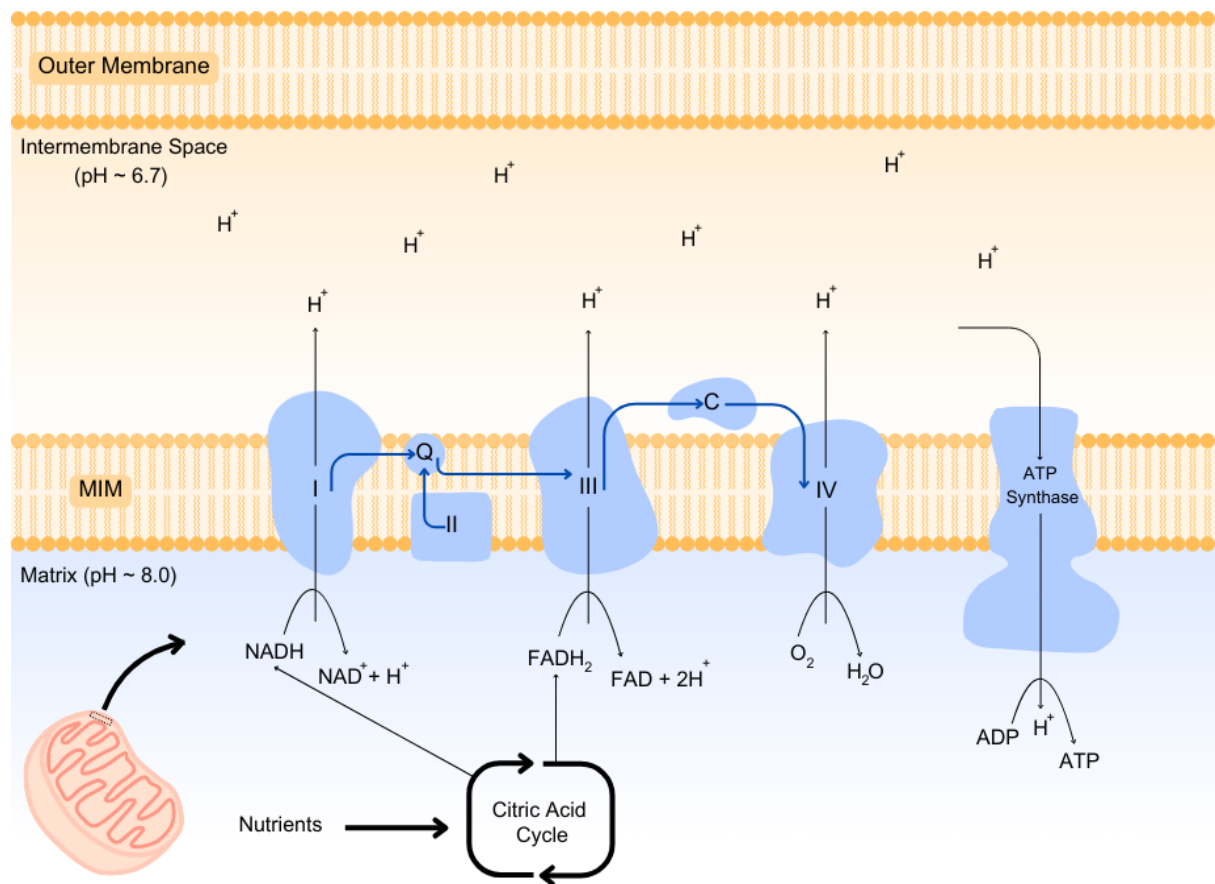
Figure 1: The process of mitochondrial OXPHOS. Nutrients are oxidised by the citric acid cycle and energy is transferred to the ETC via electron carriers NADH and FADH$_2$. Complexes I, III and IV use this energy to pump protons into the intermembrane space to produce a proton gradient. The PMF generated by this gradient drives protons back into the matrix through ATP synthase which catalyses the conversion of ADP to ATP.

1.1.2 *Mitochondrial Uncoupling*

Mitochondrial uncoupling is a process where protons are shuttled from the intermembrane space into the matrix without passing through ATP-synthase, as a result collapsing the proton gradient and inhibiting ATP formation[8]. Uncoupling is a regular physiological process occurring within cells in which proton leak from the intermembrane space is required to help regulate metabolic rate, assist in thermogenesis and prevent excess reactive oxygen species formation (ROS)[9-12]. Fatty acids such as 4-hydroxynonenal (4-HNE) and reactive species such as superoxide play a role in proton leakage through the activation of uncoupling proteins (UCPs)[12]. UCP1 and UCP2 are uncoupling proteins which have been studied extensively for decades for their differing roles and tissue distribution. UCP1 is expressed in brown and beige adipose tissue with the primary role in non-shivering thermogenesis whilst UCP2 has a broad tissue distribution and has the role of preventing excessive ROS formation[10, 13-14].

Another mechanism of mitochondrial uncoupling within cells involves repeated protonation and de-protonation of fatty acids as they travel across the MIM. This process of fatty acid movement is commonly facilitated by UCPs or by Adenine Nucleotide Translocase (ANT), a MIM transporter which primarily facilitates the import/export of ADP/ATP to and from the matrix but also assists in uncoupling[15-16]. Lastly, mitochondrial uncoupling can be induced by protonophores, which are molecules that transport protons across the MIM into the matrix either independently or facilitated by UCPs and ANT[10].

1.1.3 Small Molecule Mitochondrial Uncouplers

Protonophores are able to act as mitochondrial uncouplers as they are lipophilic enough to move through the MIM and are weakly acidic, allowing for reversible protonation/deprotonation[10, 17-18]. The anionic form of uncouplers can be protonated in the intermembrane space, travel across the MIM, release a proton into the matrix and move back across the MIM while in their anionic form repeatedly (**Figure 2**)[18]. Although cells still continue to oxidise nutrients, the lack of energy provided for ATP synthesis causes an increase in oxygen respiration and potential for mitophagy[18-21]. Potential energy is also dissipated as heat, causing rapid metabolism and consumption of calories. An example of two classical protonophores are carbonyl cyanide p-trifluoro-methoxyphenyl hydrazone (FCCP) and carbonylcyanide-3-chlorophenylhydrazone (CCCP) (**Figure 3**), which are lipophilic weak acids and can easily traffic across biological membranes while carrying protons[18].
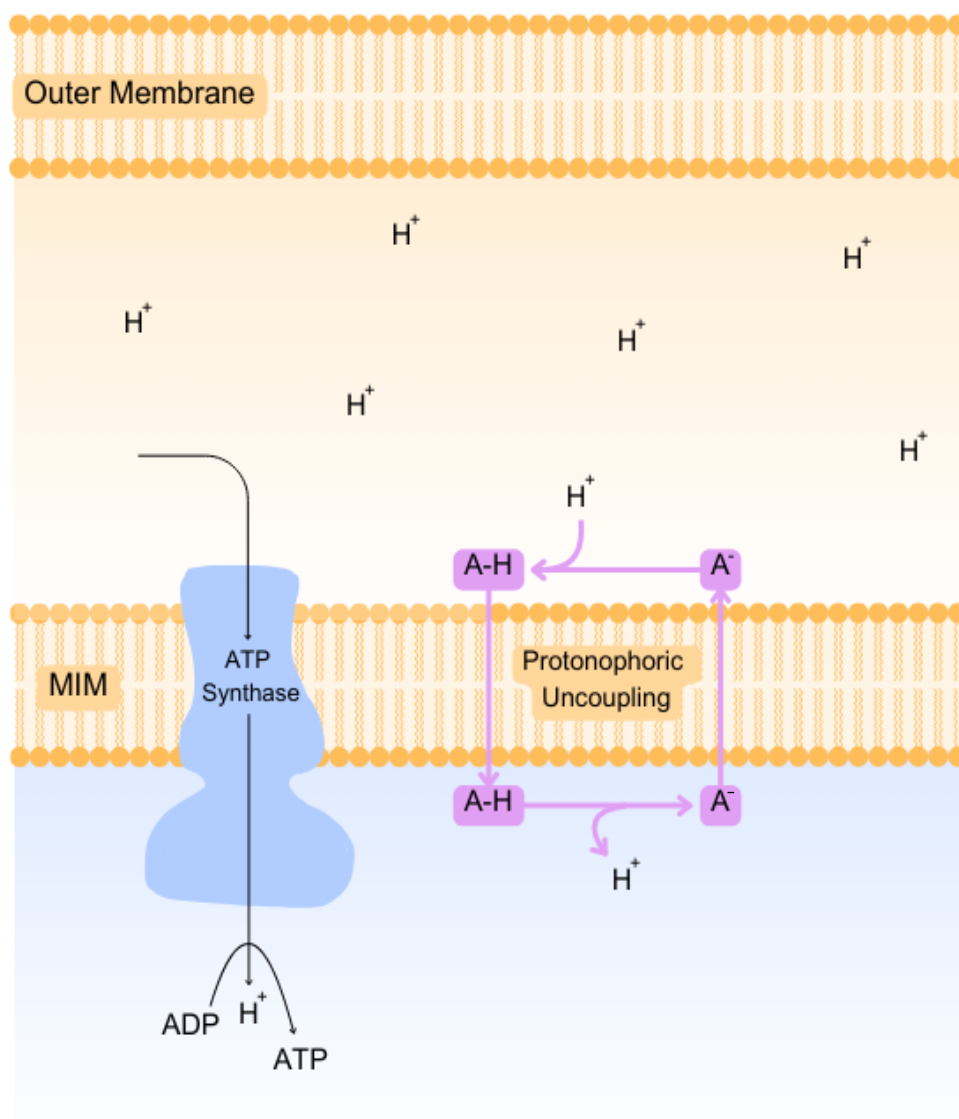
Figure 2: Mechanism of a protonophore (A) transporting protons from the intermembrane space into the matrix. After releasing the protons into the matrix, they can move back through the MIM in their anionic form and return to the intermembrane space to continue the process.
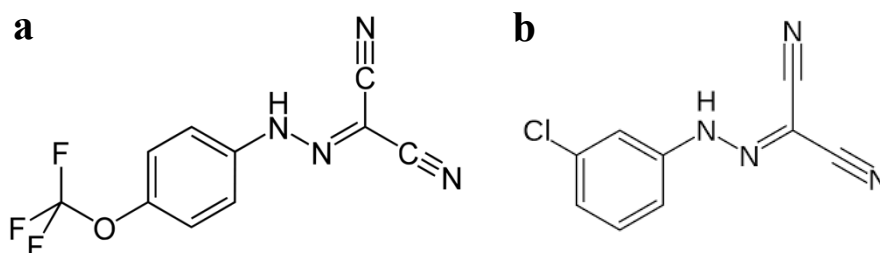
Figure 3: a) Structure of FCCP. **b)** Structure of CCCP

In contrast to protonophores like FCCP and CCCP which can transport protons across the MIM independently, UCP1 and UCP2 can facilitate proton transport across the MIM via a fatty acid-activated mechanism[22-23]. These two uncoupling proteins require activation by free fatty acids, which in the case of UCP1, remains inactive until changes in temperature cause a fatty acid-releasing cascade which activates it[23-24]. This is also known as the "flip-flop" mechanism, due to the nature of which UCPs indirectly facilitate proton transport by assisting anionic fatty acid transbilayer movement, allowing for the protonophoric cycle to continue[23]. Studies has shown that without the assistance of UCPs, the rate of anionic fatty acid flip-flop is extremely slow and as a result cellular effects caused by mitochondrial uncoupling is unlikely to occur[25].

As our understanding of the different mechanisms of protonophores has developed over time, mitochondrial uncoupling has become a prominent therapeutic strategy for its ability to affect cellular metabolism and increase energy expenditure[9-12].

1.1.4　　Potential Therapeutic Applications of Mitochondrial Uncouplers

Mitochondrial uncouplers have various therapeutic applications that have been studied extensively for almost a century including treatment of neurodegenerative diseases, cancer and more prominently weight loss.

1.1.4.1　　Neurodegenerative Diseases

Neurodegenerative diseases such as Alzheimer's Disease, Parkinson's Disease and Dementia are the leading cause for illness and disability worldwide with 1 in 3 people globally being affected[26]. These diseases are also prevalent in Australian society today, with an estimate of over 500,000 Australians diagnosed to date which is expected to almost double by 2054[27-28]. Neurodegenerative diseases are characterised by progressive functional impairment or death of neuronal cells in the central or peripheral nervous system[29]. Due to the mitochondria being an important site for energy metabolism and controlling apoptosis, in recent studies mitochondrial dysfunction has been linked to neurogenerative diseases[30]. Mitochondria is a major source for ROS, in which low concentration of ROS is required for maintaining homeostasis whilst excessive levels can be detrimental to cells as they cause oxidative stress which can damage key cellular components[29, 31]. In early stages of Alzheimer's disease, oxidative damage caused by increased ROS levels can reduce fatty acids present in neurons of the inner olfactory cortex, leading to eventual degradation of neuron cells[29, 32]. ROS generation non-linearly depends on $\Delta\Psi_m$, where small decreases in $\Delta\Psi_m$ leads to a significant reduction in ROS production[21]. A notable effect of mitochondrial uncoupling is the decrease of $\Delta\Psi_m$ as a result of proton transport across the MIM[9-12, 18, 21]. Therefore, mitochondrial uncoupling has been studied for its therapeutic potential to treat neurodegenerative diseases *in vivo* such as low-dose 2,4-dinitrophenol (DNP), lanosterol and attempts to increase expression of UCP2[21, 33-35].

1.1.4.2   Anti-cancer Agents

Cancer continues to be a major health concern worldwide, where in 2022 alone approximately 20 million new cases of cancer arose alongside 9.7 million deaths globally and one in five men or women will develop it at some point in their lifetime[36]. Cancer has had significant social and economic effects on the Australian population in particular. It is estimated that on average, one in two Australians will be diagnosed with cancer at some point in their life and one in five will die from it by the age of 85[37]. Cancer is a cellular disease where healthy cells within the body undergo genetic damage which prevents proliferation, whilst cancer cells continuously divide and can evade programmed death[38]. Contrary to initial views on cancer cell metabolism made by Walburg in 1956, research over the past few decades show that the mitochondria also plays a vital role in cancer cell metabolism and functions utilising both OXPHOS and aerobic glycolysis to produce ATP[38-40]. In many cases of chemo-resistant and metastatic cancers and cancer stem cells, they rely heavily on OXPHOS for ATP production rather than glycolysis[38, 41-42]. Cancer cell mitochondria is generally hyperpolarised ($\Delta\Psi_C \sim -220$ mV) in comparison to normal cells ($\Delta\Psi_N \sim -140$ mV), which has resulted in higher rates of mitochondrial uncoupling in comparison to normal cells, however the reason behind this selective vulnerability remains unclear[38, 43]. Uncouplers in the literature such as SR4, F16, 5MBF and TPP+C$_{10}$ have shown to preferentially accumulate in cancer cell mitochondrial matrix in comparison to normal cells[38]. Thus, mitochondrial uncoupling has potential as a therapeutic option for treating cancer due to inherent differences between mitochondria of cancer and normal cells where various types of cancer cells rely on OXPHOS for producing ATP.

1.1.4.3   *Weight Loss Treatment*

Obesity is a worldwide health problem generally caused by ingesting a greater number of calories compared to expended calories, causing an excess accumulation of body fat which leads to a plethora of health issues including type 2 diabetes, hypertension, coronary artery disease, respiratory issues and liver and gallbladder disease[44-45]. A common recommendation of treatment is lifestyle changes, such as diet and physical activity in order to achieve caloric balance[46]. This is achieved by creating a caloric deficit, eating fewer calories than required while expending more calories through physical activity. Despite treatment recommendations, as of 2022 43% of adults worldwide are overweight with 16% living with obesity[47]. Obesity has become prevalent in Australian society, with 66% of the Australian adult population in 2022 were considered overweight or obese (**Figure 4**)[48]. It has also had major economic impacts, as it affects the demand and supply of healthcare and markets such as grocery stores, fast food, restaurants, advertising, physical exercising and dieting. Obesity accounts for 2-9% of the total health budget in most developed countries, which is similar to the impact of smoking[49]. Income and prices of food influence food consumption choices greatly, where economic theory predicts an inverted U-shape relationship between income and body weight[50]. The poor are hungry and malnourished, and as their income increases, consumption of food typically increases and therefore body weight will also increase. This theory is also consistent with obesity being more common in developed countries compared to developing countries, where Indonesia for example only has 5.7% of the adult population being overweight[51].As a result of the various impacts on society and on the wellbeing of the human population, treatment options for obesity are constantly in high demand for those who struggle with adapting to lifestyle changes.
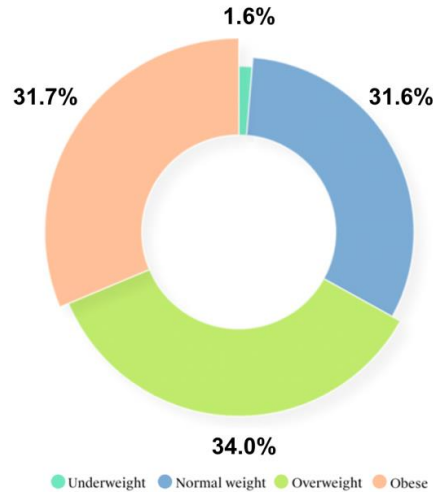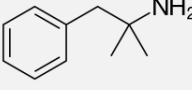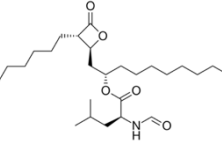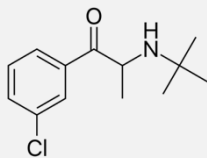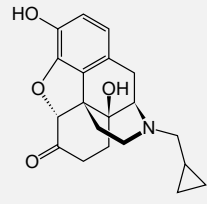
Figure 4: Australian adults by weight status in 2022, a national survey from the Australian Bureau of Statistics[48]

Anti-obesity drugs are another option for treating obesity, however they are limited by their substantial adverse effects and/or low efficacy of weight loss compared to lifestyle changes. These drugs aim to reduce appetite and/or alter metabolism to increase energy expenditure and induce weight loss through different mechanisms. Common anti-obesity drugs today target norepinephrine, dopamine, serotonin or pancreatic lipases in order to either reduce appetite, promote energy expenditure or lowering calorie absorption[52-54]. Generally, if at least 5% total weight is not lost after the first 12 weeks, the patient should gradually discontinue use and attempt other medical options such as bariatric surgery[52]. The decision on which weight loss drug is appropriate depends on the pre-existing medical conditions of the patient, as some contraindications are present for specific drugs such as cardiovascular disease, opioid addiction and pregnancy[55-56]. The Therapeutic Goods Administration (TGA) have approved phentermine, orlistat, naltrexone/bupropion and liraglutide for treatment of obesity in Australia, which are summarised in **Table 1**.

Table 1: Current drugs approved by the TGA for treating weight loss in Australia with their mechanism of action, weight loss reported in clinical trials, common side effects and their limitations.

Drug	Mechanism of Action	Weight loss	Side Effects	Limitations
Phentermine	Sympathomimetic agent which inhibits the reuptake of norepinephrine and/or dopamine in the central nervous system (CNS) to suppress appetite[57].	3-8% total body weight lost over a 12-week span when taking 30-40 mg daily[58-62]. Used to treat weight loss since 1959 but was first approved by the TGA in May 2020[63-64].	Dry mouth, insomnia and headache[49-50]. Contraindications for patients with glaucoma and/or hyperthyroidism[55-56, 58, 65].	Short treatment time due to concerns of increased risk of cardiovascular disease and potential for addiction[66-68]. Has been replaced by combination therapy with topiramate in other countries (yet to be approved by the TGA)[55-56, 60, 69]
Orlistat	Acts as a selective inhibitor of pancreatic lipases in the stomach and intestines, in turn reducing intestinal digestion of fat [52].	2.4% total body weight lost but increased to 8-11% when in combination with lifestyle changes depending on dosage[70-72]. Approved by the TGA in 2000 under the name Xenical[73].	Mild/moderate gastrointestinal events and slight interference with absorption of fat-soluble vitamins[72]. This is caused by low absorption in the gastrointestinal tract, resulting in a blockade of triglyceride digestion in the intestine[53].	Low efficacy in comparison to other anti-obesity drugs on the market. High discontinuation rate (48% in clinical trials) but patients are commonly prescribed with fibre supplements to counteract this[72, 74].
Naltrexone (above) Bupropion (below)	Naltrexone is an opioid antagonist, acting as a dopamine and norepinephrine reuptake inhibitor[75-76]. Bupropion causes stimulation of pro-opiomelanocortin (POMC) neurons in the hypothalamus, a precursor for both α-melanocyte stimulating hormone (α-MSH), which decreases food intake, and β-endorphin which sends feedback inhibition to POMC neurons to weaken the effect of α-MSH[52]. Naltrexone blocks the	6-12% body weight lost over a one-year span depending on lifestyle changes and dosage[77-80]. Approved by the TGA in August 2023 under the name Contrave[81]	Nausea, constipation, headache, depression and increased heart rate and blood pressure[77-80]	High discontinue rate (40-48%) due to adverse effects and risks for cardiovascular issues.

	negative feedback of β-endorphin, allowing for greater reduction in food intake when taken in combination.			
Liraglutide (see appendix for structure)	Glucagon like peptide-1 (GLP-1) is a hormone released in the small intestine in response to food intake which causes delayed gastric emptying and appetite suppression[82]. Liraglutide is a derivative of GLP-1 and acts as a GLP-1 receptor agonist to induce weight loss.	22-37% of patients maintained ≥ 10% body weight loss after one year of treatment[83]. Patients lost significantly more weight using liraglutide in comparison to orlistat[84-85] First approved by the TGA in January 2018 as a subcutaneous injection under the name Saxenda[86]	Nausea, hypoglycaemia and gastrointestinal intolerability[83]. Potential contraindications with patients with impaired kidneys or liver[83]. Generally well tolerated long-term.	Only available as subcutaneous injection and is not orally bioavailable.

Due to the adverse effects or low efficacy of current anti-obesity drugs, there is a need for a new drug with safer and better weight loss capabilities. Treatment is still heavily reliant on other methods which show greater weight loss results such as bariatric surgery[87]. Each of the drugs in **Table 1** have different targets and mechanisms of action. A mechanism that is not conducted by any currently approved drugs to induce weight loss is mitochondrial uncoupling.

The first instance of a mitochondrial uncoupler being used as an anti-obesity drug dates back to the 1930's with 2,4-dinitrophenol (DNP), a protonophore which uncouples the MIM through repeated protonation and deprotonation of its hydroxy group (**Figure 5**)[88].
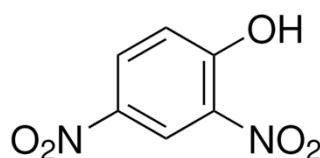
Figure 5: Structure of DNP

DNP was first used in World War I for the manufacture of ammunition and explosives in France and the US[89]. However, it was found that workers in these factories experienced substantial weight loss and hyperthermia as a result of excessive exposure to DNP[90]. By 1933, its ability to induce rapid weight loss was published by Maurice Tainter at Stanford University, causing its widespread commercialisation and use without the need of a medical prescription[91]. Tainter had treated approximately 170 obese patients for 3 months with a daily dose of 300 mg DNP orally, causing patients to lose up to 1.5 kg per week without restrictions on caloric intake[91-92].

Due to its strong uncoupling ability, the drug caused a great increase in metabolism of fats and carbohydrates. However, DNP was found to cause harsh adverse effects which has led to 72 known deaths between 1919 and 2019 worldwide[8, 17]. The most common visible side effects when used therapeutically are rashes, accompanied by yellow discolouration of skin, sclera and urine[92]. Other serious side effects include hyperthermia, nausea, vomiting, dizziness, convulsions, confusion, headache, agitation, tachycardia, diaphoresis, tachypnoea and cataracts[8, 17, 88]. As a result, the consumption of DNP was prohibited in the US in 1938 by the Federal Food, Drug and Cosmetic Act (FFDCA)[93]. Due to the rise of social media and the resurgence in popularity of body building or body sculpting, INTERPOL issued an alert to inform the general public of the dangers of consuming DNP in 2015[94]. In Australia, DNP has been classified as a schedule 10 drug since 2017, prohibiting its sale, supply and use[95]. Despite the numerous warnings, publications of deaths and prohibitions associated with the drug, it continues to be sold on the internet under various names and the demand for a weight loss drug with comparable results continues to rise. As a result of DNP's toxicity, mitochondrial uncoupling was abandoned as a mechanism for weight loss for decades.

1.1.5   *Strategies to Address Mitochondrial Uncoupler Toxicity*

As a result of DNP's full mitochondrial uncoupling activity, it has a small margin between therapeutic and toxic doses, leading to harsh adverse effects which eventually caused its prohibition. Since 2002, there has been 33 published deaths directly related to DNP use and 120 cases of intoxication between 2007-2019[17, 96-97]. These deaths were caused by cardiovascular collapse due to the lack of ATP production in cells along with the heat dissipation inducing a fever that develops into severe hyperthermia (with reported body temperatures reaching up to 43 ˚C), tachycardia and tachypnoea[8]. These fatalities have been linked with both deliberate and accidental overdoses while being used by bodybuilders, for general weight loss or from accidental occupational exposure[8, 17]. The history of DNP use suggests that it can induce rapid weight loss that exceeds any of the current anti-obesity drugs. However, due to the small difference between effective and fatal doses, it is too toxic to be used safely.

Due to the promising weight loss induced by DNP and the relatively poor efficacy of other weight loss drugs that operate by different mechanisms of action, recent attention has been directed towards the development of mild mitochondrial uncouplers. Mild uncouplers are characterised by their ability to induce uncoupling effects to a lesser extent, allowing for the ETC to still provide enough energy for ATP synthase to function adequately[98-101]. An ideal mild uncoupler could partially depolarise the MIM and increase cellular respiration without affecting ATP production, therefore having potential to be a safe weight loss drug that surpasses the current 4-11 anti-obesity drugs on the market (depending on individual country guidelines and regulations)[21, 102]. This would have significant economic impact, as Ozempic reached a total sales of approximately 19 billion USD in 2024[103]. The first instances of developing a mild uncoupler involved altering the structure of DNP in attempts to develop a

"self-limiting" protonophore by adding membrane-penetrating cation groups, such as adding a triphenylphosphonium group (TPP) known as MitoDNP (**Figure 6a**) or a photocleavable linker known as MitoPhotoDNP (**Figure 6b**)[104-105].
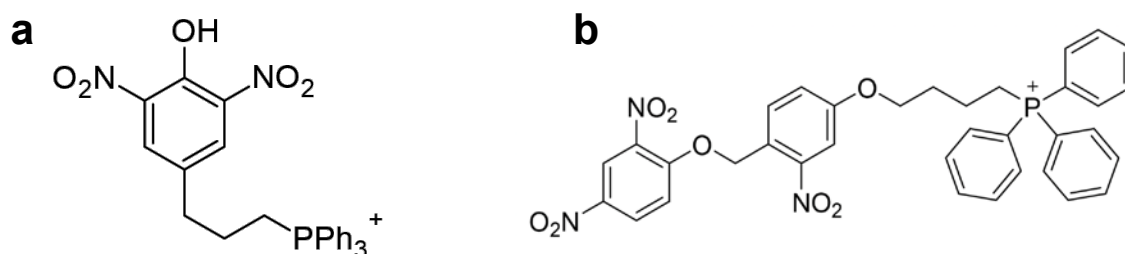
Figure 6: a) Structure of MitoDNP. **b)** Structure of MitoPhotoDNP.

However, both DNP derivatives were not able to act as a protonophores primarily due to their deprotonated form not being able to leave the mitochondrion and continue the protonophoric cycle.[104-105] Following this, mitochondria-penetrating cations such as SkQ1 and C_{12}TPP (**Figure 7**) were also investigated for their uncoupling potential as they theoretically could accumulate within the mitochondria and either leave or redistribute across the membrane when $\Delta\Psi_m$ decreases, thus being potential self-limiting protonophores[106-107]. C_{12}TPP and its alkylTPP derivatives however were unable to act as self-limiting protonophores due to multiple reasons including their lack of hydroxyl or carboxyl groups capable of carrying protons across the membrane, being trapped within the mitochondrial matrix and excessive accumulation within the mitochondria caused toxicity at higher doses[10, 106, 108]. SkQ1 on the other hand was found to act as an antioxidant rather than a protonophore, leading to decreases in reactive oxygen species (ROS) without disrupting MIM potential[106, 109-110].
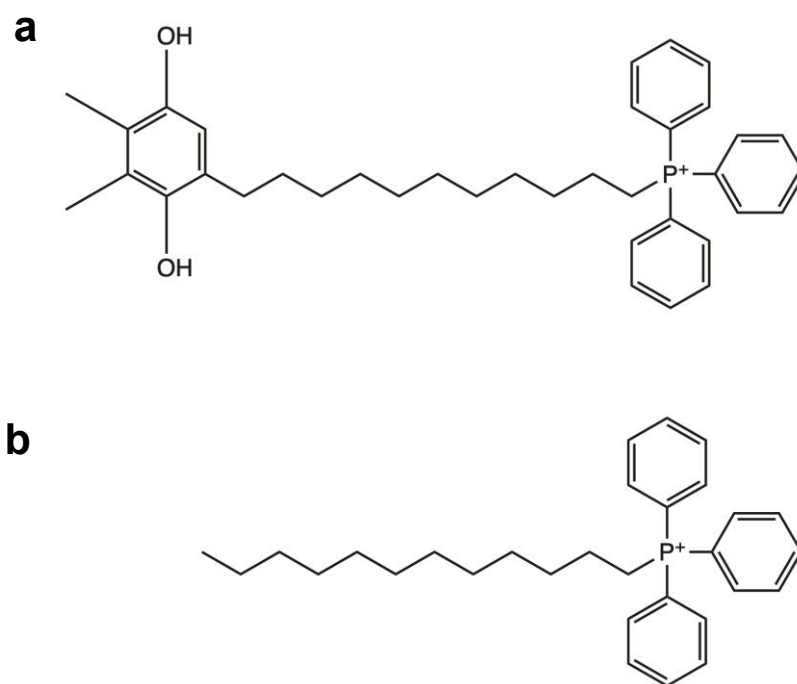
Figure 7: a) Structure of SkQ1. **b)** Structure of $C_{12}TPP$.

As an extension of the SkQ family of uncouplers, rhodamine 19 derivative C4R1 was developed[106, 111-112]. Anti-obesity effects of C4R1 were first published in 2015, where it reduced food intake and increased resting metabolic rate in a murine mouse obesity model through what was initially believed to be mitochondrial uncoupling[111]. However, it was discovered in 2023 that C4R1 does not act as a protonophore and instead binds to the β-subunit of the F1 component of ATP synthase[112]. Therefore, C4R1 should be more appropriately characterised as an ATP synthase inhibitor rather than a mitochondrial uncoupler. Thus, after decades of research on derivatives of mitochondria-penetrating cations in the SkQ family, the development of a mild mitochondrial uncoupler and its underlying mechanism remained elusive.

BAM15, a protonophore with oxadiazole, pyrazine and aniline moieties, has been studied extensively for its mitochondrial uncoupling ability for over 10 years[113-116]. It was initially characterised as a novel mitochondrial uncoupler which does not depolarise the plasma

membrane of L6 rat skeletal muscle cells, which was believed to be a cause of uncoupling toxicity[113, 117]. Following this, BAM15 was found to have anti-obesity effects in murine mouse models without signs of adverse effects[114]. Interestingly, rather than being characterised as a "mild" uncoupler, BAM15 is described as a "safe" uncoupler due to its minimal of toxicity *in vivo* and lack of understanding surrounding the exact mechanism of mild uncoupling. Subsequently, BAM15 derivatives such as SHC517, SHD865 and SHM115 (**Figure 8**) have also shown to exhibit anti-obesity effects *in vivo* but their exact mechanism which differentiates them from classical full uncouplers such as DNP and FCCP is not fully understood *[118-120]*. Similarly, other uncouplers in the literature have either been labelled as "safe" rather than mild or are simply labelled as mitochondrial uncouplers without fully distinguishing whether they are mild or full uncouplers such as OPC-163493, Ppc-1 and FR58P1a[121-123].
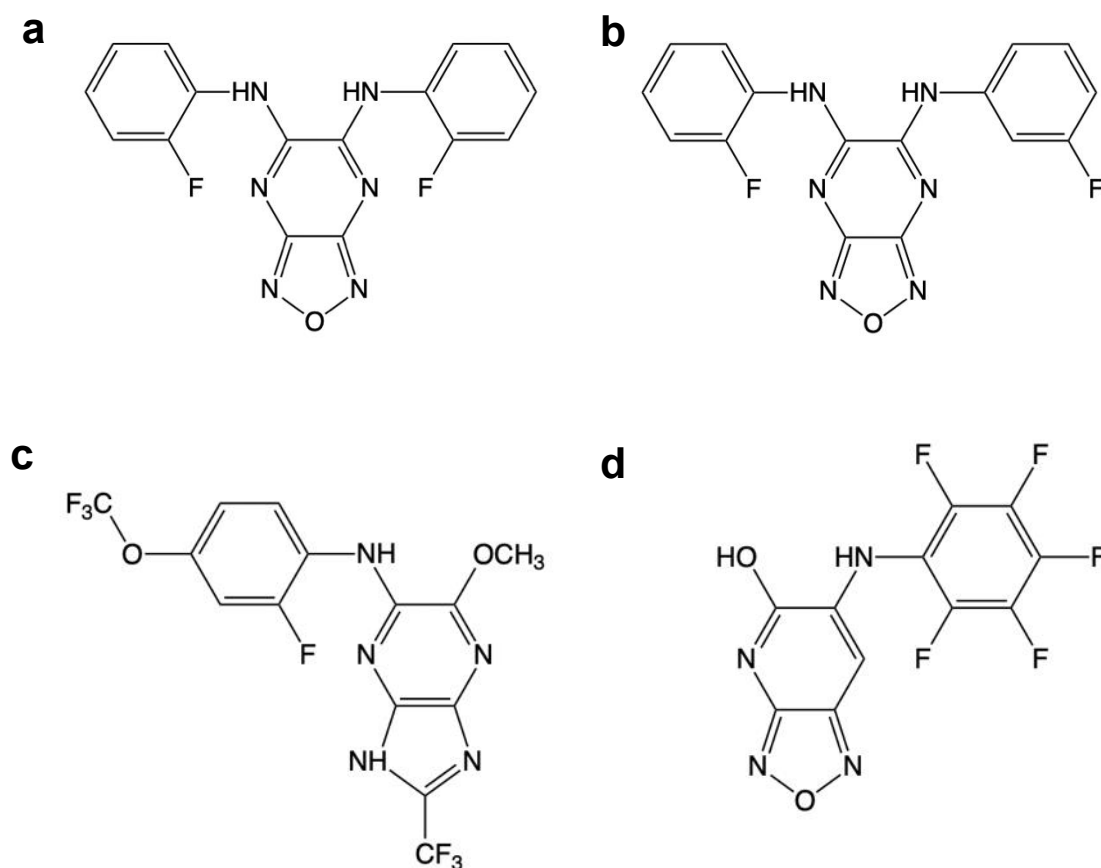
Figure 8: Structures of BAM15 (**a**), SHC517 (**b**), SHD865 (**c**) and SHM115 (**d**).

Despite these recent advancements, a structure-activity relationship (SAR) or mechanistic understanding of the properties that lead to either full or mild uncoupling is yet to be established. Most definitions on mild uncoupling focus on the fact that ATP production is not inhibited, but the reasoning behind this is yet to be proven experimentally[38, 100, 106].

1.2   Synthetic Anion Transporters (Anionophores)

Synthetic anion transporters (anionophores) are small-molecule organic compounds which assist in facilitating movement of anionic species such as Cl^- and HCO_3^- across phospholipid bilayers. These anionophores can either form channels within the membrane, which allow for the movement of ions through it or alternatively, they can form covalent bonds with the anion to form supramolecular complexes which can diffuse across the membrane and translocate the anion[124-125]. Anionophores have received significant attention due to their therapeutic applications such as treating cystic fibrosis and acting as anticancer agents[126-127]. In 2016, anion transporters were found to also facilitate the movement of protons across lipid bilayers with the assistance of free fatty acids[23]. Thus, providing an alternative mechanism to the protonophoric cycle conducted by classical uncouplers such as DNP and FCCP.

1.2.1   Anionophore Mediated Mitochondrial Uncoupling

Non-channel forming anionophores contain anion recognition moieties such as urea, thiourea or square-amide groups which bind to the guest anion, spread their negative charge across a larger surface and therefore are able to facilitate their transport across bilayer membranes[23, 124-125]. Another function of anionophores is their ability to mimic the function of UCPs by facilitating proton transport via activation by free fatty acids[22-23]. Firstly, the fatty acid in anionic form accepts a proton and travels across the membrane as a neutral species. The

fatty acid is then deprotonated, releasing a proton on the opposite side of the membrane. Lastly, the anionophore binds to the carboxylate group of the fatty acid via parallel hydrogen bonds, allowing for the fatty acid to be lipophilic enough to traverse back across the membrane and repeat the protonophoric cycle (**Figure 9**).
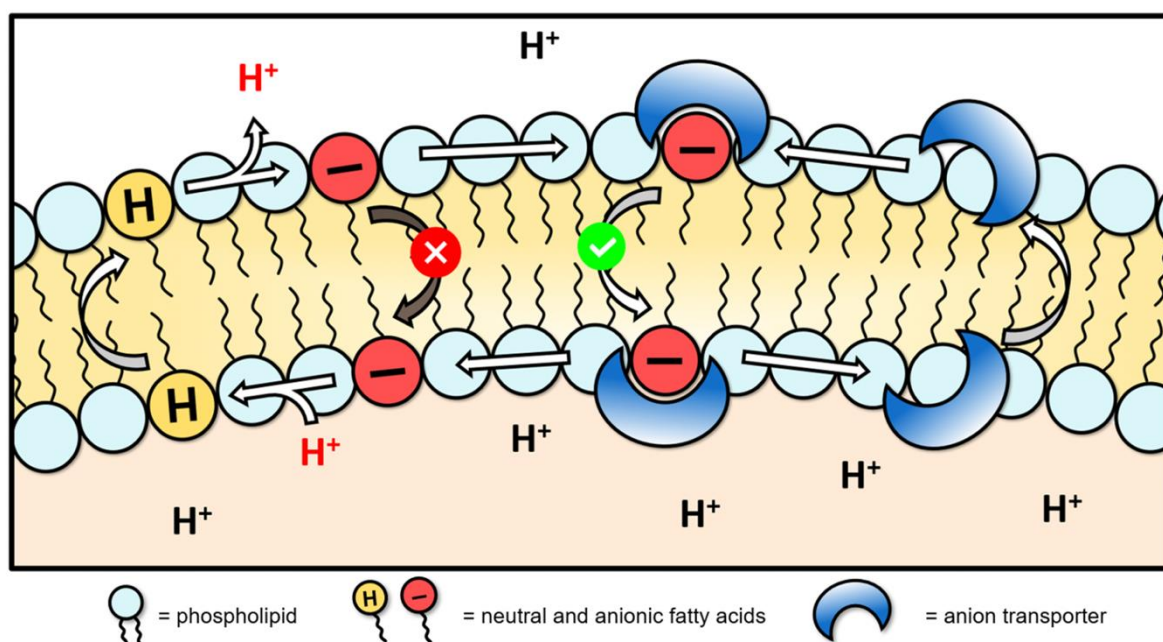
Figure 9: Fatty-acid activated proton transport mechanism via anionophores across a bilayer membrane. The anionophore binds to the fatty acid carboxylate, making it lipophilic enough to traverse back across the membrane to repeat the protonophoric cycle[22]. Diagram from the work of York *et al.* (https://doi.org/10.3390/biom13081202)[22]

This function of anionophores was first discovered by Wu and Gale and was further explored by York et al, who investigated a scaffold of bisaryl ureas and their activity as mitochondrial uncouplers through this same fatty acid activated mechanism[22-23]. The anion binding motif of bisaryl ureas were replaced with squaramide, amide and diurea groups and bisaryl rings were substituted with various electron withdrawing groups[22]. The bisaryl urea analogues inhibited OXPHOS in MDA-MB-231 cells and reduced cell viability, confirming their activity as mitochondrial uncouplers[22]. Utilising a HPTS proton transport assay developed

by Wu and Gale, the proton transport mechanisms of these anionophores across vesicle membranes were explored further such as stoichiometry of transport, proton transport rate and concentration needed to reach 50% of maximum transport (EC_{50})[22-23, 128].

1.2.2 Aryl Urea-Substituted Fatty Acids: A New Class of Mitochondrial Uncouplers

In 2020, Rawling et al reported a new class of anticancer agents: aryl urea-substituted fatty acids or "aryl ureas" (**Figure 10**)[124, 129].
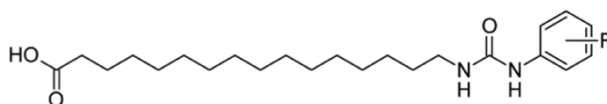
Figure 10: General structure of aryl ureas developed by Rawling et al.

In mechanistic studies, it was shown that these compounds induce apoptosis in cancer cells by acting as mitochondrial uncouplers and can operate independently of uncoupling proteins or synthetic anion transporters[124]. Aryl urea-substituted fatty acids are able to stabilise the negative charge on the carboxylate through supramolecular hydrogen bonding interactions between the urea NH protons of an aryl urea fatty acid molecule and the carboxylate of another independent aryl urea molecule. This allows the molecules to self-assemble into dimeric complexes (**Figure 11**), masking the charge of the species and permitting the anionic form to permeate the MIM[124]. Forming membrane-permeable dimeric complexes allows a complete protonophoric cycle to occur via flip-flop diffusion, leading to mitochondrial uncoupling[124, 130]. Derivatives such as aryl carbamates have also induced full mitochondrial uncoupling in MBA-MD-231 breast cancer cells via flip-flop diffusion, where they depolarised the MIM, increased cellular respiration and inhibited ATP production[22, 131-132].

Electron withdrawing substituents in the meta and para positions have shown to improve the aryl urea's ability to disrupt energy production in cancer cells[129, 133]. Thus, the 2020 aryl urea study involved preparing aryl ureas with different electron withdrawing substituents on the aromatic ring with varying polarity to assess the influence of substituent lipophilicity on activity[124]. Having chloro- and trifluoromethyl- substituents in a 3,4- or 3,5-substitution pattern appeared to improve potency in JC-1 assays and these analogues were investigated further in alkyl chain length studies[134-135].
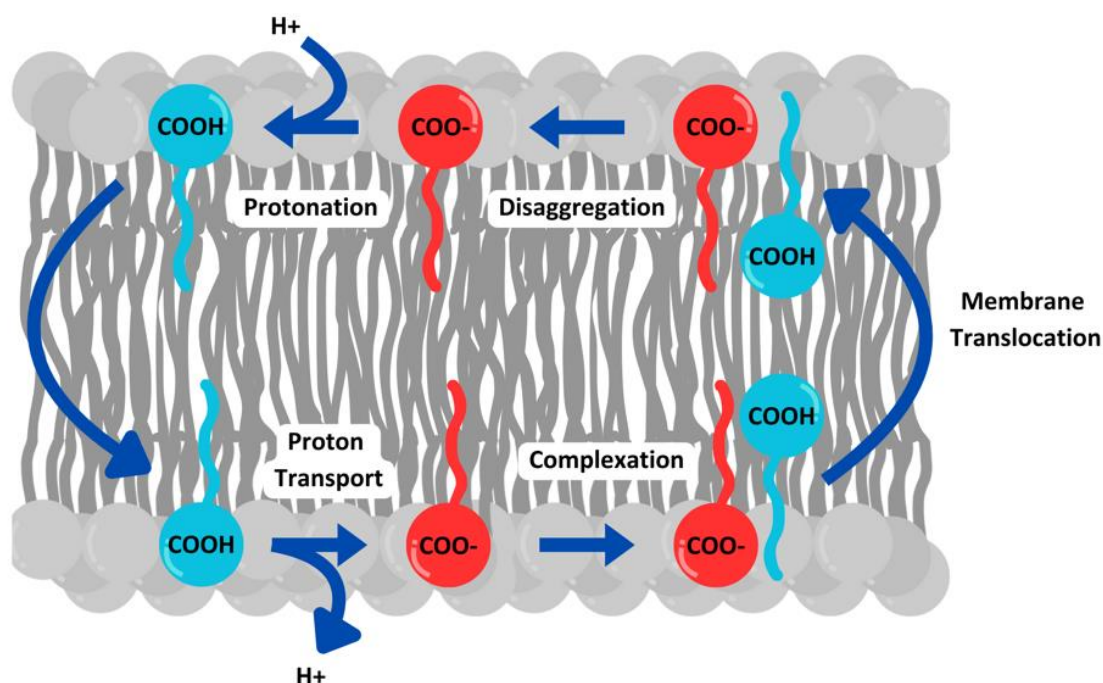
Figure 11: Proposed mechanism of uncoupling via dimer formation and flip-flop diffusion.

To further explore this new class of uncouplers, the Rawling group have investigated replacing the urea group with other anion binding units such as an amide group (aryl amides). Whereas ureas form parallel hydrogen bonds to carboxylate anions, amides bind via single hydrogen bonds via their NH group and thus have relatively lower carboxylate affinities. This change was anticipated to affect the dimerization and protonophoric activity of the amide series. In preliminary cell-based studies, it emerged that all aryl amide fatty acids were able to

diminish the proton gradient across the MIM, but a subset of amides had an activity profile consistent with mild mitochondrial uncouplers. However, investigating the underlying mechanism of mild uncouplers and distinguishing them from full uncouplers such as DNP and CCCP has been a challenge for decades. Thus, there is a growing need to further distinguish between mild and full uncouplers experimentally, which in turn could improve the screening and development of safe and effective anti-obesity drugs.

1.3   Project Aims and Thesis Structure

This thesis sought to investigate the mitochondrial uncoupling ability of aryl amide fatty acid protonophores and characterise them as full or mild uncouplers. This knowledge was then applied to the development of a library of shorter chain aryl amide fatty acids, in hopes of developing a mild uncoupler with favourable physiochemical properties for oral bioavailability and causes weight loss in murine mouse obesity models.

The specific aims of this thesis are:

1. To synthesise a library of long chain (C18) aryl amides with lipophilic electron withdrawing groups in 3,4- and 3,5- substitution patterns and assess their mitochondrial uncoupling ability *in vitro*.

2. To study anion binding and dimerization of the full and mild arylamide uncouplers using a combination of experimental and computational approaches.

3. To synthesise shorter chain (C16-C8) mild uncoupler analogues which are more "drug-like" and would have more favourable physiochemical properties for oral bioavailability.

4. Assess these short chain aryl amides for their uncoupling activity *in vitro*, proton transport mechanisms in vesicle membranes and assess the most potent analogue's potential weight loss effects *in vivo.*

To achieve these aims, aryl amides with a C18 hydrocarbon chain and an aromatic ring with chloro- and/or trifluoromethyl- substituents in either 3,4- or 3,5- substitution pattern were synthesised. Their uncoupling ability was assessed both *in vitro* in a human breast cancer cell line and through mechanistic studies investigating proton transport, anion binding and dimerisation ability. Following the C18 aryl amide scaffold, shorter chain analogues (C16, C12 and C8) were developed using substituents which promoted mild uncoupling. The aim of this short chain library was to improve physiochemical properties of aryl amides in hopes of developing a more "drug-like" mild uncoupler based on Lipinski's rules of bioavailability. Their protonophoric abilities were assessed *in vitro* using rat skeletal muscle cells and through proton transport assays. Lastly, the most potent short chain aryl amide with optimal physiochemical properties for oral bioavailability was then tested for its ability to induce weight loss *in vivo*.

In **Chapter 2**, the design, synthesis and characterisation of the long chain aryl amides and their mitochondrial effects *in vitro* including membrane potential, ATP production, cell viability and oxygen consumption rate is reported along with mechanistic studies which distinguished between mild and full uncoupling. In **Chapter 3**, the design, synthesis and characterisation of short chain aryl amides along with their uncoupling ability *in vitro*, protonophoric mechanisms across vesicle membranes and activity in murine mouse obesity models are described. Lastly, **Chapter 4** involves conclusions and suggestions for future developments whilst chemistry and cell culture experimental procedures are in **Chapter 5.**

CHAPTER 2

The role of transbilayer proton transport rate in mild mitochondrial uncoupling produced by aryl amide substituted fatty acids

2.1 Background

As described in **Chapter 1**, aryl ureas are fatty acid protonophores which have been investigated in recent years for their ability to induce mitochondrial uncoupling[129-130]. These agents differ from most protonophores such as DNP or CCCP because their acidic group is not conjugated to an extended π-system. Instead aryl urea-substituted fatty acids are able to stabilise the negative charge on the carboxylate *via* supramolecular hydrogen bonding interactions between the urea NH protons and the carboxylate of two independent molecular units. This allows the molecules to self-assemble into dimeric complexes masking the charge of the species and permitting the anionic form to permeate the MIM[124]. The addition of lipophilic and strong electron withdrawing substituents to aryl ureas appears to improve mitochondrial dysfunction[124, 129]. In this thesis, a series of aryl urea-substituted fatty acid derivates in which the urea groups were replaced with amide functional groups were prepared. Whereas ureas form parallel hydrogen bonds to carboxylate anions, amides bind via single hydrogen bonds via their NH group, and thus have relatively lower carboxylate affinities[22]. This change was anticipated to affect the dimerization and protonophoric activity of the amide series.

The objective of this chapter was to identify key determinants of mild uncoupling and experimentally distinguish between a full uncoupler and mild uncoupler using a scaffold of aryl amides, a new class of fatty acid protonophores. To achieve this, a library of aryl amides which mimics substituents and alkyl chain length of aryl ureas was prepared for *in vitro* evaluation, which is reported in this chapter.

2.2 Design of Aryl Amide Library 1 – Long Chain Analogues

Aryl Amide Library 1 was designed to investigate the mechanism of mild uncoupling and explore the effect substitution pattern has on uncoupling ability (**Figure 12**). Since lipophilic and strong electron withdrawing groups improved potency in aryl ureas, chloro- and trifluoromethyl- substituents were used in this aryl amide library[124, 129]. Similarly, the chain length of these aryl amides (C18) were identical to the aryl ureas used in a previous study investigating their flip-flop diffusion mechanism of uncoupling[124].
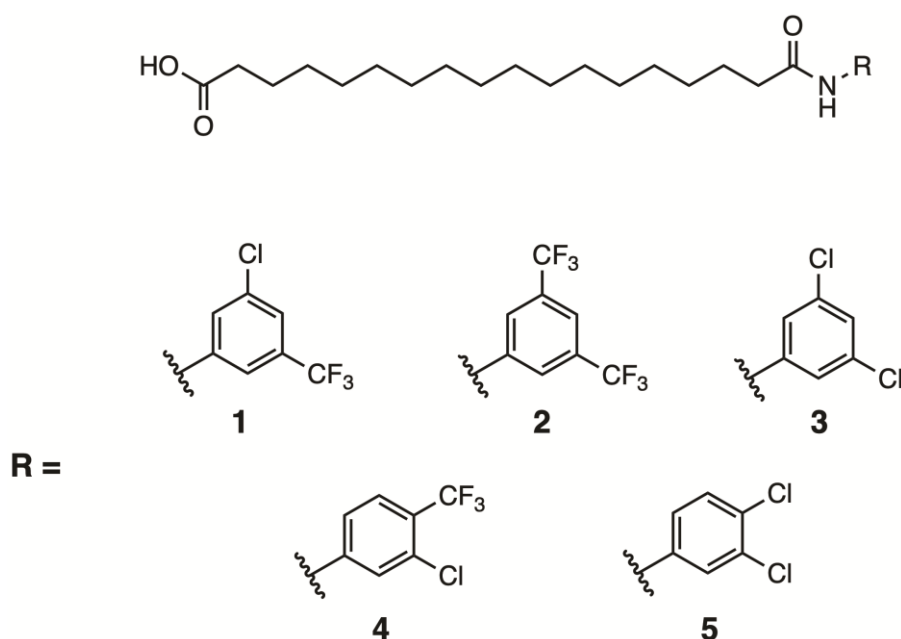
Figure 12: Chemical structures of library 1, a series of C18 aryl amides with varying aryl substituents

2.2.1 *Synthesis of Aryl Amide Library 1*

The synthesis of long chain aryl amides involved an amide coupling reaction followed by tert-butyl ester hydrolysis (**Scheme 1**).
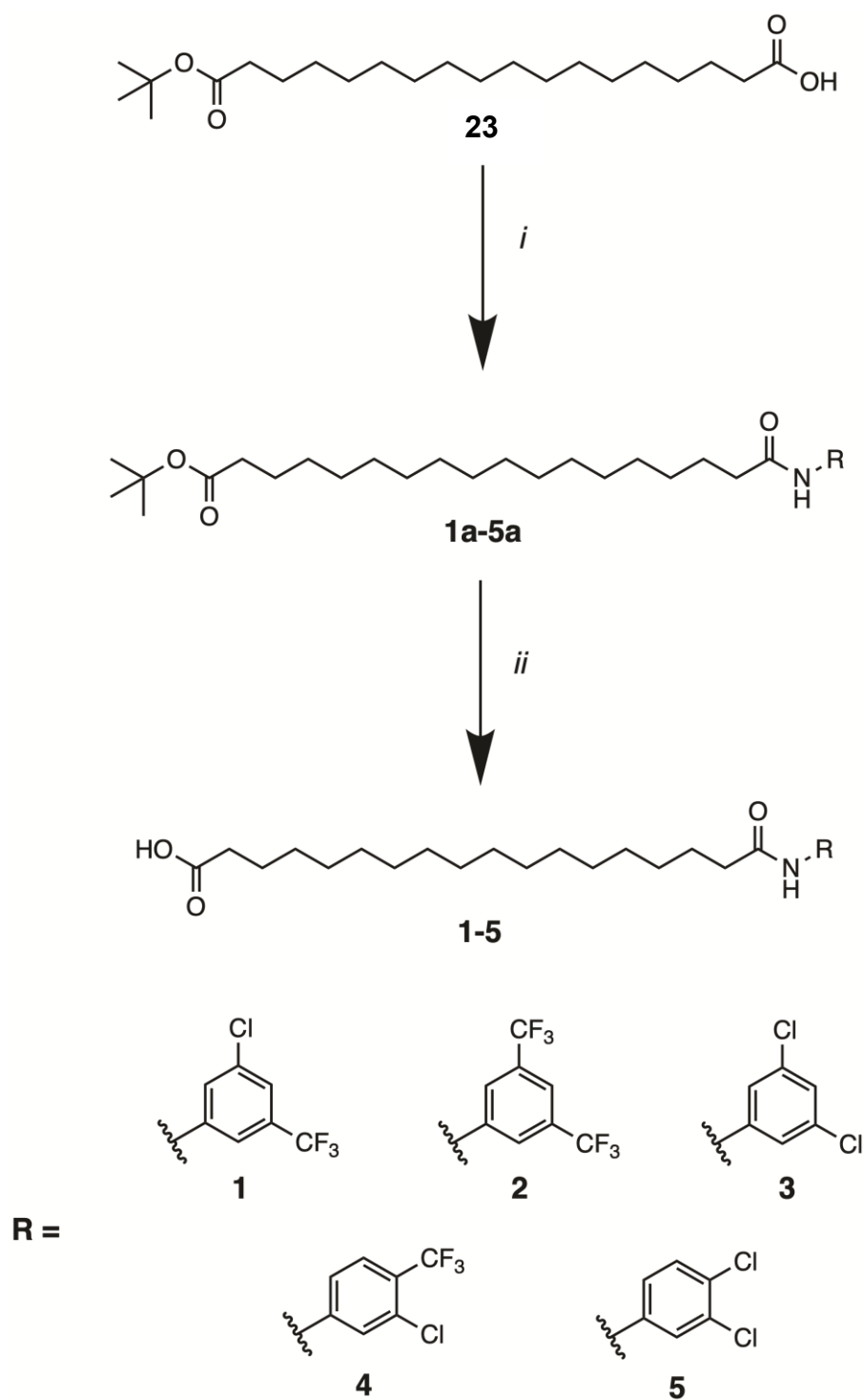
Scheme 1: General synthesis of aryl amides **1-5**. Reagents and conditions: **i)** COMU, Et₃N, RT, 3 h. **ii)** TFA, RT, 3 h

The precursor octadecanedioic acid mono tert-butyl ester (**23**) was available for purchase and obtained from a commercial supplier. **23** was then reacted with the corresponding aniline to afford aryl amide tert-butyl esters **1a-5a** through an amide coupling reaction. Amide bonds are typically formed by the union of carboxylic acids and amines, requiring the carboxylic acid to be activated by converting it into a good leaving group[136]. Coupling reagents have been used since 1955 to activate carboxylic acids, with the first group of reagents being carbodiimides such as dicyclohexylcarbodiimide (DCC)[137]. Common amide coupling reagents such as 1-ethyl-3-(3-dimethylaminopropyl) carbodiimide (EDCI) and 1-hydroxybenzotriazole (HOBt) were not suitable for this synthesis due to the anilines with electron-withdrawing substituents being poor nucleophiles, preventing adequate formation of amide bonds[138-140]. Over the past decade, COMU has shown to be a superior amide coupling reagent with safer leaving groups, greater stability, lower reaction times and assisting in forming amide bonds with high yields despite poor nucleophilic amines and/or sterically hindered acids being used[141-144]. Therefore, COMU was selected as the coupling reagent to synthesise **1a-5a**. Following the procedure outlined by El-Faham and Albericio, compound **23** was mixed with the corresponding aniline, COMU and triethylamine (Et$_3$N) in dry dimethylformamide (DMF)[143].

The reaction mixture was stirred for 5 minutes to activate the carboxylic acid before adding the corresponding substituted aniline and stirring for a further 3 hours under strict anhydrous conditions in order to prevent COMU degradation when absorbing moisture from the air and form **1a-5a**[145]. These aryl amide tert-butyl esters were then isolated by dry column vacuum chromatography (DCVC) with decent yields and characterized by ^{1}H NMR and ^{13}C NMR spectroscopy (see **appendix**).

Lastly, the tert-butyl protecting group was removed through trifluoroacetic acid (TFA) mediated hydrolysis[146]. Compounds **1a-5a** were dissolved in anhydrous dichloromethane (DCM) and TFA was added dropwise which cleaves the tert-butyl group to form a carboxylate in solution. After liquid-liquid extraction and the addition of hydrochloric acid (HCl), the carboxylate is protonated, forming the corresponding aryl amide. The success of the hydrolysis was determined by the disappearance of the tert-butyl CH_3 protons and appearance of COOH proton in ^1H NMR and ^{13}C NMR spectra (see **appendix**).

Compound purity was also assessed by absolute quantitative ^1H NMR (qNMR) spectroscopy, which involves using 1,3,5-trioxane as an internal standard in deuterated DMSO (DMSO-d_6). Purity (w/w %) was determined by calculating the proportionality between the average integration of one proton from the internal standard and a proton from the corresponding aryl amide. The purity of all aryl amides were determined to by > 95% by qNMR spectroscopy prior to *in vitro* testing.

2.3   Effects of Aryl Amides on MDA-MB-231 cell viability

Firstly, the capacity of aryl amides **1-5** (1, 10 and 40 µM, 24 hours) to reduce the viability of MDA-MB-231 breast cancer cells was assessed using MTS assays, since aryl urea fatty acids were shown to induce apoptosis in the same cell line[129]. This assay is a colorimetric method of assessing cell viability, where the tetrazolium MTS dye is reduced by living cells to form a coloured formazan product. This formazan product is measured by its absorbance at 490 nm, which is directly proportional to the number of viable cells in the population. In these assays, and all subsequent cell-based assays, the maximum test concentration of each aryl amide was 40 µM, as these compounds precipitated out of cell media at higher concentrations. As shown in **Figure 13**, aryl amide **2** was the most active in the series and reduced cell viability to 54.7 ± 4.5 % ($P < 0.001$) and 35.4 ± 6.5 % ($P < 0.0001$) of control at 10 and 40 µM respectively. 3,5-Substituted aryl amides **1** and **3** also significantly reduced cell viability at 40 µM, whereas 3,4-substituted aryl amides **4** and **5** showed no activity at all test concentrations. Thus, displaying varying effects on cellular function between aryl amides depending on substitution pattern.
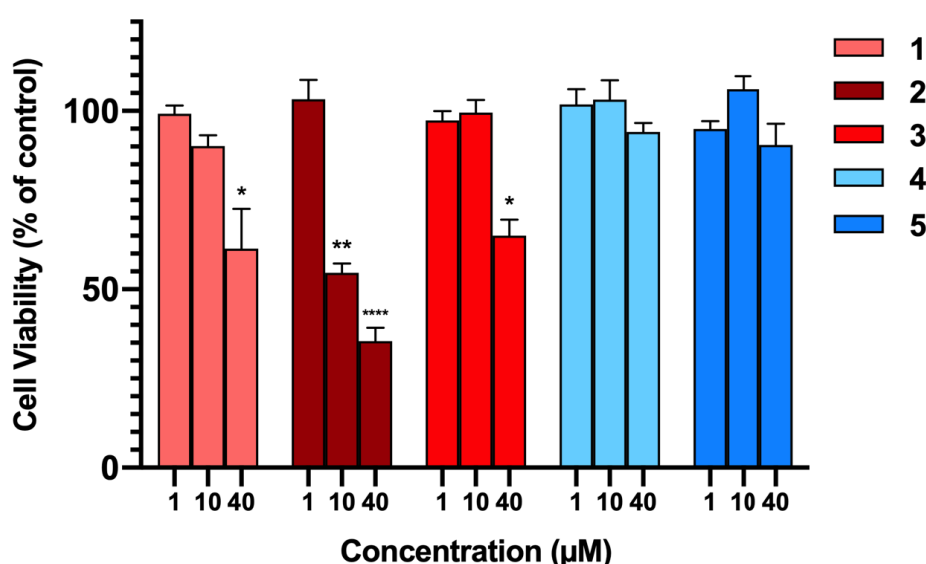
Figure 13: MTS cell viability of MDA-MB-231 breast cancer cells when treated with aryl amides **1-5** at 1, 10 and 40 µM for 24 hours. Data represents the mean ± SEM of 3 independent experiments. Difference from DMSO control: (*) $P < 0.05$, (**) $P < 0.001$, (****) $P < 0.0001$.

2.4 Effects of Aryl Amides on Mitochondrial Function of MDA-MB-231 cells

The aryl urea fatty acids, from which aryl amides **1-5** were derived, kill MDA-MB-231 cells by uncoupling OXPHOS and inducing mitochondrial dysfunction[124, 129, 133]. We therefore assessed the effects of the aryl amides on mitochondrial function. We first measured oxygen consumption rates (OCR) in MDA-MB-231 cells treated with aryl amides **1-5**, as well as the classical protonophores CCCP and DNP, using an XFe24 Seahorse analyser. Seahorse XF instrumentation provides direct real-time measurements of various metabolic functions such as OCR, extracellular acidification rate (ECAR), glycolysis, ETC-specific ATP production, and proton efflux rate (PER)[147-148]. A mito-stress test is the most common assay conducted using Seahorse XF instruments, which uses FCCP, oligomycin and rotenone/antimycin A to inhibit metabolic functions such as ATP synthase and OXPHOS in order to assess the maximal respiration of cell lines or uncouplers[147-148]. A simpler assay employs the single addition of a protonophore and measuring the OCR of cells over time, which is commonly conducted when screening for mitochondrial uncouplers[118, 149-151]. Oxygen is consumed by the ETC during OXPHOS, and OCR is expected to increase in cells treated with mitochondrial uncouplers as they increase respiration to compensate for proton leak.

To carry out these assays, MDA-MB-231 breast cancer cells were treated aryl amides **1-5** at the highest possible concentration of 40 µM and OCR was monitored over 3 hours. As shown in **Figure 14**, all aryl amides increased OCR, as well as the classical uncouplers CCCP and DNP. This data shows that all test compounds stimulated respiration in MDA-MB-231 cells, which is consistent with mitochondrial uncoupling.
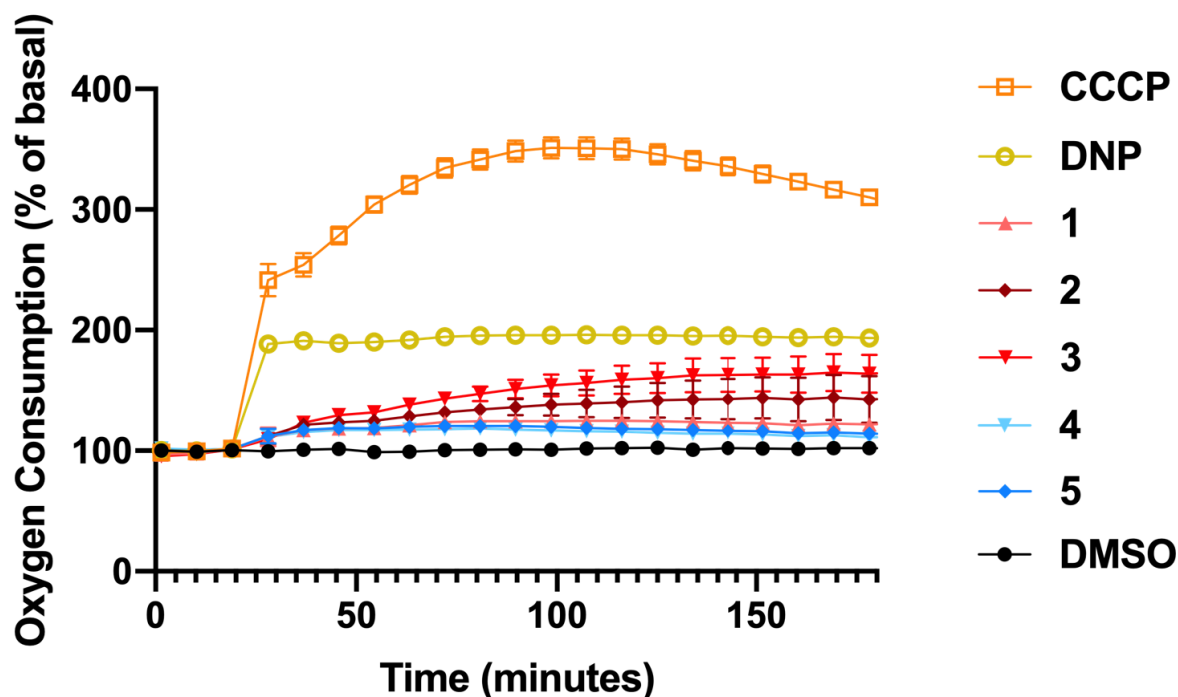
Figure 14: OCR of MDA-MB-231 breast cancer cells when treated with aryl amides **1-5** at their maximal solubility limit (40 µM) as well as CCCP (5 µM) and DNP (20 µM) over 3 hours. Data represents mean ± SEM of 3 independent experiments.

Next the capacity of the aryl amides, as well as CCCP and DNP, to depolarise the MIM in MDA-MB-231 cells was assessed using a JC-1 assay. JC-1 dye is a fluorescent cationic dye that accumulates in polarised mitochondria, forming aggregates that fluoresce red (≈590 nm)[152-153]. Upon depolarisation, JC-1 migrates to the cell cytosol where is disaggregates into monomers that fluoresces green (≈ 529 nm). Thus, the JC-1 red/green fluorescence intensity ratio can be used to determine the extent of mitochondrial depolarisation. In the JC-1 assays, MDA-MB-231 cells were treated with the aryl amides over a range of concentrations for 1 hour to capture early cellular effects of the compounds. JC-1 IC_{50} concentrations, defined as the concentration of test compounds required to shift the red/green fluorescence by 50% of control, and E_{max} values, defined as the maximum shift in JC-1 fluorescence ratio at the highest test concentration, were determined from dose-response curves (**Figure 15**) and are shown in **Table 2**.
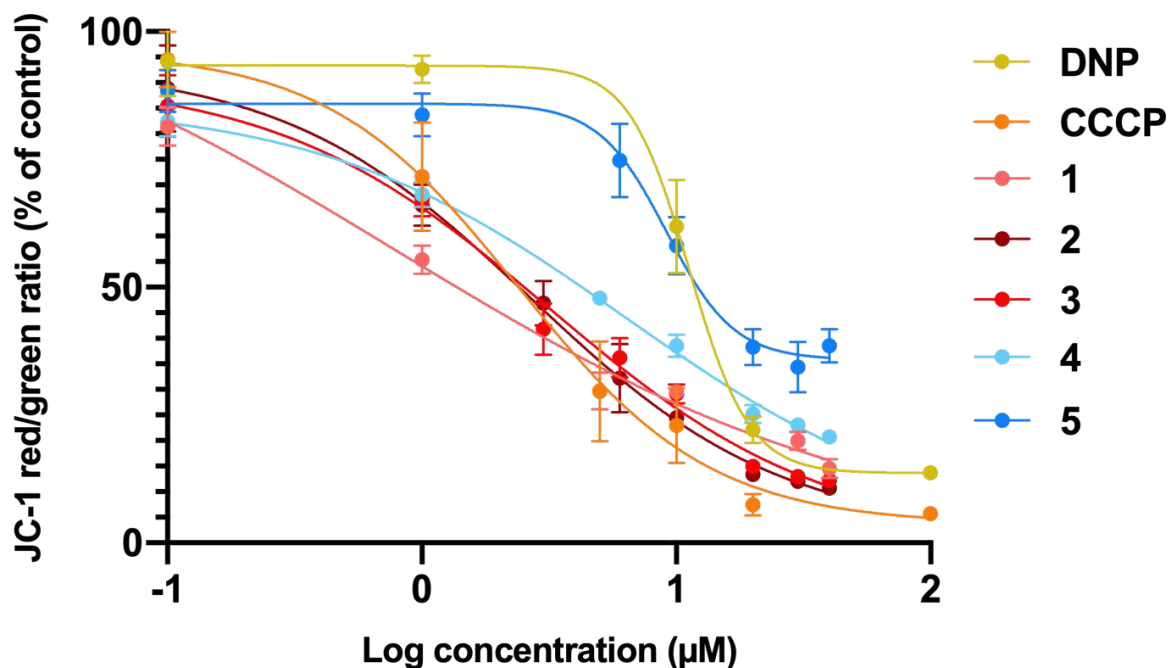
Figure 15: Dose response curve displaying JC-1 red/green fluorescence ratio which is indicative of depolarisation of MDA-MB-231 cell's MIM. Cells were treated with aryl amide **1-5** at 0.1-40 µM, DNP and CCCP at 0.1-100 µM using a JC-1 assay. Data represents the mean ± SEM of 3 independent experiments.

Table 2: Summarised JC-1 activity of aryl amides **1-5**, DNP and CCCP. Data represents the mean ± SEM of 3 independent experiments.

Compound	Relative JC-1 IC$_{50}$ (µM)	Maximum E$_{max}$ (%)
1	0.844 ± 0.37	14.6 ± 1.9
2	3.97 ± 1.8	10.7 ± 0.99
3	5.28 ± 1.7	11.7 ± 0.65
4	5.53 ± 0.3	21.1 ± 1.2
5	9.23 ± 1.4	34.1 ± 3.2
DNP	9.99 ± 1.7	13.7 ± 0.90
CCCP	3.95 ± 2.6	5.7 ± 1.3

All aryl amides **1-5** and full uncouplers CCCP and DNP were active in JC-1 assays, which indicates all compounds were able to reduce the proton gradient across the MIM in MDA-MB-231 cells. Combined with the increases in OCR observed in Seahorse data, these assays indicate that all test compounds are active mitochondrial uncouplers. The JC-1 IC_{50} concentrations of aryl amides **2-5**, which is a measure of the uncoupling potency, were similar to those of DNP and CCCP, and fell with a concentration range of 3.97 – 9.99 μM. Compound **1** had the lowest JC-1 IC_{50} concentration and is the most potent in the series.

Although all aryl amides were active uncouplers, the maximum level of depolarisation (E_{max}) achieved by each compound did vary significantly. The E_{max} values for 3,5-substituted aryl amides **1-5**, as well as the full uncouplers DNP and CCCP, were all below 15%. In contrast, the E_{max} values of the 3,4-substituted aryl amides **4** and **5** were 21.1 ± 1.2 and 34.1 ± 3.2, respectively. The E_{max} values of **4** and **5** appear to reflect their maximum level of activity, rather than resulting from lower potency or insufficiently high test concentrations. Thus, **3** and **4** have similar IC_{50} concentrations, yet the E_{max} of **4** is approximately twice that of **3**, and the dose-response curves of **4** and **5** show little increase in activity from 20-40 μM. The results imply that 3,5-substituted aryl amides **1, 2** and **3** act as full uncouplers with similar activity to that of DNP and CCCP, while **4** and **5** can only cause partial depolarisation, which is consistent with mild mitochondrial uncoupling.

2.5   Effects of Aryl Amides on ATP Production

To further characterise the uncoupling effect of the aryl amides, we assessed their capacity to inhibit ATP production in MDA-MB-231 cells using the CellTiter-Glo 2.0 Assay. Full uncouplers such as DNP and CCCP inhibit ATP synthesis by collapsing mitochondrial proton gradients to the point where the PMF is no longer strong enough to drive proton flow through ATP-synthase,[8, 18-19, 21] while mild uncoupling maintains the PMF at a level that allows ATP synthesis via OXPHOS to occur[98, 104]. CellTiter-Glo is a bioluminescence assay utilising the oxidation of luciferin into oxyluciferin, a reaction catalysed by the firefly luciferase enzyme on which ATP is dependent[154-155]. ATP is the limiting reagent of the reaction and is used to generate light; therefore, luminescence is directly proportional to the number of ATP molecules present.

As shown in **Figure 16**, all 3,5-substituted analogues (**1, 2** and **3**), along with DNP and CCCP, significantly decreased ATP production after 1-6 hr treatment at 20 μM. These relatively small decreases in ATP production are consistent with other full uncouplers in the literature[101, 123]. In contrast, ATP production was not significantly affected by 3,4-substituted aryl amides **4** and **5**. To ensure that the observed changes in intracellular ATP levels were not caused by cell death, LDH release assays were performed on MDA-MB-231 cells treated for 6 hours at 20 μM. Lactate dehydrogenase (LDH) is an intracellular enzyme that is released as cells die and therefore serves as a marker of cell death. All aryl amides failed to induce LDH release after 6 hours, (**Figure 17**), thus decreases in ATP are likely to result from inhibition of OXPHOS by uncoupling. In light of these results, it seems likely that aryl amides **4** and **5** are acting as mild mitochondrial uncouplers and depolarising the MIM without affecting ATP production.
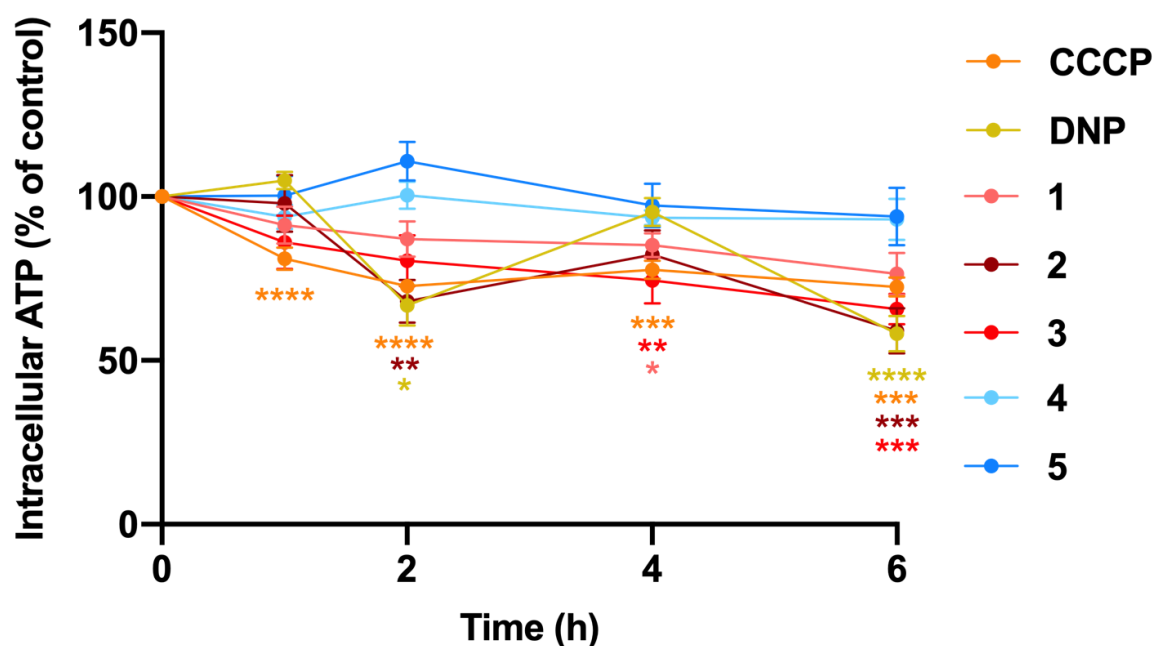
Figure 16: Intracellular ATP production in MDA-MB-231 cells when treated with amides **1-5**, DNP and CCCP at 20 μM for 1-6 hours. Data represents the mean ± SEM of 3 independent experiments. Difference from DMSO control: (*) $P < 0.05$, (**) $P < 0.01$, (***) $P < 0.001$, (****) $P < 0.0001$.
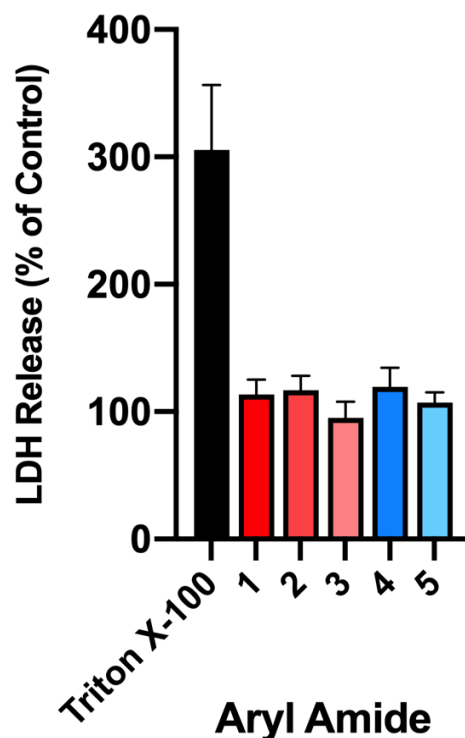
Figure 17: LDH release of MDA-MB-231 cells when treated with aryl amides **1-5** at 40 μM for 6 hours relative to DMSO control. Triton X-100 was used as a positive control which exhibits maximal LDH release.

2.6 Proton Transport of Aryl Amides Using the HPTS Assay

The *in vitro* data reveals that 3,4-substituted aryl amides induce mild mitochondrial uncoupling, while 3,5-substituted aryl amides act as full uncouplers. However, the reasons for these distinct uncoupling behaviours remain unclear. Previously reported mild uncouplers are lipophilic cations that diffuse out of mitochondria as depolarisation occurs, however this mechanism cannot apply to the aryl amides. Instead, it was hypothesised that the proton transport rates of individual aryl amides may determine the mild or full uncoupling activity. The ETC has a maximal rate in which it can pump protons into the intermembrane space and maintain the proton gradient. However, if an uncoupler is transporting protons across the MIM at a faster rate than the ETC is pumping protons into the intermembrane space, full uncoupling would arise as the proton gradient dissipates. If the uncoupler transports protons at a slower rate and does not out-pace the ETC, ATP synthesis will not be inhibited and mild uncoupling would occur.

To investigate the proton transport mechanisms driving these differences, a HPTS vesicular assay was employed. This assay utilises vesicles containing specific salt species encapsulated within a lipid membrane, allowing proton transport activity to be isolated from other cellular processes present in more complex *in vitro* assays. This simplified system provides a direct analysis of the transport process. An aqueous solution (pH 7) of potassium gluconate (100 mM), HEPES buffer (10 mM), and HPTS (1 mM), a pH-sensitive fluorescent probe, was encapsulated within large unilamellar vesicles (200 nm) composed of 1-palmitoyl-2-oleoyl-*sn*-glycero-3-phosphocholine (POPC). These vesicles were suspended in a similar solution where HPTS was not present. A pH gradient was created across the vesicle membrane by adding a NaOH pulse to the external solution, mimicking the proton gradient found in the

MIM[23]. The compound being tested in this assay facilitates the dissipation of this gradient via proton transport, which is tracked by ratiometric changes in the emission wavelengths of the HPTS dye. After 200 s, the vesicles were lysed with detergent to release all encapsulated protons and provide a 100% efflux calibration.

Dose-response studies were conducted to generate Hill plots and determine the EC_{50} value for each compound, representing the concentration of protonophore (mol%) required to achieve 50% proton efflux after 200 s. Briefly, the fractional fluorescence intensity (I_F) was calculated based on the acidic and basic forms of the HPTS probe at excited wavelengths. The I_F was plotted as a function of transporter concentration, and at $t = 200$ s each transporter concentration was fitted to an adapted Hill Equation and eventually derived to calculate EC_{50} values (please refer to Chapter 5.4.1.2 for more details). The EC_{50} values, displayed in **Table 3**, are reliable indicators of protonophoric activity, and the results partially correlate with the JC-1 IC_{50} concentrations. The 3,5-substituted compounds **1** and **2** exhibited the highest activity, with EC_{50} values of 0.060 and 0.041 mol %, respectively. The third most active compounds in the series was 3,4-substituted aryl amide **5** and 3,5-substituted aryl amide **3** ($EC_{50} = 0.14$ mol%). The Hill coefficients (n) provide insight into the relative stoichiometry of the transport event. In all cases, Hill coefficients ranging from 1.4 to 1.8 were observed. Values greater than 1 indicate a 2:1 transporter:proton stoichiometry consistent with the fatty-acid dimer transport mechanism proposed for this series of compounds. An n value of between 1 and 2 indicates the presence of both mono-deprotonated dimers and doubly deprotonated dimers, which together dissipate the pH gradient. Similar Hill coefficients across the series suggest that both classes of aryl amides operate via the same mechanism. The coexistence of these two mechanisms within the lipid bilayer has been discussed for analogous fatty acid protonophores previously[124, 131].

Table 3: EC_{50} and Hill coefficients for **1-5** in HPTS assays. CLogP values were calculated using ALOGPS 2.1[156]. HPTS data collected by Daniel McNaughton.

Aryl Amide	EC_{50} (mol %)	n	CLog P
1	0.060 ± 0.003	1.8 ± 0.1	7.28
2	0.041 ± 0.001	1.4 ± 0.1	7.19
3	0.14 ± 0.001	1.8 ± 0.02	6.95
4	0.08 ± 0.001	1.6 ± 0.01	7.27
5	0.14 ± 0.009	1.7 ± 0.14	6.94

Mitochondrial uncoupling occurs when protons bypass ATP synthase via alternative transport mechanisms. It was hypothesised, with support from the *in vitro* data, that the distinction between full and mild uncouplers lies in the proton transport rates relative to the ETC. To explore this potential differentiation between the two classes of uncouplers, the initial rate (k_i) was calculated for each compound in the HPTS assay at a loading of 0.5 mol%. This rate represents the maximum proton transport rate achieved by each protonophore when the pH gradient is steepest. The initial rates are presented in **Table 4**.

Table 4: Initial proton transport rates for aryl amides **1-5** (0.5 mol%) in HPTS assays. HPTS data collected by Dr Daniel McNaughton.

Aryl Amide	k_{ib} Base first (% s^{-1})	k_{ip} 30 s incubation (% s^{-1})	k_{ii} 300 s incubation (% s^{-1})	D (k_{ib}/k_{ip})	T (k_{ip}/k_{ii})
1	4.06	9.85	12.59	3.1	1.3
2	3.71	13.37	18.05	4.9	1.4
3	2.44	5.37	8.71	3.6	1.6
4	2.57	9.93	6.82	2.7	0.7
5	2.54	5.39	6.83	2.7	1.3

Under the original assay conditions, the initial rate trends largely mirrored those of the proton transport activity. The 3,5-substituted compounds **1** and **2** exhibited the highest initial rates (k_i = 4.06 and 3.71 % s^{-1}, respectively). In contrast, the 3,5-dichloro aryl amide **3** did not display an initial rate discernibly higher than its 3,4-substituted analogue and was again outperformed by compound **5**.

The calculated log P values for the series, presented in **Table 3**, are all greater than 6.94, which indicates they all possess a high degree of lipophilicity based on Lipinski and Verber's rules. Molecules with this structure may take longer to insert into the membrane than other small molecule protonophores. To address the effect of delayed membrane insertion on initial rate, the assay was repeated under two different incubation conditions. Firstly, the protonophore was added in an aliquot of DMSO (0.5 mol% loading) before the experiment was initiated with a NaOH base pulse after 30 s. Secondly, an incubation period of 300 s was allowed before initiating the experiment. The results of these experiments are presented in **Table 4**. Significantly, these experiments mimic pre-incorporation protocols commonly used in transport studies of highly lipophilic ionophores[157]. However, under these extended incubation conditions, the protonophores were still administrated via the extravesicular environment, a crucial consideration when evaluating their pharmaceutical potential and deliverability.

The results from the 300 s incubation assay provide the clearest distinction in proton transport rates between the 3,5- and 3,4-substituted aryl amides. Notably, compound **3**, which exhibited relatively modest proton transport rates during shorter incubation periods, emerged as the third most active compound after the extended incubation, achieving an initial rate of 8.71 % s^{-1}. Compounds **1** and **2** maintained the highest rates, with values of 12.59 % s^{-1} and

18.05 % s^{-1}, respectively. In contrast, the 3,4-substituted analogues consistently exhibited slower transport rates. Compound **4** remained the least active of the series, achieving an initial rate of 6.82 % s^{-1} after 300 s of incubation.

The constants *D*, representing the rate enhancement after 30 s incubation, and *T*, representing the rate enhancement between 30 and 300 s, were calculated to quantify the effects of incubation time on the initial proton transport rate. The values of *D* and *T* are larger for the 3,5-substituted aryl amides (**1-3**) than for the 3,4-substituted compounds (**4** and **5**), indicating that the 3,5-substituted aryl amides require more time to insert into the lipid bilayer and benefit more from extended incubation. This trend highlights a key distinction between the two classes of aryl amides. While the 3,4-substituted compounds appear to integrate more rapidly into the membrane, their overall rate of proton transport remains lower than that of their 3,5-substituted counterparts. Values of *T* < 1.0 for **4** and **5** indicate that the proton transport rates of these compounds decrease with an extended incubation.

The results suggest that the aryl substitution pattern plays a crucial role in both the membrane insertion dynamics and the proton transport rates achieved by compounds **1-5**. This role goes beyond lipophilicity, as the logP values calculated for the compounds (**Table 3**) vary minimally across the series. The 3,5-substituted compounds take longer to insert into the membrane, but once fully incorporated, they transport protons at a markedly quicker rate than their 3,4-substituted analogues. These differences in transport rate likely correlate directly with the ability of the compounds to induce either mild or full mitochondrial uncoupling.

2.7 Anion Binding Studies of Aryl Amide Esters Using ^{1}H NMR Titration

To identify possible causes of the different proton transports rates of the aryl amides, the capacity of the compounds to self-assemble into membrane permeable anionic dimers was studied, as this forms part of the rate-limiting step in their protonophoric cycle[124, 130]. Dimer formation occurs via hydrogen bonding between an amide NH from one aryl amide molecule with the carboxylate group of another. Therefore, the carboxylate (acetate) affinity of the amide groups in aryl amides **1-5** was assessed by ^{1}H NMR titration experiments. Calculating anion binding affinity involves dissolving the host molecule in an appropriate deuterated solvent where solvent-host hydrogen bonding is minimised and sequentially adding the guest anion into solution[23, 158]. As the guest anion is added, the hydrogen bond donor's (in this case the aryl amide NH) proton is shifted downfield, indicating hydrogen bond formation and complexation with the anion. These changes in chemical shift can be plotted against the concentration of the guest anion and by fitting the data into a 1:1 binding model, the binding constant (K_a) can be calculated. A 1:1 binding model was considered most likely as this binding stoichiometry was reported for the structurally related arylureas[131], however it is possible the arylamides bind to acetate via a different arrangement.

Firstly, tert-butyl ester analogues of the aryl amides (**1a-5a**) were titrated against tert-butyl ammonium acetate (TBAOAc) in acetone-d^6. Compounds **1a-5a** were selected rather than aryl amide fatty acids **1-5** in order to minimise binding interactions between the carboxylic acid group and the anion. Solutions were titrated with up to 10 equiv. of TBAOAc, and changes in resonance attributed to the NH peak were tracked with increasing concentrations of TBAOAc (**Figure 18**). The chemical shift of the aryl amide NH shifted downfield initially before plateauing at higher equivalences. The changes in chemical shift were inputted into the

Bindfit applet and fitted to a 1:1 receptor:guest binding model, which is an applicable model to fit this dataset due to aryl amides having a single NH group acting as a hydrogen bond donor[159]. Since the aryl amide tert-butyl esters are used, there is no competitive dimerisation occurring, which supports the use of this binding model further. The binding constants of each aryl amide tert-butyl ester are displayed in **Table 5**.
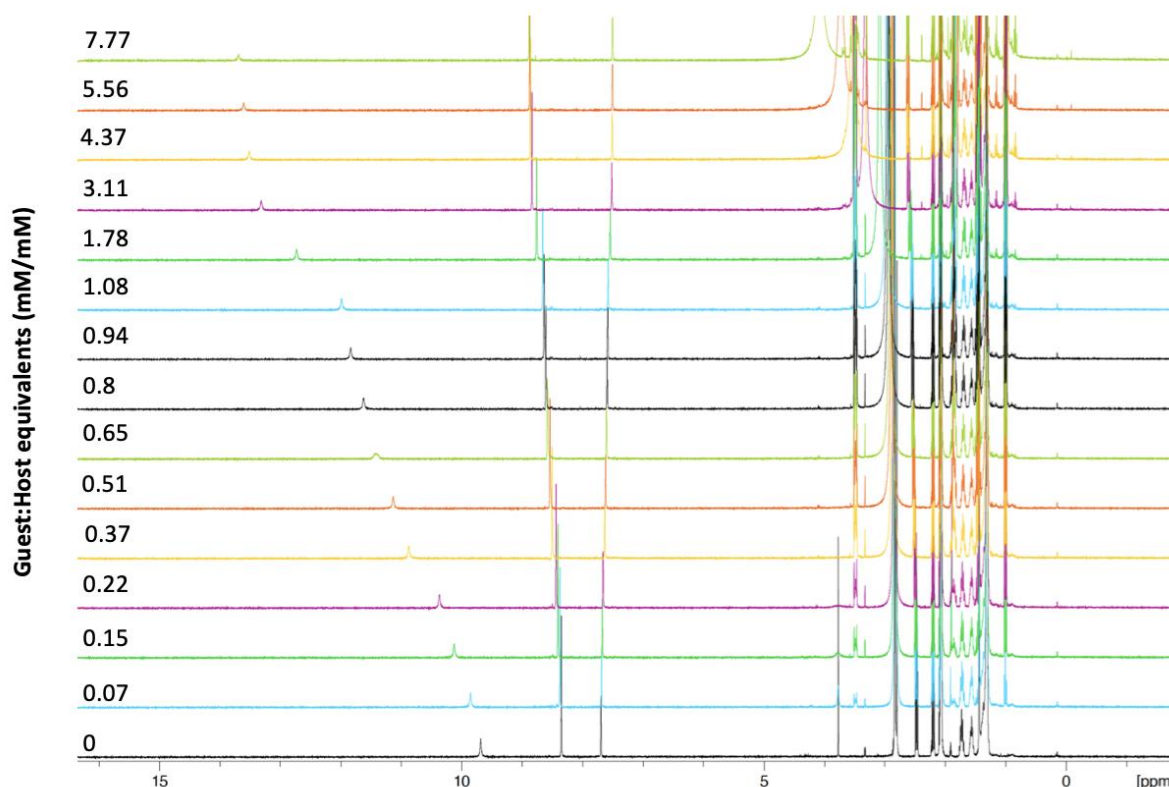
Figure 18: ^{1}H NMR titration spectra as a stack plot for aryl amide tert-butyl ester **2a** + TBAOAc in acetone-d^6 at 298 K. OAc$^-$ binding constant determined was 936.59 M^{-1} which was calculated by fitting the change in aryl amide N-H chemical shift to a 1:1 binding model on bindfit[159] with changing [OAc$^-$] from 0-9 mM/mM equivalents guest/host.

Table 5: Anion binding constants (K/M^{-1}) of aryl amide ester's to OAc^- in acetone-d^6 at 298K, calculated using a 1:1 binding model. Data represents mean ± the uncertainty of the fitted binding constant

Aryl Amide Ester	Binding Constant (K/M^{-1})
1	697 ± 4.48
2	937 ± 4.53
3	1310 ± 0.95
4	953 ± 3.60
5	926 ± 10.05

As shown in **Table 5**, all aryl amides bound to acetate with moderate affinity, but there was no clear distinction between the 3,5- and 3,4-substituted aryl amides. Indeed, the full uncoupler **3** had to the lowest acetate affinity in the series and the mild uncoupler **5** had the highest acetate affinity. Solvent choice for binding affinity studies is vital to ensure it does not provide a competing environment for forming hydrogen bonds[160]. Acetone-d^6 was used as a solvent for ^{1}H NMR titrations rather than CDCl$_3$ to minimise competitive Cl^- binding. However, acetone-d^6 is more polar and can act as a hydrogen bond acceptor, therefore opening the possibility of it competing with OAc^- for the hydrogen bonding of the aryl amide NH. Water is also one of the most competitive solvents for anion binding and if deuterated solvents are not adequately dried, it can weaken anion binding affinity of the host molecule[160-161]. Lastly, it is possible that some aryl amide esters are forming dimers with each other in this titration study, which in theory would impact their ability to bind to OAc^-.

Despite there being no clear distinction between anion binding affinities of these aryl amides to OAc^-, investigating their ability to form dimeric complexes may be more appropriate to reflect their activity *in vitro* and in HPTS assays, considering these dimers facilitate the movement of these aryl amides through lipid bilayer membranes.

2.8   Dimerisation Constants of Mild and Full Uncouplers

To further investigate whether aryl amide dimerisation impacts proton transport rate and subsequently mitochondrial uncoupling activity, concentration-dependent ^{1}H NMR studies of **1-5** in CDCl$_3$ were conducted. Deprotonation of the aryl amides was induced using 1 equiv. of tetrabutylammonium hydroxide (TBAOH). Increasing concentrations of (**1-5**)-TBAOH from 5 μM – 5 mM caused downfield shifts in the resonances attributed to the aromatic C-H protons. The concentration-dependant shifts in these resonances were fitted into a monomer-dimer aggregation model to give dimerization constants for **1-5** (**Table 6**)[159].

Table 6: Dimerisation constants of **1-5** calculated from the aromatic C-H peak chemical shifts of deprotonated **1-5** at 5 μM – 5 mM in CDCl$_3$ when fitted into a monomer-dimer aggregation model[159, 162].

Aryl Amide	Dimerisation Constant (M^{-1})	Error (%)
1	8270	± 21.30
2	8480	± 15.66
3	9290	± 17.75
4	2820	± 23.57
5	2360	± 11.51

Echoing the trends seen in previous experiments, the 3,5-substituted aryl amides **1, 2** and **3** had greater dimerisation constants than 3,4-substituted aryl amides **4** and **5**. Compound **3** with a 3,5-dichloro head group had the greatest dimerisation constant of 9290 M^{-1} whilst its 3,4-substituted counterpart **5** had the weakest dimerisation constant with 2360 M^{-1}. Aryl amides **1-3** appear to form head-to-tail dimers more readily, in turn improving their protonophoric abilities as they can facilitate proton transport at a greater rate in comparison to mild uncouplers **4** and **5**. However, this ^{1}H NMR dimerisation study does not explain whether the rate-limiting step of the protonophoric cycle of these aryl amides is dimer formation or the

speed in which these dimers move through bilayer membranes to complete the flip-flop diffusion. How substitution pattern impacts the hydrogen bond donor ability of the aryl amide NH when forming these dimeric complexes could also be explored further.

2.9   Computational Evaluation of Aryl Amide Dimers

For aryl amides to facilitate proton transport through the MIM, forming membrane permeable dimeric complexes and appears to be a key determinant in uncoupling ability. In order to determine the energetics of dimer formation, a computational evaluation of the aryl amide dimers was performed. Binding energies of dimers formed by a protonated and deprotonated aryl amine were evaluated using Gaussian 16^{163} at the M062x-D3/6-31G(d,p)//M062X-D3/6-311++G(2df,2p) level of theory. Complexes were examined in both water (to mimic the intermembrane space/matrix) and benzene (to mimic the membrane environment) using implicit solvation. In the hydrophilic environment, dimer formation of 3,5-substituted aryl amides **1-5** was more energetically favourable in comparison to 3,4-substituted aryl amides **3** and **5** (**Table 7**). However, in the hydrophobic environment this trend is not as apparent, as some 3,4-substituted aryl amides formed more stable dimers than 3,5-substituted aryl amides. Namely, mild uncoupling aryl amide **4** had a binding energy of -143.3 kJ/mol whilst in comparison full uncouplers **1** and **3** had lower binding energies of -131.5 kJ/mol and -128.6 kJ/mol respectively.

Table 7: Computational evaluation of aryl amides **1-5** dimer formation in water and benzene environments at the M062x-D3/6-31G(d,p)//M062X-D3/6-311++G(2df,2p) level of theory. Binding energy calculations were conducted by Dr Katie Wilson and Aaron Pye.

Aryl Amide	Binding Energy in Water (kJ/mol)	Binding Energy in Benzene (kJ/mol)
1	-87.1	-131.5
2	-95.6	-147.3
3	-87.9	-128.6
4	-86.5	-143.3
5	-85.9	-131.4

These fatty acid protonophores form dimeric complexes at the interface of the matrix, which is hydrophilic. The differences in trends between the modelled membrane (benzene) and solution (water) environments could be inferring that the rate-limiting step of the protonophoric cycle for these aryl amides is the stability of dimer formation between carboxylate and amide binding groups, rather than the rate of these dimers moving through the MIM. Specifically, 3,5-substituted aryl amides can form more stable dimers before moving across the MIM, which leads to faster proton transport, as a result causing full mitochondrial uncoupling. In contrast, 3,4-substituted aryl amides form less stable dimers which causes proton transport rate to decrease, thus leading to mild uncoupling.

Another factor that could influence the proton transport is the distribution and orientation of electron density around the aromatic ring of aryl amides. Notably, changes in the electron density can affect the NH group's ability to act as a hydrogen bond donor when forming a dimeric complex with a carboxylate. Measuring the dipole angle of the aromatic ring relative to the amide hydrogen bond axis provides a measure of the partial positive charge of the NH moiety, where a better alignment indicates a greater partial positive charge on the NH group and therefore a stronger hydrogen bonding ability[164-166].

To investigate this effect, the dipole angles of the aryl substituents relative to the amide hydrogen bond axis of aryl amides **1-5** were calculated using Gaussian 16[163] at the M062x-D3/6-31G(d,p)//M062X-D3/6-311++G(2df,2p) level of theory (**Table 8**). Due to aryl amides **1**, **4** and **5** being unsymmetrical, the dipole angle will differ depending on their conformation. Therefore, the average dipole angle of both conformers was used for these aryl amides after accounting for the probability of the formation of each conformer, which was calculated using the binding energies in each environment and applying them to a Boltzmann Distribution.

Table 8: Calculated dipole angles of aryl amides **1-5** at the M062x-D3/6-31G(d,p)//M062X-D3/6-311++G(2df,2p) level of theory. Aryl amides **1**, **4** and **5** are unsymmetrical molecules and therefore can have two possible conformations. The dipole angle of each conformation for these aryl amides was calculated and the probability of each conformer's formation was calculated using a Boltzmann Distribution. Displayed for the unsymmetrical aryl amides is the average dipole angle after taking this into account. Initial dipole angle calculations were conducted by Dr Katie Wilson and Aaron Pye.

Aryl Amide	Dipole Angle in Benzene	Dipole Angle in Water
1	27.24˚	19.12˚
2	28˚	21˚
3	23.4˚	16.7˚
4	35.72˚	27.91˚
5	30.54˚	22.4˚

As shown in **Table 8**, the 3,5-substituted aryl amides **1-3** had smaller dipole angles than 3,4-substituted aryl amides **4** and **5** in benzene and water environments. In both environments, mild uncoupler **4** had the highest dipole angles of 35.72˚ and 27.91˚ whilst full uncoupler **3** had the lowest dipole angles of 23.4˚ and 16.7˚. The smaller dipole angles infer that the dipole of the 3,5-substituted aromatic ring aligns better within the polarisation of the aryl amide NH group, therefore making the NH proton more positively polarised and more effective at forming strong

hydrogen bonds. In contrast, the 3,4-substituted aryl amides had greater dipole angles in both environments, inferring that the substituent's dipole does not align as well with the polarisation of the amide group. As a result, the 3,4-substituted aryl amide's NH group is generally weaker at forming hydrogen bonds in comparison to the 3,5-substituted aryl amides.

The differences in dipole alignment with the aryl amide NH group, correlates directly with the ^{1}H NMR dimerisation study (**Table 6**), where 3,5-substituted aryl amides **1-3** had greater dimerisation affinities than 3,4-substituted aryl amides **4** and **5**. Therefore, this computational evaluation provides justification as to why 3,5-substituted aryl amides form more stable dimeric complexes in comparison to 3,4-substituted aryl amides. As a result of their more energetically efficient dimer formation, 3,5-substitued aryl amides transport protons across bilayer membranes at a faster rate, causing full mitochondrial uncoupling *in vitro*. In contrast, 3,4-substituted aryl amides form less stable membrane permeable dimers, which slows down their rate of proton transport across bilayer membranes, thus leading to mild uncoupling.

2.10 Summary and Conclusions

The data presented in this chapter introduces the concept of proton transport rate being a key determinant of full or mild mitochondrial uncoupling in aryl amides, a new class of fatty acid protonophores. Despite only small structural changes in substitution pattern between analogues in library 1, great differences in *in vitro* activity were observed. Firstly, aryl amides **1-3** significantly decreased cell viability of MDA-MB-231 breast cancer cells in MTS assays at 10-40 µM, whilst **4** and **5** showed no activity at all test concentrations. These aryl amides also differed in their ability to impact mitochondrial function of MDA-MB-231 cells. All aryl amides **1-5** along with classical protonophores CCCP and DNP increased OCR, which is consistent with mitochondrial uncoupling. However, the extent in which **1-5** depolarised mitochondria varied in JC-1 assays.

Whilst aryl amides **1-5** had similar JC-1 IC_{50}'s to CCCP and DNP, which is a measure of uncoupling potency, the maximum level of depolarisation achieved by each compound varied significantly. E_{max} values of 3,5-substituted aryl amides **1-3** along with DNP and CCCP were below 15%, whereas 3,4-substituted aryl amides **4** and **5** E_{max} values ranged between 20-35%. These E_{max} values appeared to represent their maximum level of uncoupling activity, as they appear to plateau at higher concentrations in JC-1 dose-response curves. Therefore, 3,5-substituted aryl amides **1-3** act as full uncouplers with similar activity to classical uncouplers DNP and CCCP, whereas 3,4-substituted aryl amides **4** and **5** could only cause partial depolarisation which indicates mild uncoupling is occurring.

Assessing intracellular ATP production of MDA-MB-231 cells when treated with **1-5** distinguished between full and mild uncoupling further. Aryl amides **1-3**, DNP and CCCP significantly inhibited intracellular ATP levels. This is consistent with full mitochondrial uncoupling, as protons are transported from the intermembrane space across the MIM by these

protonophores and bypass ATP synthase, thus preventing sufficient energy for the catalysis of ADP to ATP. Aryl amides **4** and **5** on the other hand failed to affect ATP production. Since **4** and **5** increased OCR and depolarised mitochondria without inhibiting ATP production, they are acting as mild mitochondrial uncouplers.

The differences which distinguish full and mild uncoupling is largely unknown, as most definitions in the literature of mild uncoupling simply refer to either differences in impacting ATP production or being "self-limiting" by diffusing out of mitochondria as depolarisation occurs[98-101, 106-107]. It was hypothesised that the proton transport rates when facilitated by these aryl amides may determine full or mild uncoupling. If full uncouplers are carrying protons across the MIM at a faster rate in which the ETC pumps protons into the intermembrane space, the proton gradient dissipates and fails to provide ATP synthase with sufficient energy to produce ATP. However, mild uncoupling could occur if protons are transported across the MIM at a slower rate, in which there is sufficient energy to produce ATP whilst still inducing cellular effects such as increased OCR and partially depolarising the MIM.

HPTS assays were used to assess the proton transport mechanisms of aryl amides **1-5**. The EC_{50} values of **1-5** in HPTS assays partially correlated with the JC-1 IC_{50} concentrations, where aryl amides **1** and **2** had the lowest EC_{50} concentrations from library 1. Hill coefficients of **1-5** ranged from 1.4 to 1.8, indicating a 2:1 transporter:proton stoichiometry which is consistent with the fatty-acid dimer transport mechanism proposed by previous research into aryl urea fatty acids[23, 124, 128]. Despite having the same mechanism of movement through bilayer membranes, the initial rates of proton transport conducted by **1-5** varied. 3,5-substituted aryl amides **1-3** achieved faster rates of proton transport in comparison to 3,4-substituted aryl amides **4** and **5** when accounting for delayed bilayer membrane insertion. These differences in

transport rate correlate directly with the *in vitro* data, where these aryl amide's induced either full or mild mitochondrial uncoupling.

To identify possible causes for these different proton transport rates, ^{1}H NMR titrations were conducted to first assess the binding affinity of the aryl amide tert-butyl esters **1a-5a** with OAc⁻. However, there was no clear distinction between 3,4-substituted and 3,5-substituted aryl amides. To explore this further, their dimerisation constants were calculated when titrating against TBAOH. 3,5-substituted aryl amides **1-3** had greater dimerisation constants in comparison to 3,4-substituted aryl amides **4** and **5**, inferring that dimer stability is a key factor in their ability to facilitate proton transport.

Fatty acid protonophores form dimeric complexes with their carboxylate anion counterpart in order to facilitate their movement back through bilayer membranes and dissociate once reaching the other side of the membrane. To determine whether the rate-limiting step of the protonophoric cycle of aryl amides **1-5** is the stability of these dimeric complexes, a computational evaluation of aryl amide dimers was performed. 3,5-substituted aryl amides **1-3** appeared to have more energetically favourable dimer formation than 3,4-substituted aryl amides **4** and **5** in a hydrophilic environment which mimics the intermembrane space/matrix. However, this trend was not apparent in a hydrophobic environment which mimics the bilayer membrane. This could be inferring that the rate-limiting step of the protonophoric cycle for aryl amides is the formation of the dimers at the interface of the matrix rather than their actual rate in which these dimers transport across the membrane.

However, the only structural differences between aryl amides **1-3** and **4** and **5** is substitution pattern, which appears to be impacting their dimer formation, proton transport rate and subsequently mitochondrial uncoupling ability significantly. Comparing dipole angles of

substituents on the aromatic ring relative to the amide hydrogen bond axis appeared to explain this effect. 3,5-substituted aryl amides **1-3** had lower relative dipole angles than 3,4-substituted aryl amides **4** and **5** in benzene and water environments. Thus, inferring that the dipole of 3,5-substituents aligned with the aryl amide NH's dipole vector better, thus improving its hydrogen bond donor ability. In contrast, the larger dipole angles of 3,4-substituents infers their misalignment with the dipole vector of the amide group, therefore weakening the NH's hydrogen bond donor ability.

This correlates directly with their calculated dimerisation constants and binding energies, where 3,5-substituted aryl amides **1-3** are able to form more energetically favourable dimers in comparison to 3,4-substituted aryl amides **4** and **5**. As a result of this, **1-3** are able to transport protons across bilayer membranes at a faster rate and achieve maximal proton transport at lower concentrations in comparison to **4** and **5**. Thus, impacting their cellular effects, where **1-3** act as full mitochondrial uncouplers since they inhibit ATP production, increase OCR and depolarise the MIM greatly. In contrast, 3,4-substituted aryl amides **4** and **5** form less stable membrane permeable dimers to facilitate proton transport across bilayer membranes, thus hindering their rate of proton transport. As a result, they act as mild uncouplers as they still cause an increase OCR but without decreasing intracellular ATP levels and only partially depolarising the MIM.

These findings provide insight into the differences in efficiency between mild and full mitochondrial uncouplers in a scaffold of aryl amide fatty acid protonophores. As a result, this newfound understanding of proton transport rate being a key determinant in uncoupling ability will assist in identifying uncouplers for their therapeutic uses and widens the structural diversity of fatty acid protonophores.

CHAPTER 3

Investigation of the Effect of Chain Length on the Mitochondrial Uncoupling Ability of Aryl Amides

3.1 Background

As discussed in **Chapter 1**, there is increasing interest in recent years to develop mild mitochondrial uncouplers that can be used for therapeutic interventions in humans without the toxicity concerns of full uncouplers such as DNP. For example, within the past 5 years several 'safe' uncouplers such as BAM15 and its derivatives SHC517, SHM115 and SHD865 have been tested *in vivo* for their anti-obesity properties. These agents were generally well-tolerated in mice and showed promising activity in mouse models of obesity, but their short half-lives between 44 min – 1.4 h limits their clinical use[114, 118-120]. Thus, there remains an urgent need for safe and effective mild mitochondrial uncouplers with pharmacokinetic profiles suitable for use in humans.

Aryl amides **4** and **5** introduced in **Chapter 2** acted as mild uncouplers, however their physicochemical properties suggest these compounds are not 'drug-like' and will have poor pharmacokinetic profiles (see **Table 9**). For drugs to be orally bioavailable and drug-like, they must adhere to lipinski's rule of 5 where number of hydrogen bond acceptors, hydrogen bond donors, rotatable bonds, molecular weight and logP can impact drug absorption[167-168]. As shown in **Table 9**, these aryl amides are too lipophilic and have too many rotatable bonds to be considered drug-like, which largely arises from the long alkyl chain. Interestingly, the aryl amides share structural similarities to Vorinostat (**Figure 19**), an orally bioavailable drug currently used in Australia to treat cutaneous T-cell lymphoma (CTCL)[169]. Vorinostat has a terminal aryl amide moiety and hydroxamic acid group (a bio-isostere of carboxylic acid) connected by a C8 chain. Although Vorinostat has a different use, its similar structure to aryl amides invokes the hypothesis that shortening the C18 chain of the aryl amides may make them drug-like molecules with acceptable oral bioavailability's. Therefore, the aim of this chapter

was to develop a series of chain-shortened aryl amides and assess their protonophoric activities in cell, vesicle and animal models.

Table 9: Physiochemical properties of aryl amides **4** and **5** in relation to Lipinski's Rule of Five. The table presents calculated LogP (CLogP), molecular weight (MW) and number of hydrogen bond acceptors (HBA), hydrogen bond donors (HBD) and rotatable bonds (RB)

Aryl Amide	CLogP	MW	HBA	HBD	RB
4	7.27	492.02	2	2	16
5	6.94	458.46	2	2	16
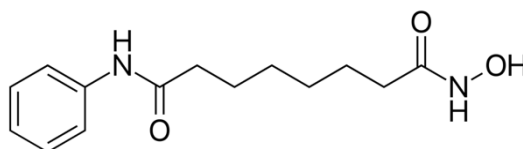
Figure 19: Structure of Vorinostat

3.2   Design of Short Chain Aryl Amides – Library 2

To develop a more drug-like mild uncoupler, a series of aryl amides with three chain lengths were studied: C16, C12 and C8 (**Figure 20**). Since Vorinostat has a C8 hydrocarbon chain and had favourable pharmacokinetics *in vivo*, C8 aryl amides were synthesised along with intermediate lengths of C12 and C16. **Table 10** displays the physiochemical properties of aryl amides **6**, **10** and **14**, with each having a 3-chloro-4-trifluoromethyl headgroup and chain lengths of C16, C12 and C8 respectively. By removing four carbons from the hydrocarbon chain of these aryl amides, LogP decreases by 1.75-1.34 and the number of rotatable bonds decrease by 4. In contrast to aryl amides **4** and **5**, aryl amides **10** and **14** satisfy Lipinski's Rules as LogP is less than or equal to 5 and the number of rotatable bonds is less than or equal to 10[167-168]. Aryl amide **6** does not satisfy Lipinski's Rules due to its high LogP of 6.76 and having 14 rotatable bonds and is therefore unlikely to have favourable oral bioavailability. Substituents

used were consistent with long chain (C18) aryl amides, with Cl- and CF_3- groups in the 3,4-position, since this substitution pattern influenced mild uncoupling as outlined in **Chapter 2**.
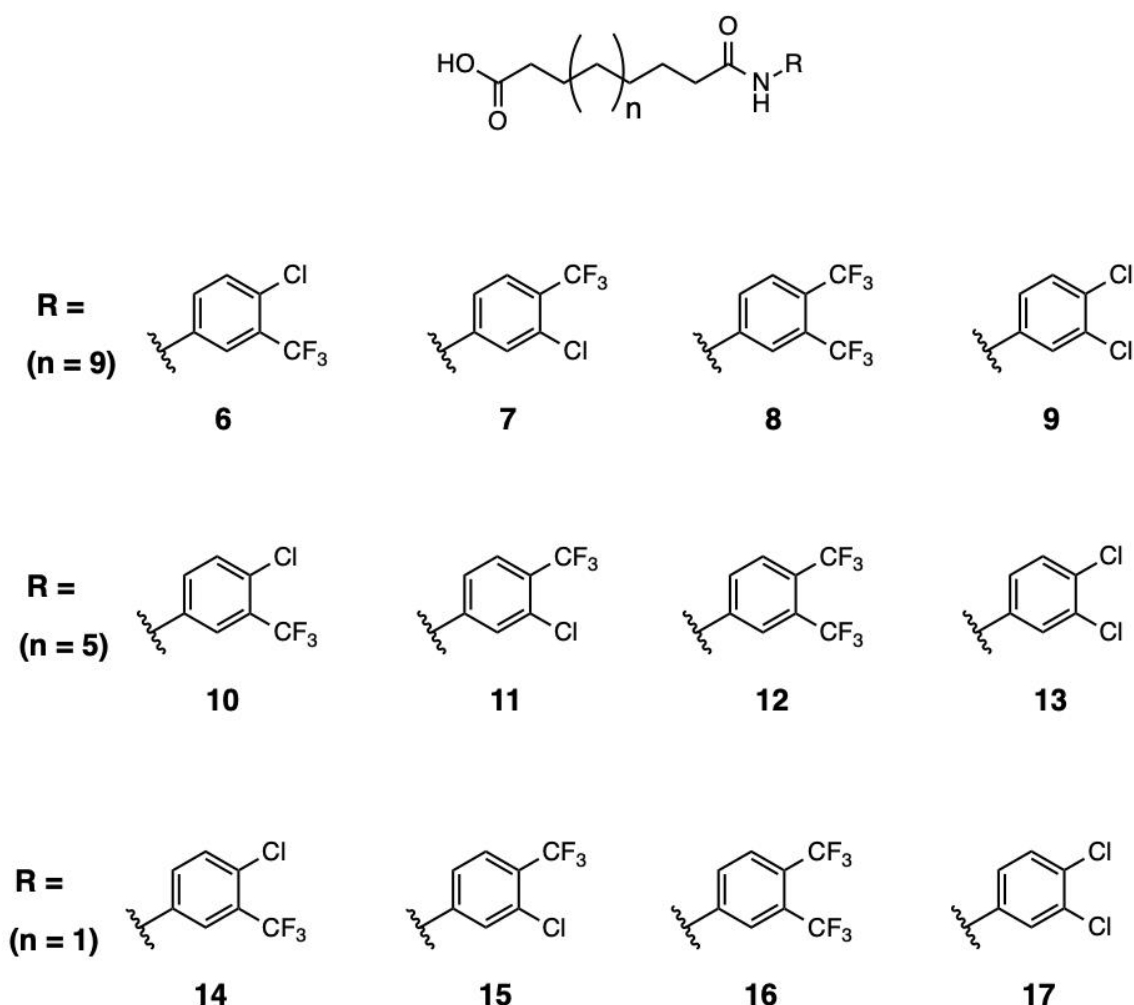
Figure 20: Chemical structures of short chain aryl amides in Library 2

Table 10: Physiochemical properties of aryl amides **6**, **10** and **14** in relation to Lipinski's Rule of Five. The table presents calculated LogP (CLogP), molecular weight (MW) and number of hydrogen bond acceptors (HBA), hydrogen bond donors (HBD) and rotatable bonds (RB). CLogP values were calculated using ALOGPS 2.1[156].

Aryl Amide	CLogP	MW	HBA	HBD	RB
6	6.76	463.97	2	2	14
10	5.01	407.86	2	2	10
14	3.67	351.75	2	2	6

3.3   Synthesis of Short Chain Aryl Amides

Shorter chain aryl amides **6-17** were synthesised as depicted in **Scheme 2**. Due to the commercial availability of 16-(*tert*-butoxy)-16-oxohexadecanoic acid (**20**), 12-methoxy-12-oxododecanoic acid (**21**) and 8-methoxy-8-oxooctanoic acid (**22**), aryl amides **6-9, 11** and **14-17** were synthesised and characterised using a similar procedure proposed in **Chapter 2.2.1** involving COMU coupling (reaction i) and ester hydrolysis (reaction ii or c). However, the ester-protected precursor **21** was not as widely commercially available and therefore aryl amides **10, 12** and **13** required a more extensive synthesis (reactions a, b, i and c).
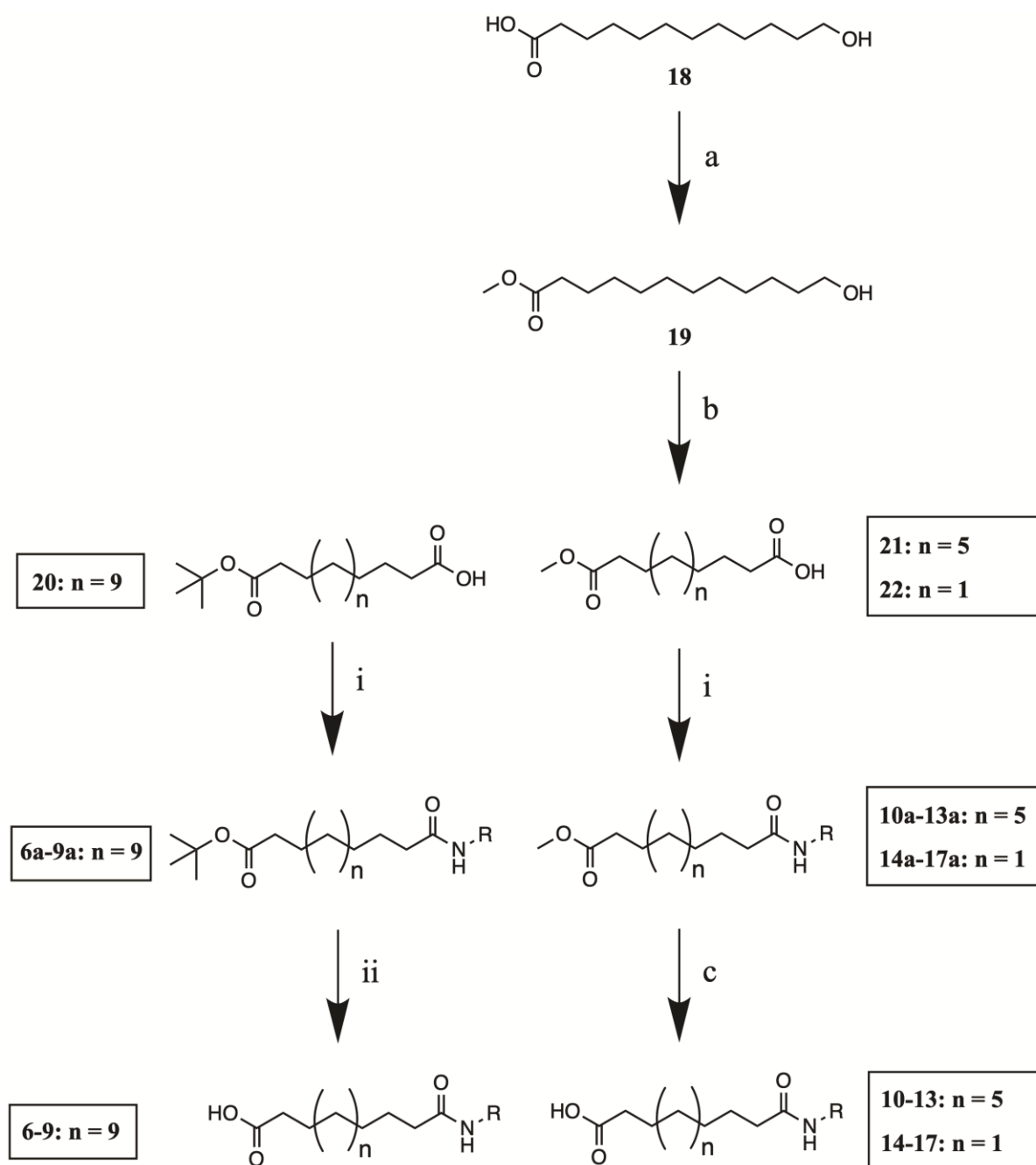
Scheme 2: General reaction scheme for the synthesis of shorter chain aryl amides **6-17**. **a)** CH$_3$I, acetone, 80 ˚C, 5 h. **b)** Jones reagent, acetone, 0 ˚C, 4.5 h. **i)** Substituted aniline, COMU, ET$_3$N, DMF, RT, 3 h. **c)** NaOH, EtOH, 40˚C, 4 h. **ii)** TFA, RT, 3 h

In order to synthesise C12 aryl amides **10, 12** and **13**, the first reaction involved the esterification of 12-hydroxydodecanoic acid (**18**) in the presence of iodomethane and potassium carbonate (K$_2$CO$_3$) in acetone (reaction a, **Scheme 2**)[170]. Initially, 1 mol of iodoethane was added to the reaction mixture and the reaction was refluxed for 5 hours at 80 ˚C. However, upon isolating the product after liquid-liquid extraction and analysing its ^{1}H NMR spectrum, remnants of **18** were present which indicated the reaction had not reached completion. Due to iodomethane's low boiling point of 42.5 ˚C, it likely evaporated before it could be subjected to nucleophilic substitution. To rectify this, sequential addition of 0.5 mol of iodomethane was added at the beginning of the reaction and the remaining 0.5 mol was added 2.5 hours later to ensure the reaction reaches completion before iodomethane evaporated[171]. As a result, methyl-12-hydroxydodecanoate (**19**) was successfully isolated as a white solid in high yield (85%).

Step b in the synthesis of the C12 aryl amides (**Scheme 2**) involved oxidising the primary alcohol group of **19** to a carboxylic acid using jones reagent[52]. Jones reagent is a mixture of chromium trioxide in diluted sulfuric acid which forms chromic acid in situ[172]. Only very acid-sensitive functional groups are incompatible with this oxidation, therefore allowing for the methyl ester group to remain unchanged. As the reaction proceeded the solution turned from red to green over time, which indicates the chromium has reduced from 6$^+$ to 3$^+$ whilst the alcohol group was oxidised to form an aldehyde initially, then converted into a carboxylic acid after 4.5 hours. After celite filtering and liquid-liquid extraction, **21** was isolated with nearly quantitative yield (98%)

Reaction i (**Scheme 2**) was covered extensively in **Chapter 2.2.1**, where COMU coupling was used to convert the COOH group to an amide and introduced an aromatic ring to

the fatty acid structure. This was followed by de-protection of the methyl ester through base-catalysed hydrolysis using NaOH (reaction c, **Scheme 2**)[173]. The reaction involved adding 1 M NaOH dropwise to the aryl amide methyl ester in ethanol (EtOH) to cleave the ester bond and form a carboxylate ion. By acidifying with HCl, the carboxylate ion protonates to form a carboxylic acid group in which the aryl amides precipitated in solution. Completion of the reaction was characterised by the disappearance of the methyl ester peak and appearance of the COOH peak in both ^1H and ^{13}C NMR spectra (see **appendix**). The purity of all aryl amides was determined to be >95% by qNMR spectroscopy prior to *in vitro* testing.

3.4   Effects of Short Chain Aryl Amides on $\Delta\Psi_m$

The ability for short chain aryl amides to depolarise mitochondria was investigated *in vitro* using a JC-1 assay, as outlined in **Chapter 2.3**. For these studies L6 rat skeletal muscle cells were used as the primary aim of this library was to develop drug-like mild uncouplers as potential weight loss drugs. JC-1 dose-response curves are shown in **Figure 21**, and the relative IC_{50} concentrations and E_{max} values are summarised in **Table 11**.

Alkyl chain length appears to affect the ability of aryl amides **6-17** to depolarise the MIM. The C16 aryl amides **6-9** induced the greatest depolarisation relative to control in the series, with $\Delta\Psi_m$ decreasing to 8-20 % of control and were the most potent of the short chain aryl amide series with relative IC_{50} values were between 1.7-6.9 µM (**Figure 21** panel **a** and **Table 11**). This extent of depolarisation along with similar IC_{50} concentrations were exhibited by C18 aryl amides **1-3** as well as DNP and CCCP, which suggests that **6-9** act as full mitochondrial uncouplers.

In contrast, C12 aryl amides **10-13** partially depolarised the MIM, with $\Delta\Psi_m$ decreasing to 18-36 % along with higher relative IC_{50}'s between 9.4-27.5 µM in comparison to **6-9**. This

extent of depolarisation was also exhibited by C18 aryl amides **4** and **5** which were characterised as mild uncouplers in **Chapter 2**, where membrane potential was decreased to 21-35 % with relative IC_{50}'s between 5.5-9.2 µM. However, it is important to note that for aryl amides **12** and **13**, their effect on $\Delta\Psi_m$ did not plateau at higher concentrations in comparison to **10** and **11** and due to solubility limitations, they could only be tested at a maximum concentration of 100 µM. Therefore, the characterisation of **12** and **13** as mild uncouplers based solely on the JC-1 data is not as definitive compared to other aryl amides in this library.

Lastly, the C8 aryl amides **14-17** had the weakest impact on $\Delta\Psi_m$ and were largely inactive. These compounds depolarised the MIM to 71-85% of control at the highest test concentration of 100 µM, and therefore relative IC_{50} concentrations could not be determined. CCCP and DNP were also tested in L6's cells and depolarised the MIM to a similar extent as in MDA-MB-231 cells outlined in **Chapter 2** (see **Table 11**). Therefore, as chain length decreases the ability for aryl amides **6-17** to impact $\Delta\Psi_m$ weakens.

.
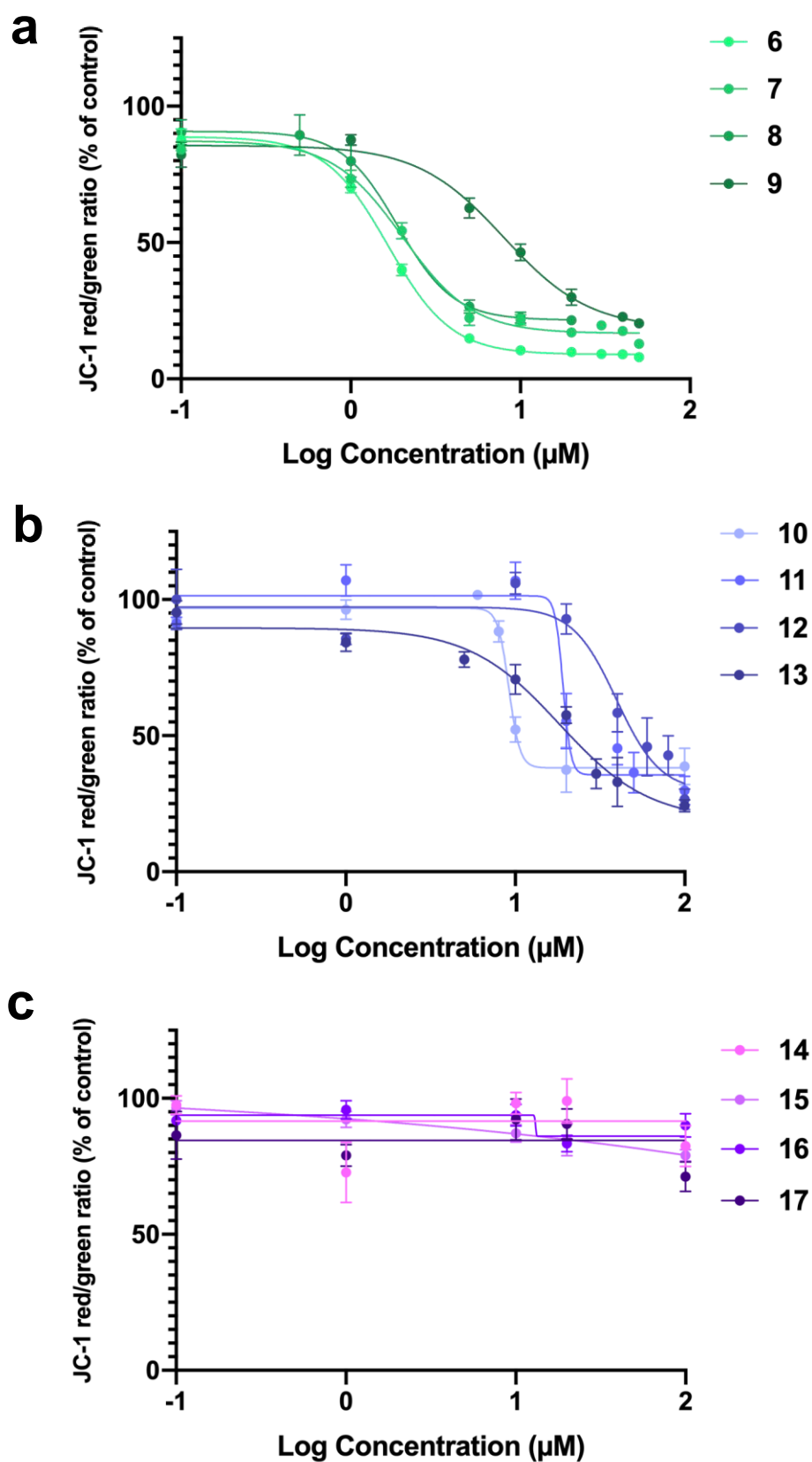
Figure 21: Dose response curves of membrane depolarisation induced by aryl amides in L6 rat skeletal muscle cells using a JC-1 assay: **a)** C16 aryl amides **6-9**. **b)** C12 aryl amides **10-13**. **c)** C8 aryl amides **14-17**. Data represents the mean ± SEM of 3 independent experiments

Table 11: Effect of aryl amides **6-17**, DNP and CCCP on $\Delta\Psi_m$ in L6 rat skeletal muscle cells using a JC-1 assay. Concentrations of aryl amides tested were between 1-100 µM. Data represents the mean ± SEM of 3 independent experiments.

Compound	Relative JC-1 IC$_{50}$ (µM)	E$_{max}$ (%)
6	1.68 ± 0.12	7.98 ± 1.2
7	2.41 ± 0.40	12.8 ± 1.5
8	6.88 ± 0.84	19.7 ± 1.3
9	2.52 ± 0.58	10.9 ± 0.85
10	9.36 ± 0.22	34.4 ± 5.2
11	22.4 ± 3.6	36.1 ± 4.2
12	18.6 ± 5.2	24.4 ± 2.5
13	27.5 ± 10	17.9 ± 2.2
14	> 100	82.8 ± 3.8
15	> 100	76.4 ± 1.5
16	> 100	74.4 ± 4.5
17	> 100	84.7 ± 3.8
DNP	9.84 ± 0.24	12.80 ± 1.36
CCCP	0.65 ± 1.12	10.21 ± 1.18

Altering alkyl chain length of aryl substituted fatty acid protonophores has been an area of interest in recent years. A study on the effect of altering carbon chain length of an aryl urea fatty acid with the same head group as aryl amides **6**, **10** and **14** was published by Murray et al in 2019[135]. The study tested chain lengths between C16-C10 and found that relative JC-1 IC$_{50}$'s ranged between 3.5 ± 1.2 µM to 7.6 ± 1.1 µM for aryl ureas with C16-C12 alkyl chains. However, the two shortest alkyl chain analogues (C11 and C10) were ineffective in depolarising the MIM with relative IC$_{50}$'s of 113 ± 1 µM and 99 ± 1 µM respectively, displaying a lack of activity similar to C8 aryl amides **14-17**[135]. Following this, a similar chain length study published in 2024 by Elmaghrabi et al investigated the *in vitro* effects of altering alkyl chain length of an aryl urea with a 3-chloro-5-trifluoromethyl head group (the same headgroup as aryl amide **1**)[174]. The study tested alkyl chain lengths C16-C11 and found that

C14 and C13 aryl ureas were the most potent in JC-1 assays, with IC_{50}'s of 4.9 ± 0.9 μM and 4.8 ± 0.8 μM respectively[174].

Interestingly, the most potent aryl amides of the C16 and C12 analogues (**6** and **10**) both had the same 3-chloro-4-trifluoromethyl head group. Similar results were seen in **Chapter 2**, where pairing of 3,4- or 3,5-substituted chloro- and trifluoromethyl- substituents led to greater potency in comparison to their other 3,4- or 3,5-substituted counterparts consisting of dichloro or bis-trifluoromethyl substituents. For aryl ureas and their derivatives, 3,4- or 3,5- substituted chloro- and trifluoromethyl- substituents appear to improve potency and promote mitochondrial dysfunction *in vitro.* This is consistent with the findings of Rawling et al in 2020, where it is reported that aryl urea substituted fatty acids with 3-trifluoromethyl-4-chloro and 3-trifluoromethyl-5-chloro head groups were the most potent in JC-1 assays, with relative JC-1 IC_{50}'s of 4.51 ± 1.1 μM and 2.9 ± 1.1 μM respectively[124]. An SAR study conducted by York et al published in 2022 involved adding substituents to a bis-aryl urea known as SR4 also found that analogues with 3,4- and 3,5- substituted chloro and trifluoromethyl groups were more potent compared to other 3,4- or 3,5- substituted counterparts, with JC-1 IC_{50}'s between 0.26 ± 0.1 μM to 1.24 ± 0.3 μM[175]. These particular head groups have also been effective in improving anti-cancer properties of other aryl urea derivatives such as with aryl carbamate fatty acids, bisaryl square amide, amide and diureas and aryl urea CTU[22, 132, 176].

3.5 Effects of Short Chain Aryl Amides on ATP Production

The JC-1 data indicated that generally the C16 aryl amides act as full uncouplers, the C12 aryl amides as mild uncouplers, and the C8 aryl amides were inactive. To further support these findings, the effects of the aryl amides **6-17** on intracellular ATP production in L6 cells was assessed using a Cell-Titer Glo assay (**Figure 22**). L6 cells were treated with each aryl amide at concentrations at least double their relative JC-1 IC_{50} concentration and intracellular ATP levels were monitored over 6 hours. Full uncouplers were expected to lower ATP levels in L6 cells, while mild uncouplers and inactive compounds were expected to have no effect on ATP production.

Similar to the JC-1 data, chain length appeared to greatly affect the extent of which aryl amides affected ATP production. C16 aryl amides **6-9** significantly decreased ATP production with the exception of **8** (**Figure 22** panel **a**). Interestingly, **8** had the depolarised the MIM in JC-1 assays to 19.7 ± 1.3 % of control, the lowest E_{max} in comparison to other C16 aryl amides. In contrast, shorter chain aryl amides **10-17** (C12 and C8) did not significantly affect ATP production (**Figure 22** panels **b** and **c**) with the exception of **13**. Out of the C12 aryl amides, **13** also had the lowest E_{max} in JC-1 assays with 17.9 ± 2.2 %.

It appears as though chain length also plays a significant role in determining mild or full uncoupling. C16 aryl amides **6,7** and **9** and C12 aryl amide **13** decreased $\Delta\Psi_m$ to a greater extent and significantly inhibited the production of ATP, similar to full uncoupling aryl amides **1-3** in **Chapter 2**. C12 aryl amides **10-12** on the other hand along with C16 aryl amide **8** partially depolarised the MIM $\Delta\Psi_m$ and did not affect ATP production significantly, similar to mild uncoupler aryl amides **4** and **5** in **Chapter 2**. Lastly, C8 aryl amides **14-17** were inactive in ATP assays. This finding is consistent with the JC-1 assay data where **14-17** only partially depolarised mitochondria at the highest test concentration of 100 μM.
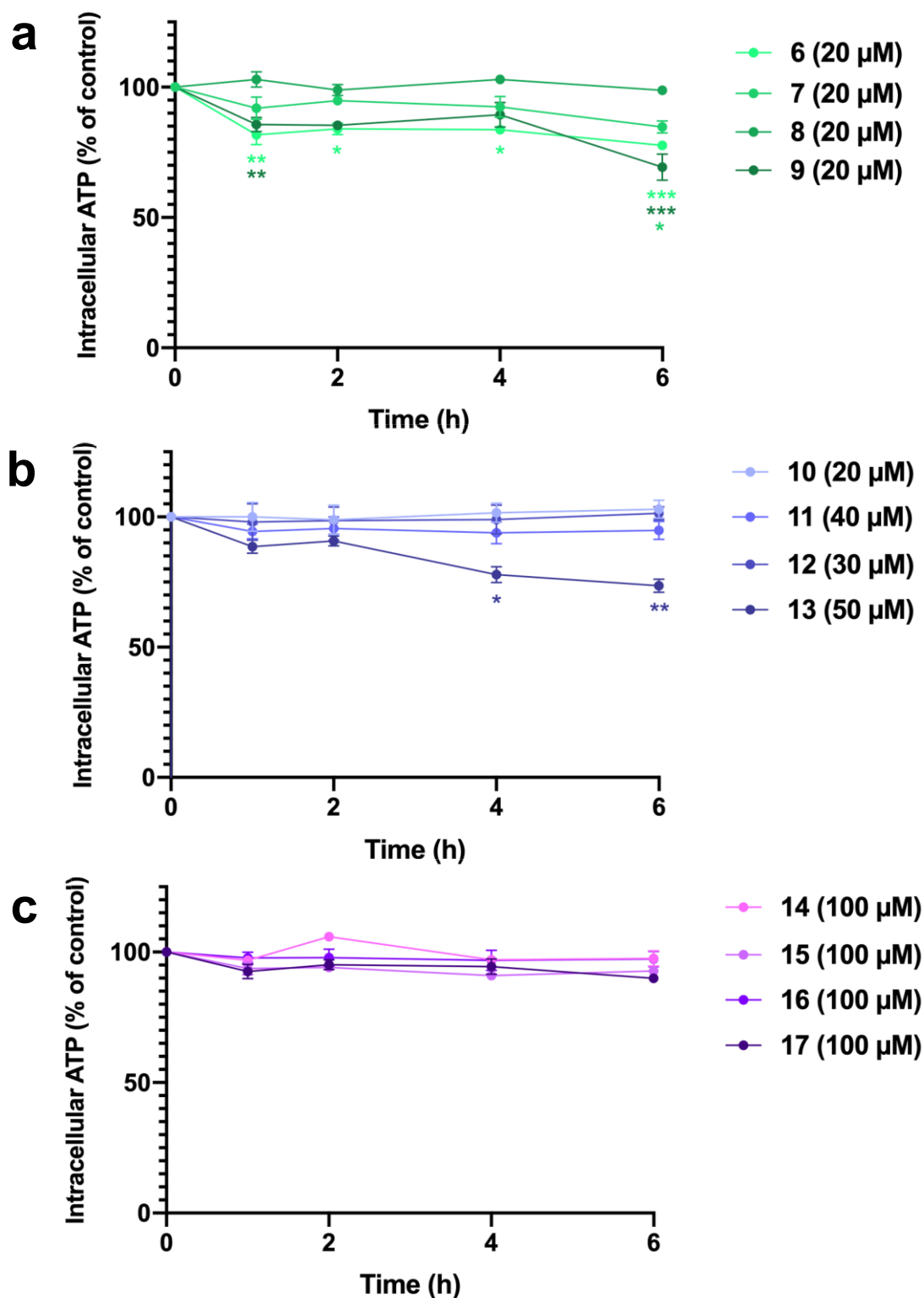
Figure 22: ATP production in L6 cells treated with aryl amides **6-17** at least double their JC-1 IC_{50} concentrations for 6 hours. **a)** ATP production when treated with C16 aryl amides **6-9**. **b)** ATP production when treated with C12 aryl amides **10-13**. **c)** ATP production when treated with C8 aryl amides **14-17**. Data represents the mean ± SEM of 3 independent experiments. Different from DMSO control: (*) $P < 0.05$, (**) $P < 0.01$, (***) $P < 0.001$

3.6   Effects of Short Chain Aryl Amides on Cellular Respiration

Next, seahorse assays were used to further characterise the effects of aryl amides **6-17** on mitochondrial function in L6 cells. Chain shortened aryl amides with the 4-chloro-3-trifluoromethyl substituted aryl rings were selected (**6**, **10** and **14**) as this substitution pattern produced the most potent analogues within each chain length series in JC-1 assays. L6 cells were treated with each aryl amide at concentrations at least double their JC-1 IC_{50} and OCR, ECAR and PER were monitored over three hours. The ECAR measures the rate in which protons are released by cells into the extracellular environment. ECAR is generally considered to be proportional to the rate of glycolysis and is expected to increase when OXPHOS is inhibited[177-178]. However, other sources of acidification within cells and pH changes within the media heavily impact ECAR[179]. Real-time ECAR data can be transformed into PER, which accounts for the buffer capacity of the media and sensor system and volume scaling factor[177-178]. PER is the sum of protons from glycolysis-derived lactate, OXPHOS-derived CO_2 generation and other proton leaking pathways[180].

As shown in **Figure 23** panel **a**, aryl amides **6** and **10** and classical full uncouplers DNP and CCCP increased OCR of L6 cells compared to control. In contrast, the shortest chain analogue **14** did not impact OCR, which was expected due to its inactivity in all other *in vitro* assays. Thus, providing further confirmation that aryl amides **6** and **10** are acting as mitochondrial uncouplers.
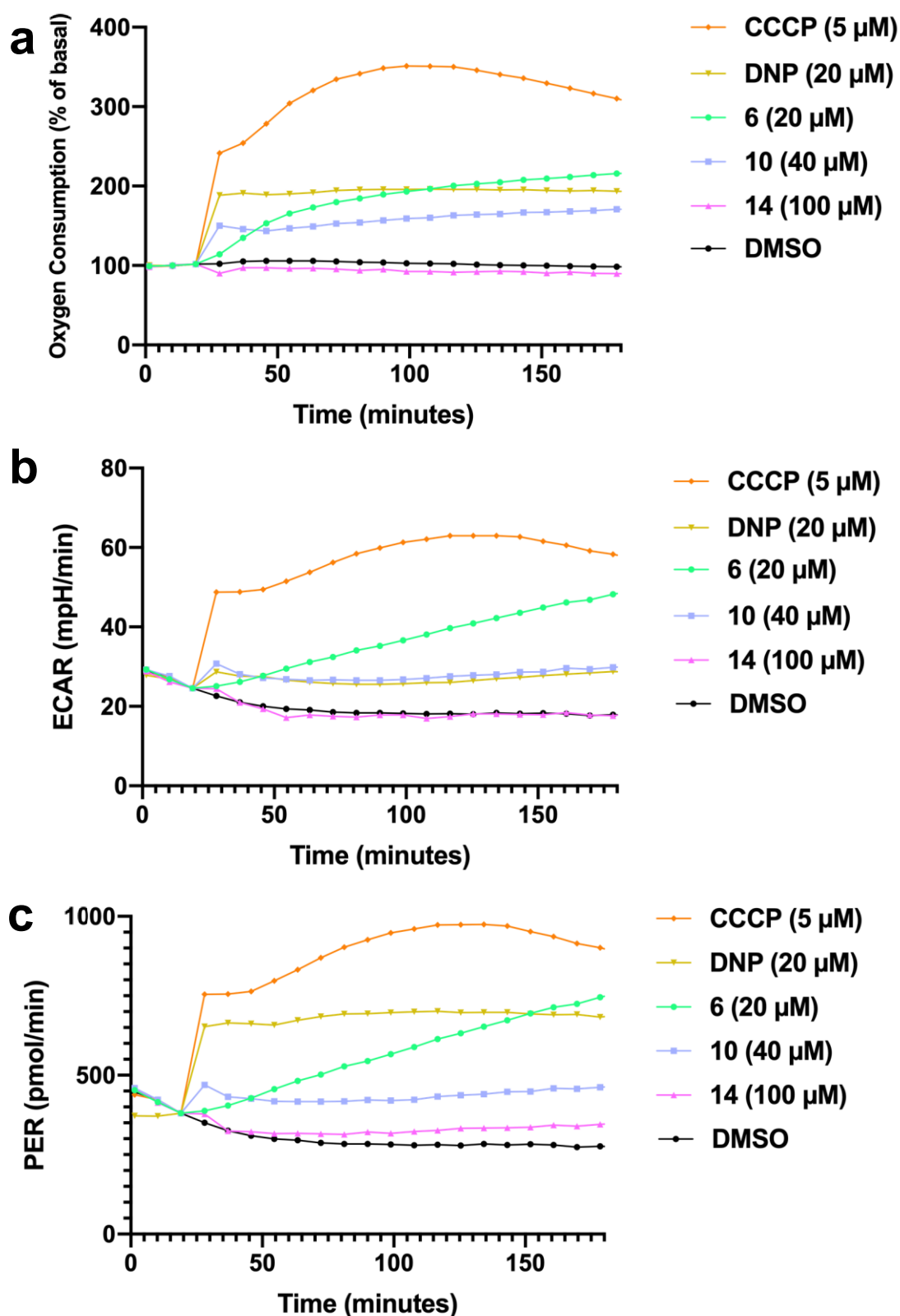
Figure 23: Seahorse assay analysis of mitochondrial function of L6 cells relative to DMSO control when treated with aryl amides **6**, **10** and **14** for 3 hours. **a)** OCR of L6 cells. **b)** ECAR of L6 cells. **c)** PER of L6 cells. Aryl amides were compared against classical full uncouplers CCCP and DNP and a 0.1% DMSO vehicle containing no uncouplers as a control.

The ECAR and PER of L6 cells when treated with aryl amides **6**, **10** and **14** as well as DNP and CCCP were measured (**Figure 23** panels **b** and **c**). DNP and CCCP produced immediate increases in ECAR and PER, while ECAR and PER increased slowly in L6 cells treated with the C16 aryl amide **6**. At the end of the assay, all 3 compounds appeared to reach similar levels, indicating that OXPHOS has been inhibited and to compensate, L6 cells increase glycolytic activity to produce ATP anaerobically. Similar to the OCR data, aryl amide **10** also increased ECAR and PER compared to control whilst **14** had minimal effects on ECAR and PER compared to control since it has been inactive in all *in vitro* assays. Overall, the Seahorse assay data provides confirmation that aryl amides **6** and **10** are acting as mitochondrial uncouplers as they inhibit OXPHOS which in turn caused an increase in OCR, PER and ECAR.

The Seahorse data, in combination with the JC-1 and ATP data, allow for a detailed characterisation of the effects of the aryl amides on mitochondrial function in L6 cells. The C16 aryl amides **6**, **7** and **9**, and the C12 aryl amide **13** all produced similar effects to CCCP, DNP and aryl amides **1-3** in **Chapter 2**. All of these compounds had E_{max} values below 17.9 ± 2.2 % in JC-1 assays and significantly inhibited ATP production in L6 cells, thus acting as full uncouplers. In contrast, C12 aryl amides **10-12** and C16 aryl amide **8** produced results similar to aryl amides **4** and **5** in **Chapter 2**. Each of these compounds had E_{max} values between 19.7 ± 1.3 % and 36.1 ± 4.2 % in JC-1 assays and lacked the ability to inhibit ATP production, thus acting as mild uncouplers. Aryl amides **6** and **10** increased OCR, ECAR and PER in L6 cells, confirming that they are acting as mitochondrial uncouplers and not causing these mitochondrial effects through an alternative mechanism. C8 aryl amides **14-17** appeared to be inactive *in vitro*, as they failed to affect $\Delta\Psi_m$, ATP production or OCR in L6 cells. Thus, confirming that they are not acting as mitochondrial uncouplers and affirms the importance of the lipophilicity of protonophores in order to effectively inhibit OXPHOS.

3.7　Effects of Short Chain Aryl Amides on Cell Viability

Since aryl amides **1-3** were shown to significantly decrease cell viability *in vitro,* the capacity for short chain aryl amides to impact cell viability of L6 rat skeletal muscle cells was assessed using an MTS assay as outlined in **Chapter 2**. Short chain aryl amides had greater solubility in cell culture media in comparison to C18 aryl amides, therefore a broader concentration range (0.1-100 µM) was used.

Despite being tested at concentrations up to 100 µM, shorter chain aryl amides did not significantly decrease cell viability of L6 cells with the exception of **12** which decreased cell viability to 56.3 % at 100 µM (**Figure 24**). Due to all aryl amides **6-17** not decreasing cell viability to below 50%, it can be assumed that the IC_{50} of all short chain aryl amides is greater than 100 µM. Therefore, shorter chain aryl amides do not appear to impact cell viability at high concentrations (100 µM) to the extent that full uncouplers such as aryl amides **1-3** did at 40 µM. However, it is important to note that MDA-MB-231 triple negative breast cancer cells are more susceptible to uncoupling due to its reliance on OXPHOS metabolism[181]. Since the aim of this chapter was to develop a safe drug-like aryl amide, cell viability and ATP production not decreasing for aryl amides **8** and **10-12** is encouraging.
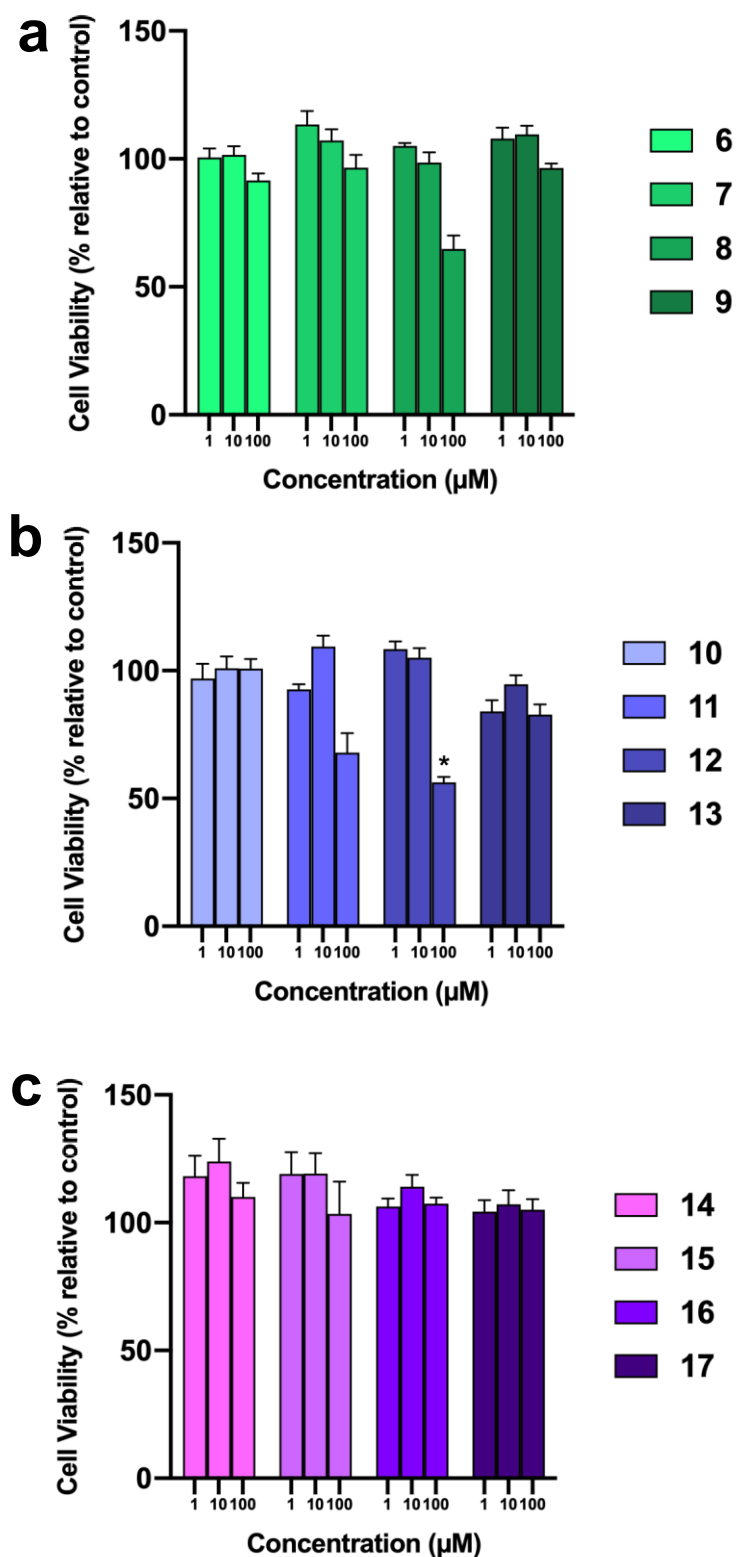
Figure 24: MTS cell viability of L6 rat skeletal muscle cells treated with: **a)** C16 aryl amides **6-9**, **b)** C12 aryl amides **10-13**, **c)** C8 aryl amides **14-17**, at concentrations 1, 10 and 100 µM for 24 hours. Data represents the mean ± SEM of 3 independent experiments. Difference from DMSO control: (*) $P < 0.05$.

In contrast to aryl amides, aryl ureas with chain lengths between C12-C16 were found to induce apoptosis in MDA-MB-231 cells[134-135]. In Murray et al's work in 2019 which involved a chain length study with an aryl urea with the same head group as aryl amides **6**, **10** and **14**, having an alkyl chain greater than C11 decreased cell viability by preventing completion of the cell cycle and impairing mitosis[135]. In Elmagrahbi et al's work in 2024 where a chain length study on an aryl urea with the same head group as aryl amide **1** in **Chapter 2** was conducted, only having an alkyl chain length greater than C12 decreased cell viability in MDA-MB-231 cells[174]. However, it is important to note that both studies involved studying ATP production and conducting annexin V-FTIC/7AAD staining rather than MTS assays to assess cell viability[135, 174]. A possible reason for this difference between aryl ureas and aryl amides could be that MDA-MB-231 cells are more susceptible to uncoupling in comparison to L6 cells[181]. Alternatively, as covered extensively in **Chapter 2**, aryl ureas form parallel hydrogen bonds to carboxylate anions to facilitate transport through the MIM, whereas aryl amides bind via single hydrogen bonds with their NH group, therefore having relatively lower carboxylate affinities which could impact their uncoupling ability.

3.8   Effect of Chain Length on Proton Transport Rate

In **Chapter 2**, it was proposed that the underlying factor that distinguishes full and mild mitochondrial uncouplers is the rate at which they can transport protons across lipid bilayer membranes. Therefore, the proton transport rates of the 4-chloro-3-trifluoromethyl substituted aryl amides **6** (C16), **10** (C12) and **14** (C8) were investigated using the HPTS assay as outlined in **Chapter 2.6**. As chain length appears to impact their activity *in vitro,* where shorter chain length weakens aryl amide's uncoupling ability, we hypothesised this is linked with their rate of proton transport across the membrane based on our findings in **Chapter 2**. The initial proton rate and EC_{50} values are presented in **Table 12**.

Table 12: Summary of HPTS transport data and CLogP of aryl amides **6**, **10** and **14**. CLogP values were calculated using ALOGPS 2.1[156]. HPTS data was collected by Dr Daniel McNaughton.

Uncoupler	Initial Rate (0.5 mol%) (% s^{-1})	EC$_{50}$ (mol%)	CLogP
6	5.30	0.0773 ± 0.011	6.7
10	0.06	1.76 ± 0.25	5.01
14	-	-	3.63

C16 aryl amide **6** had the lowest EC$_{50}$ and fastest proton transport rate of 0.0773 ± 0.011 mol% and 5.30 % s^{-1} of the short chain aryl amide series. C12 aryl amide **10** was a poor proton transporter, with an EC$_{50}$ approximately 100-fold greater than **6** and had a slow initial rate of 0.06 % s^{-1}. Lastly, C8 aryl amide **14** failed to act as a protonophore in HPTS assays, which is consistent with its inactivity *in vitro*.

The *in vitro* and HPTS data infers that as chain length decreases, the rate of proton transport facilitated by aryl amides **6**, **10** and **14** decreases, in turn weakening their uncoupling ability. A potential reason for is due to the decrease in LogP when removing CH$_2$ molecules from the hydrocarbon chain, since lipophilicity and molecular size affect anion transporter activity[134, 182-183]. In previous studies, the activity of aryl ureas were abolished when having polar substituents (even if they were also electron withdrawing) and by decreasing chain length[124, 135]. Therefore, the *in vitro* and HPTS data of the aryl amides **6-17** indicates that chain length is an important determinant of protonophoric and mitochondrial uncoupling activity. This finding is consistent with previous studies of the aryl ureas which found that alkyl chain lengths below C12 diminished their ability to cause mitochondrial dysfunction in cancer cells[135, 174].

3.9   *In Vivo* activity of Aryl Amide 10 in a murine model of obesity

The aim of this chapter was to develop a mild mitochondrial uncoupler based on the aryl amide scaffold with the shortest possible chain length. From the cell-based studies presented in **Chapters 3.4-3.9**, four chain shortened aryl amides were identified as mild uncouplers - the C16 analogue **9** and C12 analogues **10**, **11** and **12**. From these aryl amides, **10** was selected for study in a mouse model of obesity as it has the shortest chain length and greatest potency in JC-1 assays.

To conduct this study, four-week old female wild-type BALB/c mice were fed either a high fat diet (HFD) (n = 8/group) or control chow (CC) for 12 weeks and were weighed weekly. Aryl amide **10** was then administered to the mice by oral gavage daily at 1 mg/kg (low dose) and 10 mg/kg (high dose) and the mice were weighed daily for a period of 3 weeks. The average weight of the mice in each treatment group were then compared to control groups that continued on either HFD or CC without administered doses of aryl amide **10**. Fasting blood glucose and insulin levels were also monitored as readouts of efficacy, similar to other safe uncouplers tested *in vivo* such as BAM15 and SHC517[114, 118]. The results are presented in **Figures 25** and **26**.
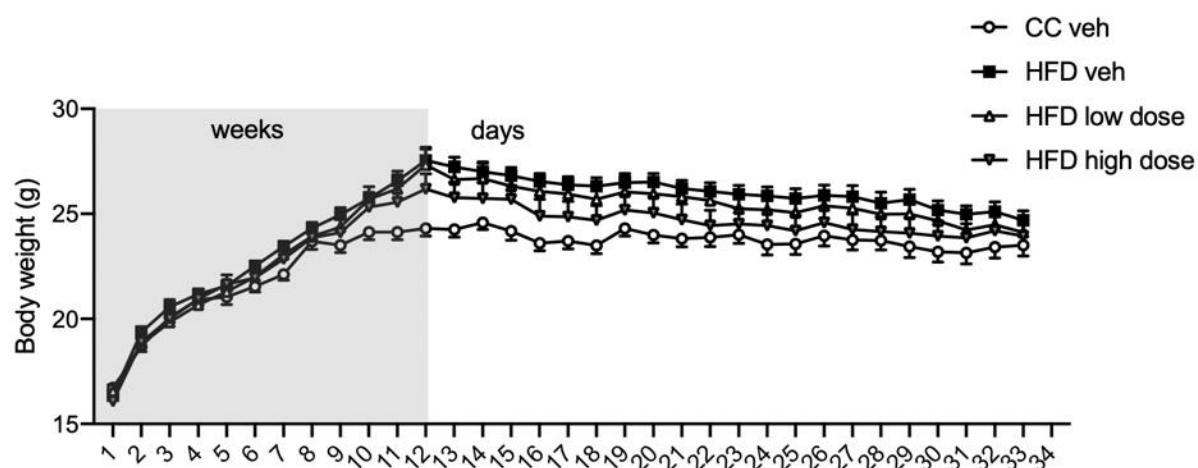
Figure 25: Body weight of female BALB/c mice on CC or HFD. Body weight was measured weekly until aryl amide **10** was administered from week 12 onwards in low and high doses, where body weight was then measured daily. Mice on CC diet and HFD veh were not administered with **10**. Data represents mean ± SEM of 8 mice per group. *In vivo* data was collected by Dr Richard Kim and Dr Chantal Donovan.
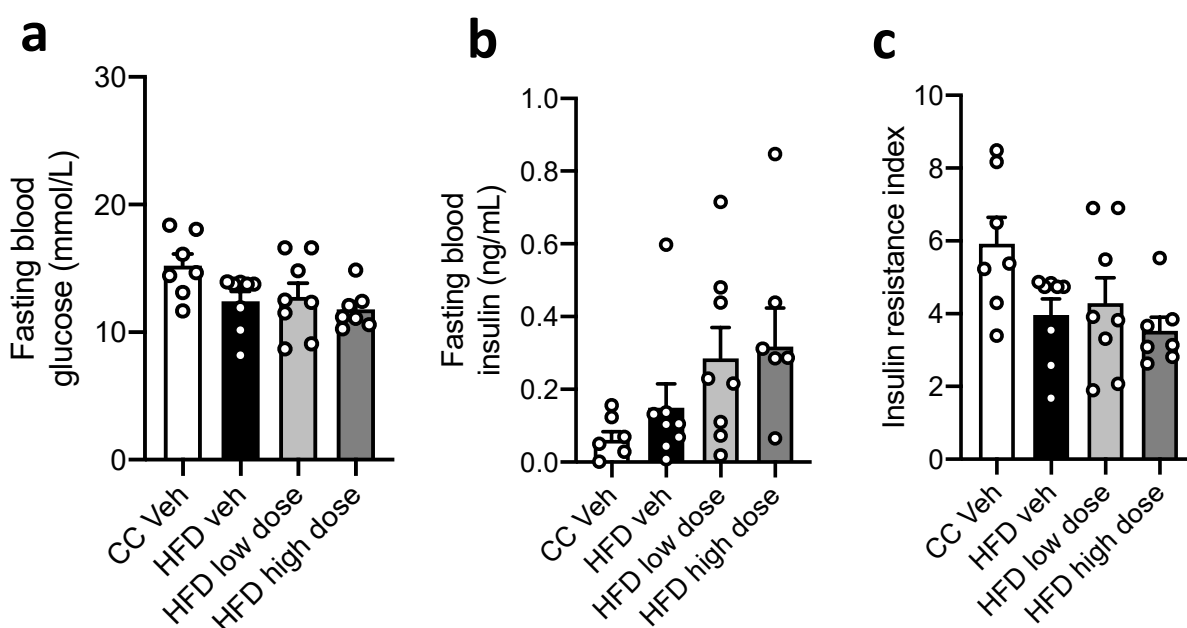
Figure 26: Effects of low and high doses of aryl amide **10** on fasting blood glucose levels (**a**), insulin levels (**b**) and calculated insulin resistance index (**c**) in mice. n=8 animals for all treatment groups, data from one study. *In vivo* data was collected by Dr Richard Kim and Dr Chantal Donovan.

The mice on the HFD appeared to increase in weight over the first 12 weeks, prior to the administration of aryl amide **10**. Upon receiving low and high doses of aryl amide **10**, the weight of on the HFD appeared to plateau and eventually decrease over the span of the next 3 weeks. The weight of the control mice (HFD veh) also followed the same trend and as a result, the weight loss between mice administered with aryl amide **10** at both high and low doses was not significantly different to control mice as per a one-way ANOVA stats test. The mice on a CC diet appeared to increase in weight from weeks 1-10, then plateaued even after being administered with **10**. Aryl amide **10** did not affect fasting blood glucose levels while insulin was increased by both low and high doses, although not significantly as per a one-way ANOVA stats test. In comparison to safe uncouplers in the literature, BAM15, SHC517 and SHD86H5 were found to decrease body fat without affecting activity or food intake and significantly affecting fasting blood and insulin levels[114, 118-119, 184].

The lack of *in vivo* activity of **10** may result from a lack of potency, poor pharmacokinetics or both. Although the alkyl chain length of **10** was reduced to C12, it still is on the cusp of having unfavourable bioavailability relative to Lipinski's rule of five due to its LogP of 5.01 and having 10 rotatable bonds (see **Table 10**)[167-168]. Furthermore, it is well known that fatty acids with a hydrocarbon chain greater than 10 carbons bind to human plasma albumin (HPA) and bovine serum albumin (BSA), which greatly reduces the concentrations of unbound drug in the blood available for target engagement[185-187]. Thus, the pharmacokinetics of **10** needs to be studied further to investigate the lack of anti-obesity effects, such as half-life, bioavailability and whether the uncoupler is being absorbed in the fats before exhibiting its protonophoric effects. Pharmacokinetics has been a challenge for some mitochondrial uncouplers such as BAM15, SHC517 and SHD865 *in vivo* and have limited their potential commercial use[114, 118-119]. Vorinostat, which has a similar structure to aryl amides **14-17**,

exhibited suboptimal pharmacokinetics both such as low bioavailability (43% for humans and 11% in rats) and a short half-life of approximately 2 hours in both human and mice studies[188]. Thus, developing a mild mitochondrial uncoupler for weight loss still remains a challenge for the scientific community.

3.10   Summary and Conclusions

The data presented in this chapter shows that chain length heavily impacts the ability for aryl amides, a new class of fatty acid protonophores, to induce mitochondrial uncoupling and the pharmacokinetics associated with chain length limit their potential use as anti-obesity drugs. When assessing each chain length for their effects on cellular function of L6 rat skeletal muscle cells, their protonophoric and uncoupling abilities differed. Aryl amides **6, 7** and **9** with the longest chain length (C16) in this library along with C12 aryl amide **13** had E_{max} values below 18 %, the lowest of Library 2. These aryl amides were also found to inhibit intracellular ATP of L6 cells, similarly to aryl amides **1**-3, DNP and CCCP, therefore confirming they act as full uncouplers. In contrast, C12 aryl amides **6, 7, 9** and C16 aryl amide **13**, partially depolarised the MIM in JC-1 assays, with E_{max} values between 20 – 40 % and did not decrease ATP production of L6 cells. This is consistent with aryl amides **4** and **5**, thus they are acting as mild uncouplers. Lastly, aryl amides **14-17** with the shortest chain length in this library (C8) were inactive in JC-1 and CellTiter Glo 2.0 assays, thus failing to decrease $\Delta\Psi_m$ and ATP production of L6 cells.

Aryl amides **6**, **10** and **14** were investigated further for their protonophoric actions. In Seahorse assays, **6** and **10** along with DNP and CCCP caused an increase in OCR, ECAR and PER in L6 cells, which is indicative of their ability to act as mitochondrial uncouplers. Consistent with other *in vitro* assays, C8 aryl amide **14** failed to stimulate cellular respiration. The reasoning behind this difference in uncoupling ability can be attributed to the rate of which these aryl amides transport protons across the MIM. C16 Aryl amide **6** transported protons at almost a 100-fold faster rate and 100-fold more potent based on its EC_{50} in comparison to C12 aryl amide **10**. Conducting a HPTS assay showed that shortening the chain length of aryl amides slowed the rate in which they facilitate proton transport. Aryl amide **14** was unable to

facilitate proton transport, proving that excessive shortening of the chain length of aryl amides diminishes uncoupling ability, which was also seen in other fatty acid protonophores[124, 134-135]. Altering chain length to improve activity has been studied for other protonophores such as ionic liquids, where although their mechanism of facilitating proton transport is different to aryl amides, increased alkyl chain length improved mitochondrial disfunction[189]. Based on the *in vitro* and HPTS data presented in this chapter, there is a clear reliance on logP/alkyl chain length of aryl amides in order to maintain uncoupling ability which was also seen in aryl ureas[135, 174].

Aryl amide **10** acted as a mild mitochondrial uncoupler *in vitro* and was the most potent of the C12 aryl amide series in JC-1 assays. Therefore, it was selected for *in vivo* testing in a murine mouse obesity model. Despite having promising effects on cellular function *in vitro* whilst being more "drug-like" than the long chain aryl amides studied in **Chapter 2**, it was unable to exhibit significant anti-obesity effects compared to control mice when 10 mg/kg (high-dose) was administered by oral gavage. Further research on investigating its bioavailability and pharmacokinetics more extensively would assist in determining the feasibility of fatty acid protonophores as weight loss drugs. The work proposed in this chapter provides insight on how alkyl chain length impacts the protonophoric capabilities of aryl amides and using the newfound knowledge of distinguishing between mild and full mitochondrial uncoupling outlined in **Chapter 2**, these short chain aryl amides were able to be characterised as either full or mild uncouplers based on their *in vitro* and proton transport data.

CHAPTER 4

Conclusions and Future Directions

4.1 Conclusions

Mitochondrial uncoupling is a promising therapeutic strategy for clinically important disease such as neurodegenerative diseases, cancer and obesity, however the toxicity of full uncouplers such as DNP limits their safe use in humans. One possible solution to this problem is the development of mild uncouplers that retain the beneficial actions of full uncouplers but lack their toxic side effects, however the development of mild uncouplers has been a significant challenge for decades. This thesis sought to address this by providing a new insight into distinguishing between full and mild uncoupling, with proton transport rate being a key determinant for this in aryl amides, a new class of fatty acid protonophores.

In **Chapter 2**, A library of C18 aryl amides (**1-5**) with varying headgroups of chloro- and/or trifluoromethyl- substituents in 3,5- and 3,4-substitution patterns were prepared. When their impact on mitochondrial function in MDA-MB-231 breast cancer cells was assessed, stark differences in activity were observed depending on the aryl amide's substitution pattern. 3,5-substituted aryl amides **1-3** had similar *in vitro* effects as classical protonophores CCCP and DNP, as they were found to increase OCR, decrease cell viability, depolarise the MIM and inhibit intracellular ATP production of MDA-MB-231 cells, inferring that they are acting as full mitochondrial uncouplers. In contrast, 3,4-substituted aryl amides **4** and **5** only partially depolarised the MIM and increased OCR without decreasing cell viability or intracellular ATP levels, consistent with mild mitochondrial uncoupling. Next the proton transport rates of the protonophores was assessed using the HPTS assay, which revealed that 3,5-substituted aryl amides **1-3** transport protons at a faster rate and reach maximal proton transport at lower concentrations in comparison to 3,4-substituted aryl amides **4** and **5**. ^{1}H NMR titrations showed that compounds **1-3** dimerise more favourably than **4** and **5**, which might explain their superior rates of transport. Computational analysis indicated that 3,5-substituted aryl amides **1-3** have

substituent dipole angles relative to the amide hydrogen bond axis more aligned with the aryl amide NH group, thus improving its ability to act as a hydrogen bond donor. Thus, this chapter explores the distinctions between mild and full uncoupling and presents proton transport rate as a key determinant in uncoupling ability.

Aryl amides **4** and **5** showed promise as mild uncouplers but lack drug-like physiochemical properties due to their high lipophilicity and number of rotatable bonds, which largely arises from their C18 alkyl chain. Therefore, the work in **Chapter 3** aimed to develop a more drug-like aryl amide which acts as a mild mitochondrial uncoupler to be tested in murine mouse obesity models for its ability to induce weight loss. A library of short chain (C16, C12 and C8) aryl amides (**6-17**) with 3,4-substituted chloro- and/or trifluoromethyl- head groups were synthesised and their uncoupling activity were assessed *in vitro* with the same methodology as **Chapter 2**. In contrast to 3,4-substituted aryl amides **4** and **5**, most C16 aryl amides acted as full uncouplers and produced similar effects as compounds **1-3**, DNP and CCCP. Notably, they fully dissipated the MIM proton gradient and as a result significantly inhibited intracellular ATP production in L6 cells. In contrast, most of the C12 aryl amides acted as mild uncouplers as they only partially depolarised the MIM and did not decrease ATP production. C8 aryl amides on the other hand were largely inactive. In HPTS assays, the same pattern in activity was observed where C16 aryl amide **6** had faster proton transport rate and a lower EC_{50} concentration than C12 aryl amide **10**, while C8 aryl amide **14** failed as a proton transporter. From this, aryl amide **10** emerged as the most potent and drug-like mild uncoupler in this library and its ability to induce weight loss was assessed in murine mouse models with HFD-induced obesity. Although mice showed no signs of adverse effects as a result of being administered **10** by oral gavage, this aryl amide failed to induce statistically significant weight loss in comparison to control mice.

This, **Chapter 3** presents the effect of contracting alkyl chain length of aryl amides on their uncoupling ability. Lipophilicity appears to play a key role in the ability for fatty acid protonophores to facilitate proton transport. As the alkyl chain is shortened, their uncoupling activity weakens to the point of inactivity once reaching C8 in length. This has implications on the feasibility of aryl amides as potential weight loss drugs, as they lack the physiochemical properties which promote oral bioavailability at chain lengths that act as uncouplers (C18, C16 and C12). Taken together **Chapter 1** and **2** demonstrate the importance of both proton transport rate and lipophilicity in determining full or mild uncoupling activity in aryl urea fatty acids.

4.2   Future Directions

Further research to substantiate the findings of **Chapter 2** involve investigating the proton transport rates of a wide variety of known full and mild uncouplers. There are various examples of compounds or drugs in the literature which are yet to be characterised as mild or full uncouplers explicitly. BAM15 and its derivatives SHC517, SHD865 and SHM115 have shown potential *in vivo* for their ability to act as "safe" uncouplers and induce weight loss[118-119, 149-150]. There are also various repurposed drugs such as Niclosamide, Nitazoxanide and Oxyclozanide despite their different therapeutic uses have shown to exhibit properties which mimic mitochondrial uncoupling such as decreasing $\Delta\Psi_m$, intracellular ATP or inducing apoptosis in cancer cells[38, 190]. The protonophores mentioned above do not operate with the same flip-flop diffusion mechanism as aryl amides. Therefore, further investigation into whether proton transport rate is also a key factor in a wide variety of mitochondrial uncouplers would be worthwhile. If this theory is upheld by other classes of protonophores, HPTS could be used as a cheap high throughput screening assay to search for new mild uncouplers to be safely used in humans.

Following from the findings in **Chapter 3**, the pharmacokinetics of C12 aryl amide **10** *in vivo* could be explored further including half-life, bioavailability and locations of tissue accumulation. Considering the difficulty of fatty acids reaching their therapeutic target due to binding to HPA and BSA, the feasibility of aryl amides as anti-obesity drugs is still unknown. Fatty acid protonophores are somewhat limited in regard to oral bioavailability due to their high lipophilicity which, as shown in **Chapter 3**, are necessary for their ability to act as uncouplers. If aryl amide **10** truly has a poor pharmacokinetic profile, HPTS assays could be used to screen for new mild uncouplers which have more drug-like physiochemical properties.

CHAPTER 5

Experimental

5.1 Materials and General Procedures

All chemical reagents, analytical grade solvents and aryl amide intermediates were purchased from Sigma Aldrich/Merck (Castle Hill, NSW, Australia) or Fluorochem (Derbyshire, United Kingdom). The purity of all tested compounds was confirmed to be $\geq 95\%$ by absolute quantitative ^{1}H NMR (qNMR) spectroscopy. Reactions were monitored by thin-layer chromatography (TLC) using silica gel 60 F_{254} plates. TLC plates were visualised with UV light and potassium permanganate TLC stain. ^{1}H and ^{13}C NMR spectra were acquired using an Agilent and/or Bruker 400/500 MHz spectrometer (500.13 MHz for ^{1}H and 125.76 MHz for ^{13}C) in deuterated chloroform ($CDCl_3$) at 298 K unless otherwise specified. Melting point determination was preformed using Stuart automatic melting point. High-resolution mass spectroscopy (HRMS) was performed on an Agilent 6510 Accurate-Mass Q-TOF Mass Spectrometer equipped with an ESI source.

5.2 Synthesis

5.2.1 General Procedure "a" for Methyl Esterification

12-hydroxydodecanoic acid (**19**) (9.25 mmol, 2.00 g), potassium carbonate (27.74 mmol, 3.83 g) and iodomethane (46.23 mmol, 2.88 mL) was dissolved in acetone (160 mL) and the mixture was refluxed for 5 hours at 80 °C. Solvent was evaporated under reduced pressure and the residue was re-dissolved in 60 mL H_2O. The solution was acidified with 1M HCl and the aqueous layer was extracted three times with DCM (100 mL). The combined organic layers were washed with brine (200 mL) and dried over a minimum amount of Mg_2SO_4. Solvent was removed under reduced pressure, leading to the isolation of methyl 12-hydroxydodecanoate (**20**) (1.91 g, 85%) in the form of a yellow oil which crystallises at room temperature.

20 – Methyl-12-hydroxydodecanoate:

Synthesised with general procedure a. Yellow solid (85%). ^{1}H NMR (500 MHz, CDCl3): δ 3.66 (s, 3H), 3.65-3.62 (t, *J* = 14 Hz, 2H), 2.31-2.28 (t, *J* = 14 Hz, 2H), 1.64-1.59 (m, *J* = 14 Hz, 2H), 1.58-1.53 (m, *J* = 14 Hz, 2H), 1.35-1.25 (m, 14H). ^{13}C NMR (125 MHz, CDCl3): δ 174.4, 77.3-76.8, 63.1, 51.4, 34.1, 32.8, 29.5-29.1, 25.7, 24.9.
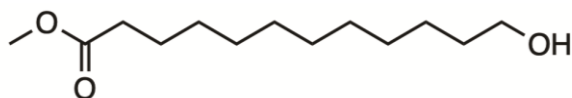
5.2.2 General Procedure "b" for Jones Oxidation

Methyl 12-hydroxydodecanoate (**20**) (7.16 mmol, 1.75 g) was dissolved in acetone (175 mL) and jones reagent (4.2 mL) was added while the solution stirred in an ice bath. The reaction mixture was left to stir for 4.5 hours while the ice melted and finished at room temperature. Isopropanol (8.75 mL) was added to the mixture which was then filtered on celite and washed with acetone. The filtrate was evaporated under reduced pressure and the residue was re-dissolved in EtOAc (150 mL). The organic layer was washed twice with brine (150 mL) and dried over a minimum amount of Mg$_2$SO$_4$. Solvent was removed under reduced pressure, leading to the isolation of 12-Methoxy-12-oxododecanoic acid (**22**) (1.813 g, 98%) in the form of a yellow oil which crystallises at room temperature.

22 – 12-Methoxy-12-oxododecanoic acid

Synthesised with general procedure b. Yellow solid (98%). ^{1}H NMR (500 MHz, CDCl3): δ 3.66 (s, 3H), 2.35-2.32 (t, *J* = 15 Hz, 2H), 2.31-2.28 (t, *J* = 15 Hz, 2H), 1.65-1.62 (m, *J* = 15 Hz, 2H), 1.61-1.58 (m, *J* = 15 Hz, 2H), 1.31-1.27 (m, 12H). ^{13}C NMR (125 MHz, CDCl3): δ 179.4, 174.4, 77.3-76.8, 51.5, 34.1-33.9, 29.3-29.0, 24.9, 24.7.
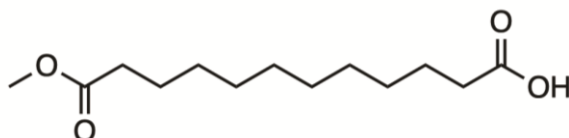
5.2.3 General Procedure "i" for COMU Coupling

While under the constant flow of nitrogen gas, either 16-Methoxy-16-hexadecanoic acid (**20**), 12-Methoxy-12-oxododecanoic acid (**21**), 8-Methoxy-8-octanoic acid (**22**) or 18-tert-butyl ester-18-octodecanoic acid (**23**) (0.77 mmol, 200 mg), COMU (0.77 mmol, 332 mg) and Et$_3$N (1.54 mmol) were dissolved in anhydrous DMF (6 mL) and stirred for 5 minutes at room temperature. The appropriately substituted aniline (0.77 mmol) was added, and the reaction mixture was stirred at room temperature for 3 hrs. The reaction mixture was diluted with EtOAc (50 mL), and the organic layer was washed with 1 M HCl twice (25 mL), saturated NaHCO$_3$ twice (25 mL) and brine twice (10 mL). The organic layer was dried over Mg$_2$SO$_4$, and EtOAc was removed under reduced pressure. The crude products were purified using stepwise gradient elution on silica gel with DCM/EtOAc (100:0 to 98:2).

1a – tert-butyl 18-((3-chloro-5-(trifluoromethyl)phenyl)amino)-18-oxooctadecanoate

Synthesised with general procedure i. White solid (64%). ^{1}H NMR (400 MHz, CdCl3): δ 7.90 (s, 1H), 7.67 (s, 1H), 7.39 (s, 1H), 7.35 (s, 1H), 2.41-2.38 (t, J = 7.4 Hz, 2H), 2.24-2.20 (t, J = 7.4 Hz, 2H), 1.78-1.71 (m, 2H), 1.62-1.58 (m, 2H), 1.47 (s, 9H), 1.39-1.27 (m, 24H). ^{13}C NMR (100 MHz, CdCl3): δ 173.5, 171.6, 139.6, 135.5, 132.7, 132.4, 122.6 (q, J = 273 Hz), 120.8, 114.4, 80.0, 77.3-76.7, 37.7, 35.7, 29.5-29.1, 28.1, 25.3, 25.2.
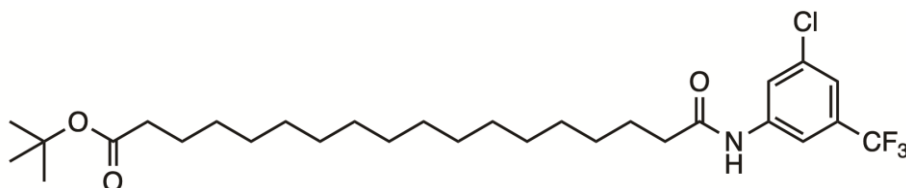
2a – tert-butyl 18-((3,5-bis(trifluoromethyl)phenyl)amino)-18-oxooctadecanoate

Synthesised with general procedure i. White solid (56%). ^{1}H NMR (400 MHz, CdCl₃): δ 8.05 (s, 2H), 7.59 (s, 1H), 7.55 (s, 1H), 2.42-2.38 (t, J = 7.4 Hz, 2H), 2.22-2.17 (t, J = 7.5 Hz, 2H), 1.77-1.70 (m, 2H), 1.57-1.53 (m, 2H), 1.44 (s, 9H), 1.38-1.25 (m, 25H). ^{13}C NMR (100 MHz, CdCl₃): δ 173.6, 171.8, 139.4, 132.5, 124.6 (q, J = 273 Hz), 119.3, 117.3, 77.3-76.7, 37.7, 35.7, 29.5-29.1, 25.3, 25.2.

3a – tert-butyl 18-((3,5-dichlorophenyl)amino)-18-oxooctadecanoate

General procedure i. White solid (42%). ^{1}H NMR (500 MHz, CDCl$_3$): δ 7.50 (s, 2H), 7.27 (s, 1H), 7.08 (s, 1H), 2.36-2.33 (t, J = 15 Hz, 2H), 2.21-2.18 (t, J = 15 Hz, 2H), 1.73-1.67 (m, J = 15 Hz, 2H), 1.58-1.55 (m, J = 15 Hz, 2H), 1.44 (s, 9H), 1.36-1.25 (m, 25H). ^{13}C NMR (125 MHz, CDCl$_3$): δ 173.5, 171.5, 139.7, 135.2, 124, 117.8, 80, 77.3-76.8, 37.7, 35.7, 29.6-29.1, 28.1, 25.4, 25.1.
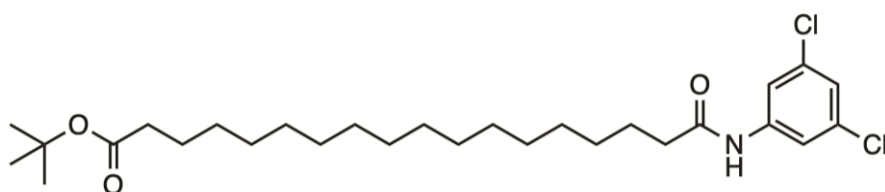
4a – tert-butyl 18-((3-chloro-4-(trifluoromethyl)phenyl)amino)-18-oxooctadecanoate

Synthesised with general procedure i. White solid (53%). ^{1}H NMR (500 MHz, DMSO-d_6): δ 7.818 (s, 1H), 7.61-7.60 (d, J = 9.0 Hz, 2H), 7.49-7.48 (d, J = 8.0 Hz, 2H), 7.35 (s, 1H), 2.39-2.36 (t, J = 7.5 Hz, 2H), 2.21-2.19 (t, J = 6.5 Hz, 2H), 1.75-1.69 (m, 2H), 1.58-1.54 (m, 2H), 1.44 (s, 9H), 1.37-1.25 (m, 25H). ^{13}C NMR (125 MHz, CDCl$_3$): δ 173.5, 171.6, 141.8, 133.1, 128.2, 123.9 (q, J = 273 Hz), 121.5, 116.7, 80, 37.8, 35.7, 29.6-29.1, 28.1, 25.3, 25.1.
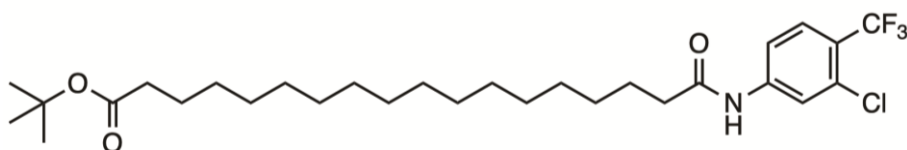
5a – *tert-butyl 18-((3,4-dichlorophenyl)amino)-18-oxooctadecanoate*

Synthesised with general procedure i. White solid (41%). ^{1}H NMR (500 MHz, CDCl$_3$): δ 7.77 (s, 1H), 7.37-7.34 (m, 2H), 7.22 (s, 1H), 2.36-2.33 (t, *J* = 15 Hz, 2H), 2.21-2.18 (t, *J* = 15 Hz, 2H), 1.72-1.68 (m, *J* = 15 Hz, 2H), 1.59-1.56 (m, *J* = 15 Hz, 2H), 1.44 (s, 9H), 1.36-1.25 (m, 25H). ^{13}C NMR (125 MHz, CDCl$_3$): δ 173.4, 171.4, 138.4, 132.8, 130.5, 121.4, 118.8, 79.9, 77.3-76.8, 37.7, 35.7, 29.6-29.1, 28.1, 25.4, 25.1.

6a – *Tert-butyl 16-((4-chloro-3-(trifluoromethyl)phenyl)amino)-16-oxohexadecanoate:*

Synthesised with general procedure i. White solid (58%). ^{1}H NMR (500 MHz, CDCl$_3$): δ 7.827 (s, 1H), 7.77-7.76 (d, *J* = 5 Hz, 1H), 7.47-7.45 (d, *J* = 10 Hz, 1H), 7.32 (s, 2H), 2.41-2.37 (t, *J* = 20 Hz, 2H), 2.24-2.20 (t, *J* = 20 Hz, 2H), 1.78-1.70 (m, 2H), 1.61-1.58 (m, 2H), 1.46 (s, 9H), 1.46-1.39 (m, 20H). ^{13}C NMR (125 MHz, CDCl$_3$): δ 173.5, 171.6, 136.8, 132, 123.6 (q, *J* = 273 Hz), 37.7, 35.7, 29.5-29.1, 28.1, 25.4, 25.1.

7a – *Tert-butyl 16-((3-chloro-4-(trifluoromethyl)phenyl)amino)-16-oxohexadecanoate:*

Synthesised with general procedure i. White solid (52%). ^{1}H NMR (500 MHz, CDCl$_3$): δ 7.81 (s, 1H), 7.62-7.60 (d, *J* = 10 Hz, 1H), 7.50-7.47 (d, *J* = 15 Hz, 1H), 7.32 (s, 1H), 2.40-2.36 (t, *J* = 20 Hz, 1H), 2.22-2.18 (t, *J* = 20 Hz, 1H), 1.76-1.68 (m, 2H), 1.60-1.54 (m, 2H), 1.44 (s, 9H), 1.37-1.25 (m, 20H). ^{13}C NMR (125 MHz, CDCl$_3$): δ 173.5, 171.7, 141.8, 133.1, 128.3 (q, *J* = 273 Hz), 121.6, 116.7, 80, 37.8, 35.7, 29.5-28.1, 25.3, 25.1.
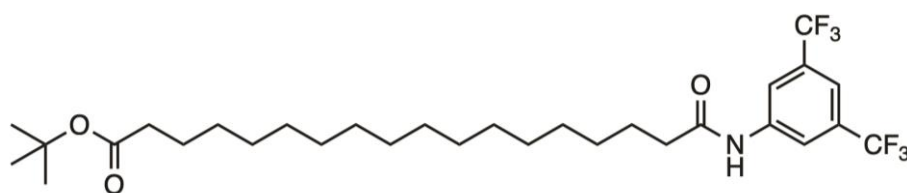

8a – *Tert-butyl 16-((3,4-bis(trifluoromethyl)phenyl)amino)-16-oxohexadecanoate:*

Synthesised with general procedure i. White solid (41%). ^{1}H NMR (500 MHz, CDCl$_3$): δ 8.02-8.00 (d, *J* = 10 Hz, 1H), 7.96 (s, 1H), 7.82-7.8 (d, *J* = 10 Hz, 1H), 7.28 (s, 1H), 2.45-2.41 (t, *J* = 20 Hz, 2H), 2.24-2.21 (t, *J* = 15 Hz, 2H), 1.78-1.74 (m, *J* = 20 Hz, 2H), 1.62-1.58 (m, *J* = 20 Hz, 2H), 1.47 (s, 9H), 1.31-1.26 (m, 20H). ^{13}C NMR (125 MHz, CDCl$_3$): δ 173.7, 172, 139.8, 126, 124.5 (q, *J* = 273 Hz), 122.7, 121.7, 120.7, 114.5, 80.1, 37.7, 35.7, 29.7-29.1, 28.1, 25.4, 25.1.

9a – *Tert-butyl 16-((3,4-dichlorophenyl)amino)-16-oxohexadecanoate*

Synthesised with general procedure i. White solid (48%). ^{1}H NMR (500 MHz, CDCl$_3$): δ 7.79 (s, 1H), 7.37 (s, 2H), 7.22 (s, 1H), 2.39-2.35 (t, *J* = 20 Hz, 2H), 2.24-2.20 (t, *J* = 20 Hz, 2H), 1.77-1.70 (m, *J* = 35 Hz, 2H), 1.62-1.55 (m, *J* = 35 Hz, 2H), 1.46 (s, 9H), 1.38-1.27 (m, 20H). ^{13}C NMR (125 MHz, CDCl$_3$): δ 173.5, 171.5, 137.4, 132.8, 130.5, 121.4, 118.9, 80, 37.7, 35.7, 29.5-29.1, 28.1, 25.4, 25.1.

10a – *Methyl 12-((4-chloro-3-(trifluoromethyl)phenyl)amino)-12-oxododecanoate:*

Synthesised with general procedure i. White solid (37%). ^{1}H NMR (500 MHz, CDCl$_3$): δ 7.834 (s, 1H), 7.77-7.75 (d, *J* = 17 Hz, 1H), 7.44 (s, 1H), 7.42 (s, 1H), 3.66 (s, 1H), 2.38-2.32 (t, *J* = 15 Hz, 2H), 2.32-2.29 (t, *J* = 15 Hz, 2H), 1.74-1.69 (m, *J* = 15 Hz, 2H), 1.62-1.58 (m, *J* = 14 Hz, 2H), 1.37-1.28 (m, 12H). ^{13}C NMR (125 MHz, CDCl$_3$): δ 174.5, 171.7, 136.8, 132, 123.6 (q, *J* = 273 Hz), 121.5, 118.6-118.6, 77.3-76.8, 51.5, 37.6, 34, 29.2-29, 25.3, 24.9.
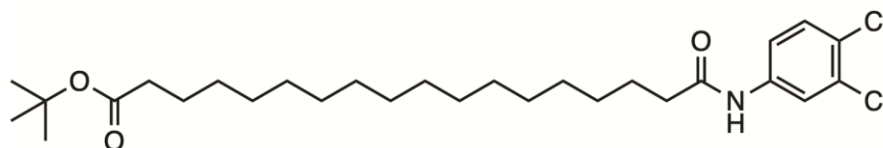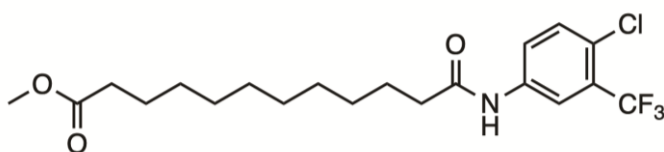
11a – *Methyl 12-((3-chloro-4-(trifluoromethyl)phenyl)amino)-12-oxododecanoate:*

Synthesised with general procedure i. White solid (55%). ^{1}H NMR (500 MHz DMSO-d_6): δ 7.90 (s, 1H), 7.67 (s, 1H), 7.41 (s, 1H), 7.35 (s, 1H), 2.41-2.38 (t, J = 15 Hz, 2H), 2.24-2.21 (t, J = 15 Hz, 2H), 1.78-1.71 (m, J = 35 Hz, 2H), 1.62-1.58 (m, J = 20 Hz, 2H), 1.47 (s, 9H), 1.39-1.28 (m, 12H). ^{13}C NMR (125 MHz, CDCl$_3$): δ 174.5, 171.7, 141.8, 133.1, 128.3-128.2 (q, J = 273 Hz), 121.6, 121.4, 116.8, 51.5, 37.8, 34.1, 29.2-29, 25.3, 24.9.
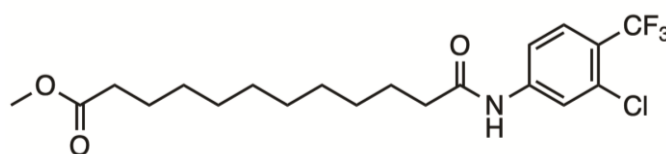
12a – *Methyl 12-((3,4-bis(trifluoromethyl)phenyl)amino)-12-oxododecanoate:*

Synthesised with general procedure i. White solid (49%). ^{1}H NMR (500 MHz, CDCl$_3$): δ 8.01-7.99 (d, J = 10 Hz, 1H), 7.96 (s, 1H), 7.83-7.81 (d, J = 10 Hz, 1H), 7.46 (s, 1H), 2.45-2.41 (t, J = 20 Hz, 2H), 2.35-2.31 (t, J = 20 Hz, 2H), 1.80-1.74 (m, J = 30 Hz, 2H), 1.66-1.57 (t, J = 35 Hz, 2H), 1.57 (s, 9H), 1.40-1.31 (m, 12H). ^{13}C NMR (125 MHz, CDCl$_3$): δ 174.5, 171.8, 141.3, 129.3-129.2 (q, J = 273 Hz), 121.5, 118.3-118.2, 51.5, 37.7, 34.1, 29.2-29, 25.2, 24.9.
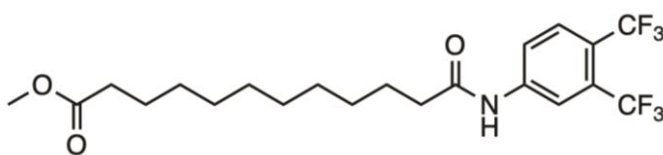
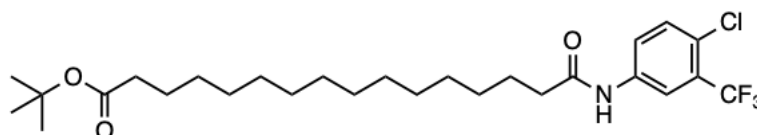**13a** – *Methyl 12-((3,4-dichlorophenyl)amino)-12-oxododecanoate:*

Synthesised with general procedure i. White solid (40%). ^{1}H NMR (500 MHz, CDCl$_3$): δ 7.77 (s, 1H), 7.35 (s, 1H), 7.34 (s, 1H), 7.25 (s, 1H), 3.67 (s, 3H), 2.36-2.33 (t, J = 15 Hz, 2H), 2.32-2.29 (t, J = 15 Hz, 2H), 1.72-1.69 (m, J = 15 Hz, 2H), 1.63-1.60 (t, J = 15 Hz, 2H), 1.36-1.28 (m, 12H). ^{13}C NMR (125 MHz, CDCl$_3$): δ 174.5, 171.6, 136.8, 131.9, 123.6, 121.4, 118.6-118.6, 77.3- 76.8, 51.5, 37.6, 34.1, 29.2-29, 25.3, 24.9
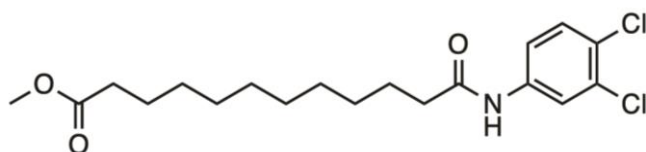
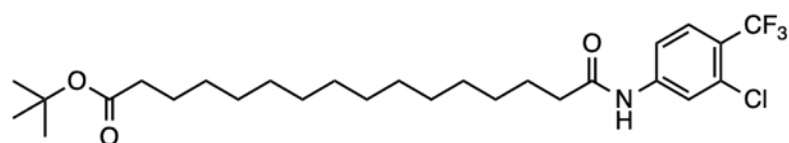**14a** – *Methyl 8-((4-chloro-3-(trifluoromethyl)phenyl)amino)-8-oxooctanoate:*

Synthesised with general procedure i. White solid (21%). ^{1}H NMR (500 MHz, CDCl$_3$): δ 7.86 (s, 1H), 7.77-7.75 (d, J = 11 Hz, 1H), 7.47 (s, 1H), 7.44-7.42 (d, J = 10.5 Hz, 1H), 3.67 (s, 3H), 2.38-2.34 (t, J = 9.5, 2H), 2.34-2.30 (t, J = 9.5 Hz, 2H), 1.76-1.72 (m, 2H), 1.66-1.62 (m, 2H), 1.42-1.39 (m, 4H). ^{13}C NMR (125 MHz, CDCl$_3$): δ 174.4, 171.5, 136.8, 132, 123.6 (q, J = 273 Hz), 121.2, 118.6, 77.3-76.7, 51.6, 37.3, 33.9, 28.5-28.5, 25-24.5.
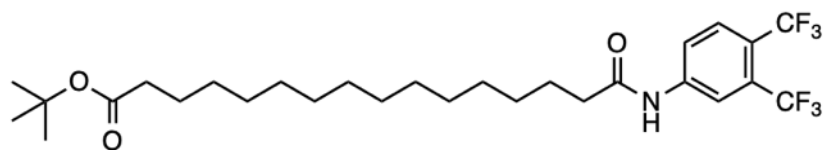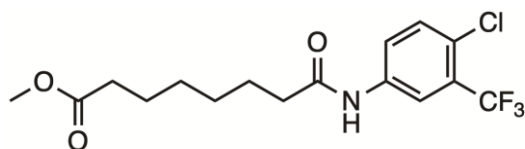
15a – *Methyl 8-((3-chloro-4-(trifluoromethyl)phenyl)amino)-8-oxooctanoate:*

Synthesised with general procedure i. White solid (53%). ^{1}H NMR (500 MHz, CDCl$_3$): δ

7.84 (s, 1H), 7.64-7.62 (d, J = 10 Hz, 1H), 7.59 (s, 1H), 7.53-7.51 (d, J = 10 Hz, 1H), 2.42-

2.33 (m, 4H), 1.78-1.74 (m, 2H), 1.68-1.64 (m, 2H), 1.41-1.39 (m, 4H). ^{13}C NMR (125 MHz,

CDCl$_3$): δ 174.4, 171.7, 141.9, 133, 128.3-128.2, 124.2, 123.7-123.3 (q, J = 273 Hz), 121.6,
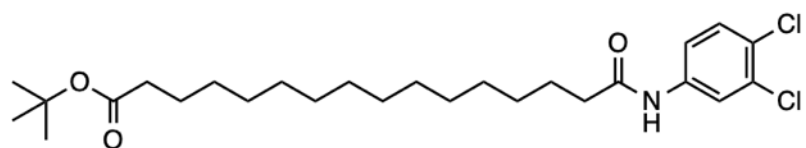
116.8, 51.6, 37.4, 33.9, 28.5, 25, 24.5.
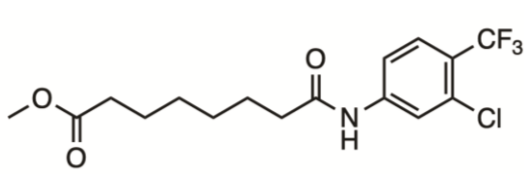
16a – *Methyl 8-((3,4-bis(trifluoromethyl)phenyl)amino)-8-oxooctanoate:*

Synthesised with general procedure i. White solid (39%). ^{1}H NMR (500 MHz, CDCl$_3$): δ 8.03-

8.01 (d, J = 10 Hz, 1H), 7.97 (s, 1H), 7.82-7.80 (d, J = 10 Hz, 1H), 7.75 (s, 1H), 2.45-2.41 (t,

J = 20 Hz, 2H), 2.37-2.34 (t, J = 15 Hz, 2H), 1.80-1.76 (m, 2H), 1.68-1.65 (m, 2H), 1.44-1.40

(m, 4H). ^{13}C NMR (125 MHz, CDCl$_3$): δ 174.5, 174.9, 141.4, 129.2, 128.9, 124.1-123.9 (q, J

= 273 Hz), 121.6, 118.3, 51.6, 37.4, 33.8, 28.4, 24.9, 24.4
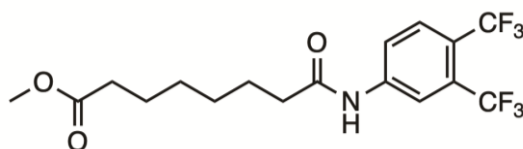
17a – *Methyl 8-((3,4-dichlorophenyl)amino)-8-oxooctanoate:*

Synthesised with general procedure i. White solid (37%). ^{1}H NMR (500 MHz, CDCl$_3$): δ 7.78 (s, 1H), 7.35 (m, 2H), 7.26 (s, 1H), 3.67 (s, 3H), 2.36-2.33 (t, J = 9 Hz, 2H), 2.32-2.28 (t, J = 9 Hz, 2H), 1.74-1.71 (m, 2H), 1.63-1.61 (m, 2H), 1.39-1.34 (m, 4H). ^{13}C NMR (125 MHz, CDCl$_3$): 174.3, 171.4, 137.5, 132.8, 130.5, 127.2, 121.4, 118.9, 77.3-76.7, 51.6, 37.4, 34, 29.1-28.6, 25.1-24.6.
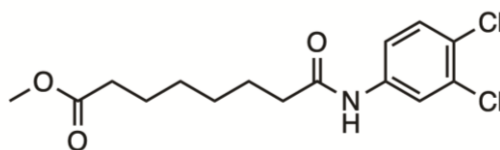
5.2.4 General Procedure "ii" for tert-Butyl Ester Hydrolysis

To a solution of aryl amide esters **1a-5a** (0.20 mmol) in dry DCM (4 mL), TFA (3 mL) was added dropwise, and the reaction mixture was stirred at room temperature for 3 hours. The resulting solution was diluted with 20 mL EtOAc, and the organic layer was washed with 0.5 M NaOH (25 mL), H$_2$O (25 mL) and 1% HCl (25 mL). The organic layer was dried with Mg$_2$SO$_4$, and the solvent was removed under reduced pressure to isolate the aryl-amides **1-5** as white solids.

1 – 18-((3-chloro-5-(trifluoromethyl)phenyl)amino)-18-oxooctadecanoic acid:

Synthesised with general procedure ii. White solid (95%). M.P. = 124-126 ˚C. ^{1}H NMR (500 MHz, DMSO-d_6): δ 10.46 (s, 1H), 7.99-7.95 (d, J = 22 Hz, 2H), 7.49 (s, 1H), 2.35-2.32 (t, J = 15 Hz, 2H), 2.18-2.15 (t, J = 15 Hz, 2H), 1.27-1.20 (m, 24H). ^{13}C NMR (100 MHz, acetone-d_6): δ 173.73, 168.63, 140.48, 134.20, 133.09, 131.58, 124.58, 123.23, 41.84, 39.11, 33.29, 29.45-28.48, 26.68, 24.77. HRMS (ESI) *m/z* [M]+ calculated for $C_{25}H_{37}ClF_3NO_3$ = 492.0144, found 492.0148. qNMR purity = 96.4 %
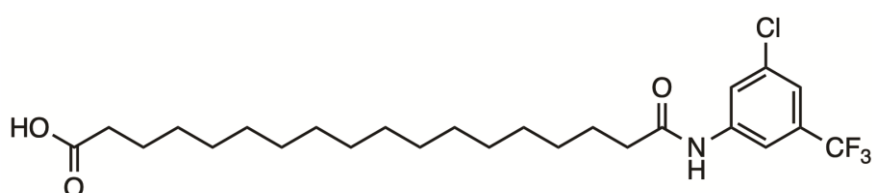
2 – 18-((3,5-bis(trifluoromethyl)phenyl)amino)-18-oxooctadecanoic acid:

Synthesised with general procedure ii. White solid (92%). M.P. = 102-104 ˚C. ^{1}H NMR (500 MHz, DMSO-d_6): δ 11.93 (s, 1H), 10.52 (s, 1H), 8.26 (s, 2H), 7.72 (s, 1H), 2.36-2.33 (t, J = 15 Hz, 2H), 2.18-2.15 (t, J = 15 Hz, 2H), 1.61-1.58 (t, J = 14 Hz, 2H), 1.48-1.45 (t, J = 14 Hz, 2H), 1.27-1.21 (m, 25H). ^{13}C NMR (125 MHz, DMSO-d_6): δ 172.87, 141.55, 131.30, 131.03, 124.78, 122.59, 119.00, 40.47-39.47, 36.89, 34.14, 29.47-28.94, 25.17, 24.95. HRMS (ESI) *m/z* [M]+ calculated for $C_{26}H_{37}F_6NO_3$ = 525.5673, found 525.5675. qNMR purity = 98.6 %
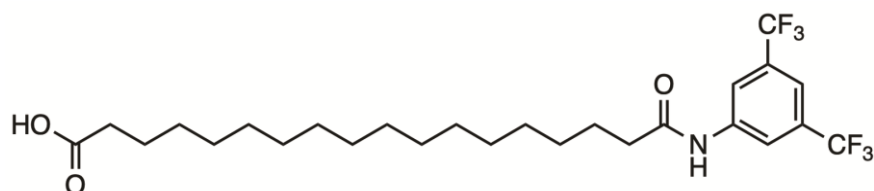
3 – 18-((3,5-dichlorophenyl)amino)-18-oxooctadecanoic acid:

Synthesised general procedure ii. White solid (88%). M.P. = 120-124 ˚C. ^{1}H NMR (500 MHz, DMSO-d_6): δ 11.93 (s, 1H), 10.19 (s, 1H), 7.65 (s, 2H), 7.23 (s, 1H), 2.31-2.28 (t, J = 15 Hz, 2H), 2.18-2.15 (t, J = 15 Hz, 2H), 1.58-1.55 (t, J = 14 Hz, 2H), 1.48-1.45 (t, J = 14 Hz, 2H), 1.26-1.22 (m, 25H). ^{13}C NMR (125 MHz, DMSO-d_6): δ 172.48, 142.03, 134.47, 122.59, 117.48, 109.98, 40.47-40.39.47, 36.89, 29.48-28.96, 25.26, 25.00. HRMS (ESI) *m/z* [M]+ calculated for $C_{24}H_{37}Cl_2NO_3$ = 458.4615, found 458.4611. qNMR purity = 98.5 %

4 – 18-((3-chloro-4-(trifluoromethyl)phenyl)amino)-18-oxooctadecanoic acid

Synthesising general procedure ii. White solid (93%). M.P. = 122-125 ˚C. ^{1}H NMR (400 MHz, CdCl$_3$): δ 10.40 (s, 1H), 8.03 (s, 1H), 7.80-7.77 (d, J = 8.8 Hz, 2H), 7.65-7.63 (d, J = 9.8 Hz, 2H), 2.36-2.33 (d, J = 14.8 Hz, 2H), 1.60-1.57 (m, 2H), 1.49-1.46 (m, 2H), 1.23 (m, 25H). ^{13}C NMR (125 MHz, DMSO-d_6): δ 174.92, 169.01, 144.01, 132.34, 130.77, 128.79, 128.09, 125.50-124.54, 122.37, 41.93, 34.12, 29.49-29.01, 26.78 24.95. HRMS (ESI) *m/z* [M]+ calculated for $C_{25}H_{37}ClF_3NO_3$ = 492.0144, found 492.0147. qNMR purity = 98.2 %

5 – 18-((3,4-dichlorophenyl)amino)-18-oxooctadecanoic acid

Synthesised with general procedure ii. White solid (93%). M.P. = 118-120 ˚C. ^{1}H NMR (500 MHz, DMSO-d_6): δ 11.93 (s, 1H), 10.14 (s, 1H), 7.99 (s, 1H), 7.54-7.52 (d, *J* = 18 Hz, 1H), 7.48-7.45 (dd, *J* = 18 Hz, 1H), 2.31-2.28 (t, *J* = 15 Hz, 2H), 2.18-52.16 (t, *J* = 15 Hz, 2H), 1.58-1.55 (t, *J* = 14 Hz, 2H), 1.48-1.45 (t, *J* = 14 Hz, 2H), 1.26-1.22 (m, 24H). ^{13}C NMR (125 MHz, DMSO-d_6): δ 174.94, 163.37, 131.03, 120.57, 119.42, 40.47-39.47, 36.83, 29.48-29.00, 25.13, 24.95. HRMS (ESI) *m/z* [M]+ calculated for $C_{25}H_{37}ClF_3NO_3$ = 492.0144, found 492.0142. qNMR purity = 97.1 %

5.2.5 General Procedure for "c" Methyl Ester Hydrolysis

To a solution of the aryl amide esters **6a-17a** (0.10 mmol) in ethanol (6 mL), 1M NaOH (2 mL) was added dropwise and the reaction mixture was stirred for 3 hours at 40 ˚C. Ethanol was removed under reduced pressure and the residue was acidified with 0.5 M HCl until pH = 2 (approximately 6 mL). The aqueous layer was extracted with chloroform 3 times (15 mL) and the combined organic layers were dried over Mg_2SO_4. Chloroform was removed under reduced pressure to isolate aryl amides **6-17**.

6 – 16-((4-chloro-3-(trifluoromethyl)phenyl)amino)-16-oxohexadecanoic acid

Synthesised with general procedure c. White solid (94%). M.P. = 86-87 ˚C. ^{1}H NMR (500 MHz, DMSO-d_6): δ 10.30 (s, 1H) 8.19 (s, 1H), 7.84-7.81 (d, J = 15 Hz, 1H), 7.65-7.63 (d, J = 10 Hz, 1H), 2.34-2.30 (t, J = 20 Hz, 2H), 2.20-2.16 (t, J = 20 Hz, 2H), 1.60-1.57 (m, 2H), 1.49-1.46 (m, 2H), 1.26-1.22 (m, 20H). ^{13}C NMR (125 MHz, DMSO-d_6): δ 175, 172.5, 139.2, 132.5, 127.1, 124.2 (q, J = 273 Hz), 118.1, 36.8, 34.1, 29.5-29, 25.3, 24.9. HRMS (ESI) m/z [M]+ calculated for $C_{23}H_{33}ClF_3NO_3$ = 463.2101 found 463.2104. qNMR purity = 96.3 %
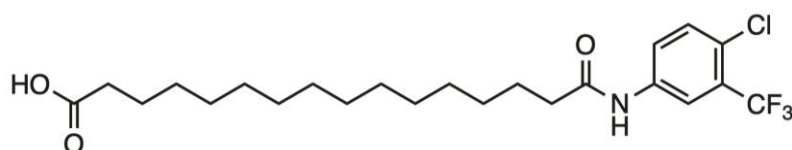
*7 – 16-((3-chloro-4-(trifluoromethyl)phenyl)amino)-16-oxohexadecanoic acid*

Synthesised with general procedure c. White solid (96%). 114-116 ˚C. ^{1}H NMR (500 MHz DMSO-d_6): δ 10.41 (s, 1H), 8.02 (s, 1H), 7.79-7.77 (d, J = 10 Hz, 1H), 7.65-7.62 (d, J = 15 Hz, 1H), 2.36-2.32 (t, J = 20 Hz, 2H), 2.19-2.16 (t, J = 15 Hz, 2H), 1.60-1.57 (m, J = 15 Hz, 2H), 1.49-1.45 (m, J = 15 Hz, 2H), 1.26-1.22 (m, 20H). ^{13}C NMR (125 MHz, DMSO-d_6): δ 175, 172.9, 144.3, 131.6, 129 (q, J = 273 Hz), 120.9, 117.4, 36.9, 34.1, 29.5-29, 25.2, 25. HRMS (ESI) m/z [M]+ calculated for $C_{23}H_{33}ClF_3NO_3$ = 463.2101, found 463.2102 qNMR purity = 95.8 %
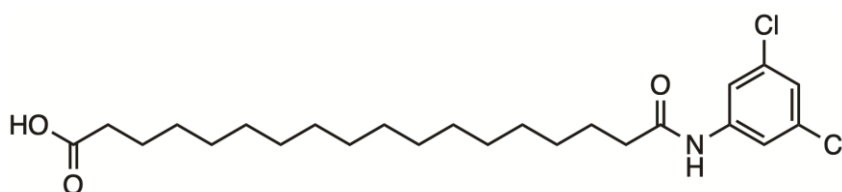
8 – *16-((3,4-bis(trifluoromethyl)phenyl)amino)-16-oxohexadecanoic acid*

Synthesised with general procedure c. White solid (88%). M.P. = 107-108 ˚C. ^{1}H NMR (500

MHz DMSO-d_6): δ 10.69 (s, 1H), 8.32 (s, 1H), 8.07-8.05 (d, J = 10 Hz, 1H), 7.99-7.96 (d, J =

15 Hz, 1H), 2.39-2.36 (t, J = 15 Hz, 2H), 2.17-2.14 (t, J = 15 Hz, 2H), 1.62-1.58 (m, J = 20

Hz, 2H), 1.48-1.45 (m, J = 15 Hz, 2H), 1.28-1.23 (m, 20H). ^{13}C NMR (125 MHz, DMSO-d_6):

δ 175.1, 173, 143.9, 142.2, 130.1, 122.1 (q, J = 273 Hz), 118.2, 117.9, 36.9, 34.5, 29.4-29.3,

29.2-29, 25.2, 25.1. HRMS (ESI) *m/z* [M]+ calculated for $C_{24}H_{33}F_6NO_3$ = 497.2365, found
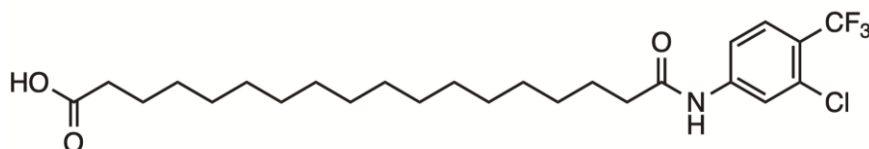
497.2361. qNMR purity = 95.1 %
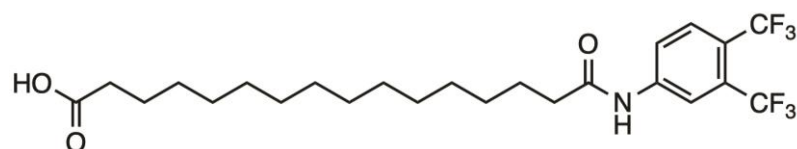
9 – *16-((3,4-dichlorophenyl)amino)-16-oxohexadecanoic acid*

Synthesised with general procedure c. White solid (91%). M.P. = 102-104. ^{1}H NMR (500 MHz

DMSO-d_6): δ 10.18 (s, 1H), 7.98 (s, 1H), 7.55-7.53 (d, J = 10 Hz, 1H), 7.48-7.45 (d, J = 15

Hz, 1H), 2.31-2.28 (t, J = 15 Hz, 2H), 2.19-2.15 (t, J = 20 Hz, 2H), 1.59-1.55 (t, J = 20 Hz,

2H), 1.49-1.45 (t, J = 20 Hz, 2H), 1.27-1.22 (m, 20H). ^{13}C NMR (125 MHz, DMSO-d_6): δ

175.04, 172.37, 139.81, 131.81, 131.08, 124.80, 120.62, 119.49, 39.67, 34.13, 29.48-29.15,

28.99, 25.33, 24.95. HRMS (ESI) *m/z* [M]+ calculated for $C_{22}H_{33}Cl_2NO_3$ = 429.1838, found
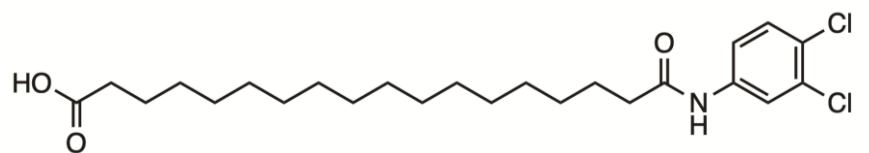
429.1842. qNMR purity = 97.3 %

10 – *12-((4-chloro-3-(trifluoromethyl)phenyl)amino)-12-oxododecanoic acid:*

Synthesised with general procedure c. White solid (90%). M.P. = 121-122 ℃. ^{1}H NMR (500 MHz, DMSO-d_6): δ 11.93 (s, 1H), 10.29 (s, 1H), 8.19-8.18 (d, J = 5 Hz, 1H), 7.83-7.81 (dd, J = 5 Hz), 7.64-7.62 (d, J = 18 Hz, 1H), 2.33-2.30 (t, J = 15 Hz, 2H), 2.18-2.15 (t, J = 15 Hz, 2H), 1.59-1.56 (t, J = 14 Hz, 2H), 1.48-1.45 (t, J = 14 Hz, 2H), 1.27-1.24 (m, 12H). ^{13}C NMR (125 MHz, DMSO- d_6): δ 172.4, 139.2, 132.5, 124.1 (q, J = 273 Hz), 118, 40.5-39.5, 36.9, 34.2, 29.3-29, 25.3, 25. HRMS (ESI) *m/z* [M]+ calculated for $C_{19}H_{25}ClF_3NO_3$ = 407.1475, found 407.1478. qNMR purity = 95.7 %
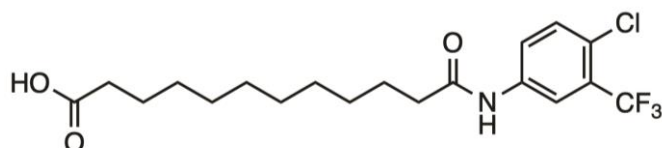
11 – *12-((3-chloro-4-(trifluoromethyl)phenyl)amino)-12-oxododecanoic acid*

Synthesised with general procedure c. White solid (92%). M.P. = 113-115 ˚C. ^{1}H NMR (500 MHz DMSO-d_6): δ 11.93 (s, 1H), 10.39 (s, 1H), 8.03 (s, 1H), 7.79-7.77 (d, J = 10 Hz, 1H), 7.65-7.63 (d, J = 10 Hz, 1H), 2.36-2.33 (t, J = 15 Hz, 2H), 2.20-2.16 (t, J = 20 Hz, 2H), 1.60-1.57 (m, J = 15 Hz, 2H), 1.50-1.47 (m, J = 15 Hz, 2H), 1.27-1.24 (m, 12H). ^{13}C NMR (125 MHz, DMSO-d_6): δ 175.1, 172.9, 144.3, 131.6, 129.1, 124.9 (q, J = 273 Hz), 122.2, 120.9, 117.4, 36.9, 34.1, 29.3-29, 25.2, 25. HRMS (ESI) *m/z* [M]+ calculated for $C_{19}H_{25}ClF_3NO_3$ = 407.1475, found 407.1477. qNMR purity = 96.5 %
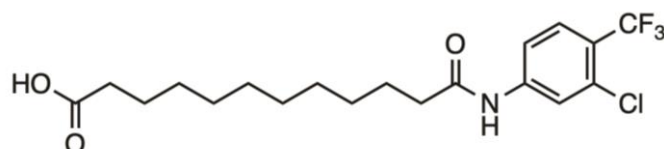
12 – *12-((3,4-bis(trifluoromethyl)phenyl)amino)-12-oxododecanoic acid:*

Synthesised with general procedure c. White solid (83%). ^{1}H NMR (500 MHz DMSO-d_6): δ 10.58 (s, 1H), 8.29 (s, 1H), 8.05-8.03 (d, J = 10 Hz, 1H), 7.98-7.96 (d, J = 10 Hz, 1H), 2.38-2.35 (t, J = 15 Hz, 2H), 2.19-2.16 (t, J = 15 Hz, 2H), 1.61-1.58 (m, J = 15 Hz, 2H), 1.48-1.45 (t, J = 15 Hz, 2H), 1.27-1.24 (m, 12H). ^{13}C NMR (125 MHz, DMSO-d_6): δ 171, 173.1, 143.8, 130, 127.6, 124.9-124.6 (q, J = 273 Hz), 120.1, 118, 36.9, 34.1, 29.3-29, 25.2, 24.9. HRMS (ESI) *m/z* [M]+ calculated for $C_{20}H_{25}F_6NO_3$= 441.1739, found 441.1743. qNMR purity = 95.2 %

13 – *12-((3,4-dichlorophenyl)amino)-12-oxododecanoic acid:*

Synthesised with general procedure c. White solid (91%). M.P. = 152-153 ℃. ^{1}H NMR (500 MHz, DMSO-d_6): δ 11.93 (s, 1H), 10.15 (s, 1H), 7.99 (s, 1H), 7.54-7.52 (d, J = 18 Hz, 1H), 7.48-7.45 (dd, J = 17 Hz, 1H), 2.31- 2.28 (t, J = 15 Hz, 2H), 2.18-2.15 (t, J = 15 Hz, 2H), 1.58-1.55 (t, J = 14 Hz, 2H), 1.48-1.45 (t, J = 14 Hz, 2H), 1.27-1.24 (m, 12H). ^{13}C NMR (125 MHz, DMSO-d_6): δ 172.4, 139.2, 132.5, 124.1, 118, 40.5-39.5, 36.9, 34.2, 29.3-29, 25.3, 25. HRMS (ESI) *m/z* [M]+ calculated for $C_{18}H_{25}Cl_2NO_3$= 373.1212, found 373.1210. qNMR purity = 97.8 %
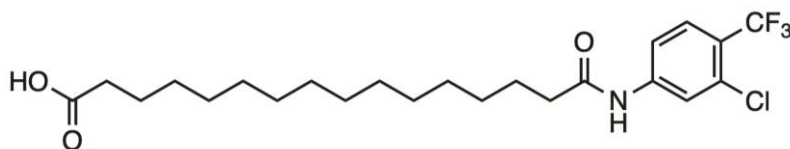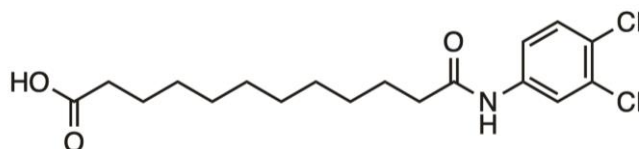
14 – *8-((4-chloro-3-(trifluoromethyl)phenyl)amino)-8-oxooctanoic acid:*

Synthesised with general procedure c. White solid (68%). M.P. = 91-93 ℃. ^{1}H NMR (500

MHz, DMSO-d_6): δ 11.98 (s, 1H), 10.31 (s, 1H), 8.20-8.19 (d, *J* = 3 Hz, 1H), 7.85-7.82 (d, *J* =

11 Hz, 1H), 7.65-7.63 (d, *J* = 11 Hz, 2H), 2.35-2.31 (t, *J* = 9 Hz, 2H), 2.22-2.18 (t, *J* = 9 Hz,

2H), 1.59 (m, 2H), 1.52-1.48 (m, 2H), 1.32 (m, 2H). ^{13}C NMR (125 MHz, DMSO-d_6): δ 174.9,

172.4, 139.2, 132.5, 124.2 (q, *J* = 273 Hz), 118.1, 40.6-39.4, 36.8, 34.1, 28.8-28.8, 25.2, 24.8.

HRMS (ESI) *m/z* [M]+ calculated for $C_{15}H_{17}ClF_3NO_3$ = 351.0849, found 351.0853. qNMR
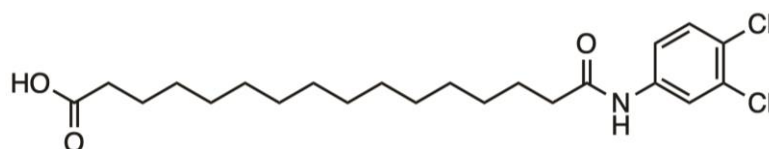
purity = 96.4 %
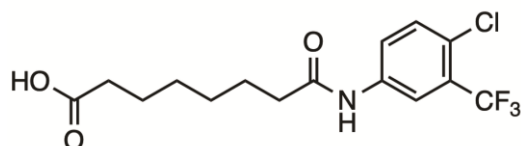
15 – *8-((3-chloro-4-(trifluoromethyl)phenyl)amino)-8-oxooctanoic acid*

Synthesised with general procedure c. White solid (75%). M.P. = 102-104 ˚C. ^{1}H NMR (500

MHz DMSO-d_6): δ 10.41 (s, 1H), 8.02 (s, 1H), 7.79-7.76 (d, *J* = 15 Hz, 1H), 7.65-7.62 (d, *J* =

15 Hz, 1H), 2.36-2.32 (t, *J* = 20 Hz, 2H), 2.21-2.17 (t, *J* = 20 Hz, 2H), 1.62-1.54 (m, 2H), 1.53-

1.46 (m, 2H), 1.31-1.28 (m, 4H). ^{13}C NMR (125 MHz, DMSO-d_6): δ 175, 172.8, 144.3, 131.6,

129.1-129 (q, *J* = 273 Hz), 120.9, 117.5, 36.9, 34.1, 28.7, 25.1, 24.8. HRMS (ESI) *m/z* [M]+

calculated for $C_{15}H_{17}ClF_3NO_3$ = 351.0849, found 351.0846. qNMR purity = 95.9 %
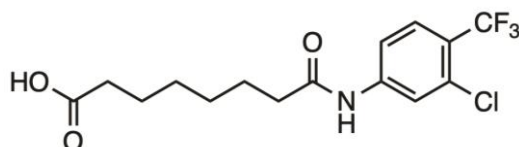
16 – *8-((3,4-bis(trifluoromethyl)phenyl)amino)-8-oxooctanoic acid:*

Synthesised with general procedure c. White solid (61%). M.P. = 112-114 ˚C. ^{1}H NMR (500 MHz DMSO-d_6): δ 10.58 (s, 1H), 8.29 (s, 1H), 8.05-8.03 (d, J = 10 Hz, 1H), 7.98-7.96 (d, J = 10 Hz, 1H), 2.39-2.35 (t, J = 20 Hz, 2H), 2.20-2.16 (t, J = 20 Hz, 2H), 1.63-1.56 (m, 2H), 1.53-1.46 (m, 2H), 1.31-1.29 (m, 4H). ^{13}C NMR (125 MHz, DMSO-d_6): δ 175, 173, 143.8, 130.1-130 (q, J = 273 Hz), 122.1, 118, 36.9, 34.1, 28.7, 25.1, 24.8. HRMS (ESI) *m/z* [M]+ calculated for $C_{16}H_{17}F_6NO_3$ = 385.1113, found 385.1118. qNMR purity = 95.3 %
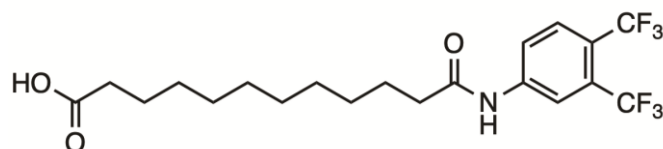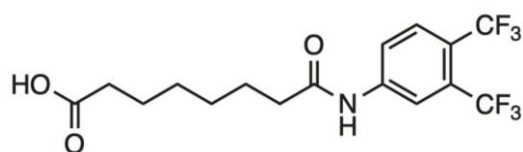

17 – *8-((3,4-dichlorophenyl)amino)-8-oxooctanoic acid:*

Synthesised with general procedure c. White solid (43%). M.P. = 122-123 ˚C. ^{1}H NMR (500 MHz, DMSO-d_6): δ 11.98 (s, 1H), 10.15 (s, 1H), 7.99 (s, 1H), 7.54-7.52 (d, J = 8.5 Hz, 1H), 7.48-7.45 (d, J = 8.5 Hz, 1H), 2.31-2.28 (t, J = 7 Hz, 2H), 2.20-2.17 (t, J = 7 Hz, 2H), 1.58-1.55 (m, 2H), 1.50-1.46 (m, 2H), 1.30-1.27 (m, 4H). ^{13}C NMR (125 MHz, DMSO-d_6): δ 174.94, 172.23, 139.85, 131.37, 124.75, 120.61, 119.47, 40.61-39.56, 36.81, 34.08, 28.78-28.76, 25.22, 24.82. HRMS (ESI) *m/z* [M]+ calculated for $C_{14}H_{17}Cl_2NO_3$ = 317.0586, found 317.0589. qNMR purity = 97.2 %
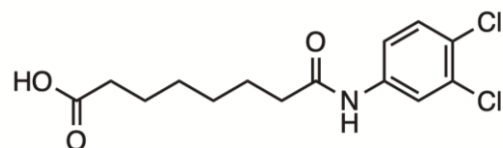
5.3   Cell Culture

5.3.1 General Cell Culture

Human tumour cell lines were obtained from ATCC (Manassas, VA). Cells were grown at 37°C in a humidified atmosphere of 5% CO2 in air in DMEM supplemented with 10% fetal bovine serum (Thermo Fisher Scientific) and 1% penicillin/streptomycin (Invitrogen). Confluent cells (80-90%) were harvested using Trypsin/EDTA after washing in PBS. Cells were treated with various concentrations of the test compounds in DMSO (final concentration 0.1%); control cells were treated with DMSO alone.

5.3.2 Seahorse Assay

Mitochondrial function was measured by determining the OCR of cells with a Seahorse XF24 extracellular flux analyser (Seahorse Bioscience, MA, USA) according to the manufacturer's protocol. MDA-MB-231 cells were seeded in a 24-well XF cell culture microplate (2.5×10^4 cells per well) and allowed to adhere overnight (37 ˚C, 5% CO_2). After 24 h, the culture media was replaced with serum-free media and left to incubate at 37 ˚C for 16-18 hours. The culture media was then replaced with buffered XF Base Medium supplemented with 2 mM L-glutamine, 10 mM glucose and 2 mM sodium pyruvate at pH = 7.4. The cells were incubated at 37 ˚C without CO_2 for one hour then OCR was measured using an XF Cell Mito Stress Test Kit (Seahorse Bioscience, MA, USA). Test compounds (at highest possible concentration where soluble), CCCP (5 µM) and DNP (20 µM) were loaded into the sensor cartridge and OCR was measured using a modified cycling program.

5.3.3 MTS Assay

Cells were seeded in a clear 96 well plate (5×10^3 cells per well) in complete media and incubated at 37 ˚C for 18-24 hours. The complete media was then replaced with serum-

free media and left to incubate at 37 ˚C for 16-18 hours. Media was then aspirated from each well, and aryl amide was added. The cells were then incubated at 37 ˚C for 24 hours before adding 15 µL of Cell Titer AQ One solution (Promega, USA) to each well. Cells were incubated for 3 hrs at 37 ˚C, and fluorescence was measured using a plate reader. Cell viability was determined relative to DMSO control.

5.3.4 JC-1 Assay

Cells were seeded in a black 96 well plate (1.5×10^4 cells per well for both MDA-MB-231 and L6 cell lines) in complete media and left to incubate for 18-24 hours at 37 ˚C. The complete media in each well was then replaced with serum-free media and left to incubate at 37 ˚C for 16-18 hours. Each well was then replaced with 100 µL of complete media stocks of each analogue (1 µL of analogue in 999 µL of complete media) at varying concentrations. Cells were incubated for 1 hour at 37 ˚C before adding 10 µL of JC-1 dye (Promega, USA) to each well (except for blank wells). The cells were again incubated for 20 minutes and centrifuged for 5 minutes at 1250 RPM. Cells were washed with 200 µL PBS twice and centrifuged in between washes. Each well was then aspirated, and 100 µL of PBS was added before measuring fluorescence using a plate reader. IC_{50} values were defined as the drug concentration which depolarised the MIM to 50% (relative to the vehicle control) and was determined using non-linear regression analysis with Prism 7.0 (GraphPad Software, CA, USA). MIM depolarisation was determined using the red/green fluorescence intensity ratio relative to DMSO controls.

5.3.5 ATP assay

Cells were seeded in a black clear bottom 96 well plate (7.5×10^3 cells per well) in complete media and incubated at 37 ˚C for 18-24 hours. The complete media in each well was then replaced with serum-free media and left to incubate at 37 ˚C for 16-18 hours. Each well

was then replaced with 100 µL of complete media stocks of each analogue (1 µL of analogue in 999 µL of complete media) at varying concentrations. The cells were then incubated at 37 ˚C for 1-6 hours after treatment with aryl amides before adding 75 µL of Cell Titer Glo solution (Promega, USA) to each well. The plate was shaken using the plate reader for 2 minutes, followed by incubating at room temperature for 10 minutes and measuring luminescence using a Tecan M1000 plate reader. ATP production was determined relative to DMSO control.

5.3.6 LDH Assay

Cells were seeded in a clear 96 well plate (5×10^3 cells per well) in complete media and left to incubate at 37 ˚C for 18-24 hours. The complete media was then replaced with serum free media and left to incubate at 37 ˚C for 16-18 hours. Media was then aspirated from each well and aryl amide stocks were added. The cells were then incubated at 37 ˚C for 6 hours and 3 µL of media was taken out of each well and added to 97 µL of LDH storage buffer. These solutions containing media were frozen at -20 ˚C until the day of the assay. After thawing, 50 µL of media sample was transferred to a black 96 well clear bottom plate along with 50 µL of LDH detection reagent in the same wells. The plate was incubated for 60 minutes at room temperature and luminescence was recorded using a Tecan M1000 plate reader. LDH release determined relative to DMSO control

5.4 Mechanistic Studies

5.4.1 HPTS Assay

The HPTS Assay was conducted by Dr Daniel McNaughton following the procedure outlined in the supplementary information section of a 2016 study conducted by Wu & Gale[23]. HPTS assays were conducted using POPC LUVs (200 nm diameter) vesicles were loaded with an internal solution containing pH-sensitive fluorescent dye HPTS (1 mM), HEPES buffer (10 mM) and potassium gluconate (100 mM). An external solution of HEPES buffer (10 mM) and potassium gluconate (100 mM) was also prepared, and both solutions were buffered to pH 7.

Unilamellar vesicles were prepared following a procedure outlined previously by the Gale group[.23]. A chloroform solution of POPC (37.5 mM, 4 mL) was transferred to a pre-weighed round-bottom flask, and the solvent was removed using a rotary evaporator. The pressure was lowered slowly to ensure the formation of a smooth lipid film. Subsequently, the film was dried in vacuo for 4-24 h, and the mass of lipid was recorded. The lipids were rehydrated with 4 mL of internal solution (this number should correspond to the volume of POPC solution used initially) and vortexed until all lipids were removed from the sides of the flask and were suspended in solution. The lipids were subjected to 9 cycles of freeze-thaw by freezing using a dry ice/acetone bath and thawing in lukewarm water. Following this, the vesicles were left to rest at room temperature for 30 min. The lipids were extruded through a 200 nm polycarbonate membrane 25 times to form monodisperse vesicles. Only 1 mL of solution was extruded at a time before being collected. Finally, any residual unencapsulated salt from the internal solution was using a B19 column packed with hydrated G-25 Sephadex®, which had been pre-saturated with the respective external solution. The lipid suspensions were diluted with the external solution to afford a stock solution (10 mL) of a known concentration.

5.4.1.1 Assay Conditions

For a given experiment, the prepared vesicles were diluted to a concentration of 0.1 mM in a 4.5 mL plastic cuvette. A pH gradient is required to drive transport through the vesicle membrane in these experiments before the transporter is added. An aliquot of aqueous NaOH solution (25 µL, 0.5 M) was added to increase the pH of the external solution by approx. one pH unit to pH 8.0. Following this, valinomycin (5 µL of 25 µM DMSO solution, 0.05 mol%) was added to each cuvette. Transport was initiated with the addition of the transporter as a DMSO solution (5 µL) and ended with the addition of detergent (Triton X-100 (10% v/v in water), 25 µL) at $t = 210$ s to lyse the vesicles, and a final fluorescence intensity reading was recorded at $t = 300$ s to signify 100% proton efflux.

5.4.1.2 Dose-Response Hill Analysis

The changes in the fluorescent activity of intravesicular HPTS were used to detect pH changes during the experiments, and hence represent proton efflux. The acidic and basic forms of the HPTS probe were excited at $\lambda_{ex} = 403$ nm and $\lambda_{ex} = 460$ nm, respectively, and the fluorescence emission of both forms recorded at $\lambda_{em} = 510$ nm. The intensity ratio of basic form to acidic form was determined, and the fractional fluorescence intensity (I_F) was calculated using the equation:

$$I_f = \frac{R_t - R_0}{R_d - R_0}$$

Where R_t is the ratiometric fluorescence value at a given time (t), R_0 is the ratiometric fluorescence value at $t = 0$ s and R_d is the fluorescence ratiometric value recorded at $t = 280$ s following the addition of detergent.

Dose-response experiments were performed at a minimum of five transporter concentrations plus a blank DMSO control run. I_F was plotted as a function of transporter concentration (mol%, with respect to lipid concentration). The I_F value at $t = 200$ s for each tested transporter concentration was fit to an adapted Hill Equation, using Origin 2021b (Academic), given as:

$$y = y_0 + (y_{max} - y_0)\frac{x^n}{k^n + x^n}$$

Where y_0 is the I_F value at $t = 200$ s for the DMSO blank run, y_{max} is the maximum I_F value, n is the Hill coefficient, and k is a derived parameter. A derived equation was used to calculate the EC_{50} value, the transporter concentration required to facilitate 50% chloride efflux, given as:

$$EC_{50} = k(\frac{0.5}{y_1 - y_0})^{1/n}$$

Where k and n are the derived parameters from the Hill equation, y_0 is the percentage chloride efflux at $t = 0$ s, and y_1 is the percentage chloride efflux at $t = 280$ s.

5.4.1.3   Incubation Studies

Additional experiments were conducted to assess the effect of protonophore incubation on the rate of proton efflux. Experiments were completed for each compound at the same loading of protonophore (0.5 mol%) and performed under three conditions. 1.) Base addition first, followed by protonophore addition to initiate the experiment ($t = 0$ s incubation). 2.) Protonophore addition first, followed by base addition to initiate the experiment. This provides a brief incubation after protonophore is added while the experiment and fluorimeter are prepared ($t = 30$ s incubation). 3.) Protonophore addition first, followed by base addition to initiate the experiment after a $t = 300$ s interval ($t = 300$ s incubation). The efflux plots of these

experiments were depicted on the same axes for qualitative comparison. The initial rates and incubation enhancement factors were calculated to provide a quantitative analysis.

5.4.2 Anion Binding ^{1}H NMR Studies

Aryl amide esters **1a-5a** were dissolved in acetone-d^6 subject to ^{1}H NMR measurements on a Bruker AVANCE III 400 NMR Spectrometer. TBA-OAc in acetone-d^6 was sequentially added to the NMR tube, varying in concentrations of 0.1 – 30 mM. The chemical shift of the N-H peak at various concentrations was fitted to a 1:1 binding model to retrieve anion binding constants[191].

5.4.3 Concentration-Dependent ^{1}H NMR Studies

A suspension of aryl amides **1-5** in CDCl3 was treated with 1.0 equivalent of tetrabutylammonium hydroxide (TBAOH, ~40% in H2O) and sonicated for 20 min to give a clear solution of (**1-5**)-TBAOH at 5 mM. The solution was diluted to various concentrations in CDCl3 and subject to ^{1}H NMR measurements on a Bruker AVANCE III 400 NMR Spectrometer. The chemical shifts of two aromatic C-H peaks at various concentrations were fitted to a monomer-dimer equilibrium model to retrieve dimerisation constants[159, 162].

5.4.4 Computational Evaluation

Both truncated and complete aryl amide structures were constructed using GaussView 6[192]. Aryl amide dimers were constructed using the optomized monomeric structures. All DFT calculations performed using Gaussian 16, revision C.01[163] at the M062x-D3/6-31G(d, p)//M062X-D3/6-311++G(2df,2p) level of theory. Implicit solvation in benzene (e=2.2706) and water (e=78.3553) was carried out using the SMD model for all calculations.

For calculating dipole angle of aryl amides **1**, **4** and **5**, the probability of the formation of their two possible conformers were calculated using a Boltzmann Distribution given as:

$$p_i = \frac{1}{Q} \exp\left(-\frac{\varepsilon_i}{kT}\right) = \frac{\exp\left(-\frac{\varepsilon_i}{kT}\right)}{\sum_{j=1}^{M} \exp\left(-\frac{\varepsilon_j}{kT}\right)}$$

Where p_i is the probability of formation of the conformer, T is the temperature (298 K), k is typically a Boltzmann constant but in this case it is the gas constant R (0.00831 kJ/mol·K) and ε_1 is the energy states of the conformer. The average bond angle was calculated by addition of the bond angles of each conformer when considering their probabilities:

$$\theta_{average} = (\theta_1 \times p_1) + (\theta_2 \times p_2)$$

Where $\theta_{average}$ is the average dipole angle for that aryl amide, θ_1 and θ_2 are the dipole angles of the conformers and p_1 and p_2 are the probabilities of the formation of each conformer.

5.5 Mice Studies

5.5.1 Mice and Ethics

All studies were performed under the protocol approved by the Animal Care and Ethics Committee at The University of Newcastle (A-2019-928). Six-8 week old female wild-type BALB/c mice (Animal Resource Centre, Western Australia, Australia or Central Animal House, Newcastle, Australia) were housed under specific pathogen free (SPF) conditions in the Hunter Medical Research Institute PC2 Facility (Newcastle, Australia) and maintained on a 12-hour day-night cycle with food and water available *ad libitum*. Mice were either placed on a high fat diet (HFD; 60% energy derived from lipids, 15% energy from protein [SF14-154], Specialty Feeds, Glen Forrest, Western Australia, Australia) or control chow (CC) diet (16% energy derived from lipids, 21% energy from protein [SF09-091], Specialty Feeds, Australia)

as outlined in model Figures throughout and we have previously established[193]. Following euthanasia by intraperitoneal (i.p.) injection with sodium pentobarbitone (60 mg/kg) in 200μl phosphate buffered saline (PBS), parametrial, retroperitoneal and inguinal fat pads were collected and weighed to confirm HFD-induced increase in weight and adiposity. Gastrocnemius muscle weight was also recorded. Following 9 weeks of HFD or CC, mice were administered EP4 (1 mg/kg or 10 mg/kg; oral gavage) or PBS (oral gavage) on days 21-34.

On day 35 of the study protocol, mice were anaesthetised with a mixture of ketamine (100mg/kg, Parnell Laboratories, Alexandria, New South Wales, Australia) and xylazine (10mg/kg, Troy Laboratories, Smithfield, New South Wales, Australia) in 200μL PBS i.p. Following tracheostomy, cannulae were inserted into the trachea and ligated. Rn and Rrs (tidal volume of 8mL/kg at a respiratory rate of 450 breaths/min) were measured in response to increasing doses of nebulised methacholine (up to 10mg/mL, 15μL saline; Sigma-Aldrich, Sydney, Australia) and expressed as a percentage change to saline nebulization. Mice were subsequently euthanized by intraperitoneal (i.p.) injection with sodium pentobarbitone (60mg/kg) in 200μL phosphate buffered saline (PBS) and BALF collected.

5.5.2 *Glucose and insulin measurements (blood)*

In some groups, mice were fasted for 12 hours prior to euthanasia by i.p. injection with sodium pentobarbitone (60mg/kg) in 200 μL phosphate buffered saline (PBS). Blood was immediately collected via cardiac puncture and glucose measured using an Accu-Chek glucose monitor. Blood was clotted at room temperature, centrifuged (300 x*g*, 10 mins), serum collected and ran fresh using an Ultra-Sensitive Mouse Insulin ELISA Kit (Cat no. 90080; Crystal Chem, IL, USA) as per the manufacturer's instructions.

5.5.3 Statistics

Comparisons between two groups were made using unpaired *t*-tests where appropriate. Comparisons between multiple groups were made using a One-way ANOVA and Fisher's LSD Post Test where appropriate. Analyzes were performed using GraphPad Prism Software (version 10.4.0). All data points shown are representative of individual mice. No data has been pooled. *$P<0.05$ was considered statistically significant.

CHAPTER 6

Appendix

Figure 27: Structure of Liraglutide
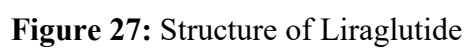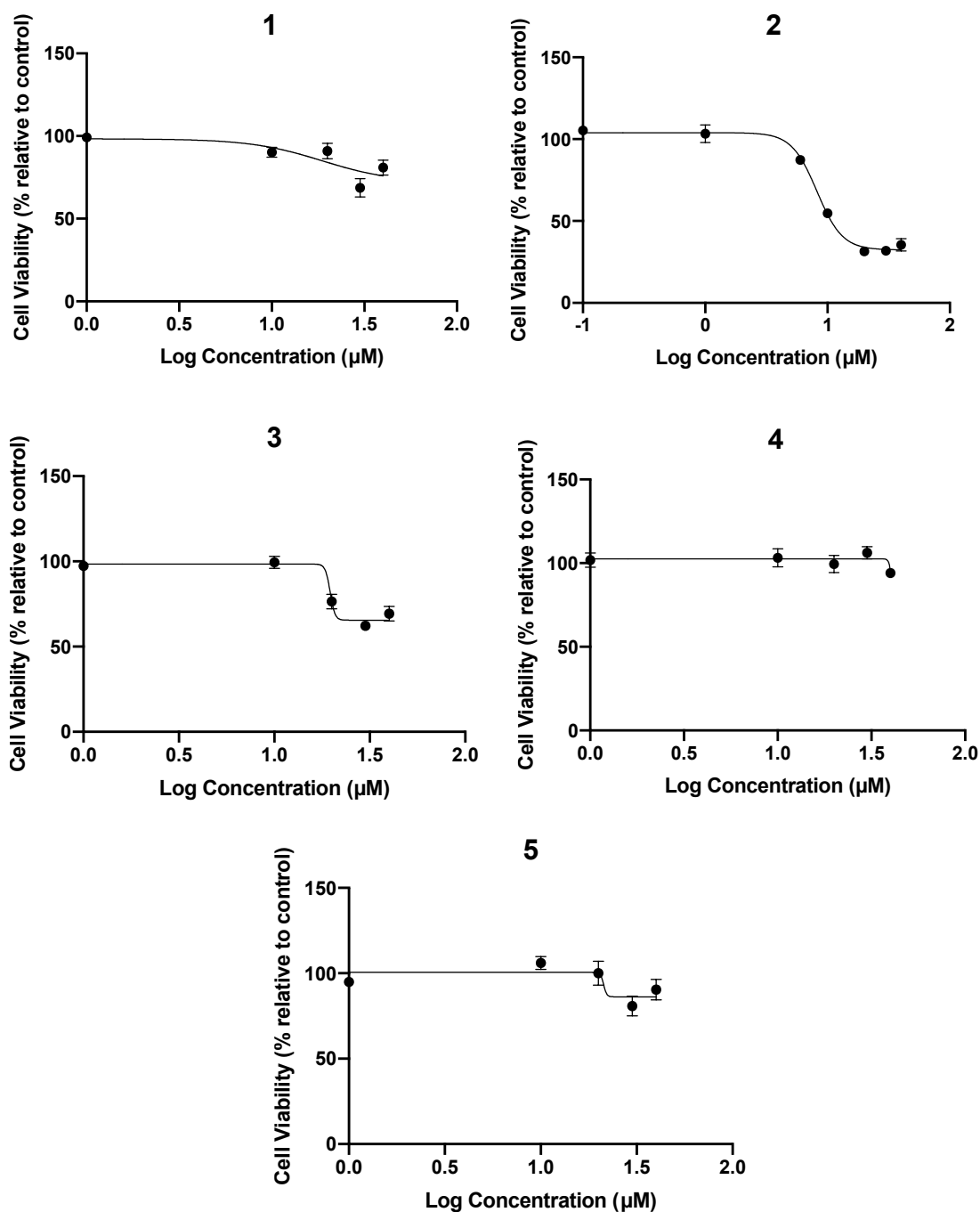
Figure 28: MTS Cell viability of aryl amides. Dose-response curves of cell viability (%) relative to control of MDA-MB-231 breast cancer cells when treated with aryl amides **1-5** for 24 hours at concentrations between 0.1 μM to 40 μM using an MTS assay. Only aryl amide **2** had an $IC_{50} < 100$ with 7.15 ± 1.5 μM. Data represents mean $\pm$ SEM of three independent experiments.
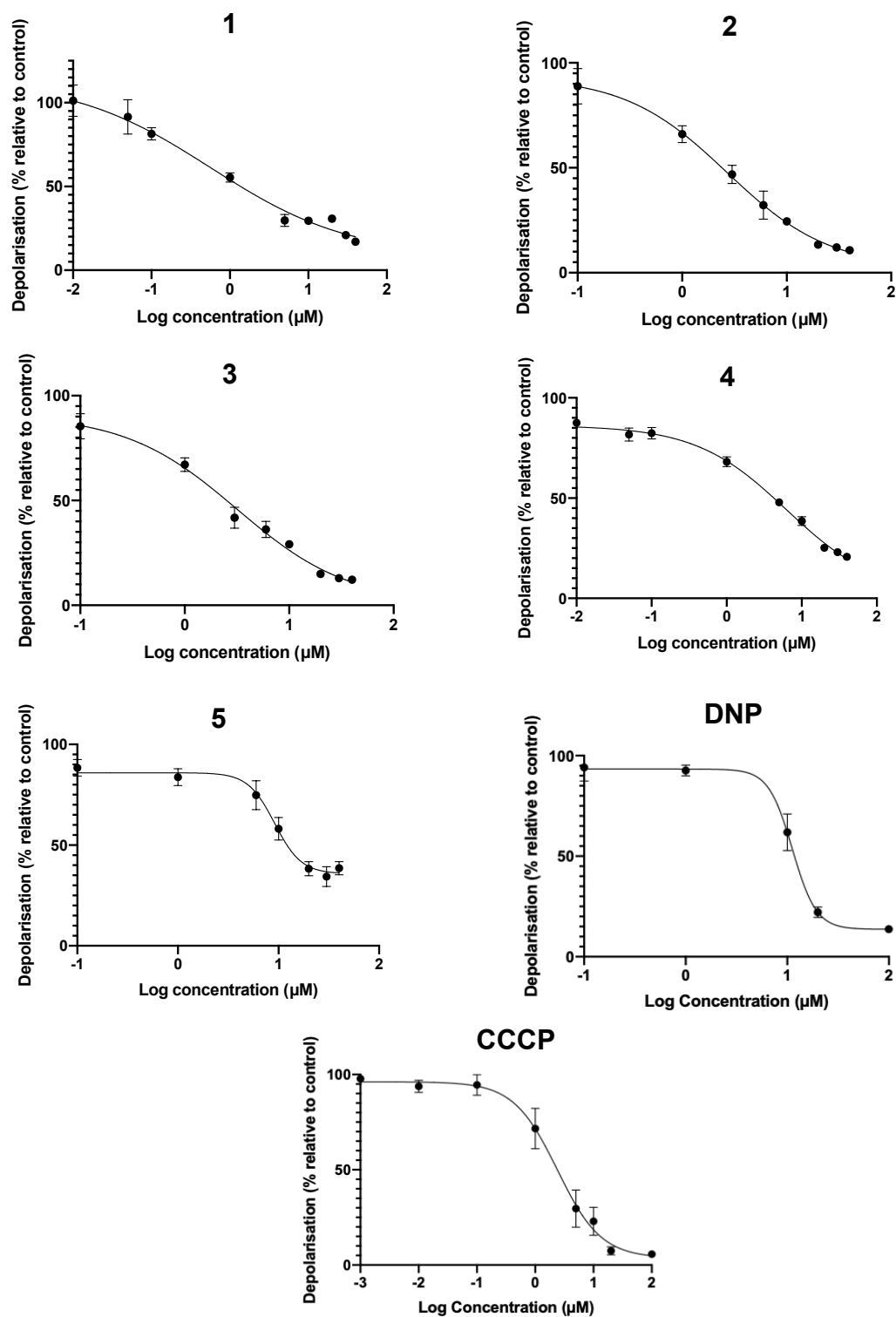
Figure 29: Aryl amides effect on membrane potential. Individual dose-response curves of membrane depolarisation (%) relative to control of MDA-MB-231 breast cancer cells when treated with aryl amides **1-5** for 1 hour at concentrations between 0.1 µM to 40 µM using a JC-1 assay. CCCP and DNP tested at concentrations of 0.01-100 µM Data represents mean ± SEM of three independent experiments.

Figure 30: Hill plot analysis of H^+/OH^- transport facilitated by compound **1** measured using the KGluc assay. NaOH (5 mM) and valinomycin (0.05 mol%) were added to the vesicles before the addition of **1** at 0 s. Detergent was added at $t = 210$ s to lyse the vesicles. Compound concentrations are shown as compound-to-lipid molar ratios. Error bars represent standard deviations from two repeats.
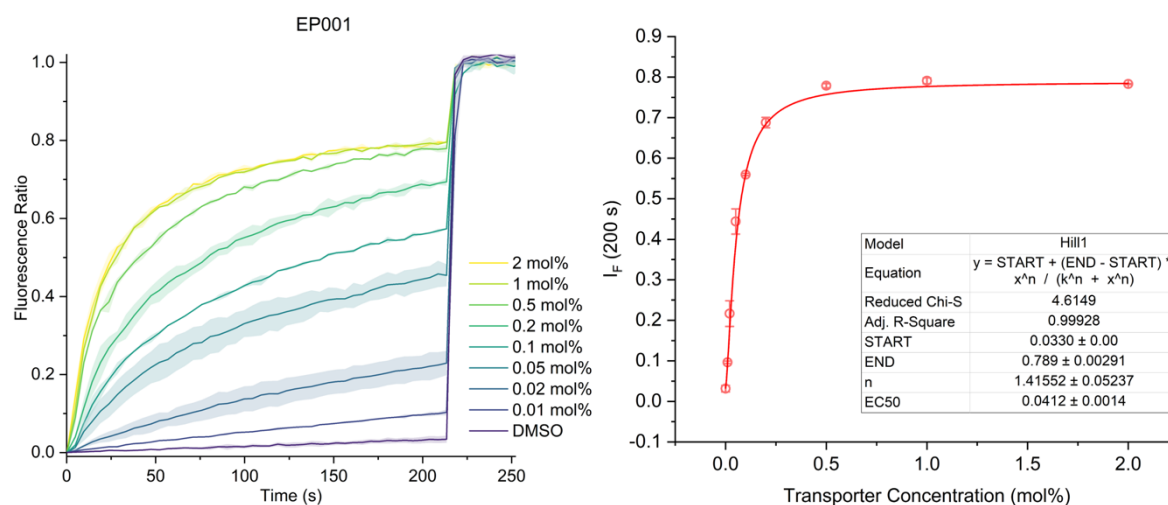
Figure 31: Hill plot analysis of H^+/OH^- transport facilitated by compound **2** measured using the KGluc assay. NaOH (5 mM) and valinomycin (0.05 mol%) were added to the vesicles before the addition of **2** at 0 s. Detergent was added at $t = 210$ s to lyse the vesicles. Compound concentrations are shown as compound-to-lipid molar ratios. Error bars represent standard deviations from two repeats.
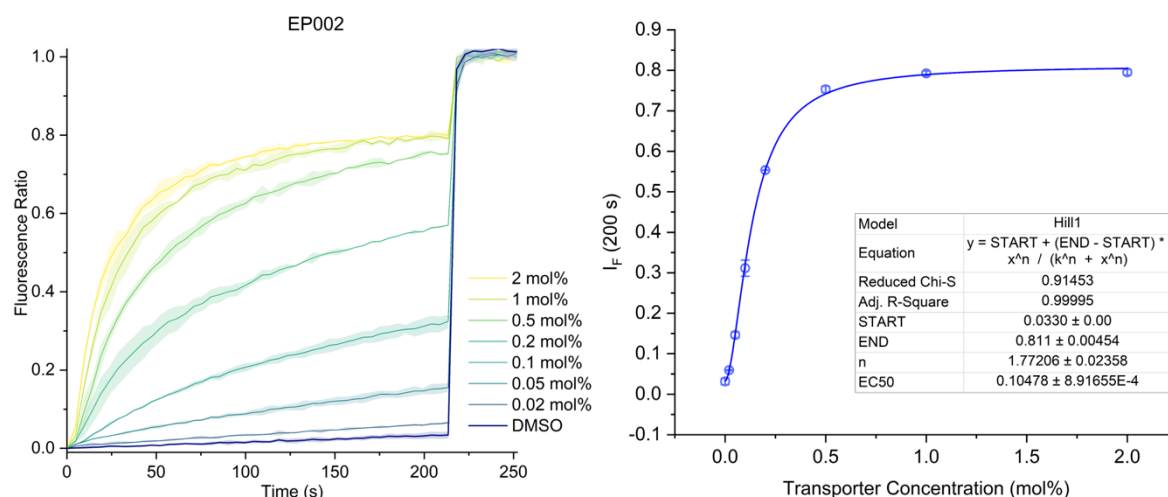
Figure 32: Hill plot analysis of H$^+$/OH$^-$ transport facilitated by compound **3** measured using the KGluc assay. NaOH (5 mM) and valinomycin (0.05 mol%) were added to the vesicles before the addition of **3** at 0 s. Detergent was added at $t = 210$ s to lyse the vesicles. Compound concentrations are shown as compound-to-lipid molar ratios. Error bars represent standard deviations from two repeats.
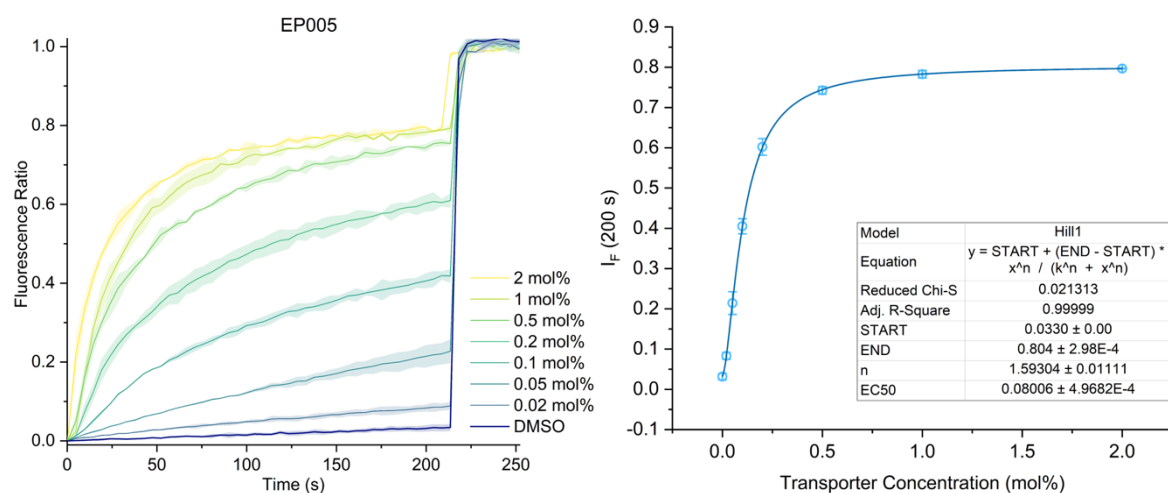
Figure 33: Hill plot analysis of H$^+$/OH$^-$ transport facilitated by compound **4** measured using the KGluc assay. NaOH (5 mM) and valinomycin (0.05 mol%) were added to the vesicles before the addition of **4** at 0 s. Detergent was added at $t = 210$ s to lyse the vesicles. Compound concentrations are shown as compound-to-lipid molar ratios. Error bars represent standard deviations from two repeats.
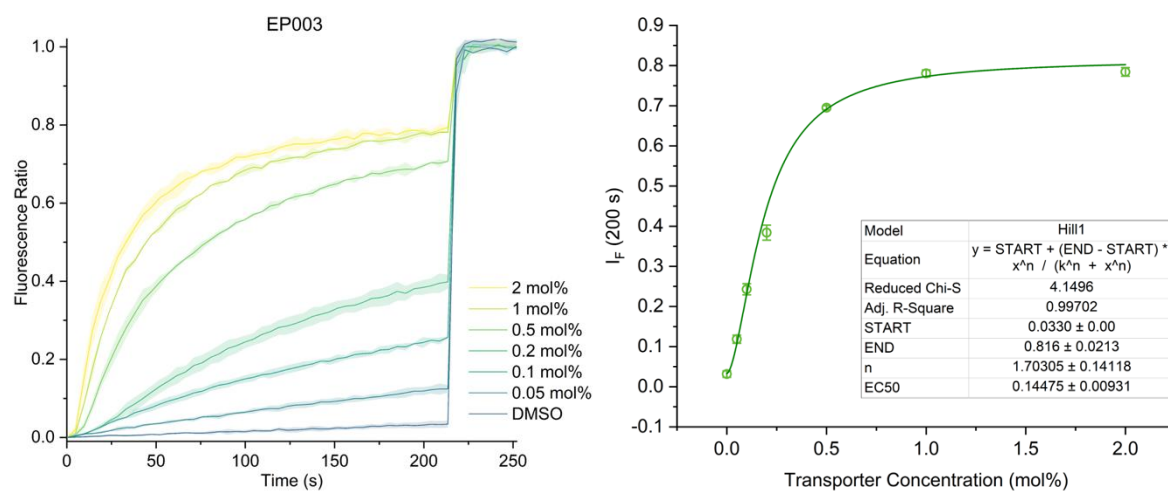
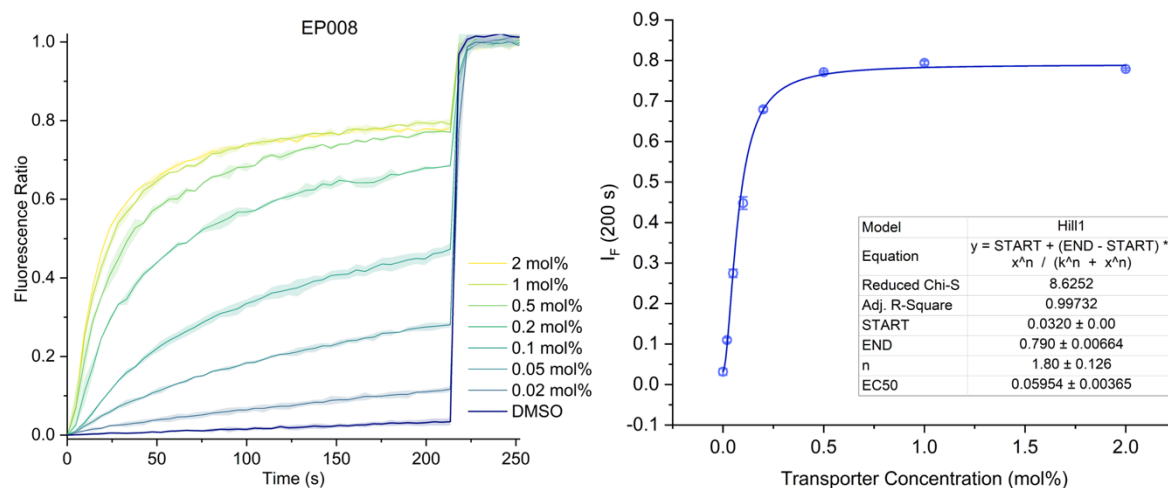**Figure 34:** Hill plot analysis of H⁺/OH⁻ transport facilitated by compound **5** measured using the KGluc assay. NaOH (5 mM) and valinomycin (0.05 mol%) were added to the vesicles before the addition of **5** at 0 s. Detergent was added at $t = 210$ s to lyse the vesicles. Compound concentrations are shown as compound-to-lipid molar ratios. Error bars represent standard deviations from two repeats.

Figure 35: The HPTS efflux plots for compound **1** (0.5 mol%) measured using the KGluc assay under three incubation conditions. Valinomycin (0.05 mol%) were added to the vesicles in each experiment before the addition of **1** and NaOH (5 mM) in various orders. 0 s incubation represents base-first addition followed by protonophore initiation. 40 s incubation represents protonophore-first addition followed by base initiation. 300 s incubation represents protonophore first addition followed by base initiation after a 300 s period. Detergent was added at $t = 210$ s to lyse the vesicles. Error bars represent standard deviations from two repeats.
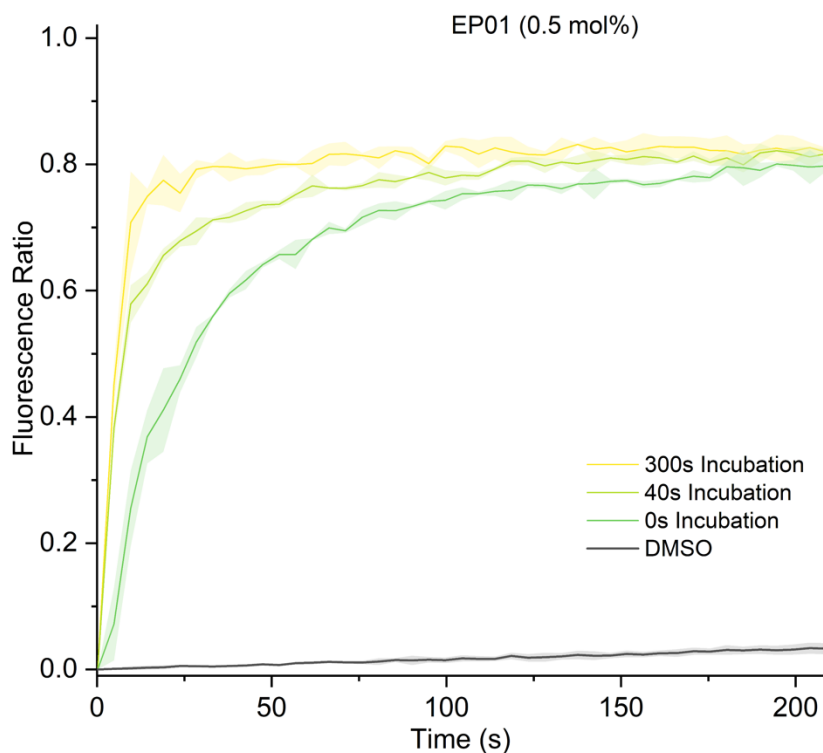
Figure 36: The HPTS efflux plots for compound **2** (0.5 mol%) measured using the KGluc assay under three incubation conditions. Valinomycin (0.05 mol%) were added to the vesicles in each experiment before the addition of **2** and NaOH (5 mM) in various orders. 0 s incubation represents base-first addition followed by protonophore initiation. 40 s incubation represents protonophore-first addition followed by base initiation. 300 s incubation represents protonophore first addition followed by base initiation after a 300 s period. Detergent was added at $t = 210$ s to lyse the vesicles. Error bars represent standard deviations from two repeats.
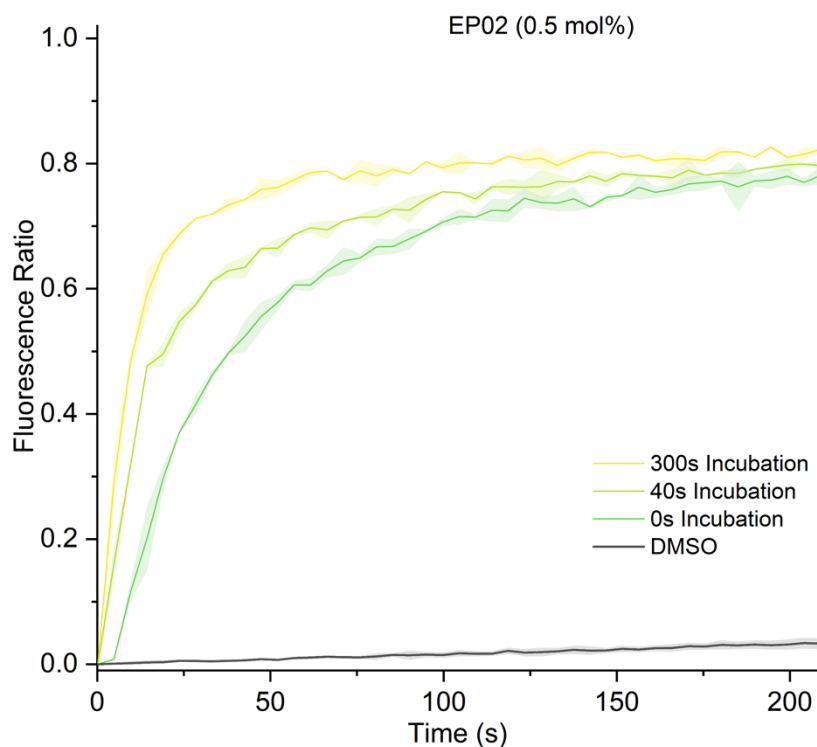
Figure 37: The HPTS efflux plots for compound **3** (0.5 mol%) measured using the KGluc assay under three incubation conditions. Valinomycin (0.05 mol%) were added to the vesicles in each experiment before the addition of **3** and NaOH (5 mM) in various orders. 0 s incubation represents base-first addition followed by protonophore initiation. 40 s incubation represents protonophore-first addition followed by base initiation. 300 s incubation represents protonophore first addition followed by base initiation after a 300 s period. Detergent was added at $t = 210$ s to lyse the vesicles. Error bars represent standard deviations from two repeats.
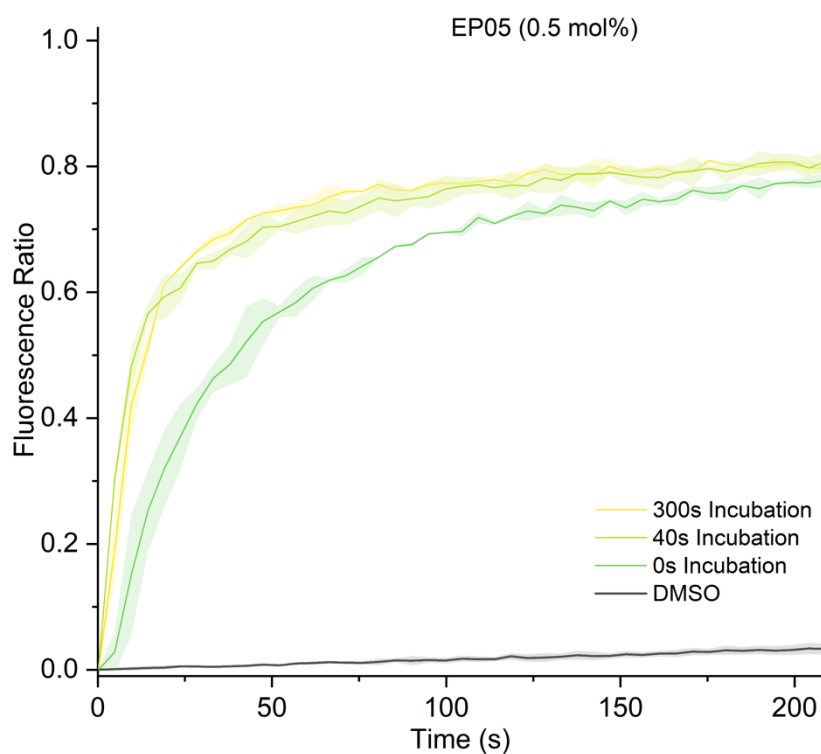
Figure 38: The HPTS efflux plots for compound **4** (0.5 mol%) measured using the KGluc assay under three incubation conditions. Valinomycin (0.05 mol%) were added to the vesicles in each experiment before the addition of **4** and NaOH (5 mM) in various orders. 0 s incubation represents base-first addition followed by protonophore initiation. 40 s incubation represents protonophore-first addition followed by base initiation. 300 s incubation represents protonophore first addition followed by base initiation after a 300 s period. Detergent was added at $t = 210$ s to lyse the vesicles. Error bars represent standard deviations from two repeats.
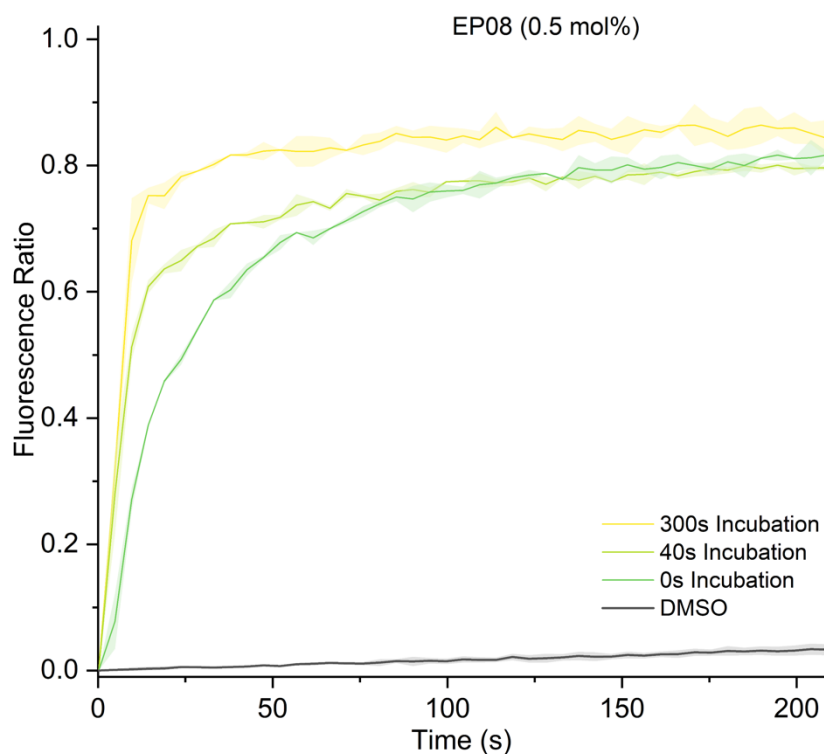
132
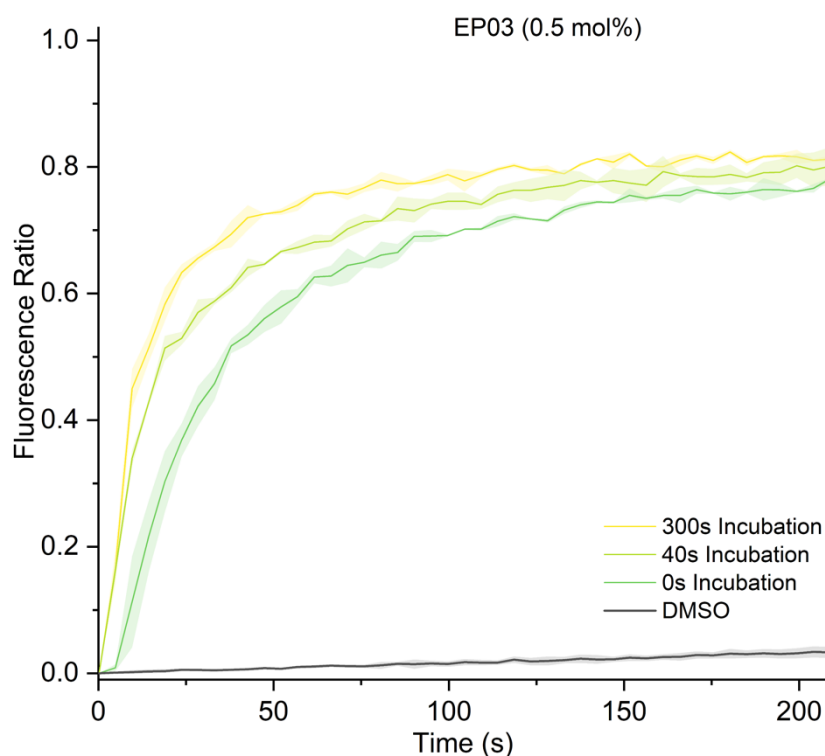
Figure 39: The HPTS efflux plots for compound **5** (0.5 mol%) measured using the KGluc assay under three incubation conditions. Valinomycin (0.05 mol%) were added to the vesicles in each experiment before the addition of **5** and NaOH (5 mM) in various orders. 0 s incubation represents base-first addition followed by protonophore initiation. 40 s incubation represents protonophore-first addition followed by base initiation. 300 s incubation represents protonophore first addition followed by base initiation after a 300 s period. Detergent was added at $t = 210$ s to lyse the vesicles. Error bars represent standard deviations from two repeats.
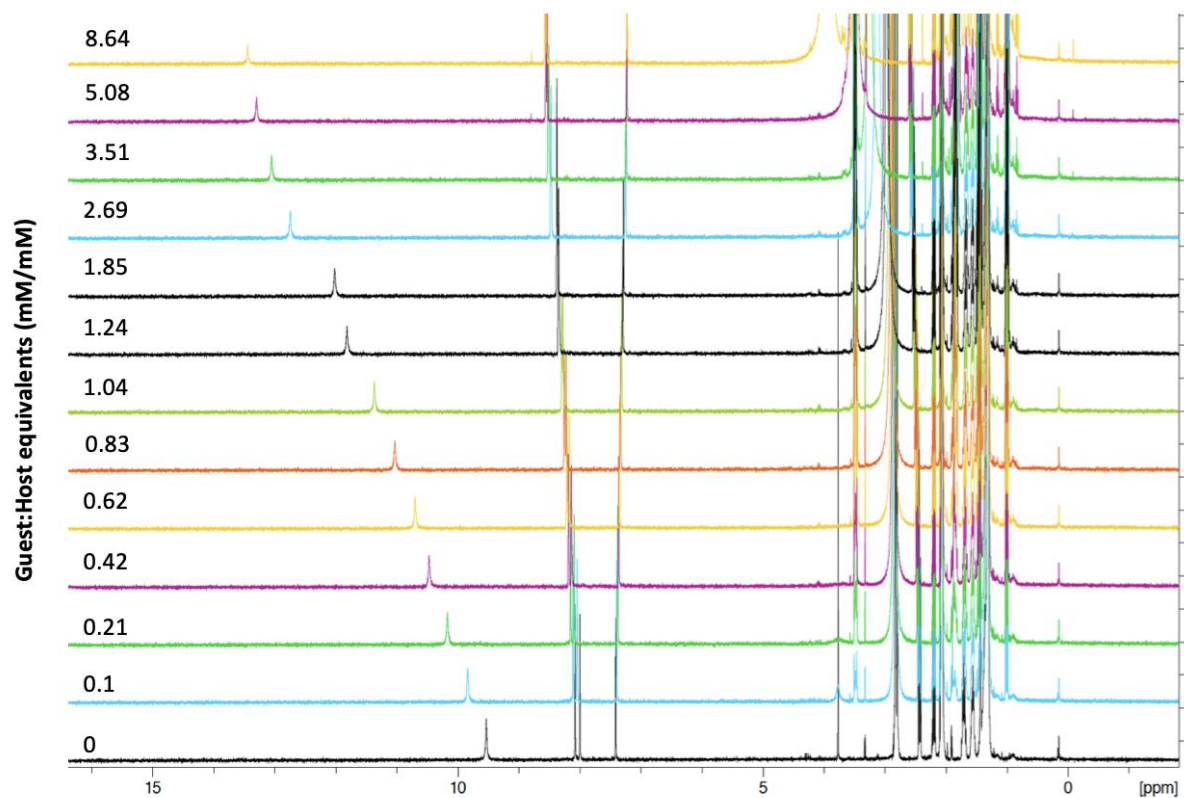
Figure 40: ^{1}H NMR titration spectra as a stack plot for aryl amide ester **1a** + TBAOAc in acetone-*d* at 298 K. OAc[−] binding constant determined was 696.58 M^{−1} calculated by fitting the change in aryl amide N-H chemical shift to a 1:1 binding model on bindfit with changing [OAc[−]] from 0-9 mM/mM equivalents guest/host. Full plot details can be found using the following link: http://app.supramolecular.org/bindfit/view/1514c8b3-3e72-419f-a53d-b7484aa4abab
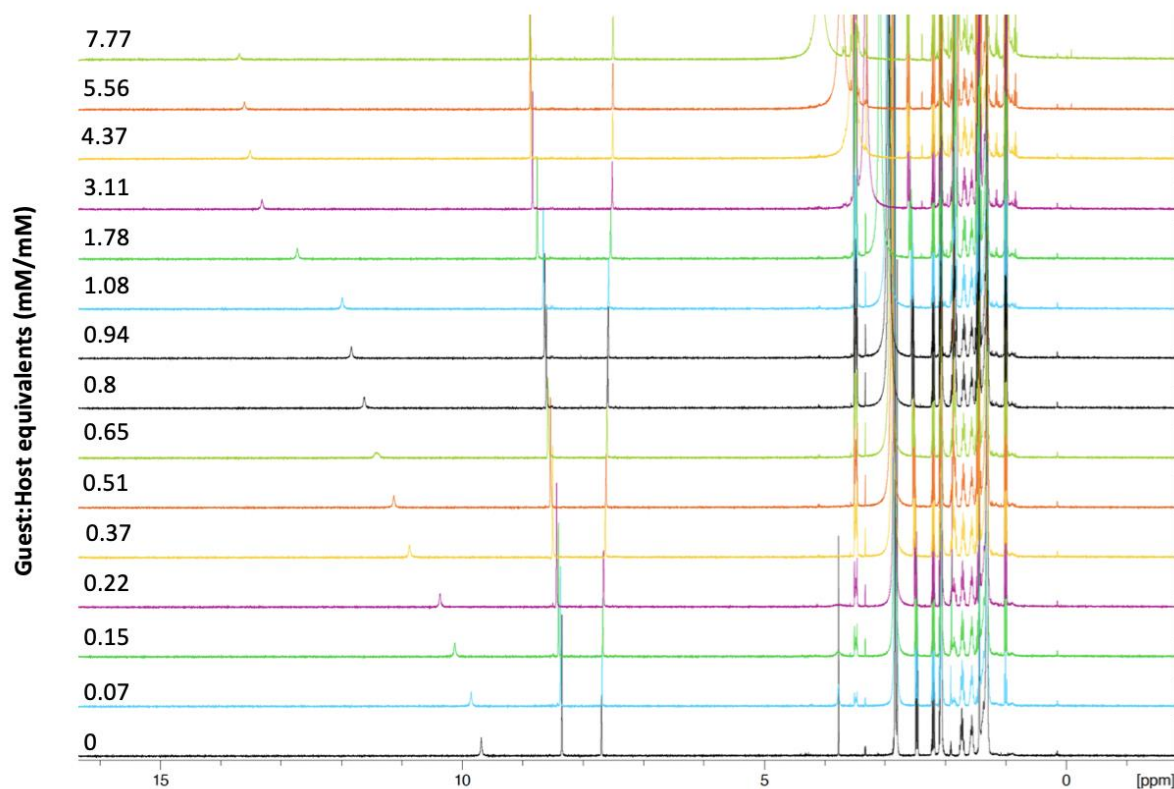
Figure 41: ^{1}H NMR titration spectra as a stack plot for aryl amide ester **2a** + TBAOAc in acetone-*d* at 298 K. OAc$^-$ binding constant determined was 936.59 M^{-1} calculated by fitting the change in aryl amide N-H chemical shift to a 1:1 binding model on bindfit with changing [OAc$^-$] from 0-9 mM/mM equivalents guest/host. Full plot details can be found using the following link: http://app.supramolecular.org/bindfit/view/b82b2376-ca35-417a-bd6e-591a2e05b24e
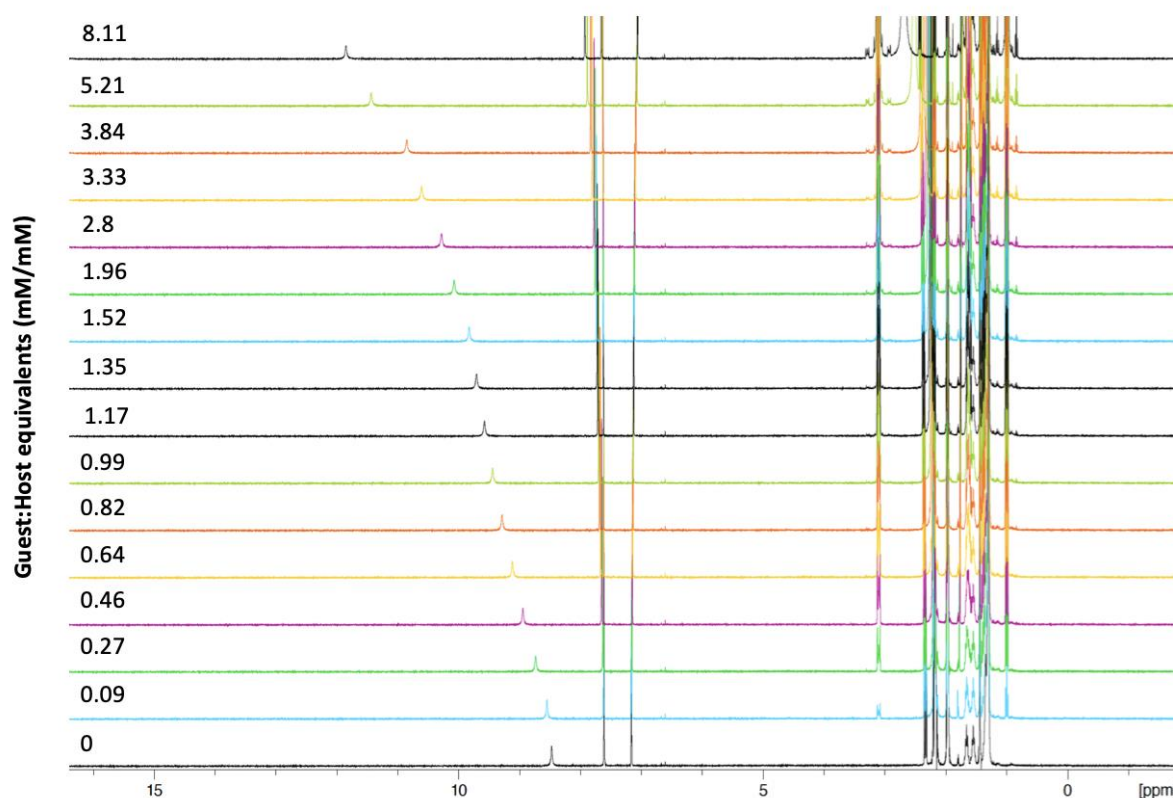
Figure 42: [^1]H NMR titration spectra as a stack plot for aryl amide ester **3a** + TBAOAc in acetone-*d* at 298 K. OAc⁻ binding constant determined was 1306.84 M⁻¹ calculated by fitting the change in aryl amide N-H chemical shift to a 1:1 binding model on bindfit with changing [⁻OAc] from 0-9 mM/mM equivalents guest/host. Full plot details can be found using the following link: http://app.supramolecular.org/bindfit/view/f4dd8115-47ca-4123-b567-0cc5c188e8ba
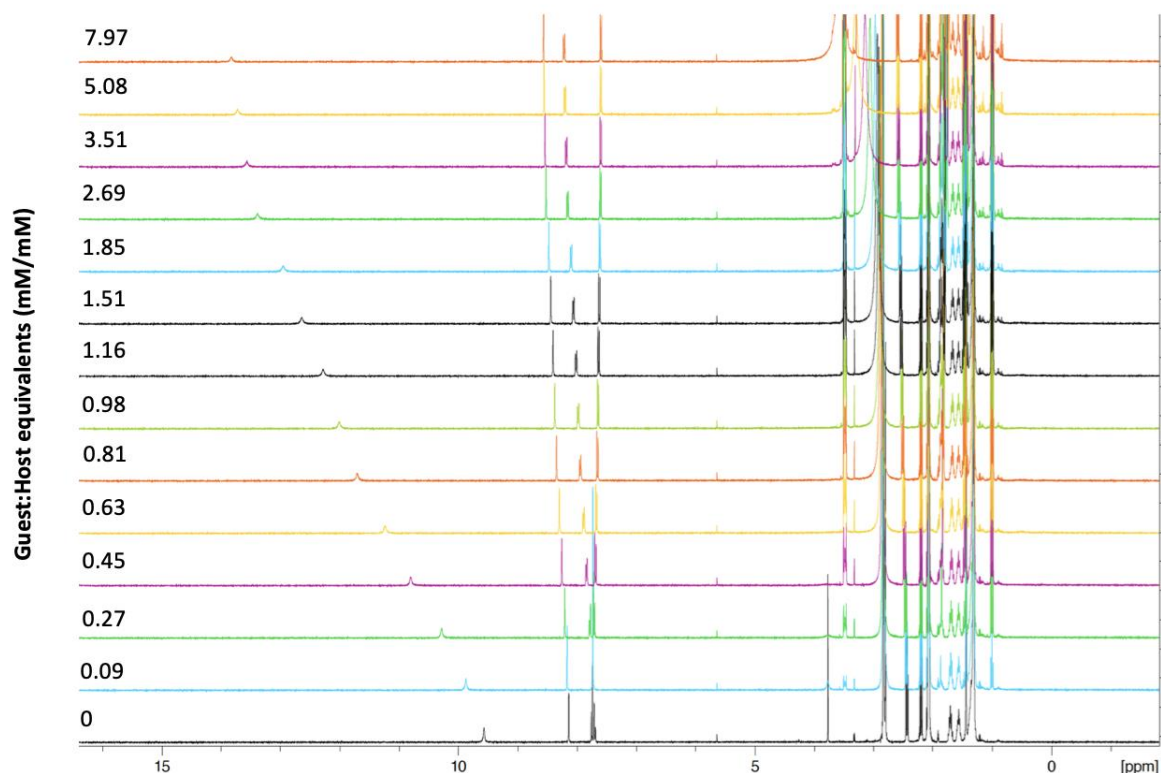
Figure 43: ^{1}H NMR titration spectra as a stack plot for aryl amide ester **4a** + TBAOAc in acetone-*d* at 298 K. OAc⁻ binding constant determined was 818.91 M⁻¹ calculated by fitting the change in aryl amide N-H chemical shift to a 1:1 binding model on bindfit with changing [OAc⁻] from 0-9 mM/mM equivalents guest/host. Full plot details can be found using the following link: http://app.supramolecular.org/bindfit/view/fe0176a1-9258-4168-96f6-a26c6b76e236
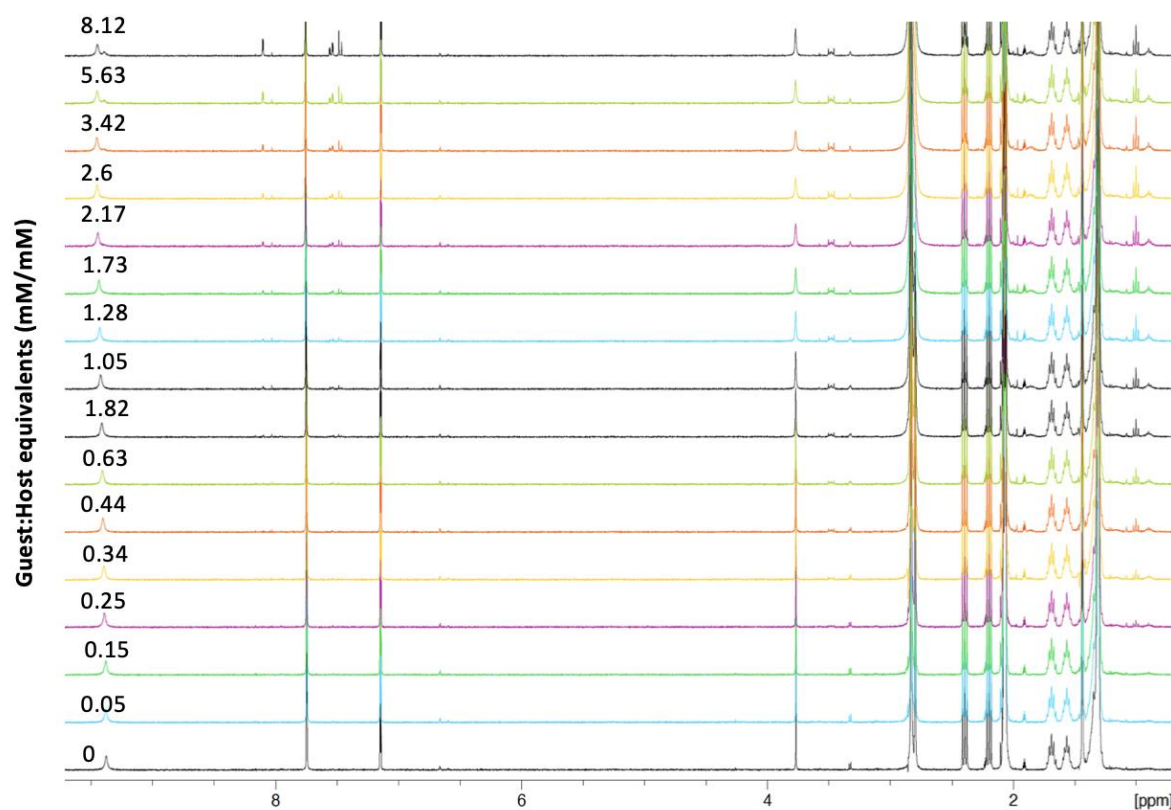
Figure 44: ^{1}H NMR titration spectra as a stack plot for aryl amide ester **5a** + TBAOAc in acetone-*d* at 298 K. OAc⁻ binding constant determined was 936.10 M⁻¹ calculated by fitting the change in aryl amide N-H chemical shift to a 1:1 binding model on bindfit with changing [OAc⁻] from 0-9 mM/mM equivalents guest/host. Full plot details can be found using the following link: http://app.supramolecular.org/bindfit/view/22a84dca-1990-4be8-9bf7-0391e2a25b5a
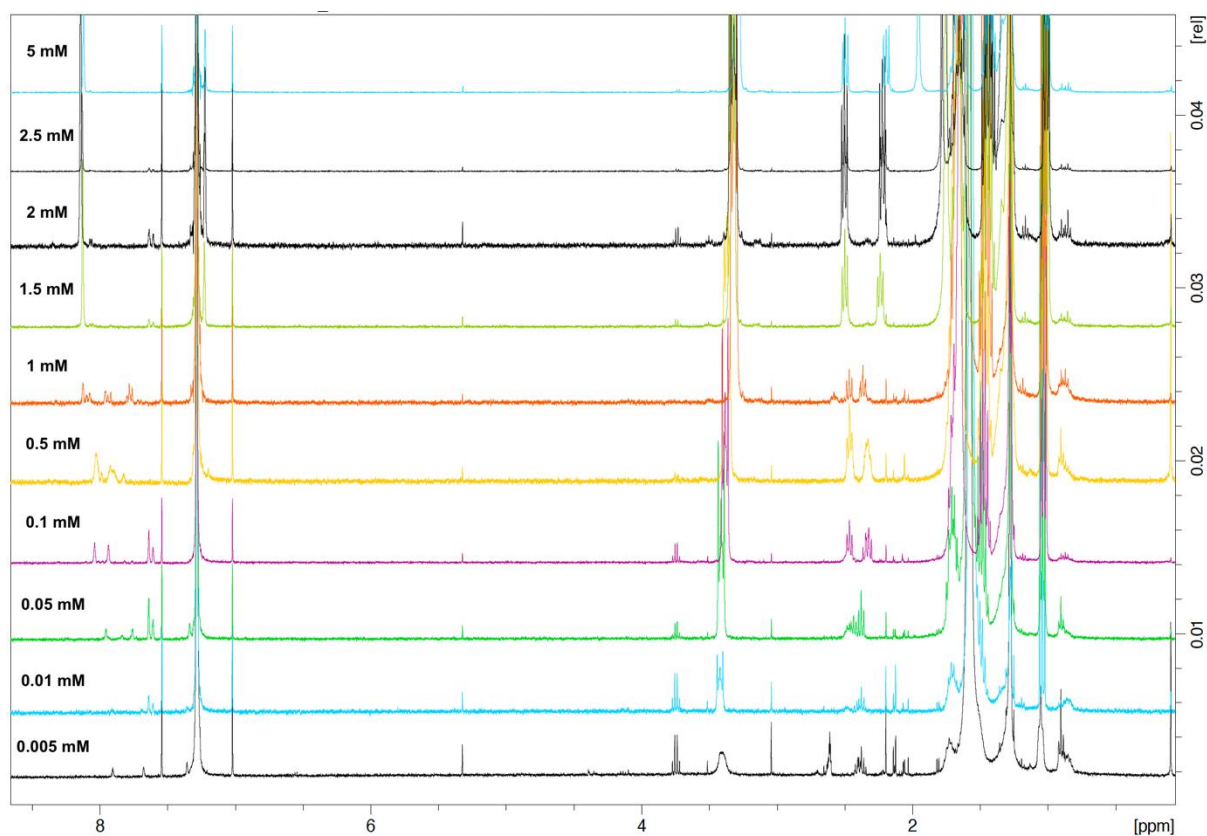
Figure 45: Concentration-dependent ^{1}H NMR titration spectra as a stack plot for aryl amide **1** + TBAOH in CDCl$_3$ at 298 K. Dimerisation constant determined was 8274.73 M^{-1} and calculated by fitting the average chemical shifts of two aromatic C-H peaks to a NMR Dimer Aggregation model on bindfit with concentrations of **1** between 5-0.005 mM.
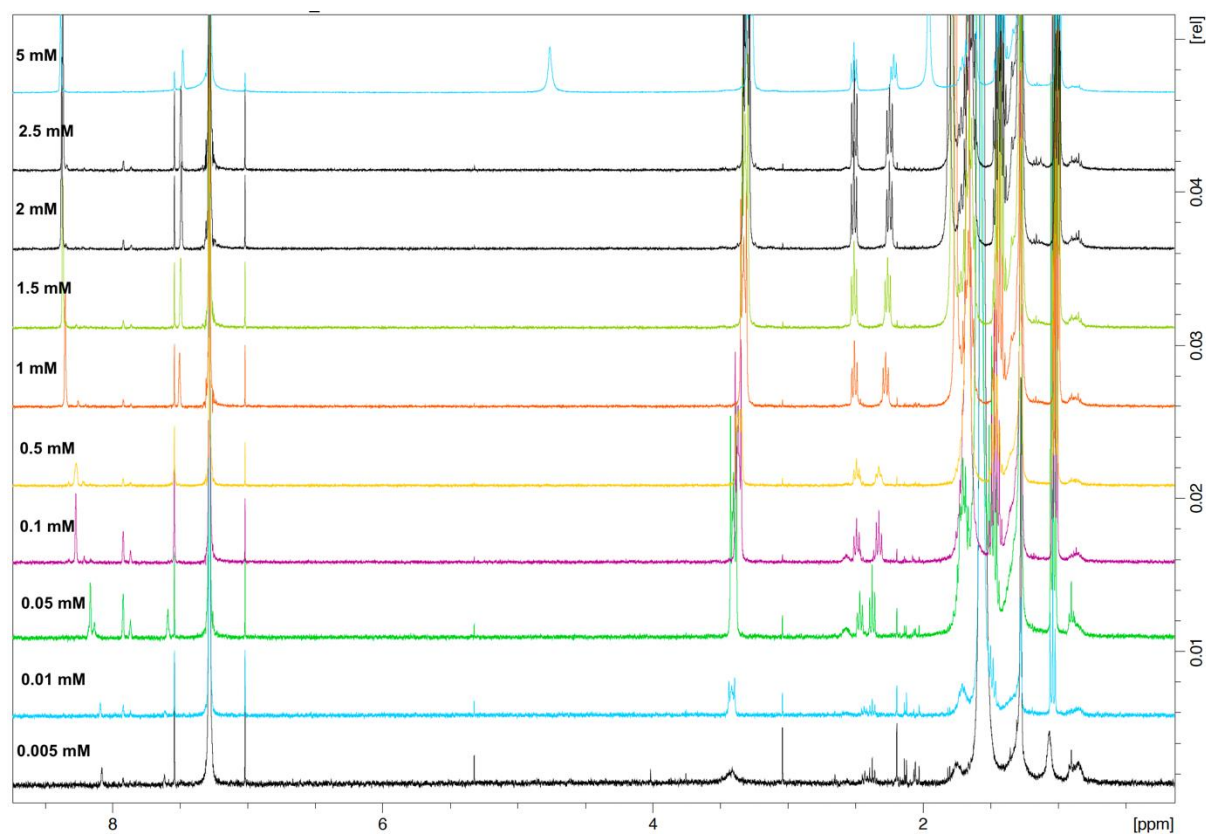
Figure 46: Concentration-dependent ^{1}H NMR titration spectra as a stack plot for aryl amide **2** + TBAOH in CDCl$_3$ at 298 K. Dimerisation constant determined was 8483.76 M^{-1} and calculated by fitting the average chemical shifts of two aromatic C-H peaks to a NMR Dimer Aggregation model on bindfit with concentrations of **2** between 5-0.005 mM.
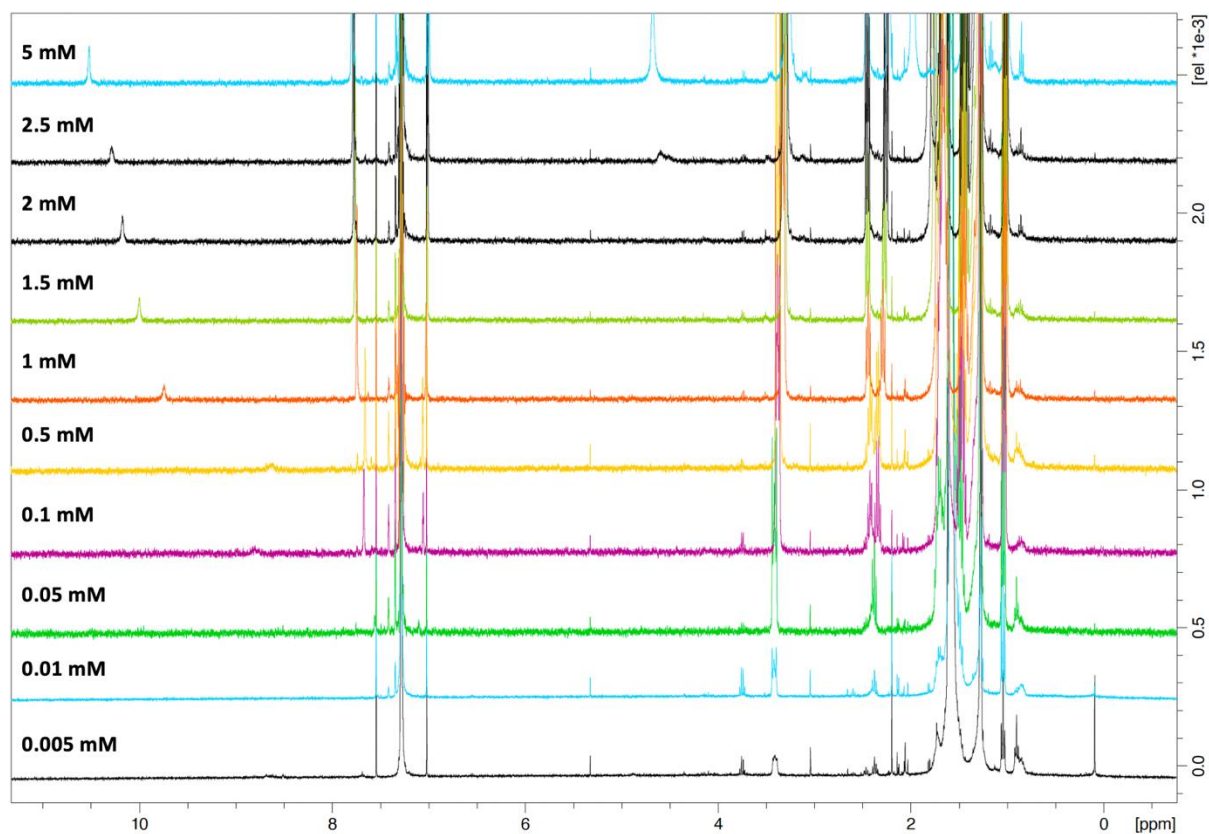
Figure 47: Concentration-dependent ^{1}H NMR titration spectra as a stack plot for aryl amide **3** + TBAOH in CDCl$_3$ at 298 K. Dimerisation constant determined was 9297.37 M^{-1} and calculated by fitting the average chemical shifts of two aromatic C-H peaks to a NMR Dimer Aggregation model on bindfit with concentrations of **3** between 5-0.005 mM.
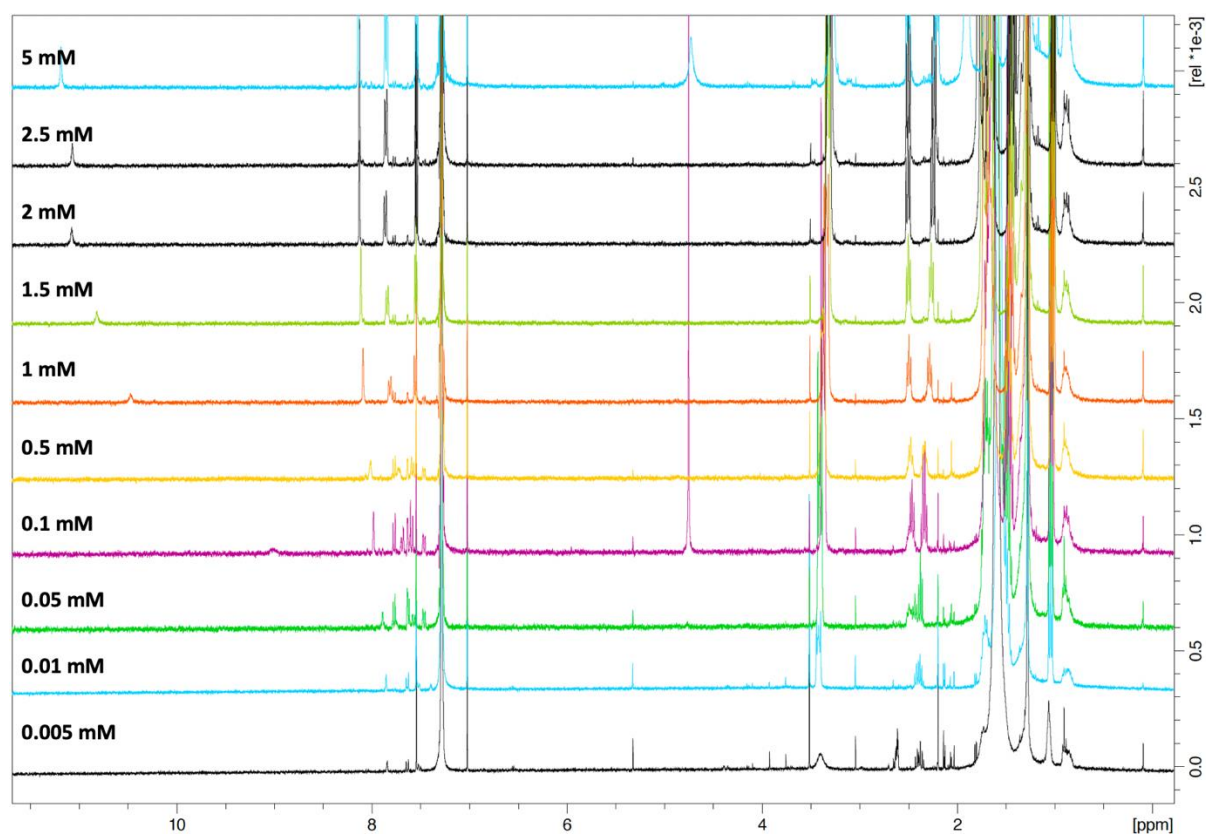
Figure 48: Concentration-dependent ^{1}H NMR titration spectra as a stack plot for aryl amide **4** + TBAOH in CDCl$_3$ at 298 K. Dimerisation constant determined was 2825.96 M^{-1} and calculated by fitting the average chemical shifts of two aromatic C-H peaks to a NMR Dimer Aggregation model on bindfit with concentrations of **4** between 5-0.005 mM.
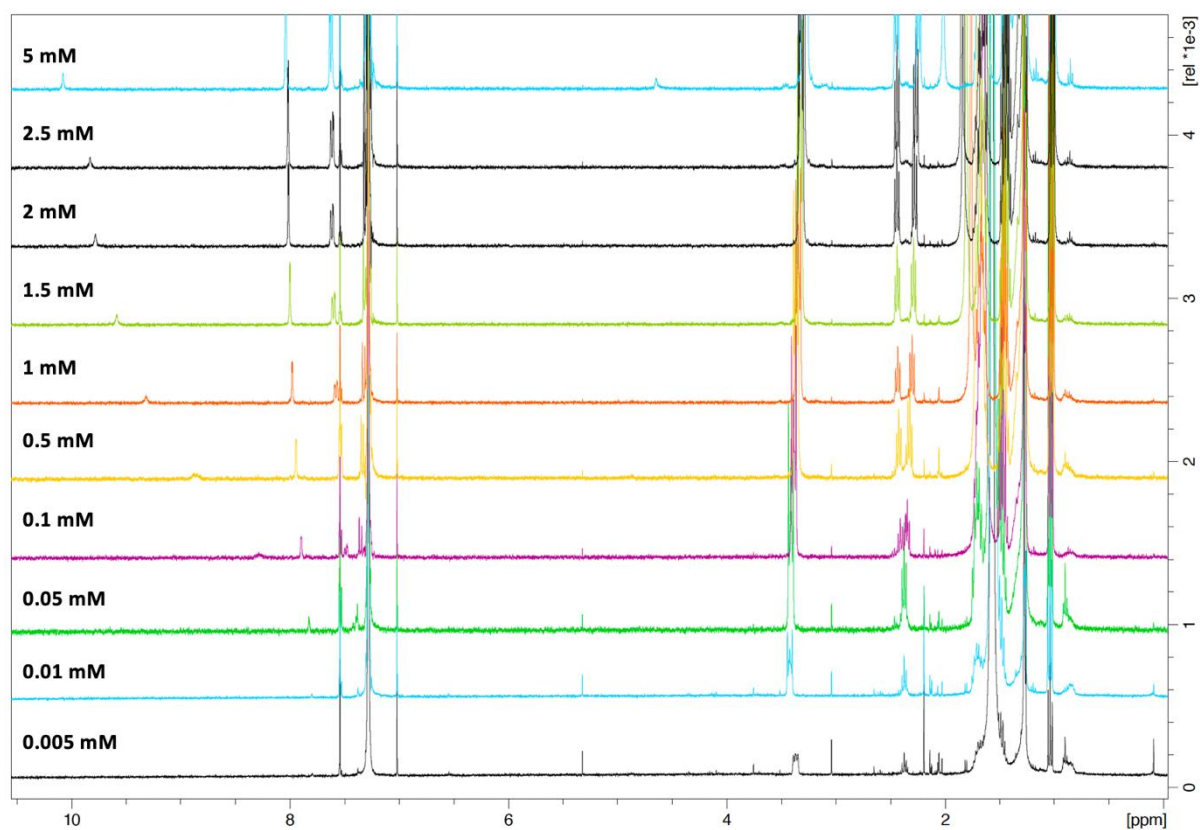
Figure 49: Concentration-dependent ^{1}H NMR titration spectra as a stack plot for aryl amide **5** + TBAOH in CDCl₃ at 298 K. Dimerisation constant determined was 2366.56 M^{-1} and calculated by fitting the average chemical shifts of two aromatic C-H peaks to a NMR Dimer Aggregation model on bindfit with concentrations of **5** between 5-0.005 mM.
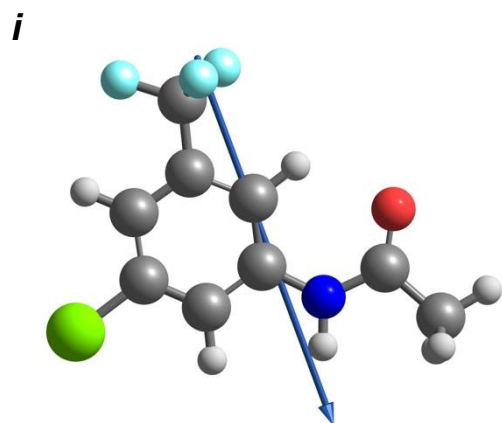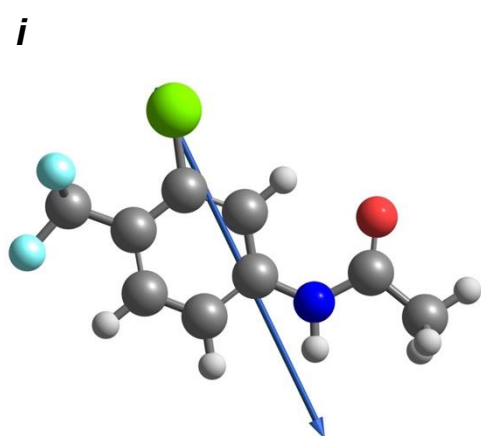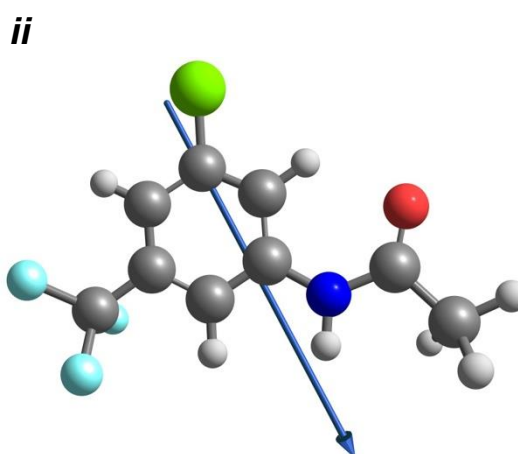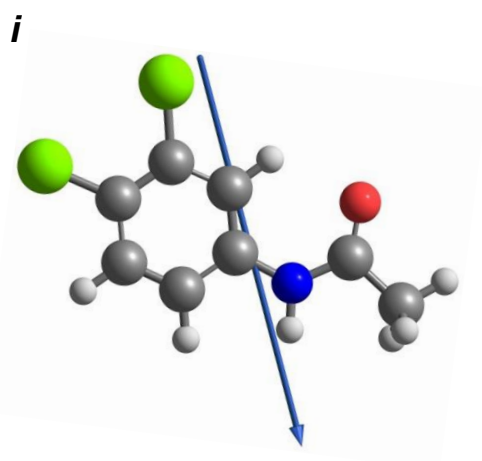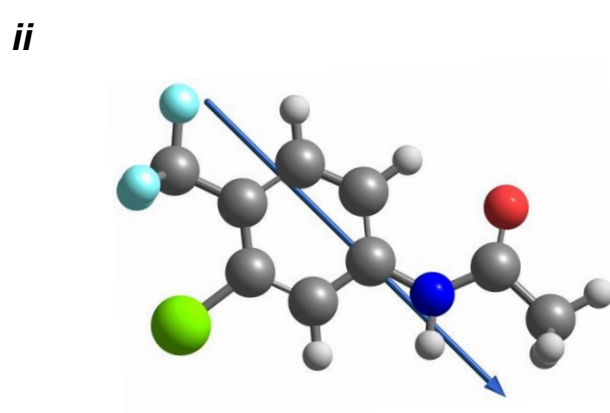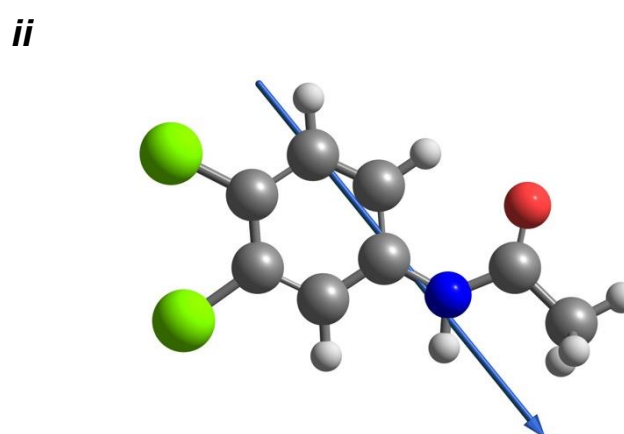
Figure 50: Two possible conformers of aryl amides **1**, **4** and **5** respectively in which their dipole angle relative to the hydrogen bond axis was measured.
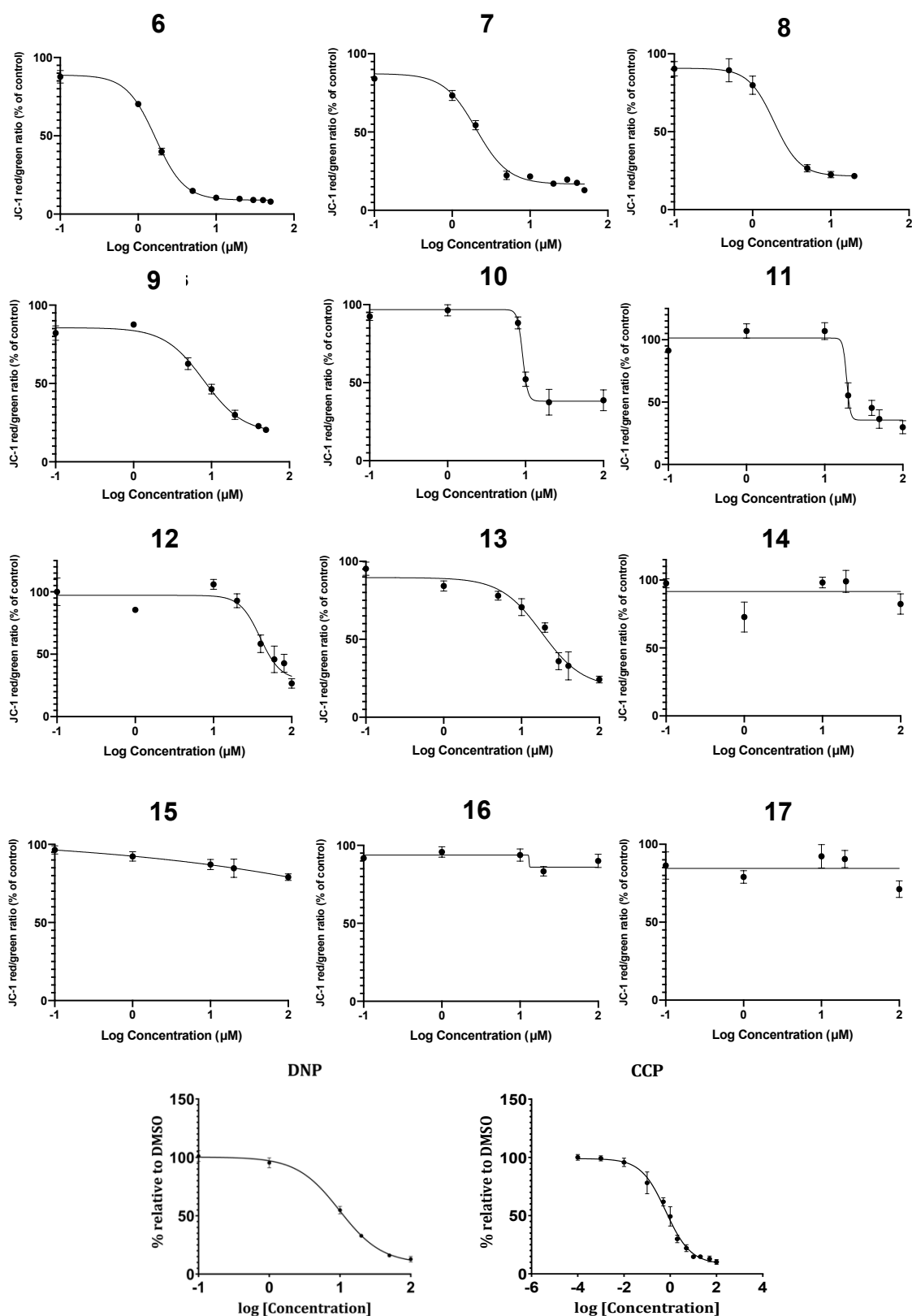
Figure 51: Short chain aryl amides effect on membrane potential. Individual dose-response curves of membrane depolarisation (%) relative to control of L6 rat skeletal muscle cells when treated with aryl amides **6-17** and DNP for 1 hour at concentrations between 0.1 µM to 100

μM using a JC-1 assay. CCCP tested at concentrations of 0.01-100 µM Data represents mean ± SEM of three independent experiments.
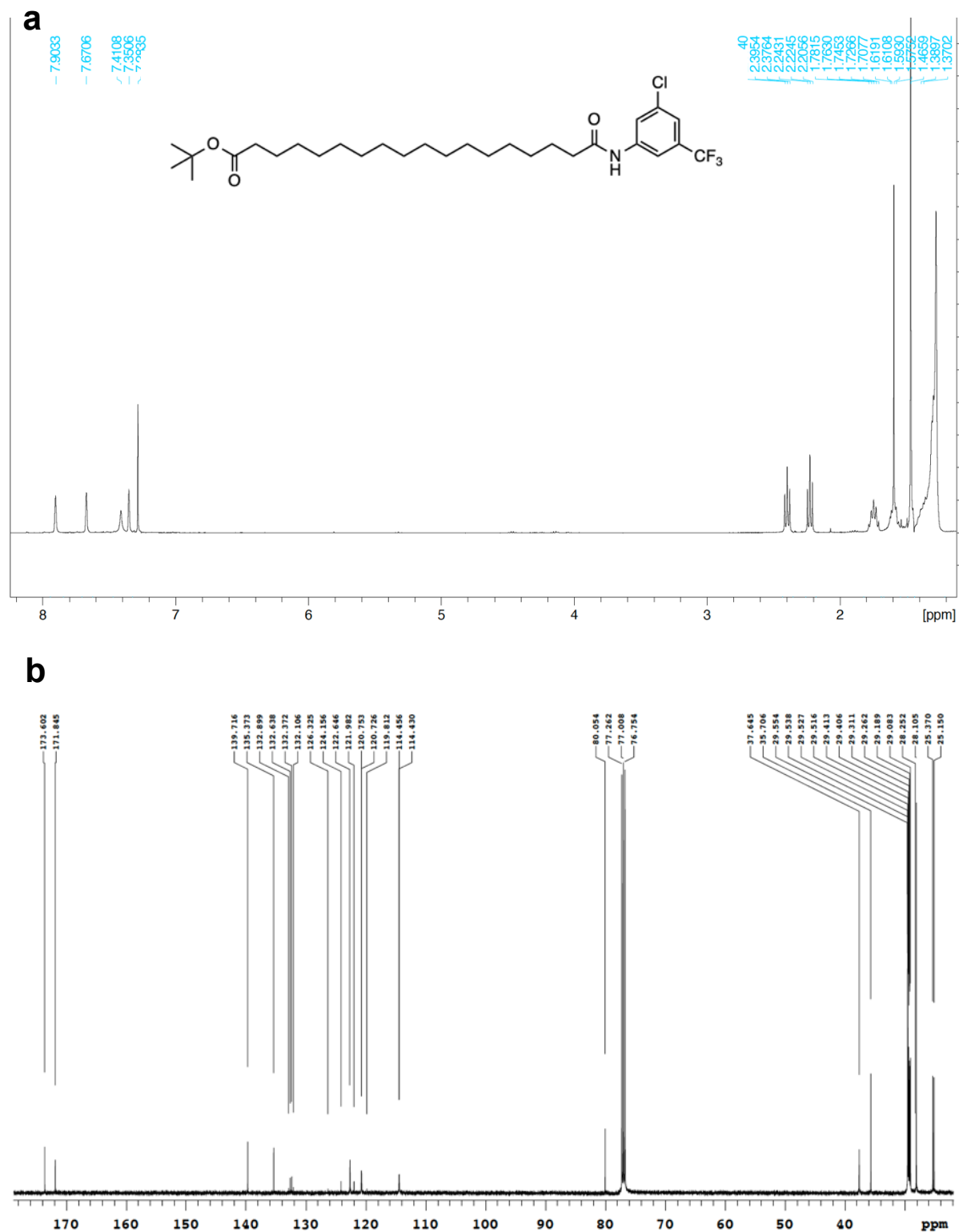
Figure 52: a) ^{1}H NMR spectrum of **1a** (400 MHz, CDCl$_3$). **b)** ^{13}C NMR spectrum of **1a** (125 MHz, CDCl$_3$)

Figure 53: a) ^{1}H NMR spectrum of **1** (500 MHz, DMSO-d_6). **b)** ^{13}C NMR spectrum of **1** (125 MHz, DMSO-d_6)
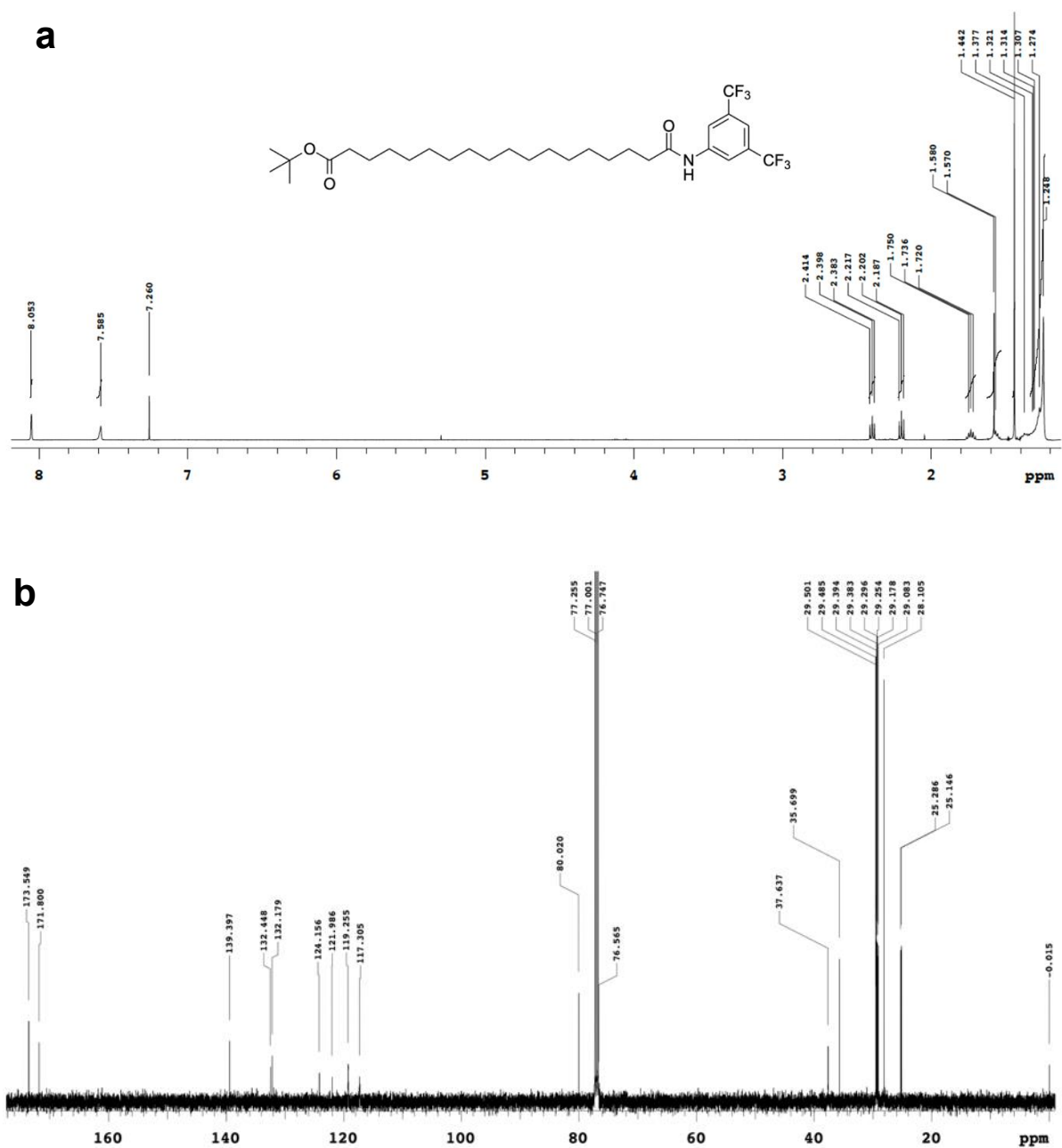
Figure 54: a) ^{1}H NMR spectrum of **2a** (400 MHz, CDCl$_3$). **b)** ^{13}C NMR spectrum of **2a** (125 MHz, CDCl$_3$)
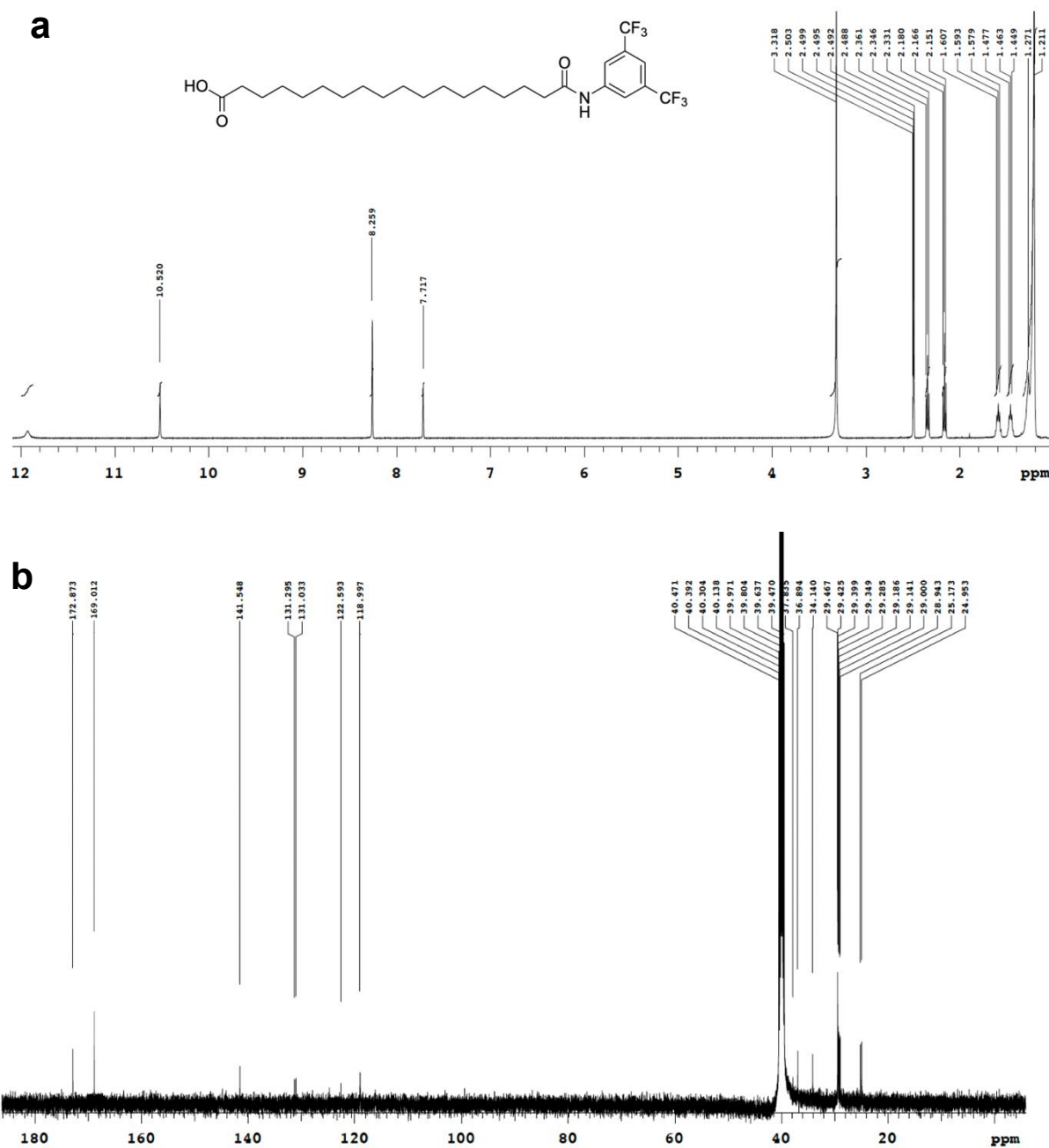
Figure 55: a) ^{1}H NMR spectrum of **2** (400 MHz, DMSO-d_6). **b)** ^{13}C NMR spectrum of **2** (500 MHz, DMSO-d_6).
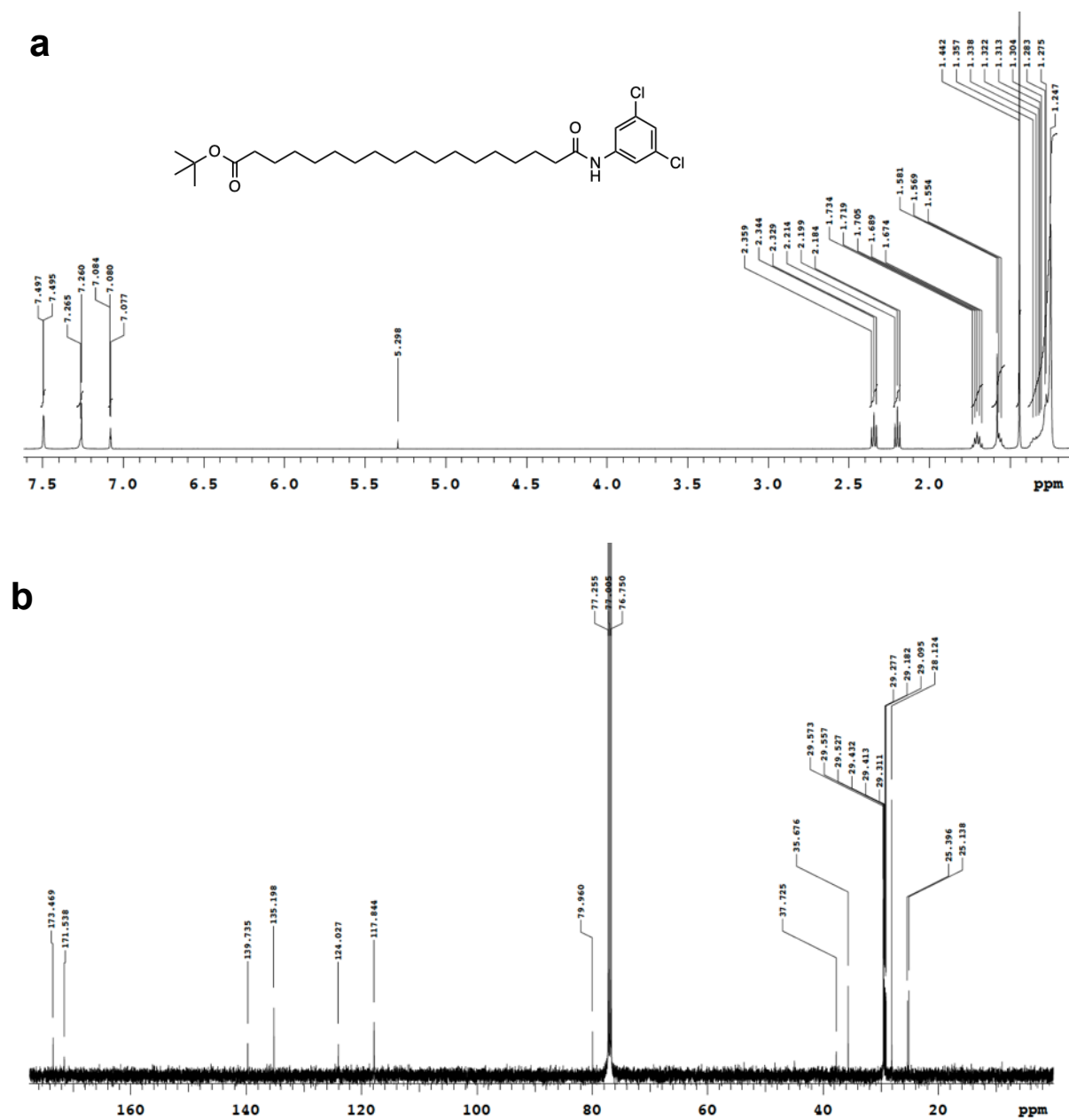
Figure 56: a) ^{1}H NMR spectrum of **3a** (400 MHz, CDCl$_3$). **b)** ^{13}C NMR spectrum of **3a** (500 MHz, CDCl$_3$).
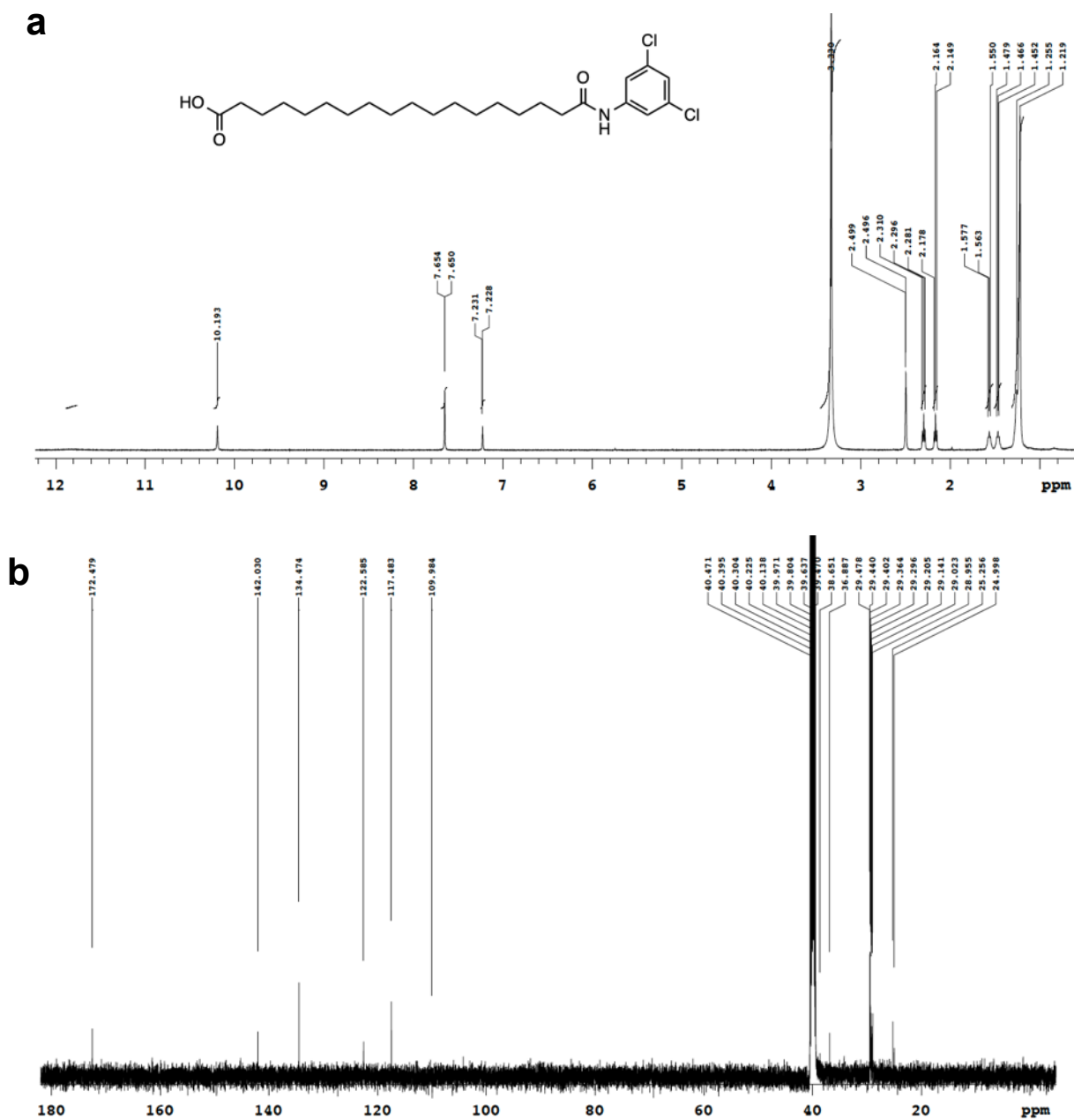
Figure 57: a) ^{1}H NMR spectrum of **3** (400 MHz, DMSO-d_6). **b)** ^{13}C NMR spectrum of **3** (500 MHz, DMSO-d_6).

a

b
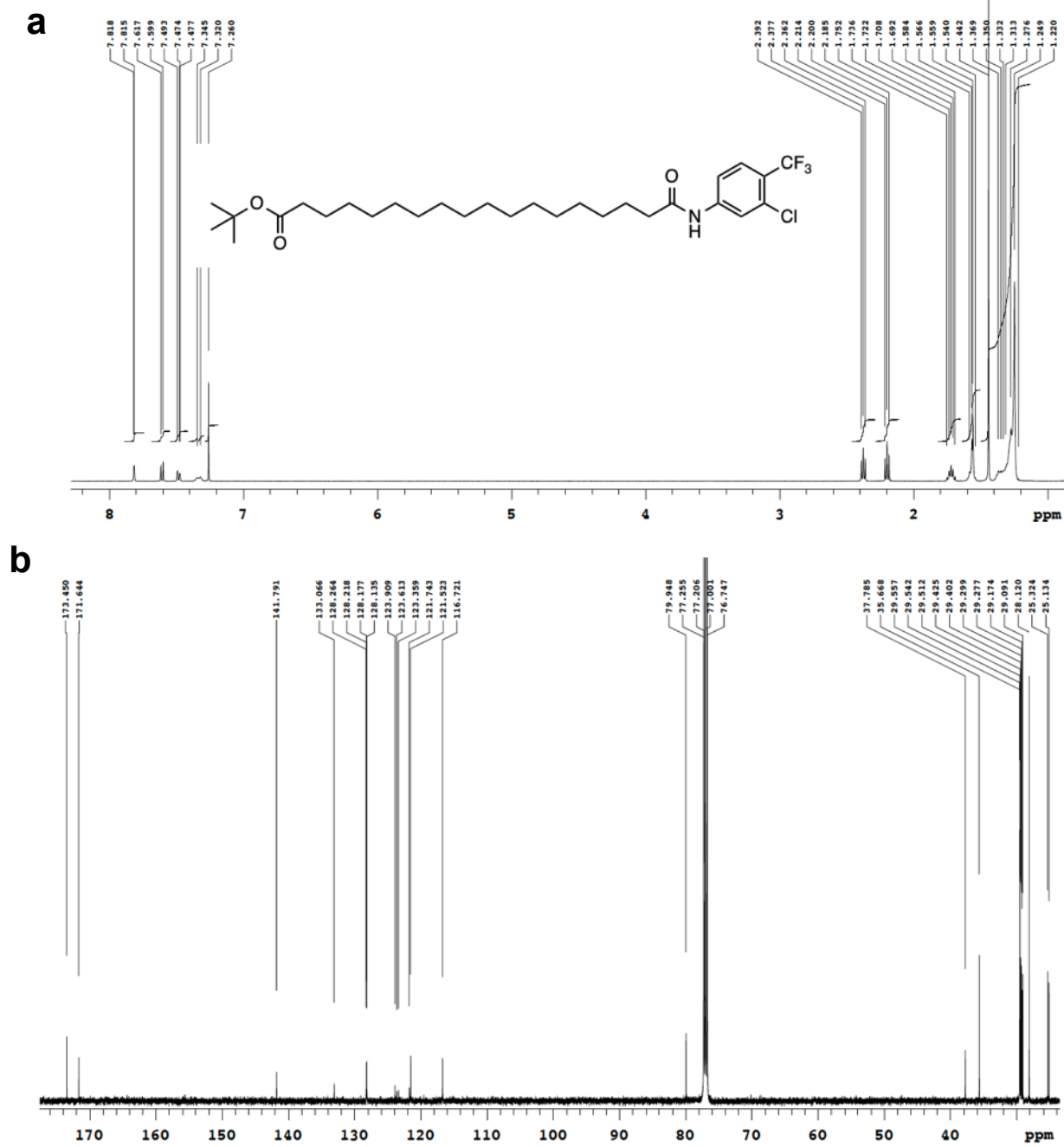
Figure 58: a) ^{1}H NMR spectrum of **4a** (400 MHz, CDCl$_3$). b) ^{13}C NMR spectrum of **4a** (500 MHz, CDCl$_3$).

Figure 59: a) ^{1}H NMR spectrum of **4** (500 MHz, DMSO-d_6). **b)** ^{13}C NMR spectrum of **4** (500 MHz, DMSO-d_6).
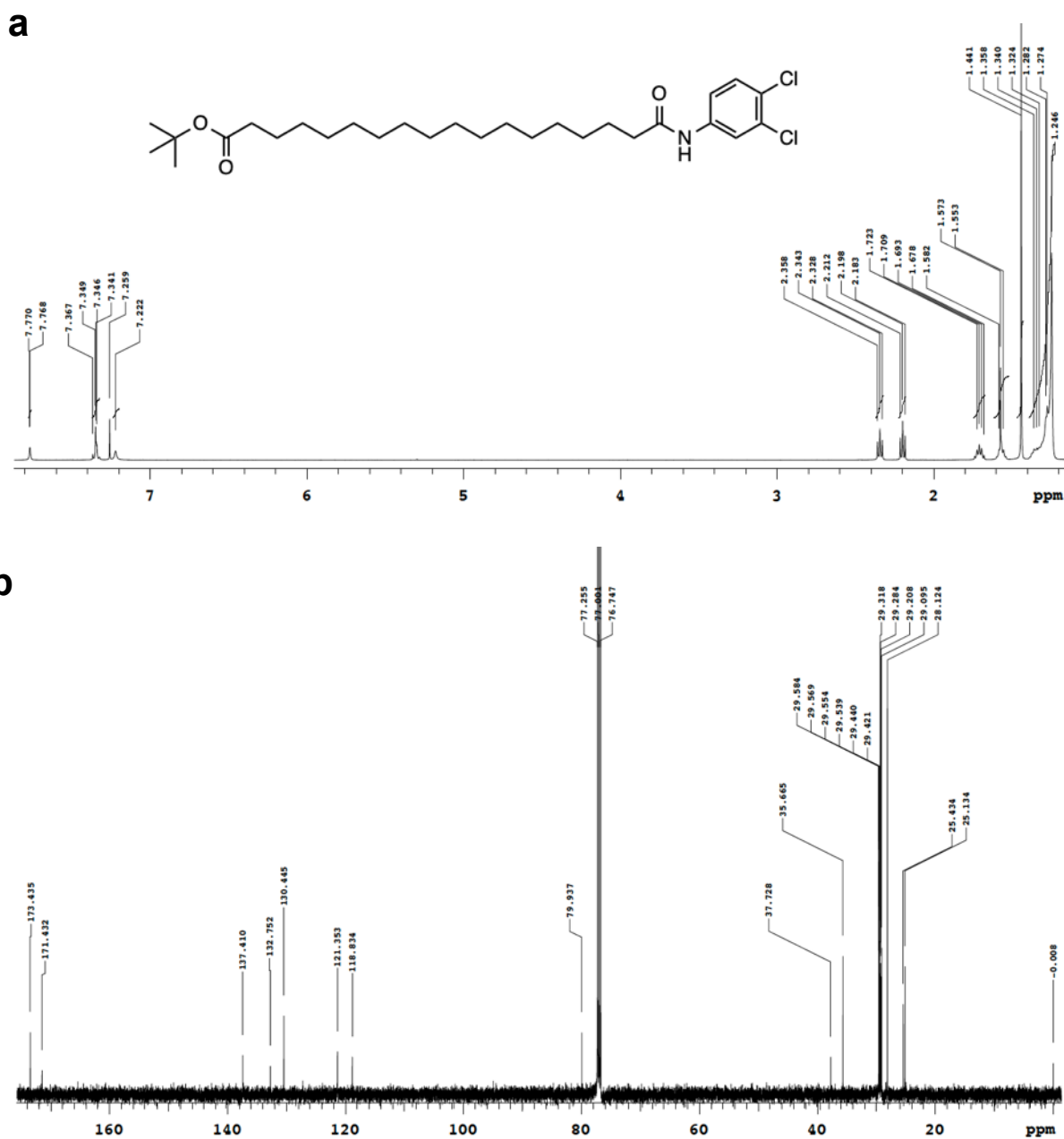
Figure 60: a) ^{1}H NMR spectrum of **5a** (500 MHz, CDCl$_3$). **b)** ^{13}C NMR spectrum of **5a** (500 MHz, CDCl$_3$).
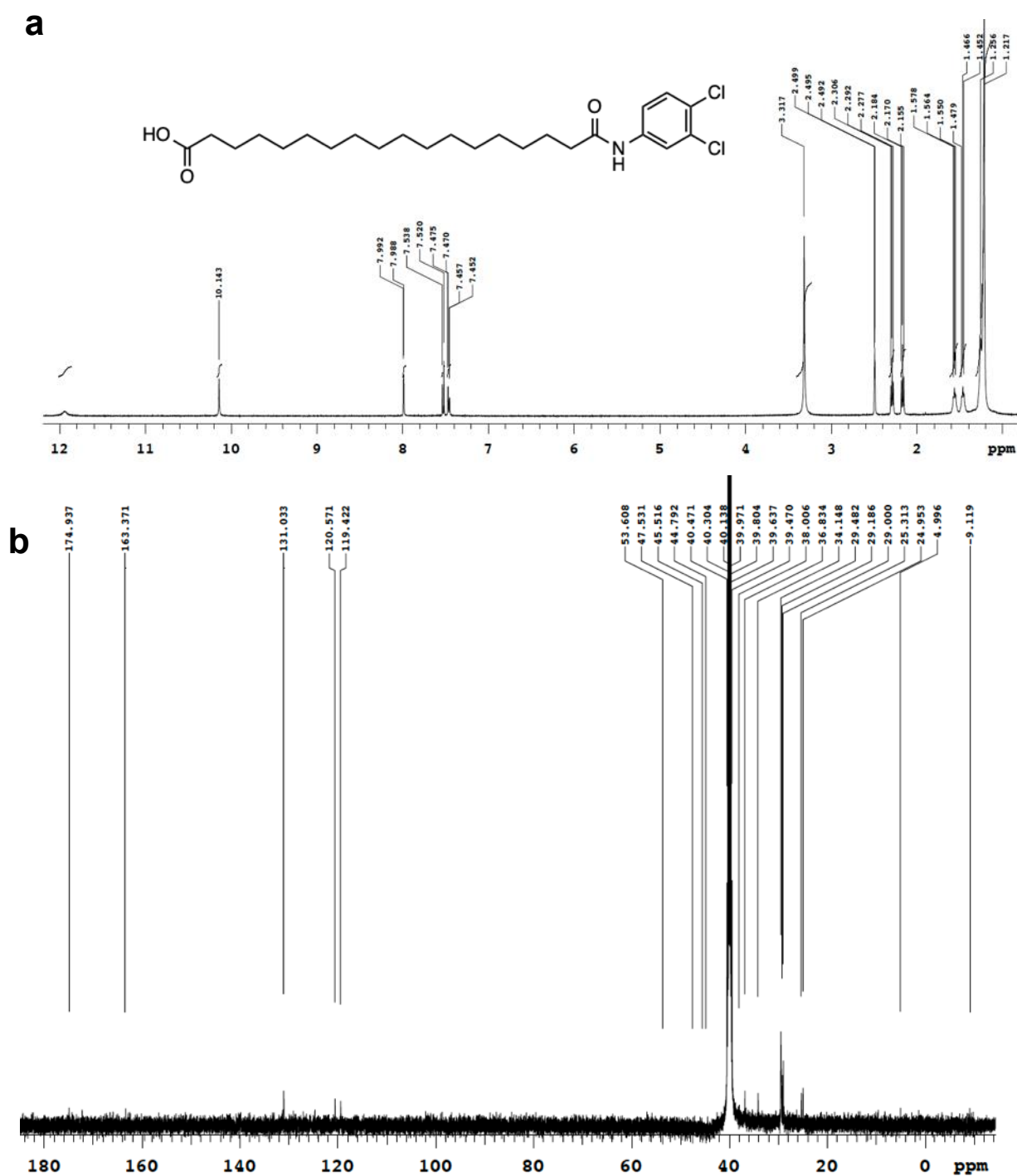
Figure 61: a) ^{1}H NMR spectrum of **5** (500 MHz, DMSO-d_6). **b)** ^{13}C NMR spectrum of **5** (500 MHz, DMSO-d_6).
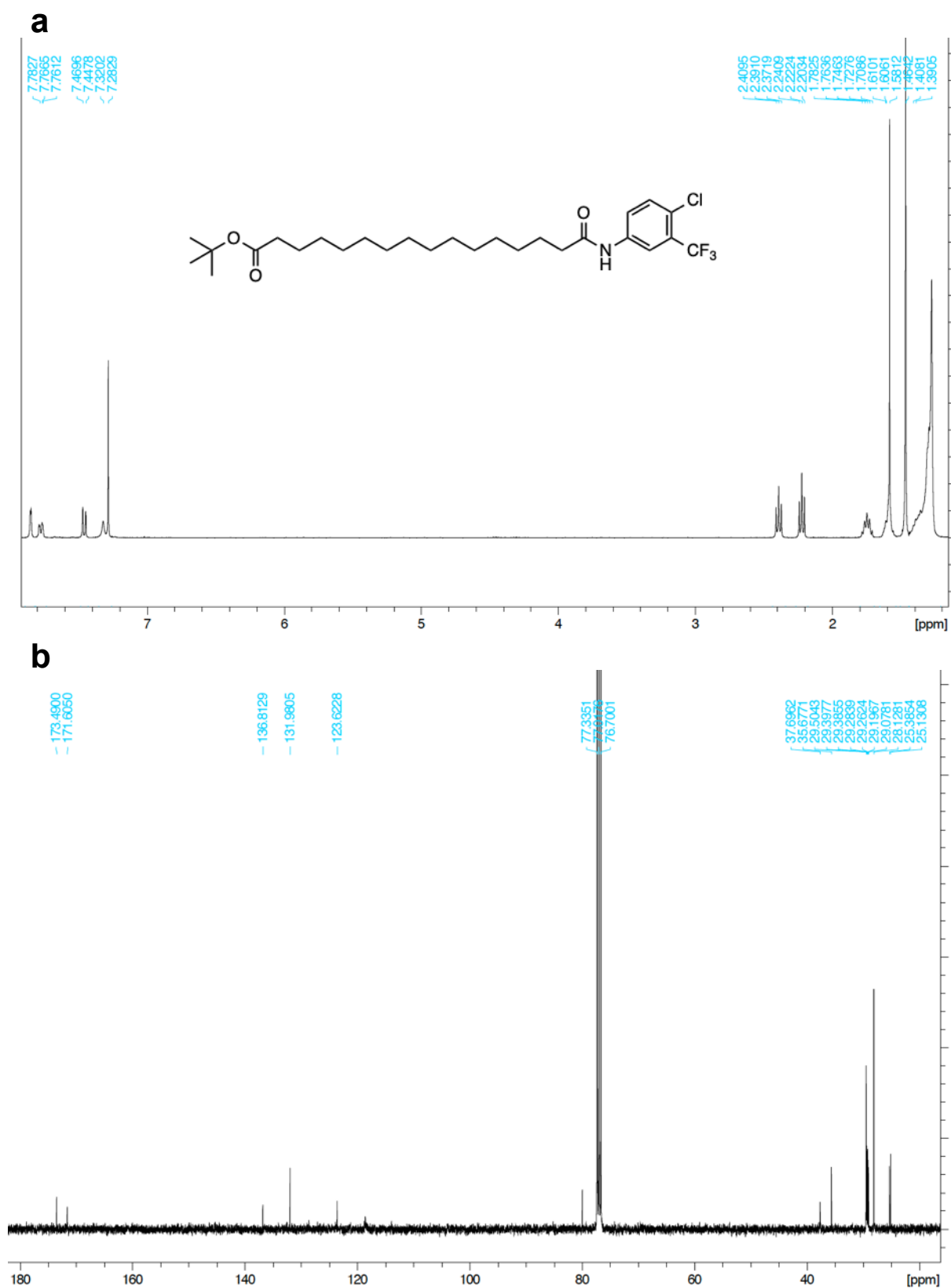
Figure 62: a) ^{1}H NMR spectrum of **6a** (500 MHz, CDCl$_3$). **b)** ^{13}C NMR spectrum of **6a** (500 MHz, CDCl$_3$).

Figure 63: a) ^{1}H NMR spectrum of **6** (500 MHz, DMSO-d_6). **b)** ^{13}C NMR spectrum of **6** (500 MHz, DMSO-d_6).
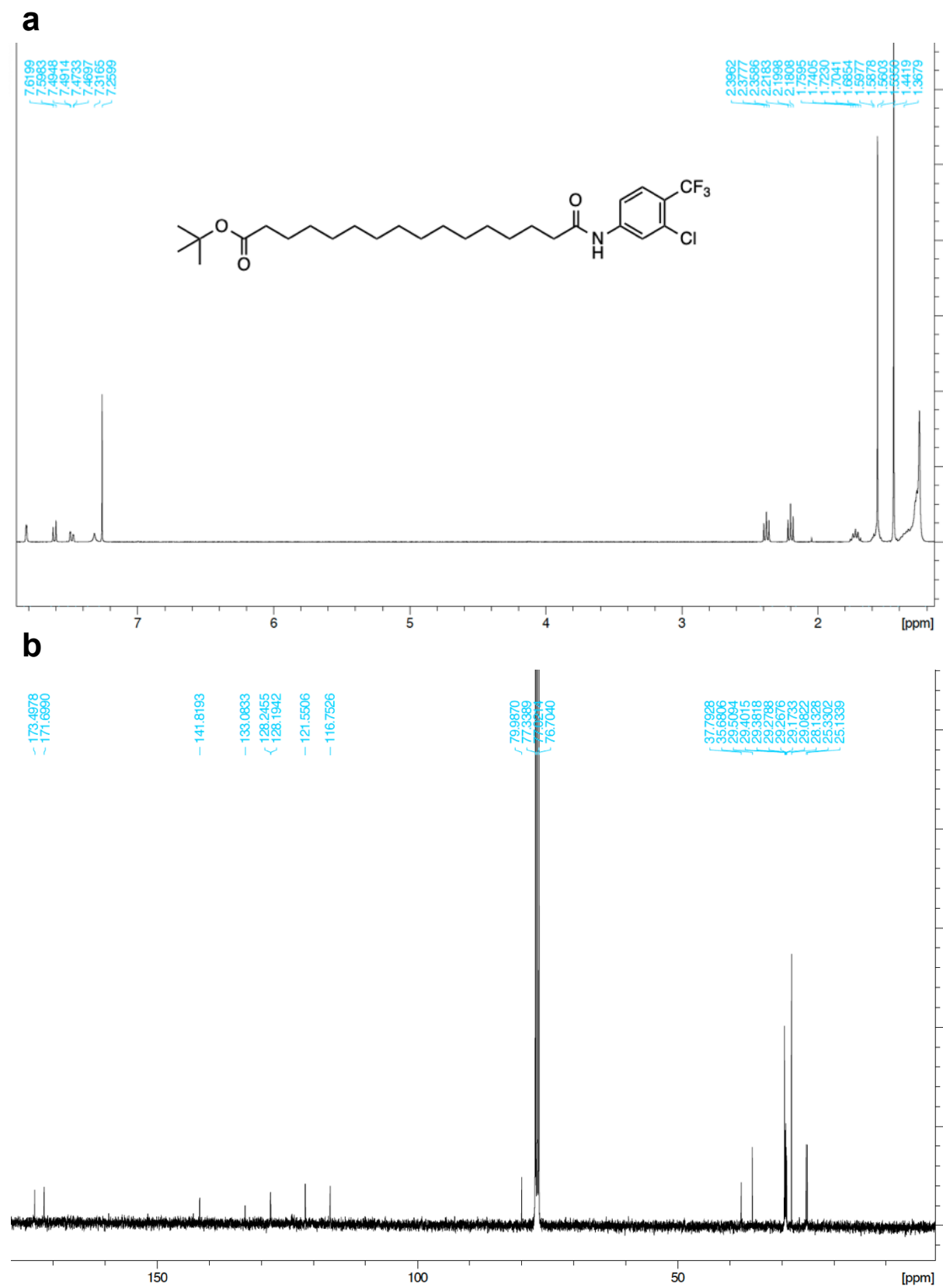
Figure 64: a) ^{1}H NMR spectrum of **7a** (500 MHz, CDCl$_3$). **b)** ^{13}C NMR spectrum of **7a** (500 MHz, CDCl$_3$).
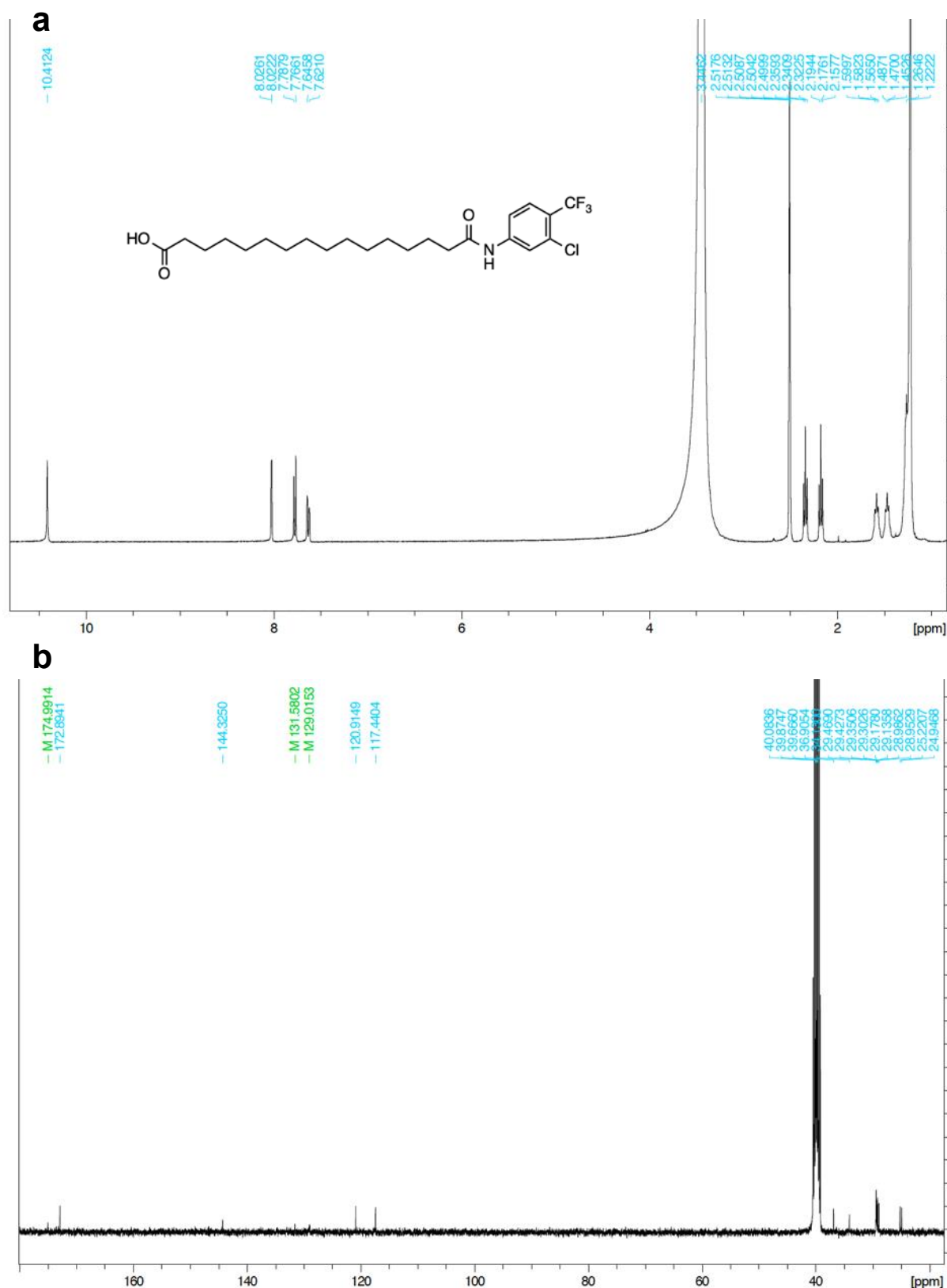
Figure 65: a) ^{1}H NMR spectrum of **7** (500 MHz, DMSO-d_6). **b)** ^{13}C NMR spectrum of **7** (500 MHz, DMSO-d_6).
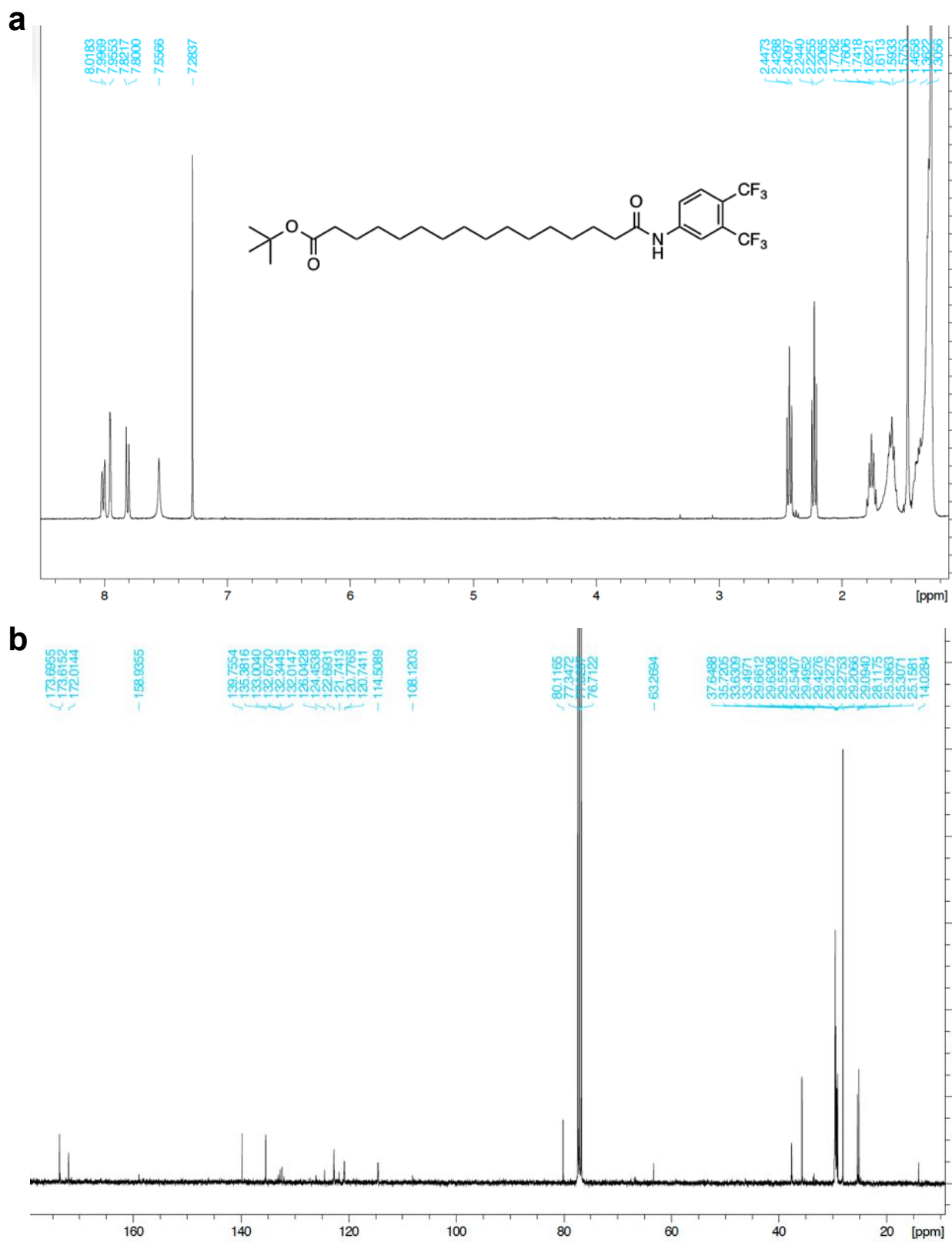
Figure 66: a) ^{1}H NMR spectrum of **8a** (500 MHz, CDCl$_3$). **b)** ^{13}C NMR spectrum of **8a** (500 MHz, CDCl$_3$).
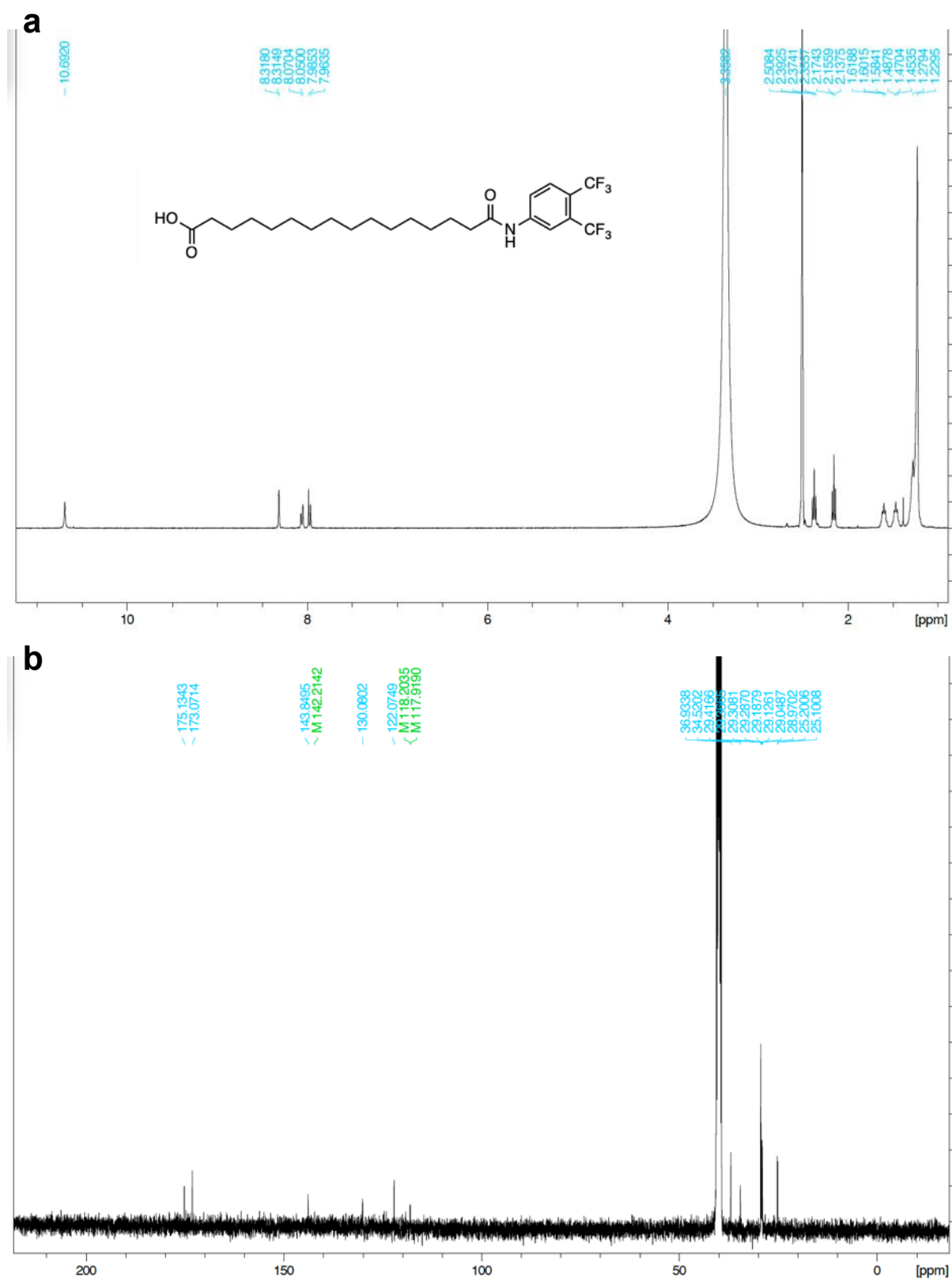
Figure 67: a) ^{1}H NMR spectrum of **8** (500 MHz, DMSO-d_6). **b)** ^{13}C NMR spectrum of **8** (500 MHz, DMSO-d_6).
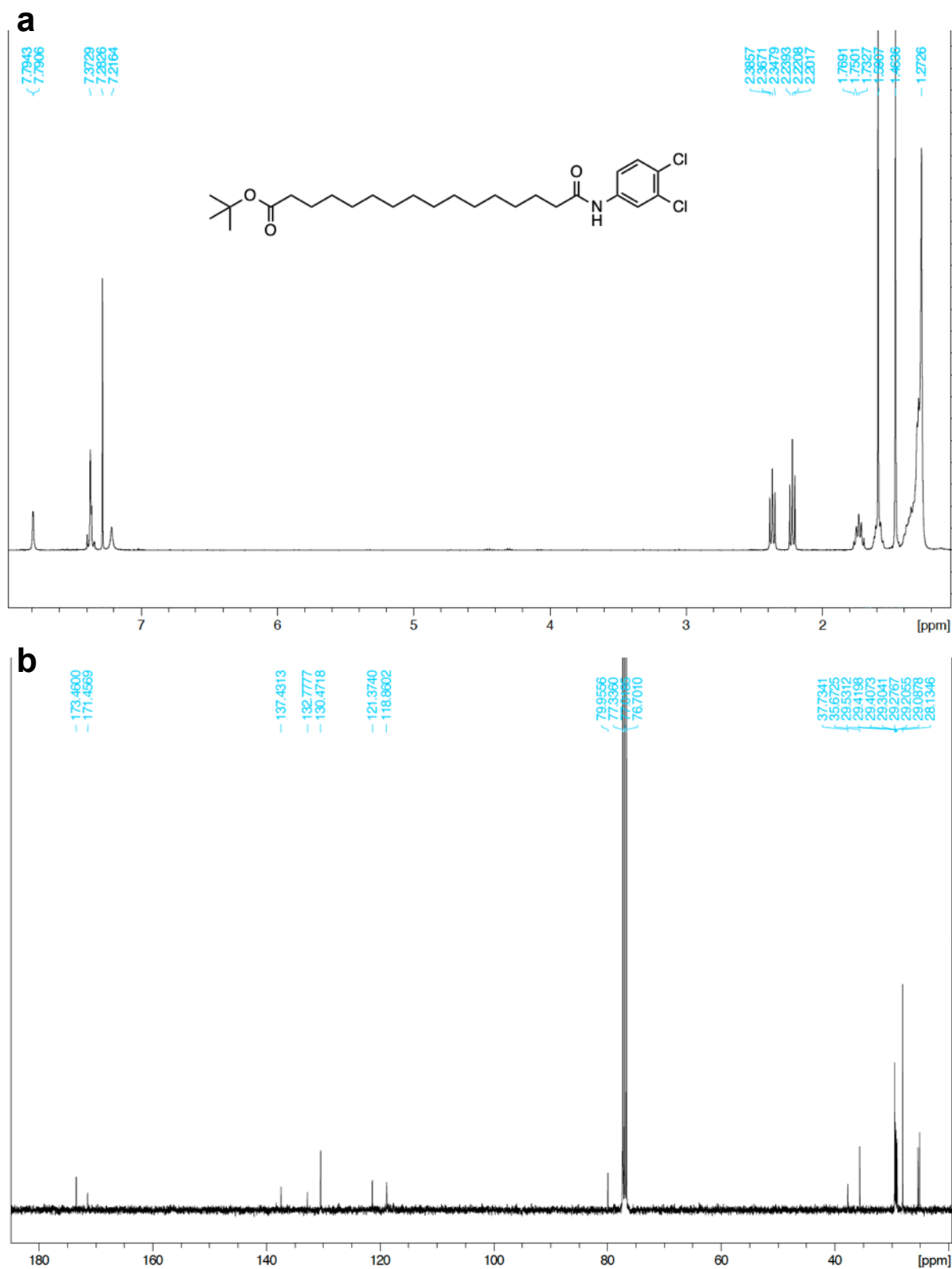
Figure 68: a) ^{1}H NMR spectrum of **9a** (500 MHz, CDCl$_3$). **b)** ^{13}C NMR spectrum of **9a** (500 MHz, CDCl$_3$).

Figure 69: a) ^{1}H NMR spectrum of **9** (500 MHz, DMSO-d_6). **b)** ^{13}C NMR spectrum of **9** (500 MHz, DMSO-d_6).
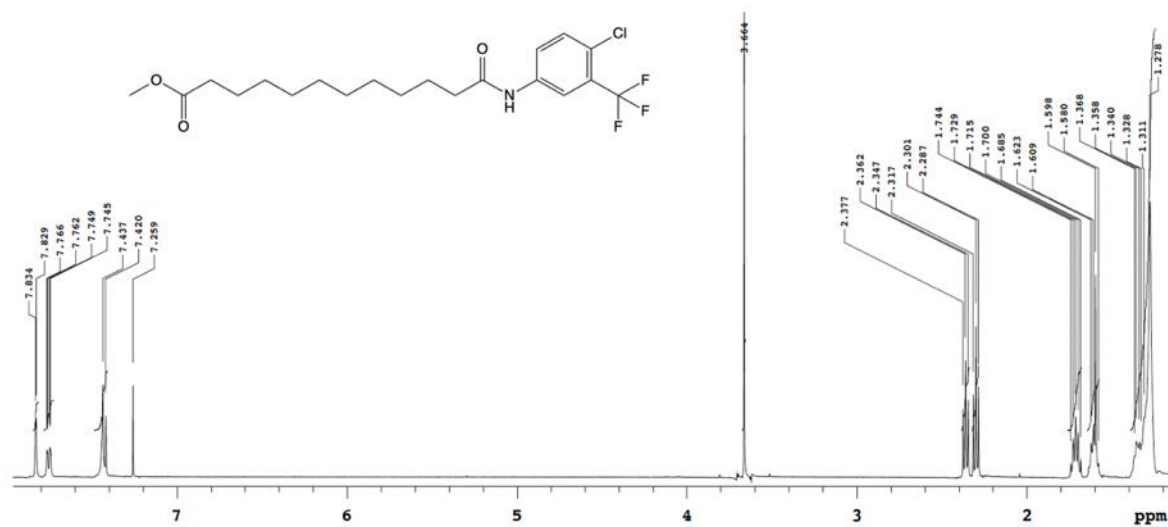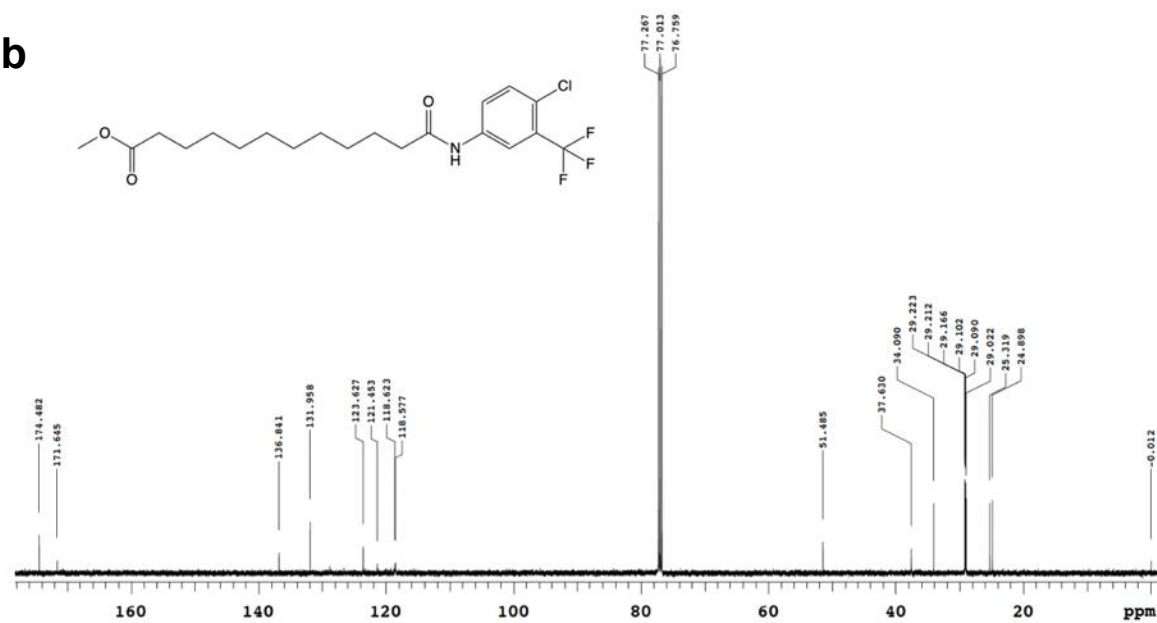
Figure 70: a) ^{1}H NMR spectrum of **10a** (400 MHz, CDCl$_3$). **b)** ^{13}C NMR spectrum of **10a** (125 MHz, CDCl$_3$).
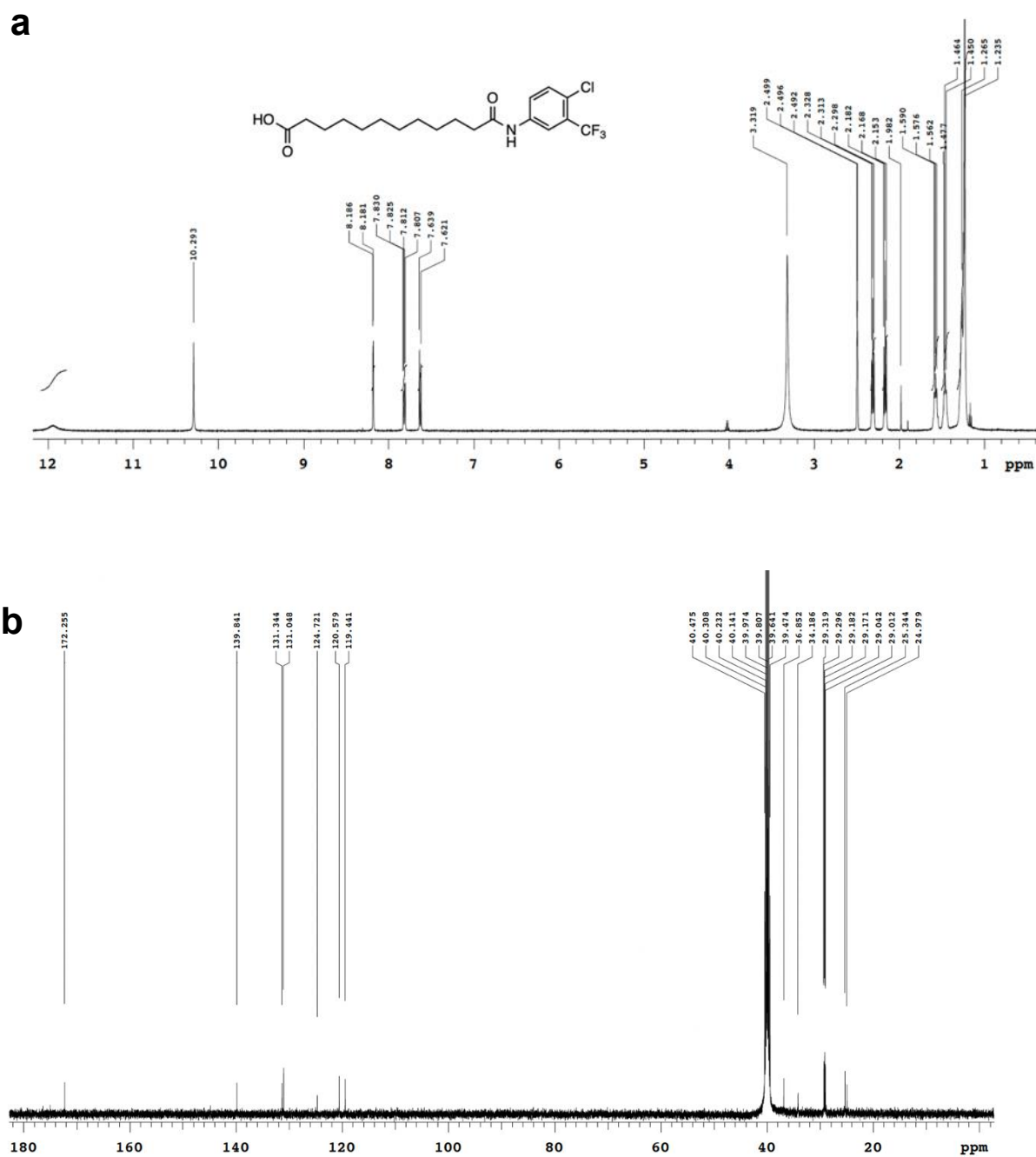
Figure 71: a) ^{1}H NMR spectrum of **10** (400 MHz, DMSO-d_6). **b)** ^{13}C NMR spectrum of **10** (125 MHz, DMSO-d_6).
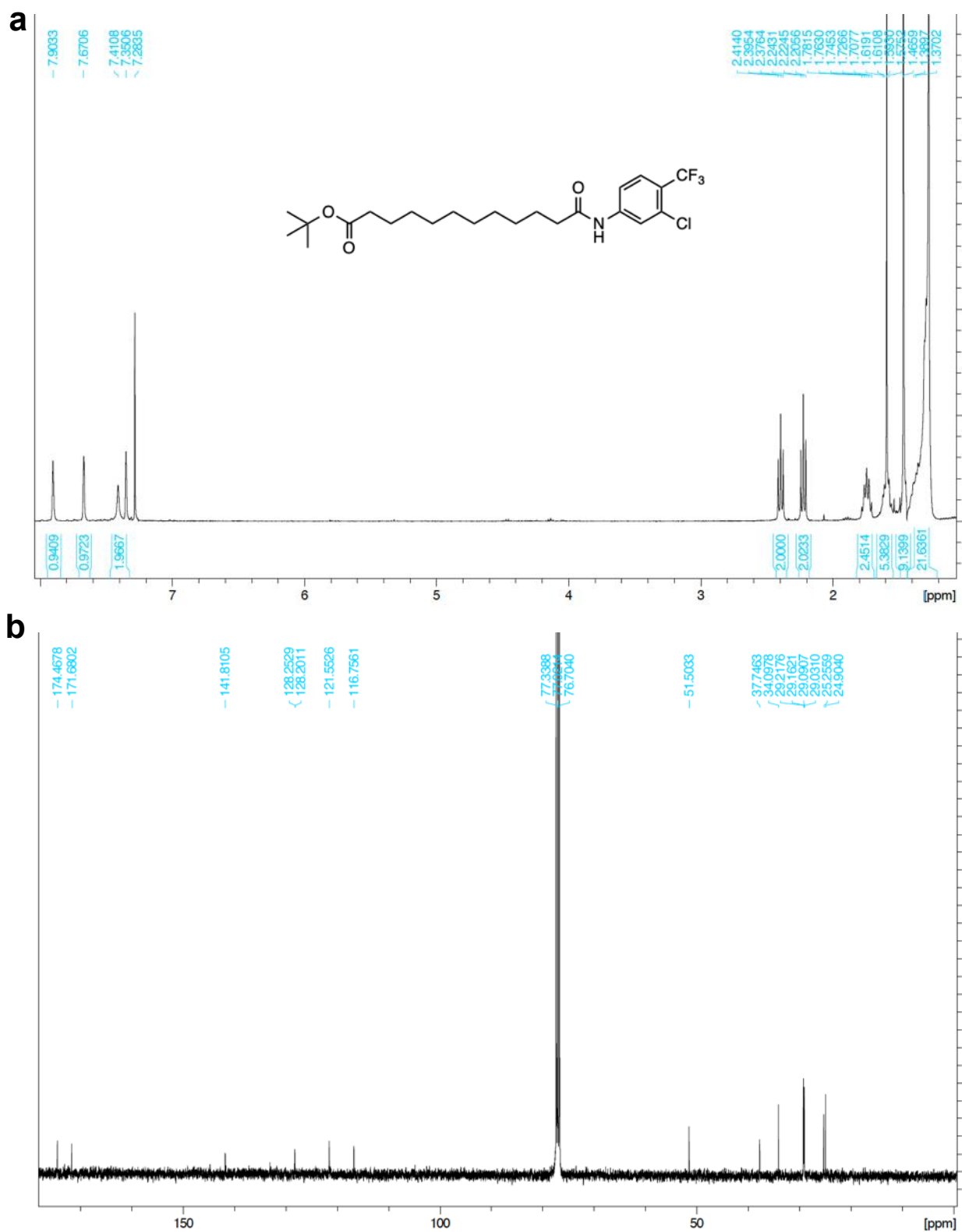
Figure 72: a) ^{1}H NMR spectrum of **11a** (500 MHz, CDCl$_3$). **b)** ^{13}C NMR spectrum of **11a** (125 MHz, CDCl$_3$).
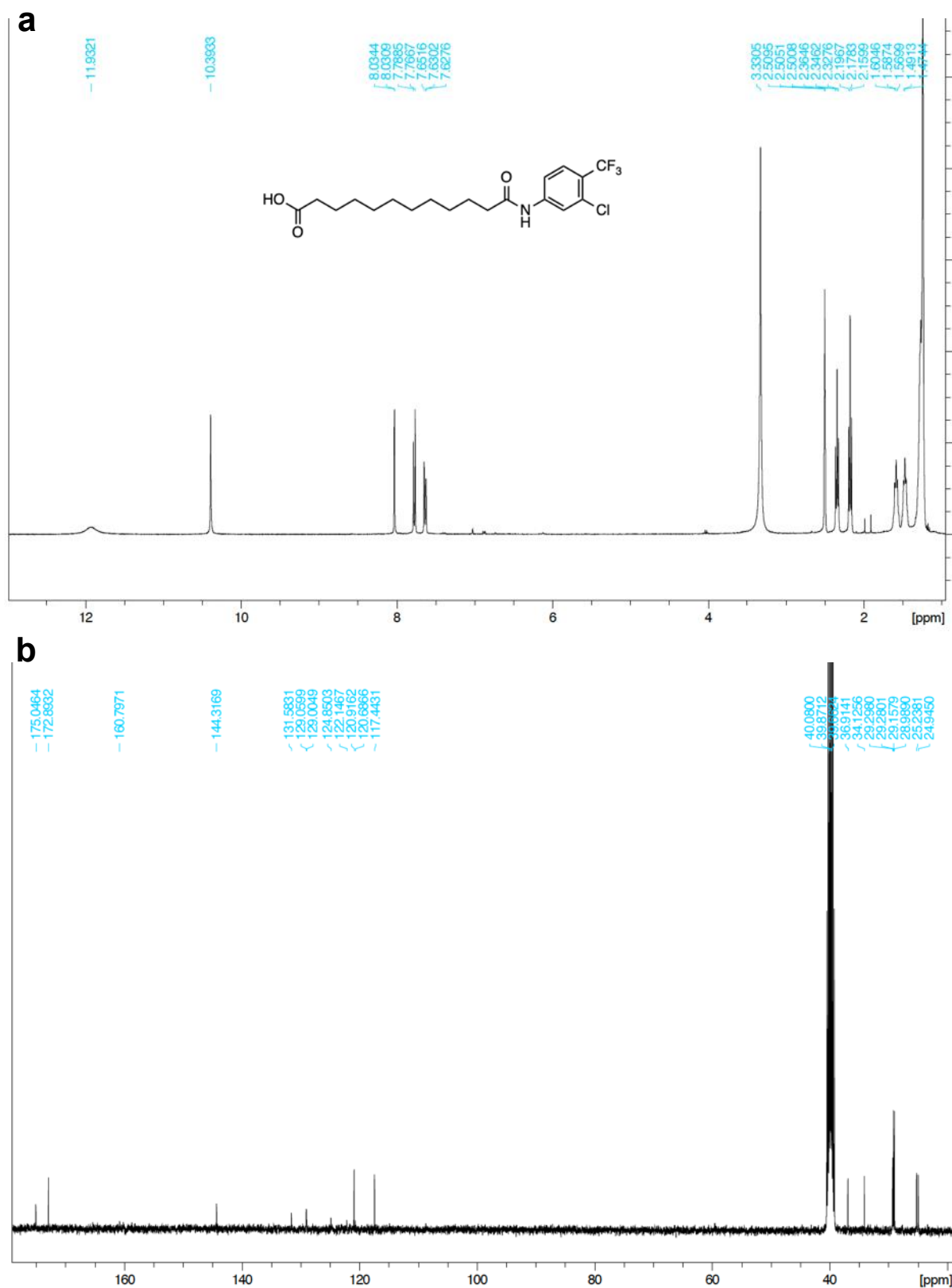
Figure 73: a) ^{1}H NMR spectrum of **11** (500 MHz, DMSO-d_6). **b)** ^{13}C NMR spectrum of **11** (125 MHz, DMSO-d_6).
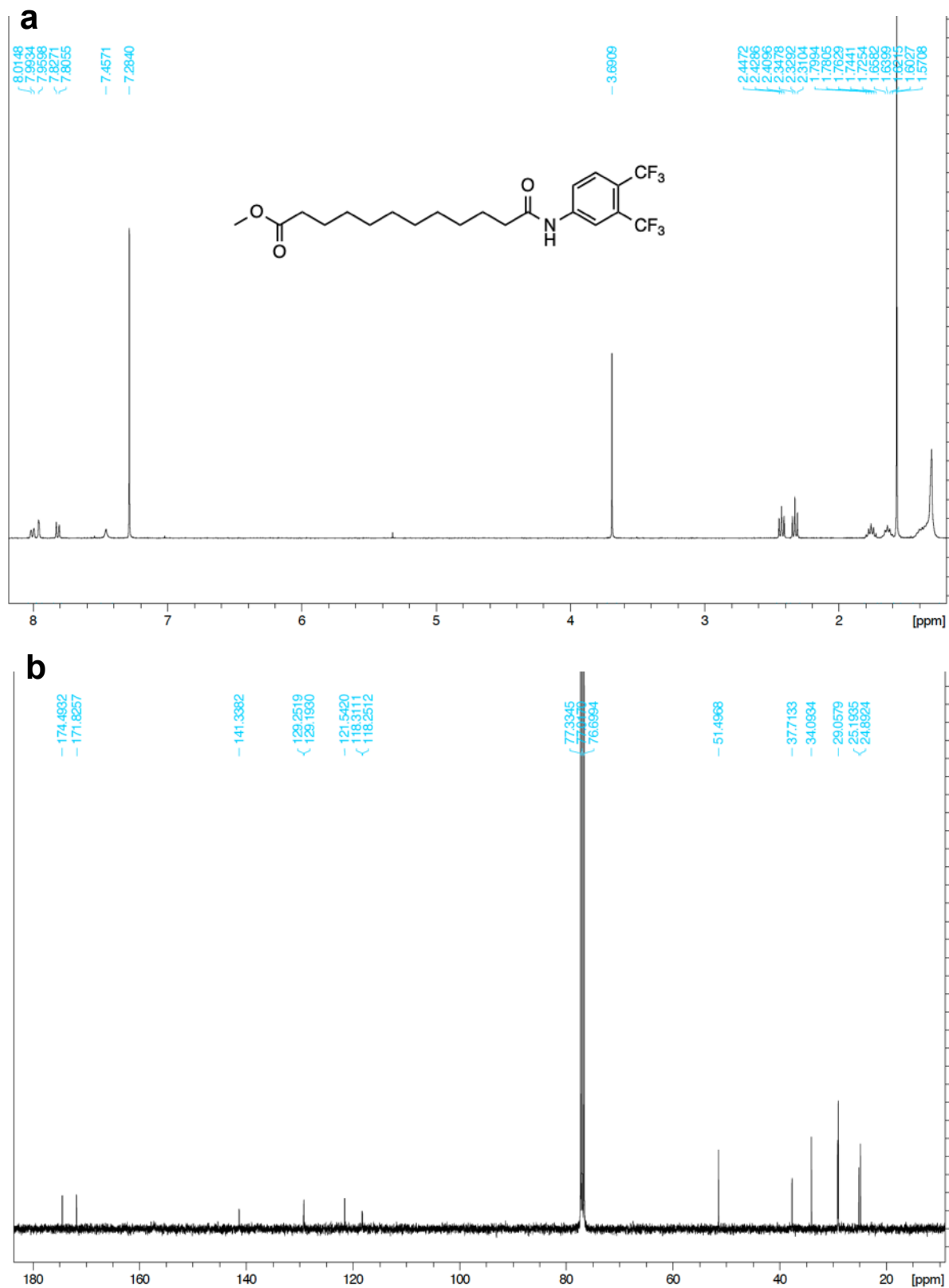
Figure 74: a) ^{1}H NMR spectrum of **12a** (500 MHz, CDCl$_3$). **b)** ^{13}C NMR spectrum of **12a** (125 MHz, CDCl$_3$).
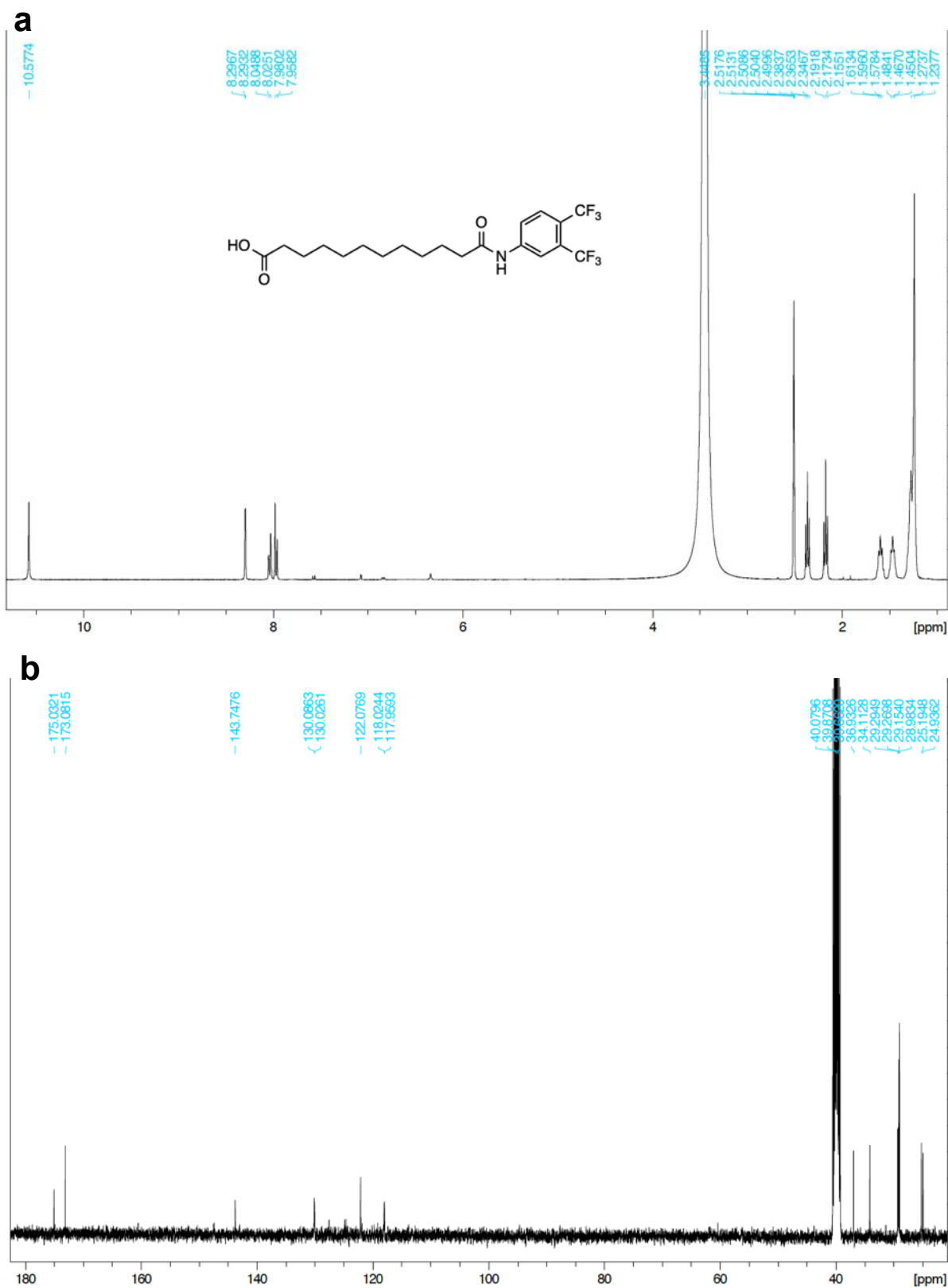
Figure 75: a) ^{1}H NMR spectrum of **12** (500 MHz, DMSO-d_6). **b)** ^{13}C NMR spectrum of **12** (125 MHz, DMSO-d_6).
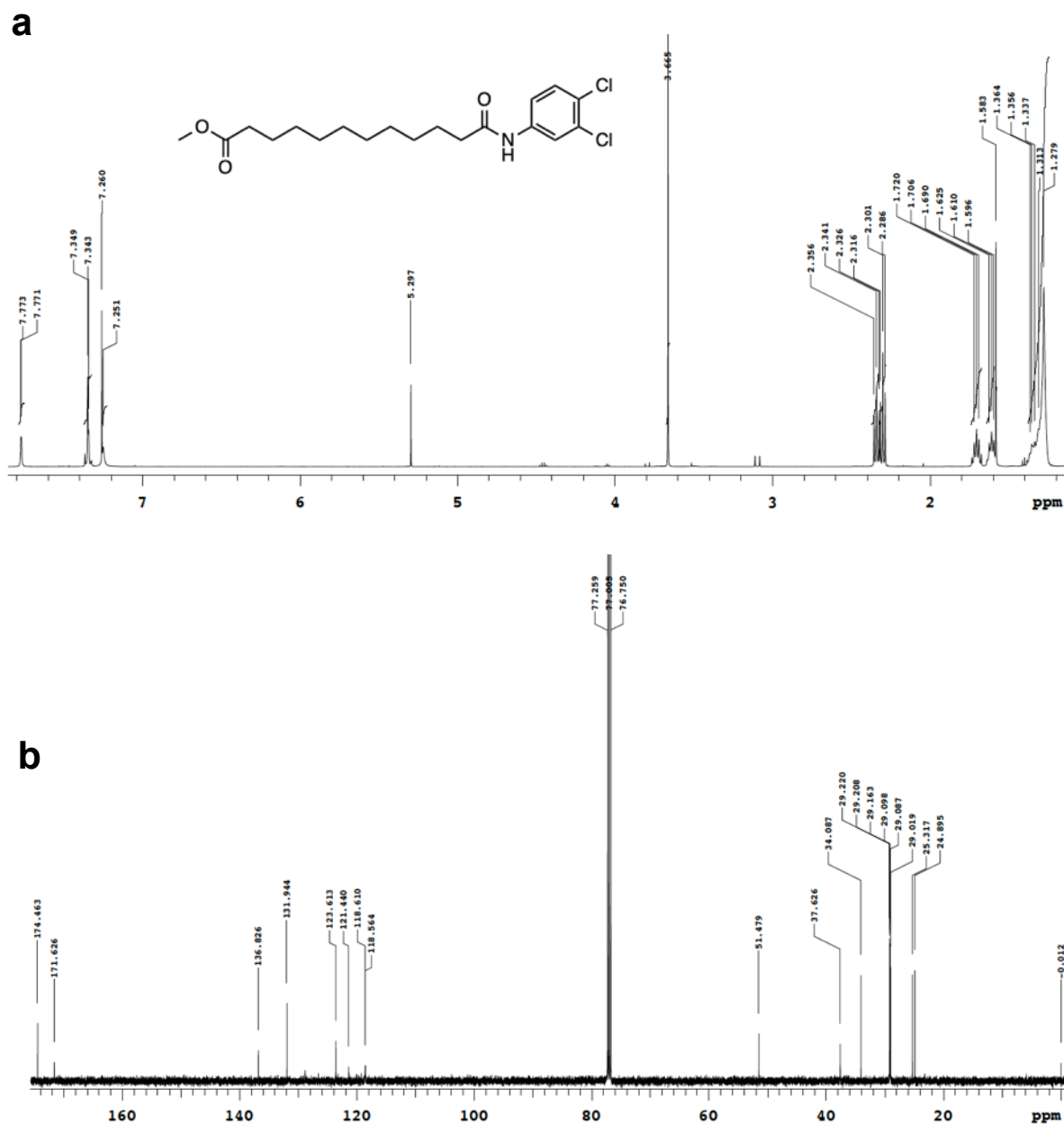
Figure 76: a) ^{1}H NMR spectrum of **13a** (400 MHz, CDCl$_3$). **b)** ^{13}C NMR spectrum of **13a** (125 MHz, CDCl$_3$).
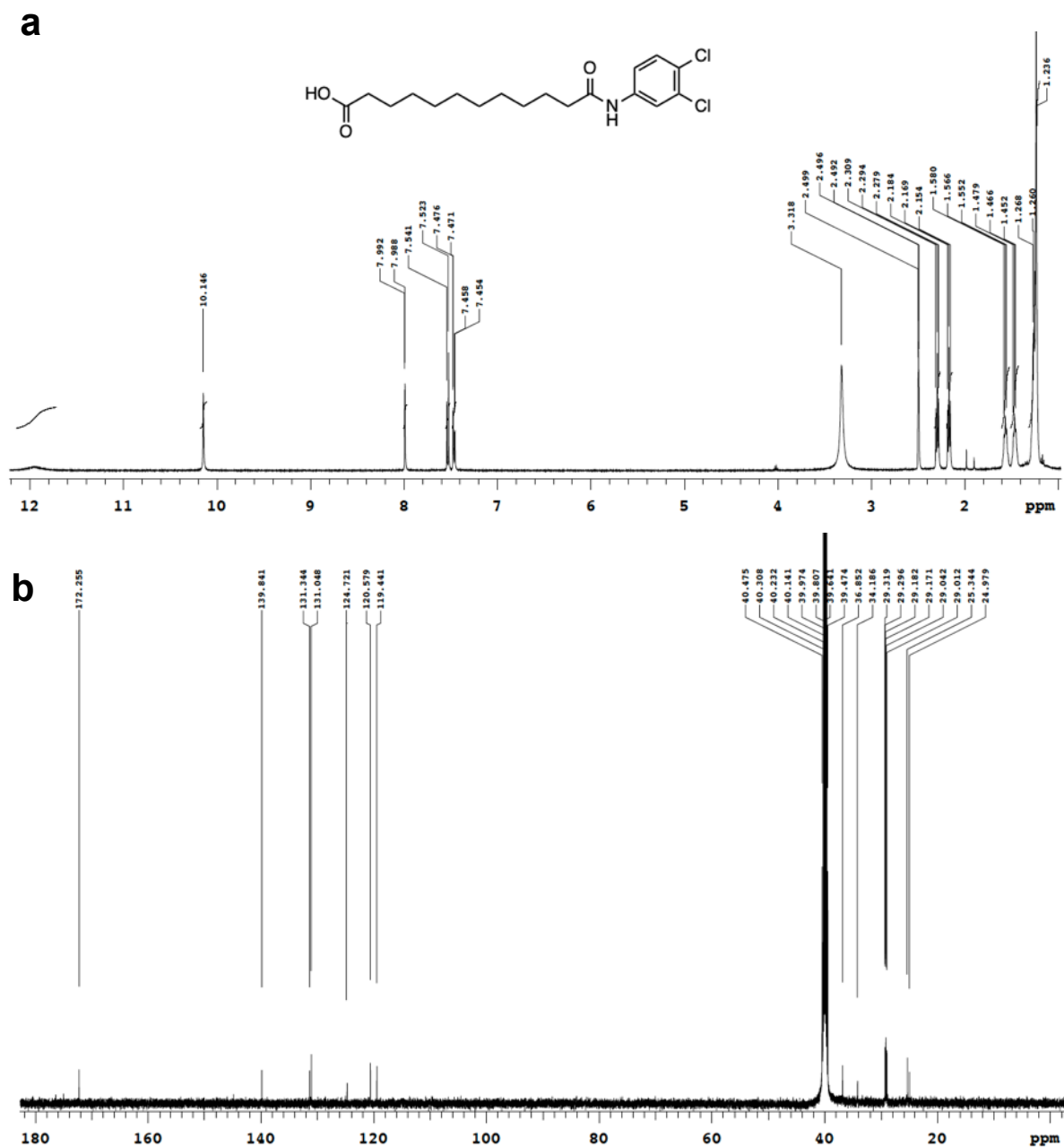
Figure 77: a) ^{1}H NMR spectrum of **13** (400 MHz, DMSO-d_6). **b)** ^{13}C NMR spectrum of **13** (125 MHz, DMSO-d_6).

172
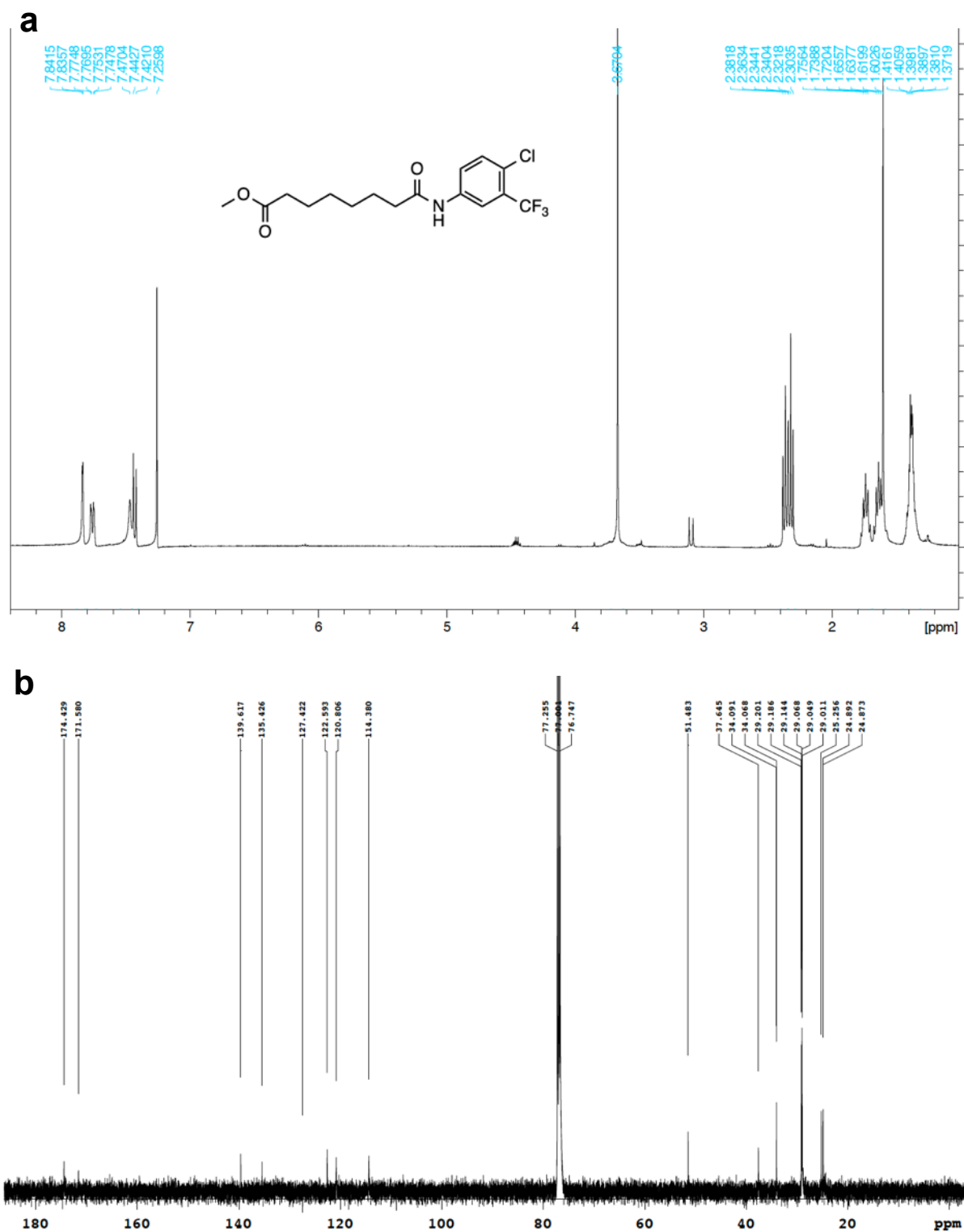
Figure 78: a) ^{1}H NMR spectrum of **14a** (500 MHz, CDCl$_3$). **b)** ^{13}C NMR spectrum of **14a** (125 MHz, CDCl$_3$).
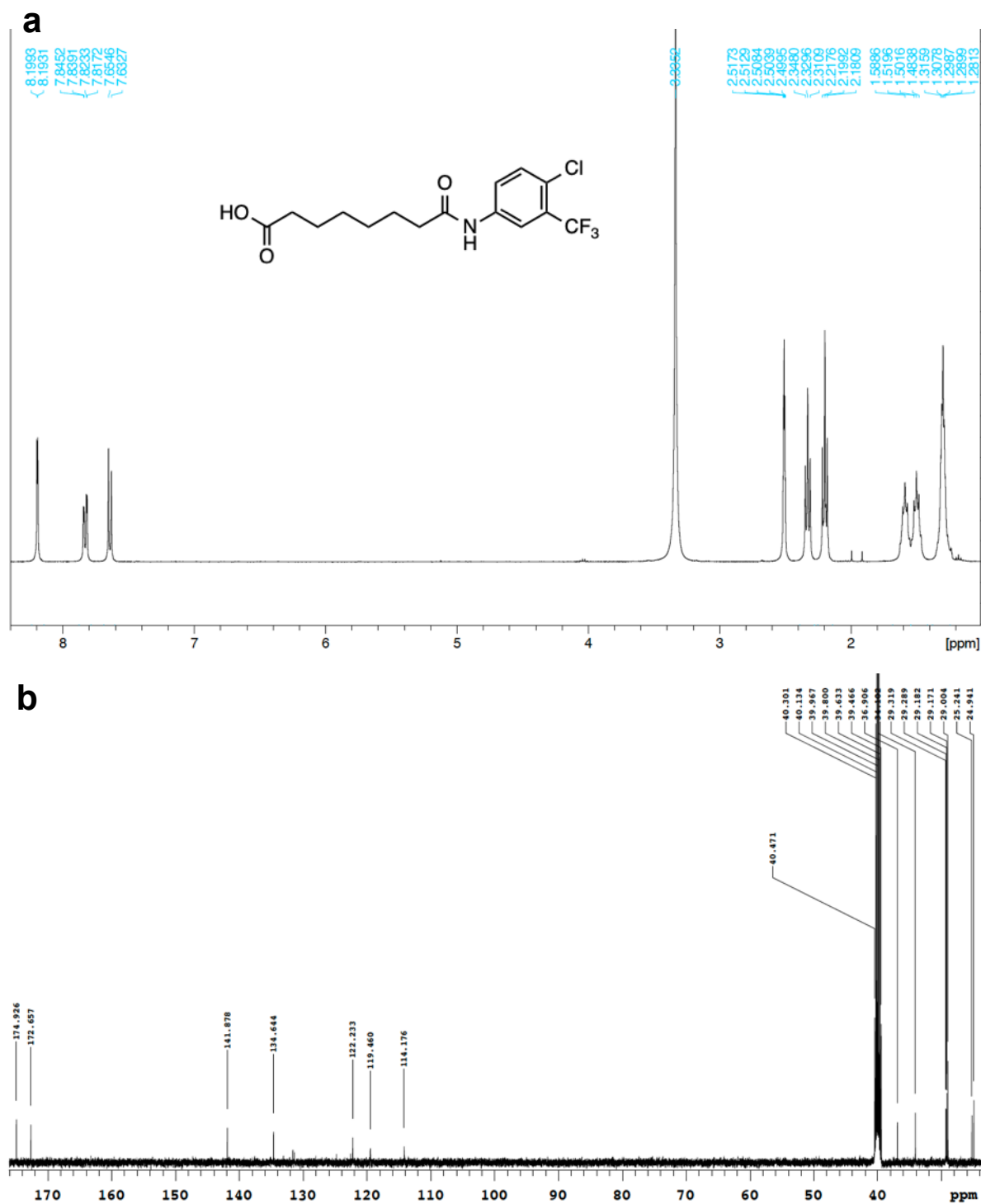
Figure 79: a) ^{1}H NMR spectrum of **14** (500 MHz, DMSO-d_6). **b)** ^{13}C NMR spectrum of **14** (125 MHz, DMSO-d_6).
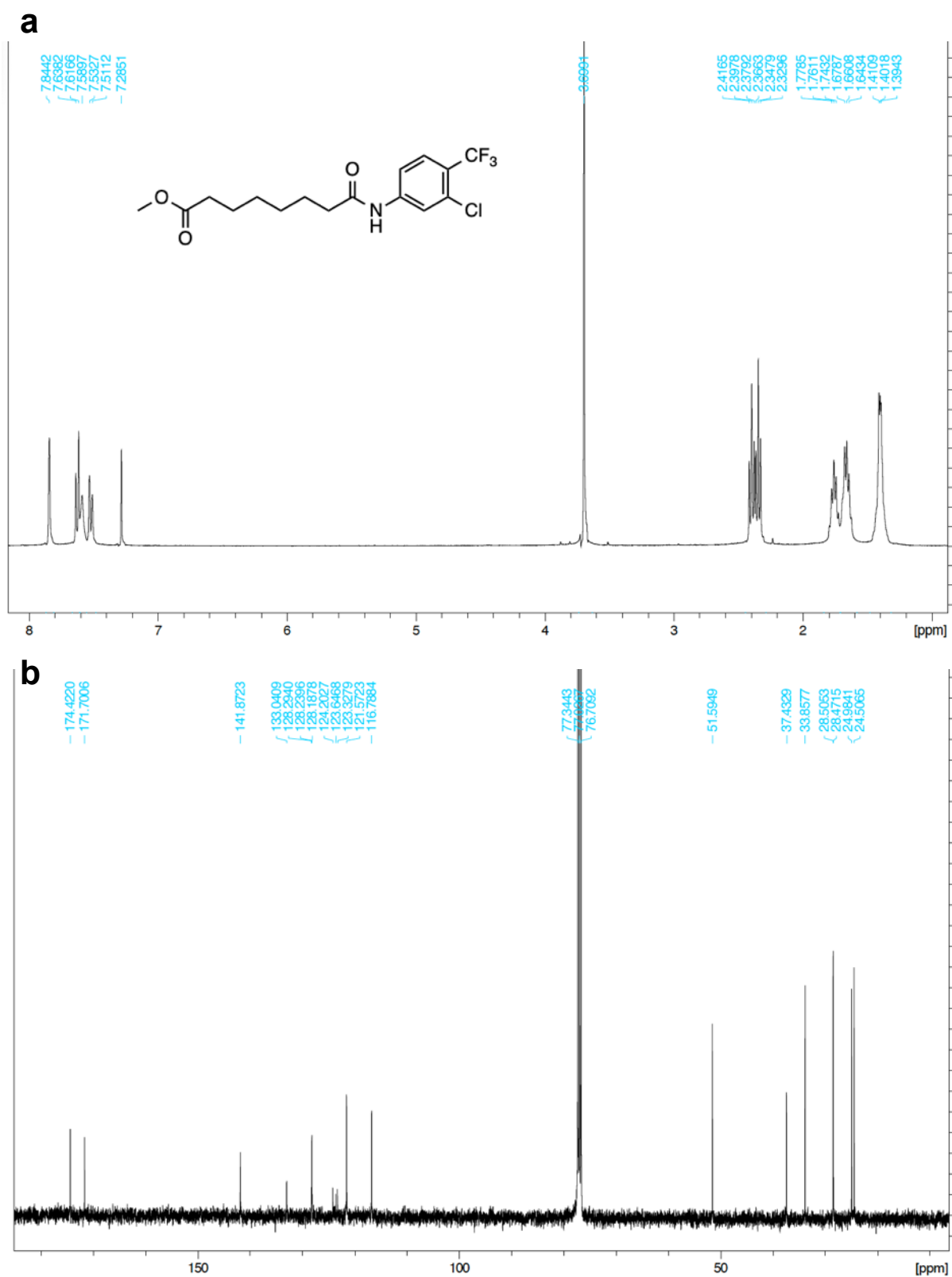
Figure 80: a) ^{1}H NMR spectrum of **15a** (500 MHz, CDCl$_3$). **b)** ^{13}C NMR spectrum of **15a** (125 MHz, CDCl$_3$).
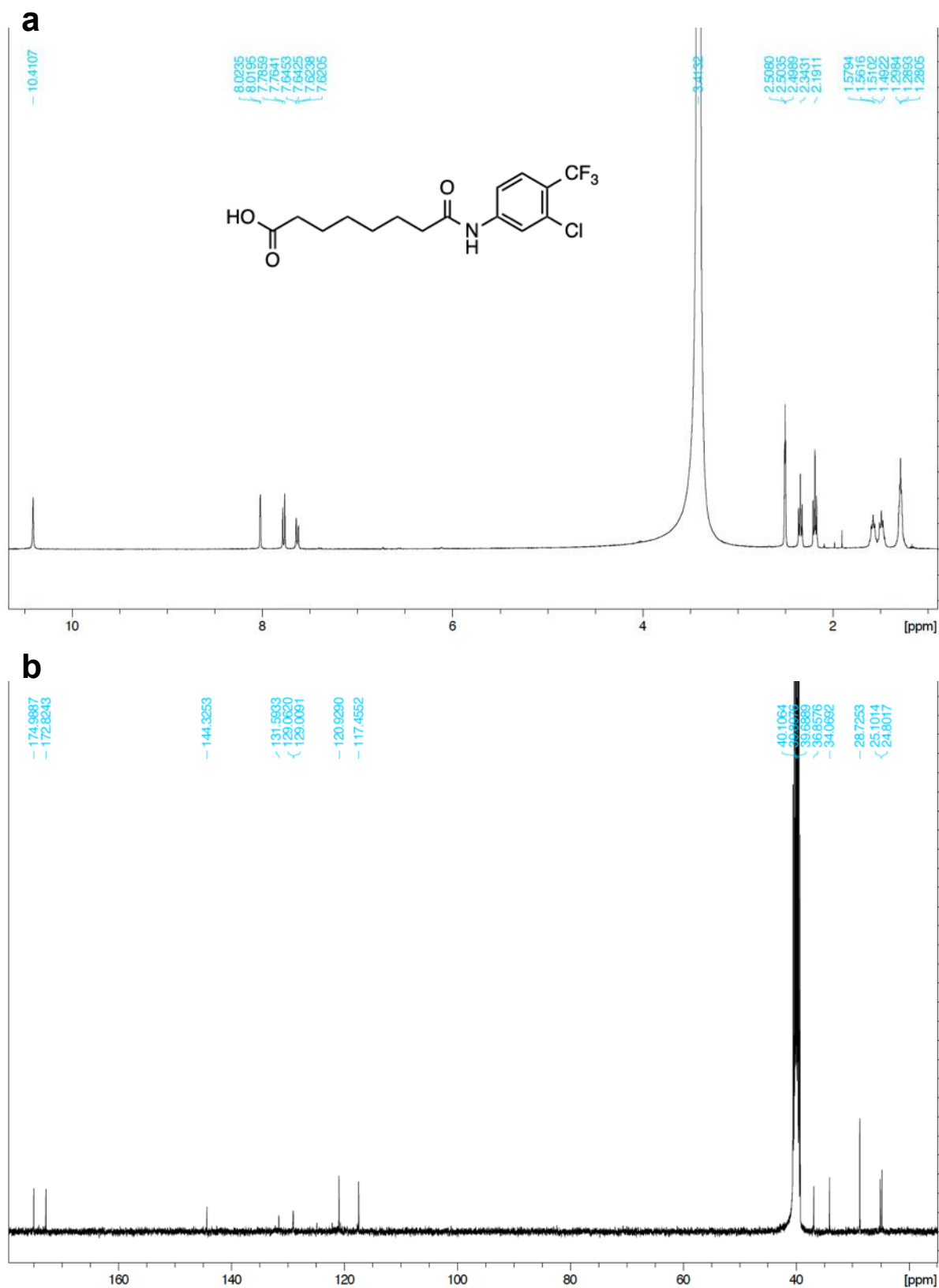
Figure 81: a) ^{1}H NMR spectrum of **15** (500 MHz, DMSO-d_6). **b)** ^{13}C NMR spectrum of **15** (125 MHz, DMSO-d_6).
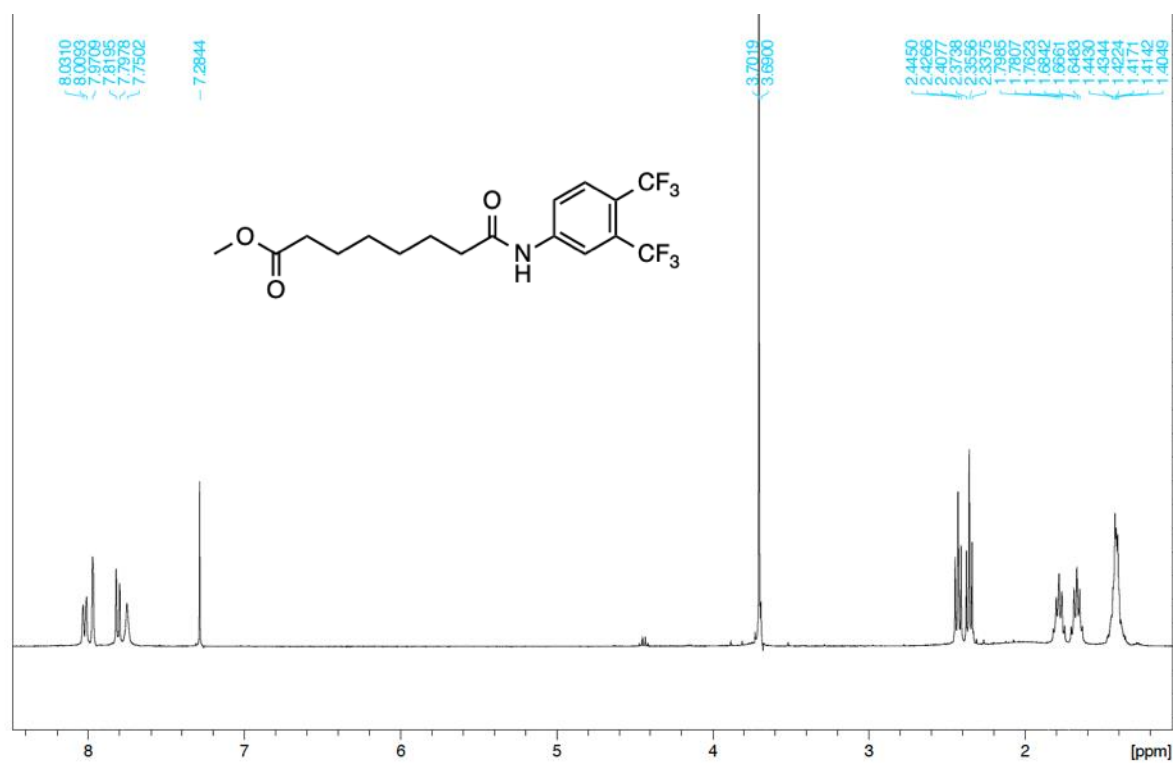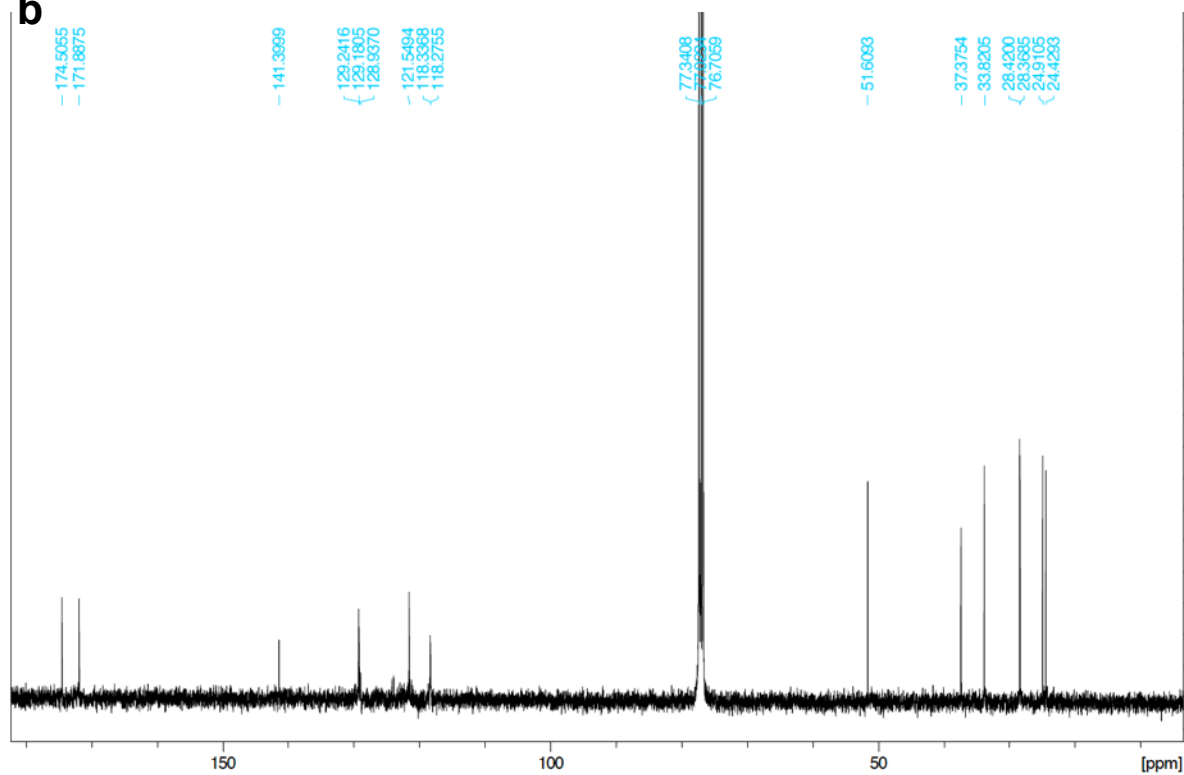
Figure 82: a) ^{1}H NMR spectrum of **16a** (500 MHz, CDCl$_3$). **b)** ^{13}C NMR spectrum of **16a** (125 MHz, CDCl$_3$).
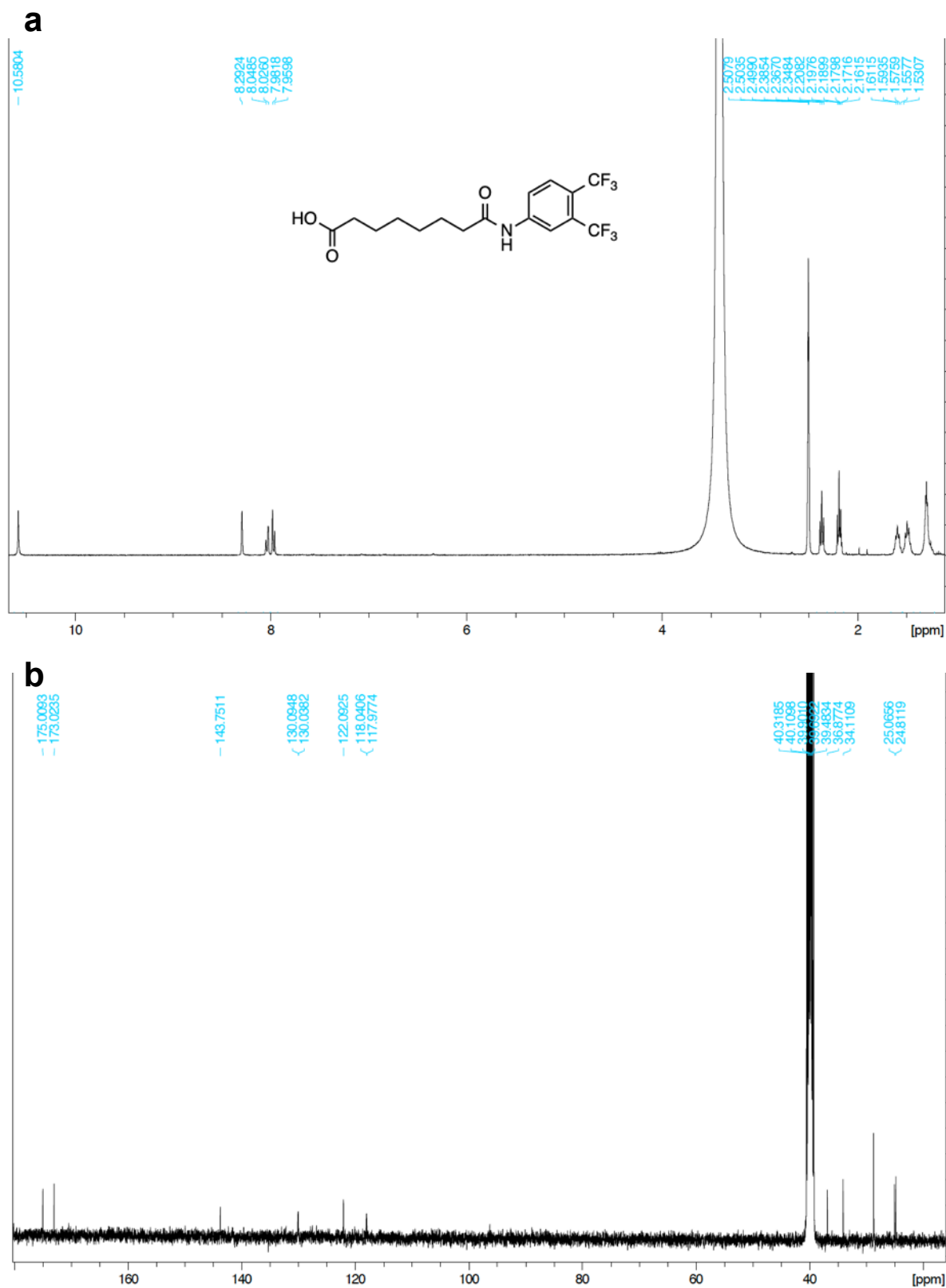
Figure 83: ^{1}H NMR spectrum of **16** (500 MHz, DMSO-d_6). **b)** ^{13}C NMR spectrum of **16** (125 MHz, DMSO-d_6).
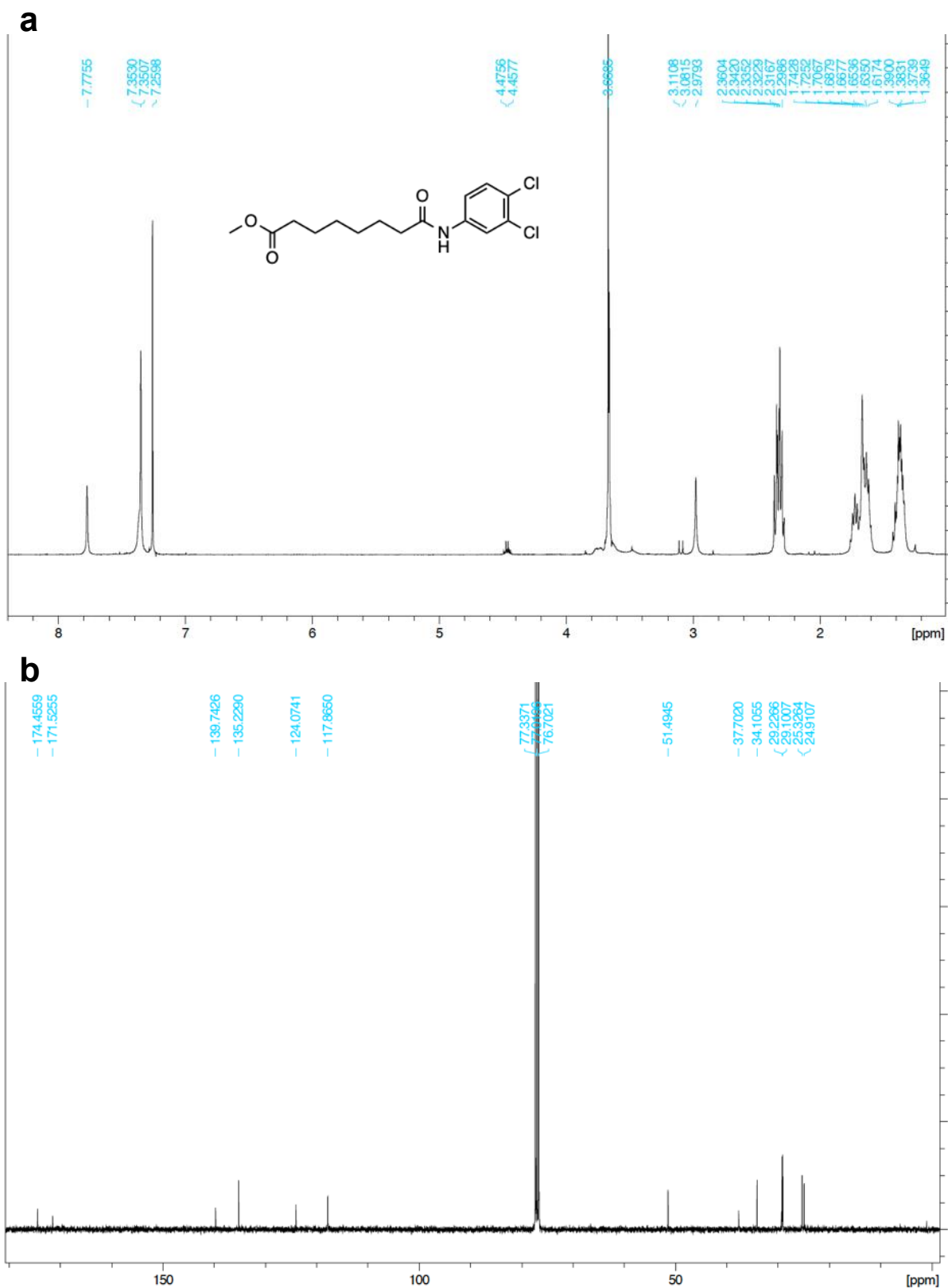
Figure 84: a) ^{1}H NMR spectrum of **17a** (500 MHz, CDCl$_3$). **b)** ^{13}C NMR spectrum of **17a** (125 MHz, CDCl$_3$).

Figure 85: a) ^{1}H NMR spectrum of **17** (400 MHz, DMSO-d_6). **b)** ^{13}C NMR spectrum of **17** (125 MHz, DMSO-d_6).
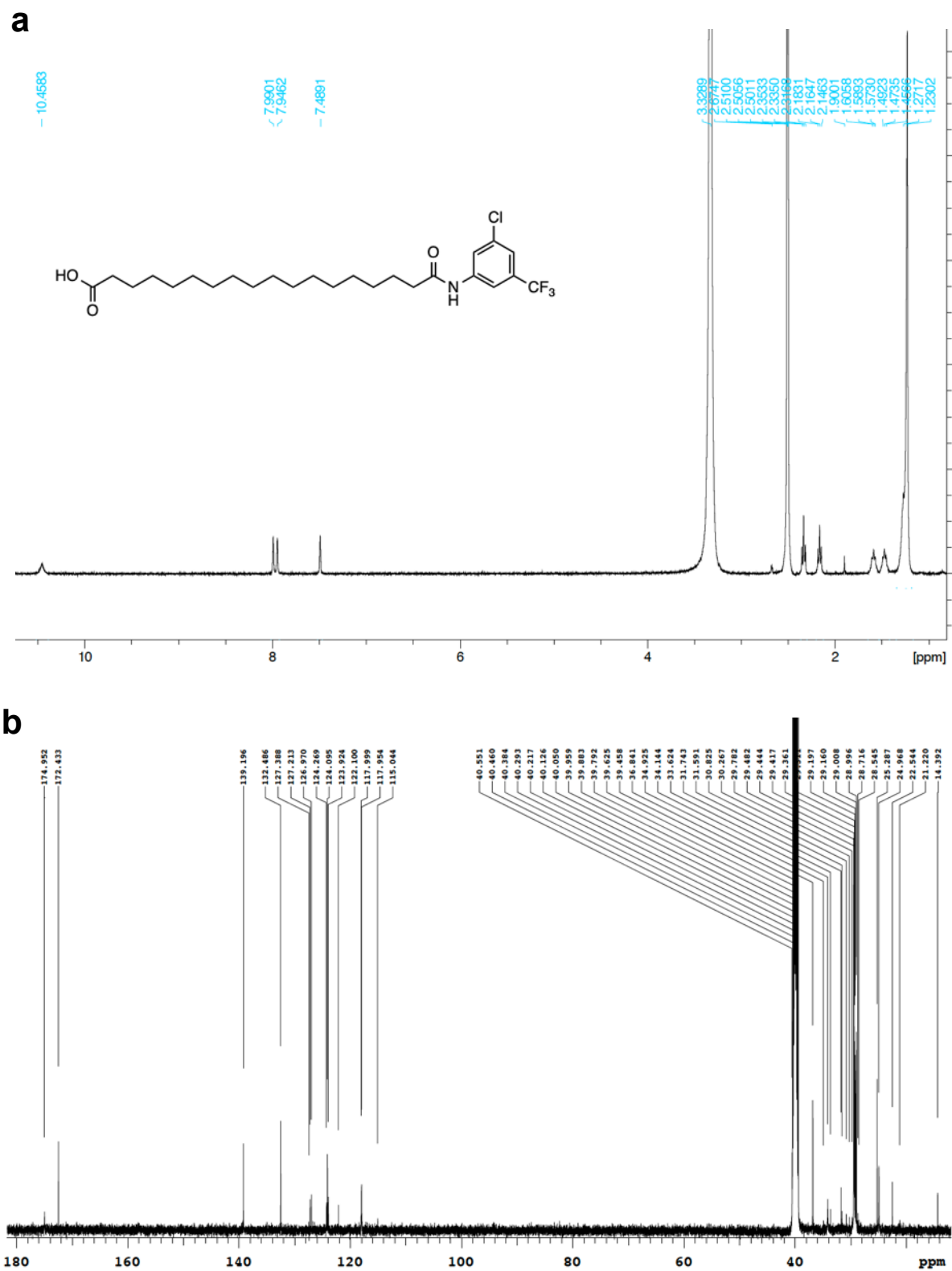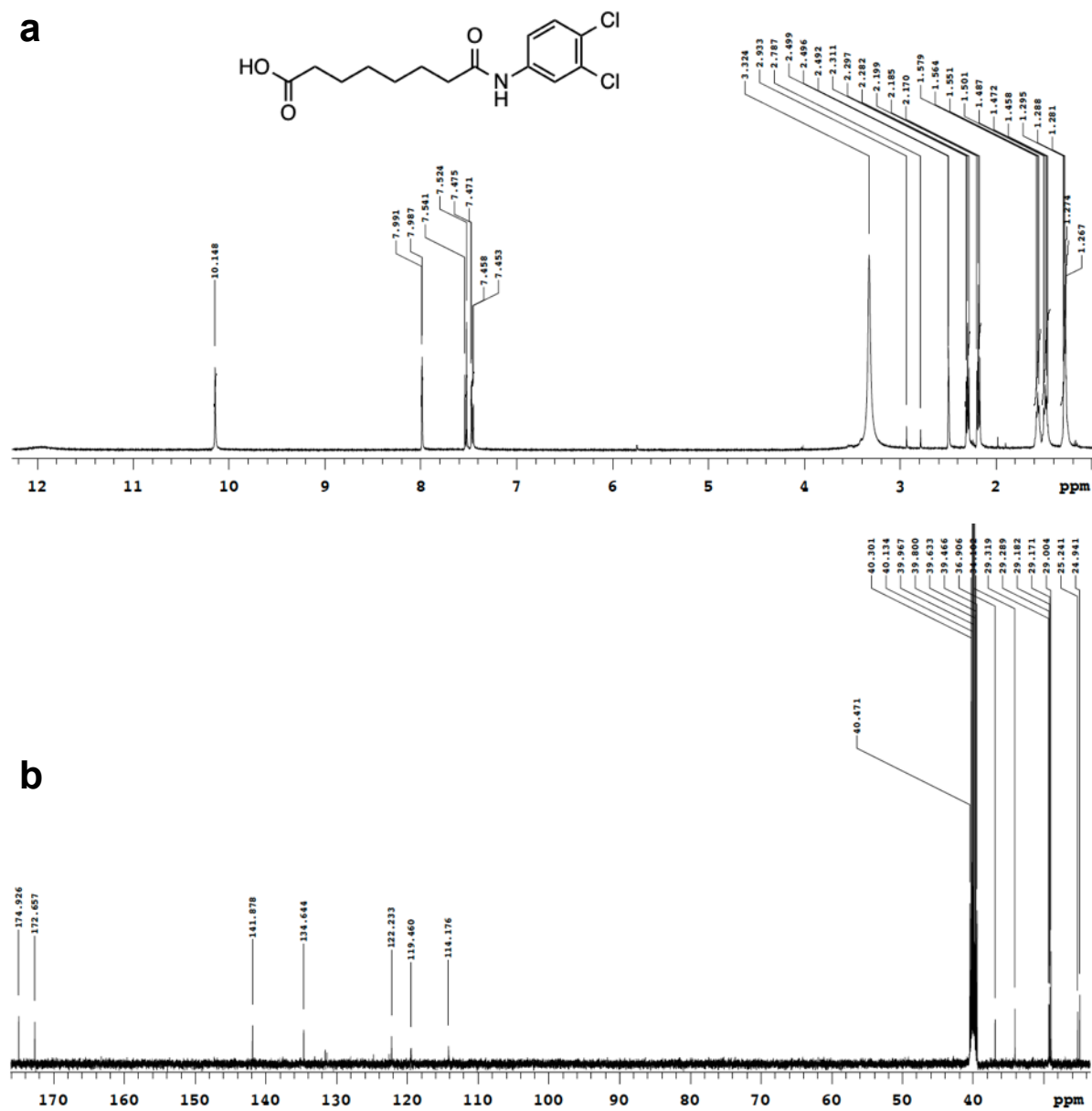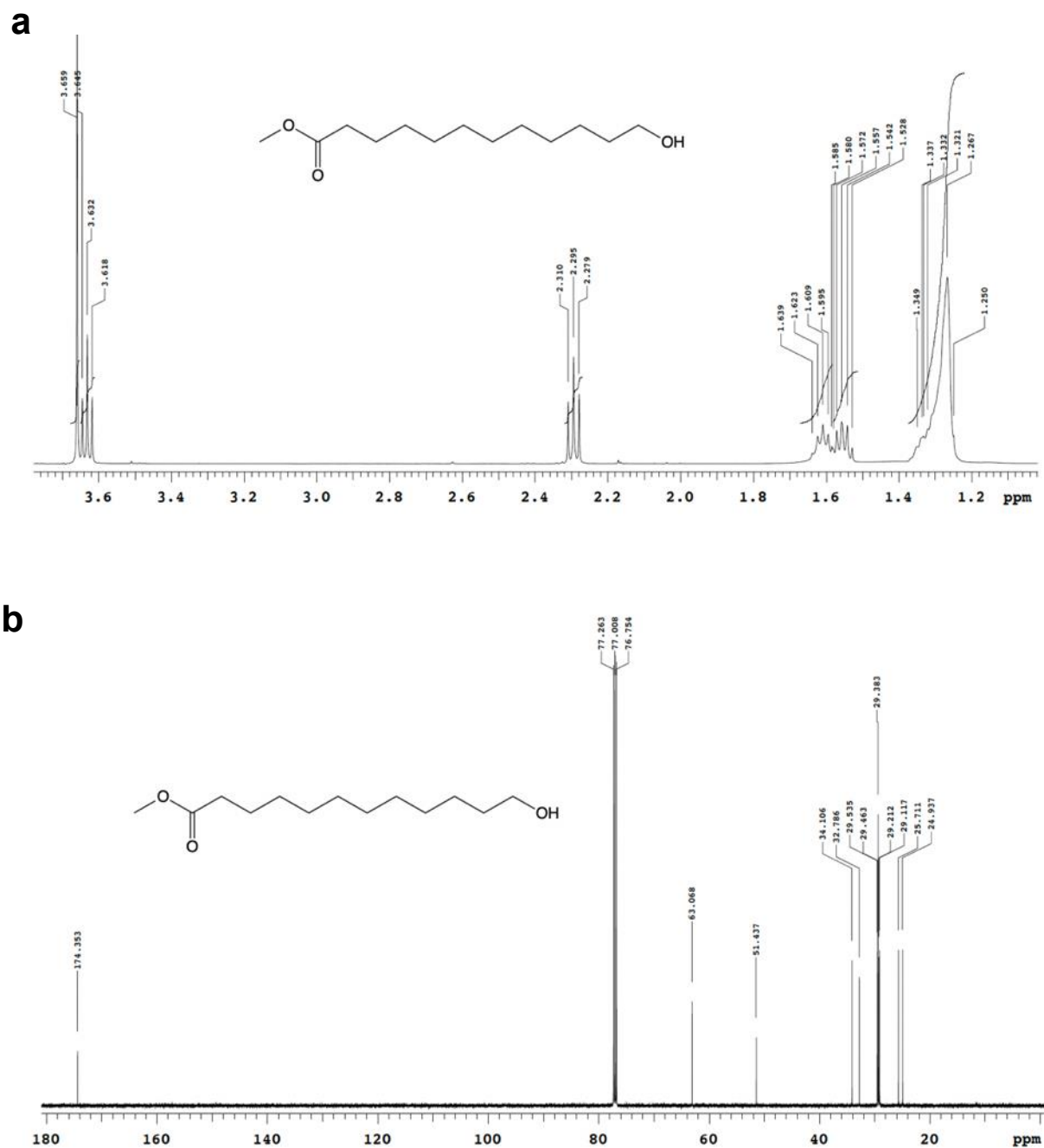
Figure 86: a) ^{1}H NMR spectrum of **19** (400 MHz, CDCl$_3$). **b)** ^{13}C NMR spectrum of **19** (125 MHz, CDCl$_3$).
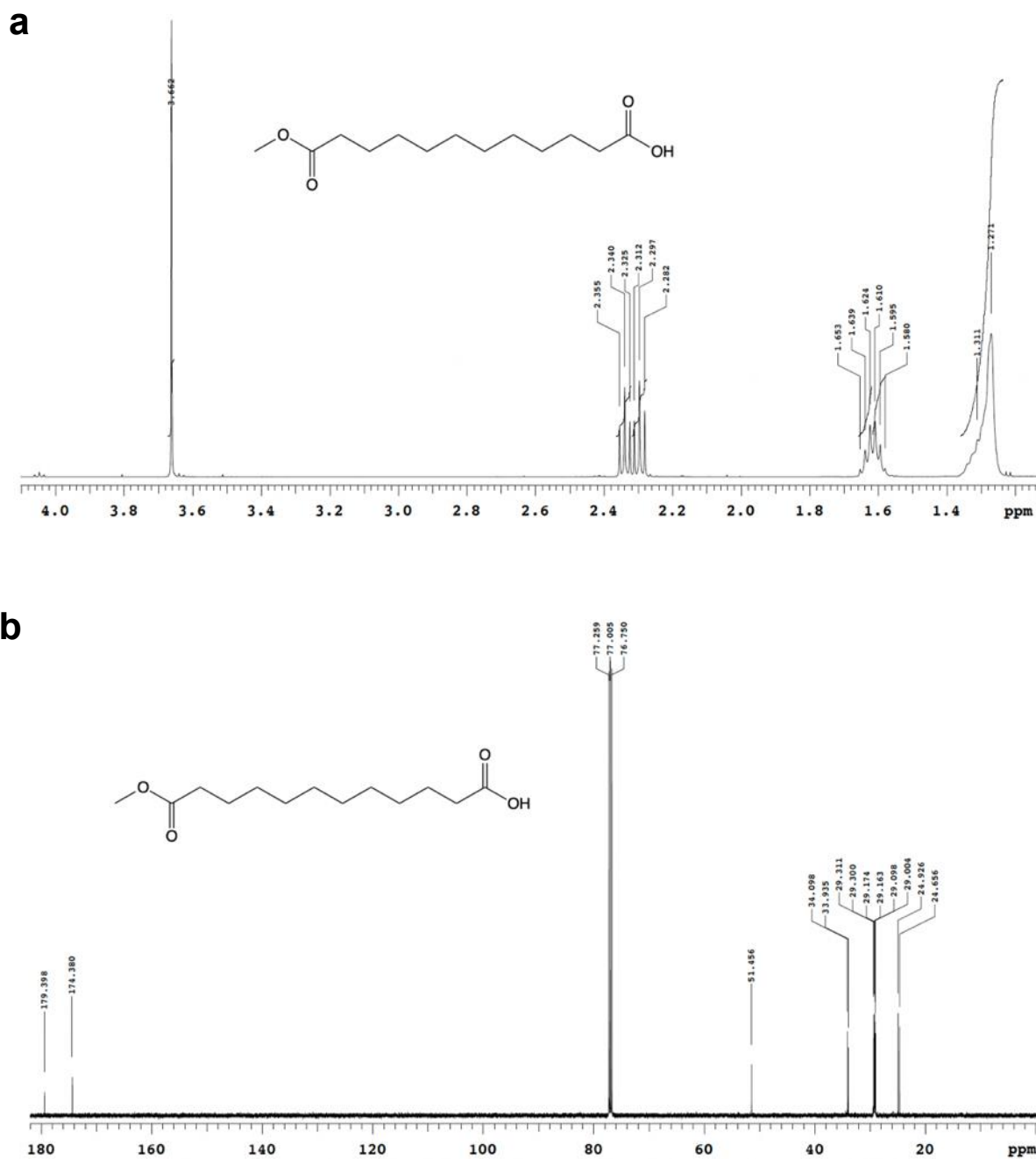
Figure 87: a) ^{1}H NMR spectrum of **20** (400 MHz, CDCl$_3$). **b)** ^{13}C NMR spectrum of **20** (125 MHz, CDCl$_3$)

CHAPTER 7

References

1.   Alberts B., J. A. L. J., Raff M., Roberts K., Walter P., Electron-transport chains and their proton pumps. Molecular Biology of the Cell, 2002. https://www.ncbi.nlm.nih.gov/books/NBK26904/ (accessed 11 June 2020).

2.   Uzman, A., Molecular biology of the cell (4th ed.): Alberts, B., Johnson, A., Lewis, J., Raff, M., Roberts, K., and Walter, P. *Biochemistry and Molecular Biology Education* **2003,** *31* (4), 212-214.

3.   Jonckheere, A. I.; Smeitink, J. A. M.; Rodenburg, R. J. T., Mitochondrial ATP synthase: architecture, function and pathology. *Journal of inherited metabolic disease* **2012,** *35* (2), 211-225.

4.   Alberts B., J. A. L. J., Raff M., Roberts K., Walter P., Molecular Biology of the Cell. In *Electron-transport chains and their proton pumps* [Online] 2002. https://www.ncbi.nlm.nih.gov/books/NBK26904/ (accessed 11 June 2020).

5.   Mitchell, P., Coupling of phosphorylation to electron and hydrogen transfer by a chemi-osmotic type of mechanism. *Nature* **1961,** *191*, 144-8.

6.   Blanc, F. E. C.; Hummer, G., Mechanism of proton-powered c-ring rotation in a mitochondrial ATP synthase. *Proceedings of the National Academy of Sciences* **2024,** *121* (11), e2314199121.

7.   Neupane, P.; Bhuju, S.; Thapa, N.; Bhattarai, H. K., ATP Synthase: Structure, Function and Inhibition. *Biomolecular Concepts* **2019,** *10* (1), 1-10.

8.   Grundlingh, J.; Dargan, P. I.; El-Zanfaly, M.; Wood, D. M., 2,4-dinitrophenol (DNP): a weight loss agent with significant acute toxicity and risk of death. *J Med Toxicol* **2011,** *7* (3), 205-212.

9.   Rolfe, D. F.; Newman, J. M.; Buckingham, J. A.; Clark, M. G.; Brand, M. D., Contribution of mitochondrial proton leak to respiration rate in working skeletal muscle and liver and to SMR. *Am J Physiol* **1999,** *276* (3), C692-9.

10.   Childress, E. S.; Alexopoulos, S. J.; Hoehn, K. L.; Santos, W. L., Small Molecule Mitochondrial Uncouplers and Their Therapeutic Potential. *JOURNAL OF MEDICINAL CHEMISTRY* **2018,** *61* (11), 4641-4655.

11.   Ricquier, D.; Bouillaud, F., Mitochondrial uncoupling proteins: from mitochondria to the regulation of energy balance. *J Physiol* **2000,** *529 Pt 1* (Pt 1), 3-10.

12.   Mailloux, R. J.; Harper, M. E., Uncoupling proteins and the control of mitochondrial reactive oxygen species production. *Free Radic Biol Med* **2011,** *51* (6), 1106-15.

13.   Divakaruni, A. S.; Brand, M. D., The regulation and physiology of mitochondrial proton leak. *Physiology (Bethesda)* **2011,** *26* (3), 192-205.

14.   Nedergaard, J.; Golozoubova, V.; Matthias, A.; Asadi, A.; Jacobsson, A.; Cannon, B., UCP1: the only protein able to mediate adaptive non-shivering thermogenesis and metabolic inefficiency. *Biochim Biophys Acta* **2001,** *1504* (1), 82-106.

15.   Bround, M. J.; Bers, D. M.; Molkentin, J. D., A 20/20 view of ANT function in mitochondrial biology and necrotic cell death. *J Mol Cell Cardiol* **2020,** *144*, A3-a13.

16.   Cunha, F. M.; Caldeira da Silva, C. C.; Cerqueira, F. M.; Kowaltowski, A. J., Mild mitochondrial uncoupling as a therapeutic strategy. *Curr Drug Targets* **2011,** *12* (6), 783-9.

17.   Sousa, D.; Carmo, H.; Roque Bravo, R.; Carvalho, F.; Bastos, M. d. L.; Guedes de Pinho, P.; Dias da Silva, D., Diet aid or aid to die: an update on 2,4-dinitrophenol (2,4-DNP) use as a weight-loss product. *Archives of Toxicology* **2020**.

18.   Demine, S.; Renard, P.; Arnould, T., Mitochondrial Uncoupling: A Key Controller of Biological Processes in Physiology and Diseases. *Cells* **2019,** *8* (8), 795.

19.   Wallace, K. B.; Starkov, A. A., Mitochondrial targets of drug toxicity. *Annu Rev Pharmacol Toxicol* **2000,** *40*, 353-88.

20.   Harper, J. A.; Dickinson, K.; Brand, M. D., Mitochondrial uncoupling as a target for drug development for the treatment of obesity. *Obes Rev* **2001,** *2* (4), 255-65.

21.   Zorov, D. B.; Andrianova, N. V.; Babenko, V. A.; Pevzner, I. B.; Popkov, V. A.; Zorov, S. D.; Zorova, L. D.; Plotnikov, E. Y.; Sukhikh, G. T.; Silachev, D. N., Neuroprotective Potential of Mild Uncoupling in Mitochondria. Pros and Cons. *Brain Sci* **2021,** *11* (8).

22.   York, E.; McNaughton, D. A.; Duman, M.-N.; Gale, P. A.; Rawling, T., Fatty Acid-Activated Proton Transport by Bisaryl Anion Transporters Depolarises Mitochondria and Reduces the Viability of MDA-MB-231 Breast Cancer Cells. *Biomolecules* **2023,** *13* (8), 1202.

23.   Wu, X.; Gale, P. A., Small-Molecule Uncoupling Protein Mimics: Synthetic Anion Receptors as Fatty Acid-Activated Proton Transporters. *Journal of the American Chemical Society* **2016,** *138* (50), 16508-16514.

24.   Nicholls, D. G., The physiological regulation of uncoupling proteins. *Biochimica et Biophysica Acta (BBA) - Bioenergetics* **2006,** *1757* (5), 459-466.

25.   Brunaldi, K.; Miranda, M. A.; Abdulkader, F.; Curi, R.; Procopio, J., Fatty acid flip-flop and proton transport determined by short-circuit current in planar bilayers. *Journal of Lipid Research* **2005,** *46* (2), 245-251.

26.   WHO Over 1 in 3 People Affected by Neurological Conditions—The Leading Cause of Illness and Disability Worldwide. https://www.who.int/news/item/14-03-2024-over-1-in-3-people-affected-by-neurological-conditions--the-leading-cause-of-illness-and-disability-worldwide (accessed 4 June).

27.   Bivol, S.; Mellick, G. D.; Gratten, J.; Parker, R.; Mulcahy, A.; Mosley, P. E.; Poortvliet, P. C.; Campos, A. I.; Mitchell, B. L.; Garcia-Marin, L. M.; Cross, S.; Ferguson, M.; Lind, P. A.; Loesch, D. Z.; Visscher, P. M.; Medland, S. E.; Scherzer, C. R.; Martin, N. G.; Rentería, M. E., Australian Parkinson's Genetics Study (APGS): pilot (n=1532). *BMJ Open* **2022,** *12* (2), e052032.

28.	Australia, D. Dementia Facts and Figures. https://www.dementia.org.au/about-dementia/dementia-facts-and-figures (accessed 10th Feb).

29.	Gu, Y.-y.; Zhao, X.-r.; Zhang, N.; Yang, Y.; Yi, Y.; Shao, Q.-h.; Liu, M.-x.; Zhang, X.-l., Mitochondrial dysfunction as a therapeutic strategy for neurodegenerative diseases: Current insights and future directions. *Ageing Research Reviews* **2024,** *102*, 102577.

30.	Wang, Y.; Xu, E.; Musich, P. R.; Lin, F., Mitochondrial dysfunction in neurodegenerative diseases and the potential countermeasure. *CNS Neuroscience & Therapeutics* **2019,** *25* (7), 816-824.

31.	Zorov, D. B.; Juhaszova, M.; Sollott, S. J., Mitochondrial Reactive Oxygen Species (ROS) and ROS-Induced ROS Release. *Physiological Reviews* **2014,** *94* (3), 909-950.

32.	Jurcau, A., Insights into the Pathogenesis of Neurodegenerative Diseases: Focus on Mitochondrial Dysfunction and Oxidative Stress. *International Journal of Molecular Sciences* **2021,** *22* (21), 11847.

33.	Lim, L.; Jackson-Lewis, V.; Wong, L. C.; Shui, G. H.; Goh, A. X. H.; Kesavapany, S.; Jenner, A. M.; Fivaz, M.; Przedborski, S.; Wenk, M. R., Lanosterol induces mitochondrial uncoupling and protects dopaminergic neurons from cell death in a model for Parkinson's disease. *Cell Death & Differentiation* **2012,** *19* (3), 416-427.

34.	Geisler, J. G.; Marosi, K.; Halpern, J.; Mattson, M. P., DNP, mitochondrial uncoupling, and neuroprotection: A little dab'll do ya. *Alzheimers & Dementia* **2017,** *13* (5), 582-591.

35.	Hass, D. T.; Barnstable, C. J., Cell Autonomous Neuroprotection by the Mitochondrial Uncoupling Protein 2 in a Mouse Model of Glaucoma. *Frontiers in Neuroscience* **2019,** *13*.

36.	Bray, F.; Laversanne, M.; Sung, H.; Ferlay, J.; Siegel, R. L.; Soerjomataram, I.; Jemal, A., Global cancer statistics 2022: GLOBOCAN estimates of incidence and mortality

worldwide for 36 cancers in 185 countries. *CA: A Cancer Journal for Clinicians* **2024,** *74* (3), 229-263.

37.   Health, A. I. o.; Welfare, Cancer in Australia: Actual incidence data from 1982 to 2013 and mortality data from 1982 to 2014 with projections to 2017. *Asia-Pacific Journal of Clinical Oncology* **2018,** *14* (1), 5-15.

38.   Shrestha, R.; Johnson, E.; Byrne, F. L., Exploring the therapeutic potential of mitochondrial uncouplers in cancer. *Mol Metab* **2021,** *51*, 101222.

39.   Vasan, K.; Werner, M.; Chandel, N. S., Mitochondrial Metabolism as a Target for Cancer Therapy. *Cell Metabolism* **2020,** *32* (3), 341-352.

40.   Warburg, O., On the Origin of Cancer Cells. *Science* **1956,** *123* (3191), 309-314.

41.   Hirpara, J.; Eu, J. Q.; Tan, J. K. M.; Wong, A. L.; Clement, M.-V.; Kong, L. R.; Ohi, N.; Tsunoda, T.; Qu, J.; Goh, B. C.; Pervaiz, S., Metabolic reprogramming of oncogene-addicted cancer cells to OXPHOS as a mechanism of drug resistance. *Redox Biology* **2019,** *25*, 101076.

42.   Guerra, F.; Arbini, A. A.; Moro, L., Mitochondria and cancer chemoresistance. *Biochimica et Biophysica Acta (BBA) - Bioenergetics* **2017,** *1858* (8), 686-699.

43.   Chen, H.; Wang, J.; Feng, X.; Zhu, M.; Hoffmann, S.; Hsu, A.; Qian, K.; Huang, D.; Zhao, F.; Liu, W.; Zhang, H.; Cheng, Z., Mitochondria-targeting fluorescent molecules for high efficiency cancer growth inhibition and imaging††Electronic supplementary information (ESI) available. See DOI: 10.1039/c9sc01410a. *Chemical Science* **2019,** *10* (34), 7946-7951.

44.   Morton, G. J.; Cummings, D. E.; Baskin, D. G.; Barsh, G. S.; Schwartz, M. W., Central nervous system control of food intake and body weight. *Nature* **2006,** *443* (7109), 289-95.

45.   Kopelman, P. G., Obesity as a medical problem. *Nature* **2000,** *404* (6778), 635-643.

46.   Health, N. I. o., Clinical Guidelines on the Identification, Evaluation, and Treatment of Overweight and Obesity in Adults--The Evidence Report. National Institutes of Health. *Obes Res* **1998,** *6 Suppl 2*, 51s-209s.

47.   WHO Obesity and Overweight. https://www.who.int/news-room/fact-sheets/detail/obesity-and-overweight (accessed 4 June).

48.   Statistics, A. B. o. Weight Circumference and BMI. https://www.abs.gov.au/statistics/health/health-conditions-and-risks/waist-circumference-and-bmi/latest-release#:~:text=Over%20the%20last%20decade%2C%20the,31.7%25%20over%20the%20same%20period.

49.   Finkelstein, E. A.; Fiebelkorn, I. C.; Wang, G., National medical spending attributable to overweight and obesity: how much, and who's paying? *Health Aff (Millwood)* **2003,** *Suppl Web Exclusives*, W3-219-26.

50.   Lakdawalla, D.; Philipson, T., The growth of obesity and technological change. *Economics and human biology* **2009,** *7* (3), 283-293.

51.   OECD, Obesity Update. Organisation for Economic Co-operation and Development: 2017; p 3.

52.   Bray, G. A., Medical treatment of obesity: the past, the present and the future. *Best Pract Res Clin Gastroenterol* **2014,** *28* (4), 665-84.

53.   Bray, G. A.; Greenway, F. L., Pharmacological treatment of the overweight patient. *Pharmacol Rev* **2007,** *59* (2), 151-84.

54.   Tak, Y. J.; Lee, S. Y., Long-Term Efficacy and Safety of Anti-Obesity Treatment: Where Do We Stand? *Current Obesity Reports* **2021,** *10* (1), 14-30.

55.   Allison, D. B.; Gadde, K. M.; Garvey, W. T.; Peterson, C. A.; Schwiers, M. L.; Najarian, T.; Tam, P. Y.; Troupin, B.; Day, W. W., Controlled-release

phentermine/topiramate in severely obese adults: a randomized controlled trial (EQUIP). *Obesity (Silver Spring)* **2012,** *20* (2), 330-42.

56.   Gadde, K. M.; Allison, D. B.; Ryan, D. H.; Peterson, C. A.; Troupin, B.; Schwiers, M. L.; Day, W. W., Effects of low-dose, controlled-release, phentermine plus topiramate combination on weight and associated comorbidities in overweight and obese adults (CONQUER): a randomised, placebo-controlled, phase 3 trial. *Lancet* **2011,** *377* (9774), 1341-52.

57.   Bray, G. A., Medications for weight reduction. *Med Clin North Am* **2011,** *95* (5), 989-1008.

58.   Kim, K. K.; Cho, H.-J.; Kang, H.-C.; Youn, B.-B.; Lee, K.-R., Effects on Weight Reduction and Safety of Short-Term Phentermine Administration in Korean Obese People. *Yonsei Medical Journal* **2006,** *47* (5), 614.

59.   Weintraub, M.; Hasday, J. D.; Mushlin, A. I.; Lockwood, D. H., A Double-blind Clinical Trial in Weight Control: Use of Fenfluramine and Phentermine Alone and in Combination. *Archives of Internal Medicine* **1984,** *144* (6), 1143-1148.

60.   Aronne, L. J.; Wadden, T. A.; Peterson, C.; Winslow, D.; Odeh, S.; Gadde, K. M., Evaluation of phentermine and topiramate versus phentermine/topiramate extended-release in obese adults. *Obesity* **2013,** *21* (11), 2163-2171.

61.   Bays, H. E.; Lazarus, E.; Primack, C.; Fitch, A., Obesity pillars roundtable: Phentermine – Past, present, and future. *Obesity Pillars* **2022,** *3*, 100024.

62.   Hollander, P.; Bays, H. E.; Rosenstock, J.; Frustaci, M. E.; Fung, A.; Vercruysse, F.; Erondu, N., Coadministration of canagliflozin and phentermine for weight management in overweight and obese individuals without diabetes: a randomized clinical trial. *Diabetes Care* **2017,** *40* (5), 632-639.

63.   Bray, G. A.; Ryan, D. H., Medical therapy for the patient with obesity. *Circulation* **2012,** *125* (13), 1695-703.

64.   TGA, T. G. A. Phentermine GENERICHEALTH. https://www.tga.gov.au/resources/prescription-medicines-registrations/phentermine-generichealth-phentermine-gh-phentermine-lapl-lupin-australia-pty-limited (accessed 15 August).

65.   Kang, J. G.; Park, C. Y.; Kang, J. H.; Park, Y. W.; Park, S. W., Randomized controlled trial to investigate the effects of a newly developed formulation of phentermine diffuse-controlled release for obesity. *Diabetes, Obesity and Metabolism* **2010,** *12* (10), 876-882.

66.   Hendricks, E. J.; Srisurapanont, M.; Schmidt, S. L.; Haggard, M.; Souter, S.; Mitchell, C. L.; De Marco, D. G.; Hendricks, M. J.; Istratiy, Y.; Greenway, F. L., Addiction potential of phentermine prescribed during long-term treatment of obesity. *Int J Obes (Lond)* **2014,** *38* (2), 292-8.

67.   Lewis, K. H.; Fischer, H.; Ard, J.; Barton, L.; Bessesen, D. H.; Daley, M. F.; Desai, J.; Fitzpatrick, S. L.; Horberg, M.; Koebnick, C.; Oshiro, C.; Yamamoto, A.; Young, D. R.; Arterburn, D. E., Safety and Effectiveness of Longer-Term Phentermine Use: Clinical Outcomes from an Electronic Health Record Cohort. *Obesity* **2019,** *27* (4), 591-602.

68.   Velazquez, A.; Apovian, C. M., Updates on obesity pharmacotherapy. *Ann N Y Acad Sci* **2018,** *1411* (1), 106-119.

69.   Kelly, A. S.; Bensignor, M. O.; Hsia, D. S.; Shoemaker, A. H.; Shih, W.; Peterson, C.; Varghese, S. T., Phentermine/Topiramate for the Treatment of Adolescent Obesity. *NEJM Evidence* **2022,** *1* (6).

70.   O'Meara, S.; Riemsma, R.; Shirran, L.; Mather, L.; Ter Riet, G., A systematic review of the clinical effectiveness of orlistat used for the management of obesity. *Obesity Reviews* **2004,** *5* (1), 51-68.

71.   Sjöström, L.; Rissanen, A.; Andersen, T.; Boldrin, M.; Golay, A.; Koppeschaar, H. P.; Krempf, M., Randomised placebo-controlled trial of orlistat for weight loss and prevention of weight regain in obese patients. European Multicentre Orlistat Study Group. *Lancet* **1998,** *352* (9123), 167-72.

72.   Torgerson, J. S.; Hauptman, J.; Boldrin, M. N.; Sjostrom, L., XENical in the prevention of diabetes in obese subjects (XENDOS) study: a randomized study of orlistat as an adjunct to lifestyle changes for the prevention of type 2 diabetes in obese patients. *Diabetes Care* **2004,** *27* (1), 155-61.

73.   (TGA), T. G. A. XENICAL orlistat 120mg capsule blister pack (61598). https://www.tga.gov.au/resources/artg/61598 (accessed 29 November).

74.   Yanovski, S. Z.; Yanovski, J. A., Long-term drug treatment for obesity: a systematic and clinical review. *JAMA* **2014,** *311* (1), 74-86.

75.   Bouza, C.; Angeles, M.; Munoz, A.; Amate, J. M., Efficacy and safety of naltrexone and acamprosate in the treatment of alcohol dependence: a systematic review. *Addiction* **2004,** *99* (7), 811-28.

76.   Foley, K. F.; DeSanty, K. P.; Kast, R. E., Bupropion: pharmacology and therapeutic applications. *Expert Review of Neurotherapeutics* **2006,** *6*, 1249+.

77.   Apovian, C. M.; Aronne, L.; Rubino, D.; Still, C.; Wyatt, H.; Burns, C.; Kim, D.; Dunayevich, E., A randomized, phase 3 trial of naltrexone SR/bupropion SR on weight and obesity-related risk factors (COR-II). *Obesity* **2013,** *21* (5), 935-943.

78.   Greenway, F. L.; Fujioka, K.; Plodkowski, R. A.; Mudaliar, S.; Guttadauria, M.; Erickson, J.; Kim, D. D.; Dunayevich, E., Effect of naltrexone plus bupropion on weight loss

in overweight and obese adults (COR-I): a multicentre, randomised, double-blind, placebo-controlled, phase 3 trial. *The Lancet* **2010,** *376* (9741), 595-605.

79.   Hollander, P.; Gupta, A. K.; Plodkowski, R.; Greenway, F.; Bays, H.; Burns, C.; Klassen, P.; Fujioka, K., Effects of Naltrexone Sustained- Release/Bupropion Sustained-Release Combination Therapy on Body Weight and Glycemic Parameters in Overweight and Obese Patients With Type 2 Diabetes. *Diabetes Care* **2013,** *36* (12), 4022-4029.

80.   Wadden, T. A.; Foreyt, J. P.; Foster, G. D.; Hill, J. O.; Klein, S.; O'Neil, P. M.; Perri, M. G.; Pi-Sunyer, F. X.; Rock, C. L.; Erickson, J. S.; Maier, H. N.; Kim, D. D.; Dunayevich, E., Weight Loss With Naltrexone SR/Bupropion SR Combination Therapy as an Adjunct to Behavior Modification: The COR-BMOD Trial. *Obesity* **2011,** *19* (1), 110-120.

81.   (TGA), T. G. A. CONTRAVET (iNova Pharmaceuticals (Australia) Pty Ltd). https://www.tga.gov.au/resources/prescription-medicines-registrations/contrave-inova-pharmaceuticals-australia-pty-ltd (accessed 4/12).

82.   Van Can, J.; Sloth, B.; Jensen, C. B.; Flint, A.; Blaak, E. E.; Saris, W. H. M., Effects of the once-daily GLP-1 analog liraglutide on gastric emptying, glycemic parameters, appetite and energy metabolism in obese, non-diabetic adults. *International Journal of Obesity* **2014,** *38* (6), 784-793.

83.   Mehta, A.; Marso, S. P.; Neeland, I. J., Liraglutide for weight management: a critical review of the evidence. *Obesity Science & Practice* **2017,** *3* (1), 3-14.

84.   Astrup, A.; Carraro, R.; Finer, N.; Harper, A.; Kunesova, M.; Lean, M. E.; Niskanen, L.; Rasmussen, M. F.; Rissanen, A.; Rössner, S.; Savolainen, M. J.; Van Gaal, L., Safety, tolerability and sustained weight loss over 2 years with the once-daily human GLP-1 analog, liraglutide. *Int J Obes (Lond)* **2012,** *36* (6), 843-54.

85.   Astrup, A.; Rössner, S.; Van Gaal, L.; Rissanen, A.; Niskanen, L.; Al Hakim, M.; Madsen, J.; Rasmussen, M. F.; Lean, M. E., Effects of liraglutide in the treatment of obesity: a randomised, double-blind, placebo-controlled study. *Lancet* **2009,** *374* (9701), 1606-16.

86.   (TGA), T. G. A. SAXENDA (Novo Nordisk Pharmaceuticals Pty Ltd). https://www.tga.gov.au/resources/prescription-medicines-registrations/saxenda-novo-nordisk-pharmaceuticals-pty-ltd (accessed 4/12).

87.   Hachem, A.; Brennan, L., Quality of Life Outcomes of Bariatric Surgery: A Systematic Review. *Obesity Surgery* **2016,** *26* (2), 395-409.

88.   Türkay, M., 2, 4 - Dinitrophenol Toxicity-Bound Mortality in Patients Doing Bodybuilding. **2014**.

89.   Freeman, N.; Moir, D.; Lowis, E.; Tam, E., 2,4-Dinitrophenol: 'diet' drug death following major trauma. *Anaesth Rep* **2021,** *9* (1), 106-109.

90.   Roger, G. P., A Study of the Munitions Intoxications in France. *Public Health Reports (1896-1970)* **1919,** *34* (43), 2335-2374.

91.   Tainter, M. L.; Stockton, A. B.; Cutting, W. C., Use of dinitrophenol in obesity and related conditions: A progress report. *Journal of the American Medical Association* **1933,** *101* (19), 1472-1475.

92.   Tainter, M. L.; Cutting, W. C.; Stockton, A. B., Use of Dinitrophenol in Nutritional Disorders : A Critical Survey of Clinical Results. *Am J Public Health Nations Health* **1934,** *24* (10), 1045-1053.

93.   Agency, F. S. Food Standards Agency issues urgent advice on consumption of 'fat burner' capsules containing DNP. http://www.food.gov.uk/news/pressreleases/2003/jun/fatburnpress (accessed 31 January).

94.   INTERPOL, Imminent Threat: 2,4-dinitrophenol (DNP). Re- emergence of an unauthorized weight-loss product presenting a lethal risk for the consumer. New Orleans, 2015.

95.   Cairns, R.; Raubenheimer, J.; Brown, J. A.; McArdle, K.; Buckley, N. A., 2,4-Dinitrophenol exposures and deaths in Australia after the 2017 up-scheduling. *Med J Aust* **2020,** *212* (9), 434-434.e1.

96.   MHRA, DNP (2,4 Dinitrophenol) toxicity. England, 2019.

97.   Skolding, L., "Slimming pill" drug to be classified as poison after at least 33 deaths. *Independent* 2023.

98.   Antonenko, Y. N.; Denisov, S. S.; Silachev, D. N.; Khailova, L. S.; Jankauskas, S. S.; Rokitskaya, T. I.; Danilina, T. I.; Kotova, E. A.; Korshunova, G. A.; Plotnikov, E. Y.; Zorov, D. B., A long-linker conjugate of fluorescein and triphenylphosphonium as mitochondria-targeted uncoupler and fluorescent neuro- and nephroprotector. *Biochim Biophys Acta* **2016,** *1860* (11 Pt A), 2463-2473.

99.   Severin, F. F.; Severina, II; Antonenko, Y. N.; Rokitskaya, T. I.; Cherepanov, D. A.; Mokhova, E. N.; Vyssokikh, M. Y.; Pustovidko, A. V.; Markova, O. V.; Yaguzhinsky, L. S.; Korshunova, G. A.; Sumbatyan, N. V.; Skulachev, M. V.; Skulachev, V. P., Penetrating cation/fatty acid anion pair as a mitochondria-targeted protonophore. *Proc Natl Acad Sci U S A* **2010,** *107* (2), 663-8.

100.   Gao, J. L.; Zhao, J.; Zhu, H. B.; Peng, X.; Zhu, J. X.; Ma, M. H.; Fu, Y.; Hu, N.; Tai, Y.; Xuan, X. C.; Dong, D. L., Characterizations of mitochondrial uncoupling induced by chemical mitochondrial uncouplers in cardiomyocytes. *Free Radic Biol Med* **2018,** *124*, 288-298.

101.   Shrestha, R.; Johnson, E.; Byrne, F. L., Exploring the therapeutic potential of mitochondrial uncouplers in cancer. *Mol Metab* **2021,** *51*, 101222.

102.   Rawling T., C. C., Aryl-substituted retro-amide fatty acid data summary. University of Technology Sydney: 2019.

103.   Ma, J. Novo Nordisk is losing Canadian patent protection on a blockbuster drug after not paying a small fee. https://fortune.com/2025/06/17/novo-nordisk-ozempic-wegovy-semaglutide-canada-patent-protection-fee/ (accessed 19 June).

104.   Blaikie, F. H.; Brown, S. E.; Samuelsson, L. M.; Brand, M. D.; Smith, R. A.; Murphy, M. P., Targeting dinitrophenol to mitochondria: limitations to the development of a self-limiting mitochondrial protonophore. *Biosci Rep* **2006,** *26* (3), 231-43.

105.   Chalmers, S.; Caldwell, S. T.; Quin, C.; Prime, T. A.; James, A. M.; Cairns, A. G.; Murphy, M. P.; McCarron, J. G.; Hartley, R. C., Selective Uncoupling of Individual Mitochondria within a Cell Using a Mitochondria-Targeted Photoactivated Protonophore. *Journal of the American Chemical Society* **2012,** *134* (2), 758-761.

106.   Severin, F. F.; Severina, I. I.; Antonenko, Y. N.; Rokitskaya, T. I.; Cherepanov, D. A.; Mokhova, E. N.; Vyssokikh, M. Y.; Pustovidko, A. V.; Markova, O. V.; Yaguzhinsky, L. S.; Korshunova, G. A.; Sumbatyan, N. V.; Skulachev, M. V.; Skulachev, V. P., Penetrating cation/fatty acid anion pair as a mitochondria-targeted protonophore. *Proceedings of the National Academy of Sciences* **2010,** *107* (2), 663-668.

107.   Kelso, G. F.; Porteous, C. M.; Coulter, C. V.; Hughes, G.; Porteous, W. K.; Ledgerwood, E. C.; Smith, R. A.; Murphy, M. P., Selective targeting of a redox-active ubiquinone to mitochondria within cells: antioxidant and antiapoptotic properties. *J Biol Chem* **2001,** *276* (7), 4588-96.

108.   Kalinovich, A. V.; Mattsson, C. L.; Youssef, M. R.; Petrovic, N.; Ost, M.; Skulachev, V. P.; Shabalina, I. G., Mitochondria-targeted dodecyltriphenylphosphonium (C12TPP) combats high-fat-diet-induced obesity in mice. *International Journal of Obesity* **2016,** *40* (12), 1864-1874.

109. Ježek, J.; Engstová, H.; Ježek, P., Antioxidant mechanism of mitochondria-targeted plastoquinone SkQ1 is suppressed in aglycemic HepG2 cells dependent on oxidative phosphorylation. *Biochimica et Biophysica Acta (BBA) - Bioenergetics* **2017,** *1858* (9), 750-762.

110. Skulachev, V. P.; Vyssokikh, M. Y.; Chernyak, B. V.; Averina, O. A.; Andreev-Andrievskiy, A. A.; Zinovkin, R. A.; Lyamzaev, K. G.; Marey, M. V.; Egorov, M. V.; Frolova, O. J.; Zorov, D. B.; Skulachev, M. V.; Sadovnichii, V. A., Mitochondrion-targeted antioxidant SkQ1 prevents rapid animal death caused by highly diverse shocks. *Scientific Reports* **2023,** *13* (1), 4326.

111. Kalinovich, A. V.; Shabalina, I. G., Novel Mitochondrial Cationic Uncoupler C4R1 Is an Effective Treatment for Combating Obesity in Mice. *Biochemistry (Mosc)* **2015,** *80* (5), 620-8.

112. Zorova, L. D.; Pevzner, I. B.; Khailova, L. S.; Korshunova, G. A.; Kovaleva, M. A.; Kovalev, L. I.; Serebryakova, M. V.; Silachev, D. N.; Sudakov, R. V.; Zorov, S. D.; Rokitskaya, T. I.; Popkov, V. A.; Plotnikov, E. Y.; Antonenko, Y. N.; Zorov, D. B., Mitochondrial ATP Synthase and Mild Uncoupling by Butyl Ester of Rhodamine 19, C4R1. *Antioxidants (Basel)* **2023,** *12* (3).

113. Kenwood, B. M.; Weaver, J. L.; Bajwa, A.; Poon, I. K.; Byrne, F. L.; Murrow, B. A.; Calderone, J. A.; Huang, L.; Divakaruni, A. S.; Tomsig, J. L.; Okabe, K.; Lo, R. H.; Cameron Coleman, G.; Columbus, L.; Yan, Z.; Saucerman, J. J.; Smith, J. S.; Holmes, J. W.; Lynch, K. R.; Ravichandran, K. S.; Uchiyama, S.; Santos, W. L.; Rogers, G. W.; Okusa, M. D.; Bayliss, D. A.; Hoehn, K. L., Identification of a novel mitochondrial uncoupler that does not depolarize the plasma membrane. *Mol Metab* **2013,** *3* (2), 114-123.

114. Alexopoulos, S. J.; Chen, S. Y.; Brandon, A. E.; Salamoun, J. M.; Byrne, F. L.; Garcia, C. J.; Beretta, M.; Olzomer, E. M.; Shah, D. P.; Philp, A. M.; Hargett, S. R.;

Lawrence, R. T.; Lee, B.; Sligar, J.; Carrive, P.; Tucker, S. P.; Philp, A.; Lackner, C.; Turner, N.; Cooney, G. J.; Santos, W. L.; Hoehn, K. L., Mitochondrial uncoupler BAM15 reverses diet-induced obesity and insulin resistance in mice. *Nature Communications* **2020,** *11* (1).

115.   Zunica, E. R. M.; Axelrod, C. L.; Cho, E.; Spielmann, G.; Davuluri, G.; Alexopoulos, S. J.; Beretta, M.; Hoehn, K. L.; Dantas, W. S.; Stadler, K.; King, W. T.; Pergola, K.; Irving, B. A.; Langohr, I. M.; Yang, S.; Hoppel, C. L.; Gilmore, L. A.; Kirwan, J. P., Breast cancer growth and proliferation is suppressed by the mitochondrial targeted furazano[3,4-b]pyrazine BAM15. *Cancer & Metabolism* **2021,** *9* (1), 36.

116.   Tai, Y.; Li, L.; Peng, X.; Zhu, J.; Mao, X.; Qin, N.; Ma, M.; Huo, R.; Bai, Y.; Dong, D., Mitochondrial uncoupler BAM15 inhibits artery constriction and potently activates AMPK in vascular smooth muscle cells. *Acta Pharmaceutica Sinica B* **2018,** *8* (6), 909-918.

117.   Park, K. S.; Jo, I.; Pak, K.; Bae, S. W.; Rhim, H.; Suh, S. H.; Park, J.; Zhu, H.; So, I.; Kim, K. W., FCCP depolarizes plasma membrane potential by activating proton and Na+ currents in bovine aortic endothelial cells. *Pflugers Arch* **2002,** *443* (3), 344-52.

118.   Chen, S. Y.; Beretta, M.; Alexopoulos, S. J.; Shah, D. P.; Olzomer, E. M.; Hargett, S. R.; Childress, E. S.; Salamoun, J. M.; Aleksovska, I.; Roseblade, A.; Cranfield, C.; Rawling, T.; Quinlan, K. G. R.; Morris, M. J.; Tucker, S. P.; Santos, W. L.; Hoehn, K. L., Mitochondrial uncoupler SHC517 reverses obesity in mice without affecting food intake. *METABOLISM-CLINICAL AND EXPERIMENTAL* **2021,** *117*.

119.   Beretta, M.; Dai, Y.; Olzomer, E. M.; Vancuylenburg, C. S.; Santiago-Rivera, J. A.; Philp, A. M.; Hargett, S. R.; Li, K.; Shah, D. P.; Chen, S.-Y.; Alexopoulos, S. J.; Li, C.; Harris, T. E.; Lee, B.; Wathier, M.; Cermak, J. M.; Tucker, S. P.; Turner, N.; Bayliss, D. A.; Philp, A.; Byrne, F. L.; Santos, W. L.; Hoehn, K. L., Liver-Selective Imidazolopyrazine Mitochondrial Uncoupler SHD865 Reverses Adiposity and Glucose Intolerance in Mice. *Diabetes* **2023,** *73* (3), 374-384.

120.   Murray, J. H.; Burgio, A. L.; Beretta, M.; Hargett, S. R.; Harris, T. E.; Olzomer, E.; Grams, R. J.; Garcia, C. J.; Li, C.; Salamoun, J. M.; Hoehn, K. L.; Santos, W. L., Oxadiazolopyridine Derivatives as Efficacious Mitochondrial Uncouplers in the Prevention of Diet-Induced Obesity. *J Med Chem* **2023,** *66* (6), 3876-3895.

121.   Okamoto, T.; Shimada, T.; Matsumura, C.; Minoshima, H.; Ban, T.; Itotani, M.; Shinohara, T.; Fujita, S.; Matsuda, S.; Sato, S.; Kanemoto, N., New Approach to Drug Discovery of a Safe Mitochondrial Uncoupler: OPC-163493. *ACS Omega* **2021,** *6* (26), 16980-16988.

122.   Suzuki, T.; Kikuchi, H.; Ogura, M.; Homma, M. K.; Oshima, Y.; Homma, Y., Weight Loss by Ppc-1, a Novel Small Molecule Mitochondrial Uncoupler Derived from Slime Mold. *PLoS One* **2015,** *10* (2), e0117088.

123.   Urra, F. A.; Muñoz, F.; Córdova-Delgado, M.; Ramírez, M. P.; Peña-Ahumada, B.; Rios, M.; Cruz, P.; Ahumada-Castro, U.; Bustos, G.; Silva-Pavez, E.; Pulgar, R.; Morales, D.; Varela, D.; Millas-Vargas, J. P.; Retamal, E.; Ramírez-Rodríguez, O.; Pessoa-Mahana, H.; Pavani, M.; Ferreira, J.; Cárdenas, C.; Araya-Maturana, R., FR58P1a; a new uncoupler of OXPHOS that inhibits migration in triple-negative breast cancer cells via Sirt1/AMPK/β1-integrin pathway. *Scientific Reports* **2018,** *8* (1).

124.   Rawling, T.; MacDermott-Opeskin, H.; Roseblade, A.; Pazderka, C.; Clarke, C.; Bourget, K.; Wu, X.; Lewis, W.; Noble, B.; Gale, P. A.; O'Mara, M. L.; Cranfield, C.; Murray, M., Aryl urea substituted fatty acids: a new class of protonophoric mitochondrial uncoupler that utilises a synthetic anion transporter. *Chemical Science* **2020,** *11* (47), 12677-12685.

125.   Macreadie, L. K.; Gilchrist, A. M.; McNaughton, D. A.; Ryder, W. G.; Fares, M.; Gale, P. A., Progress in anion receptor chemistry. *Chem* **2022,** *8* (1), 46-118.

126.   Li, H.; Valkenier, H.; Thorne, A. G.; Dias, C. M.; Cooper, J. A.; Kieffer, M.; Busschaert, N.; Gale, P. A.; Sheppard, D. N.; Davis, A. P., Anion carriers as potential treatments for cystic fibrosis: transport in cystic fibrosis cells, and additivity to channel-targeting drugs. *Chemical Science* **2019,** *10* (42), 9663-9672.

127.   Busschaert, N.; Park, S.-H.; Baek, K.-H.; Choi, Y. P.; Park, J.; Howe, E. N. W.; Hiscock, J. R.; Karagiannidis, L. E.; Marques, I.; Félix, V.; Namkung, W.; Sessler, J. L.; Gale, P. A.; Shin, I., A synthetic ion transporter that disrupts autophagy and induces apoptosis by perturbing cellular chloride concentrations. *Nature Chemistry* **2017,** *9* (7), 667-675.

128.   York, E.; McNaughton, D. A.; Roseblade, A.; Cranfield, C. G.; Gale, P. A.; Rawling, T., Structure-Activity Relationship and Mechanistic Studies of Bisaryl Urea Anticancer Agents Indicate Mitochondrial Uncoupling by a Fatty Acid-Activated Mechanism. *ACS Chem Biol* **2022,** *17* (8), 2065-2073.

129.   Rawling, T.; Choucair, H.; Koolaji, N.; Bourget, K.; Allison, S. E.; Chen, Y.-J.; Dunstan, C. R.; Murray, M., A Novel Arylurea Fatty Acid That Targets the Mitochondrion and Depletes Cardiolipin To Promote Killing of Breast Cancer Cells. *Journal of Medicinal Chemistry* **2017,** *60* (20), 8661-8666.

130.   Gale, P. A.; Davis, J. T.; Quesada, R., Anion transport and supramolecular medicinal chemistry. *Chemical Society Reviews* **2017,** *46* (9), 2497-2519.

131.   York, E.; McNaughton, D. A.; Gertner, D. S.; Gale, P. A.; Murray, M.; Rawling, T., Expanding the π-system of fatty acid-anion transporter conjugates modulates their mechanism of proton transport and mitochondrial uncoupling activity. *Chemistry – A European Journal* **2024**.

132.   Macdermott-Opeskin, H.; Clarke, C.; Wu, X.; Roseblade, A.; York, E.; Pacchini, E.; Roy, R.; Cranfield, C.; Gale, P. A.; O'Mara, M. L.; Murray, M.; Rawling, T., Protonophoric

and mitochondrial uncoupling activity of aryl-carbamate substituted fatty acids. *Organic & Biomolecular Chemistry* **2023,** *21* (1), 132-139.

133.   Al-Zubaidi, Y.; Pazderka, C.; Koolaji, N.; Rahman, M. K.; Choucair, H.; Umashankar, B.; Bourget, K.; Chen, Y.; Rawling, T.; Murray, M., Aryl-urea fatty acids that activate the p38 MAP kinase and down-regulate multiple cyclins decrease the viability of MDA-MB-231 breast cancer cells. *European Journal of Pharmaceutical Sciences* **2019,** *129*, 87-98.

134.   Murray, M.; Elmaghrabi, Y.; Roseblade, A.; Rahman, M. K.; Rawling, T., Carbon chain length in a novel anticancer aryl-urea fatty acid modulates mitochondrial targeting, reactive oxygen species production and cell killing. *ChemMedChem* **2024,** *n/a* (n/a), e202400281.

135.   Murray, M.; Roseblade, A.; Chen, Y.; Bourget, K.; Rawling, T., Carbon Chain Length Modulates MDA-MB-231 Breast Cancer Cell Killing Mechanisms by Mitochondrially Targeted Aryl−Urea Fatty Acids. *ChemMedChem* **2020,** *15* (2), 247-255.

136.   Valeur, E.; Bradley, M., Amide bond formation: beyond the myth of coupling reagents. *Chemical Society Reviews* **2009,** *38* (2), 606-631.

137.   Sheehan, J. C.; Hess, G. P., A New Method of Forming Peptide Bonds. *Journal of the American Chemical Society* **1955,** *77*, 1067-1068.

138.   Valeur, E.; Bradley, M., Amide bond formation: beyond the myth of coupling reagents. *Chem Soc Rev* **2009,** *38* (2), 606-31.

139.   Due-Hansen, M. E.; Pandey, S. K.; Christiansen, E.; Andersen, R.; Hansen, S. V. F.; Ulven, T., A protocol for amide bond formation with electron deficient amines and sterically hindered substrates. *Organic & Biomolecular Chemistry* **2016,** *14* (2), 430-433.

140. SubirÛs-Funosas, R.; Khattab, S. N.; Nieto-Rodriguez, L.; El-Faham, A.; Albericio, F., Advances in Acylation Methodologies Enabled by Oxyma-Based Reagents. *ChemInform* **2014,** *45*.

141. Brandt, G. E. L.; Blagg, B. S. J., Monoenomycin: A Simplified Trienomycin A Analogue that Manifests Anticancer Activity. *ACS medicinal chemistry letters* **2011,** *2* (10), 735-740.

142. El-Faham, A.; Subirós-Funosas, R.; Albericio, F., A Novel Family of Onium Salts Based Upon Isonitroso Meldrum's Acid Proves Useful as Peptide Coupling Reagents. *European Journal of Organic Chemistry* **2010,** *2010* (19), 3641-3649.

143. El-Faham, A.; Albericio, F., COMU: a third generation of uronium-type coupling reagents. *J Pept Sci* **2010,** *16* (1), 6-9.

144. MacMillan, D. S.; Murray, J.; Sneddon, H. F.; Jamieson, C.; Watson, A. J. B., Evaluation of alternative solvents in common amide coupling reactions: replacement of dichloromethane and N,N-dimethylformamide. *Green Chemistry* **2013,** *15* (3), 596-600.

145. Subirós-Funosas, R.; Nieto-Rodriguez, L.; Jensen, K. J.; Albericio, F., COMU: scope and limitations of the latest innovation in peptide acyl transfer reagents. *J Pept Sci* **2013,** *19* (7), 408-14.

146. Wuts P., G. T., Protection for the Carboxyl Group. In *Greene's Protective Groups in Organic Synthesis*, 2006; pp 533-646.

147. Wu, M.; Neilson, A.; Swift, A. L.; Moran, R.; Tamagnine, J.; Parslow, D.; Armistead, S.; Lemire, K.; Orrell, J.; Teich, J.; Chomicz, S.; Ferrick, D. A., Multiparameter metabolic analysis reveals a close link between attenuated mitochondrial bioenergetic function and enhanced glycolysis dependency in human tumor cells. *Am J Physiol Cell Physiol* **2007,** *292* (1), C125-36.

148. Caines, J. K.; Barnes, D. A.; Berry, M. D., The Use of Seahorse XF Assays to Interrogate Real-Time Energy Metabolism in Cancer Cell Lines. Springer US: 2022; pp 225-234.

149. Alexopoulos, S. J.; Chen, S.-Y.; Brandon, A. E.; Salamoun, J. M.; Byrne, F. L.; Garcia, C. J.; Beretta, M.; Olzomer, E. M.; Shah, D. P.; Philp, A. M.; Hargett, S. R.; Lawrence, R. T.; Lee, B.; Sligar, J.; Carrive, P.; Tucker, S. P.; Philp, A.; Lackner, C.; Turner, N.; Cooney, G. J.; Santos, W. L.; Hoehn, K. L., Mitochondrial uncoupler BAM15 reverses diet-induced obesity and insulin resistance in mice. *Nature Communications* **2020,** *11* (1), 2397.

150. Murray, J. H.; Burgio, A. L.; Beretta, M.; Hargett, S. R.; Harris, T. E.; Olzomer, E.; Grams, R. J.; Garcia, C. J.; Li, C.; Salamoun, J. M.; Hoehn, K. L.; Santos, W. L., Oxadiazolopyridine Derivatives as Efficacious Mitochondrial Uncouplers in the Prevention of Diet-Induced Obesity. *Journal of Medicinal Chemistry* **2023,** *66* (6), 3876-3895.

151. Salamoun, J. M.; Garcia, C. J.; Hargett, S. R.; Murray, J. H.; Chen, S.-Y.; Beretta, M.; Alexopoulos, S. J.; Shah, D. P.; Olzomer, E. M.; Tucker, S. P.; Hoehn, K. L.; Santos, W. L., 6-Amino[1,2,5]oxadiazolo[3,4-b]pyrazin-5-ol Derivatives as Efficacious Mitochondrial Uncouplers in STAM Mouse Model of Nonalcoholic Steatohepatitis. *Journal of Medicinal Chemistry* **2020,** *63* (11), 6203-6224.

152. Sivandzade, F.; Bhalerao, A.; Cucullo, L., Analysis of the Mitochondrial Membrane Potential Using the Cationic JC-1 Dye as a Sensitive Fluorescent Probe. *Bio Protoc* **2019,** *9* (1), e3128.

153. Reers, M.; Smith, T. W.; Chen, L. B., J-aggregate formation of a carbocyanine as a quantitative fluorescent indicator of membrane potential. *Biochemistry* **1991,** *30* (18), 4480-6.

154. Bioarray, C. ATP Cell Viability Assay. https://www.creative-bioarray.com/support/atp-cell-viability-

assay.htm#:~:text=The%20measurement%20of%20ATP%20using,a%20luminometer%20or%20Beta%20Counter. (accessed 17 November).

155.   Nguyen, L. T.; Zajíčková, M.; Mašátová, E.; Matoušková, P.; Skálová, L., The ATP bioluminescence assay: a new application and optimization for viability testing in the parasitic nematode Haemonchus contortus. *Vet Res* **2021,** *52* (1), 124.

156.   Tetko, I. V.; Tanchuk, V. Y., Application of associative neural networks for prediction of lipophilicity in ALOGPS 2.1 program. *J Chem Inf Comput Sci* **2002,** *42* (5), 1136-45.

157.   McNaughton, D. A.; Ryder, W. G.; Gilchrist, A. M.; Wang, P.; Fares, M.; Wu, X.; Gale, P. A., New insights and discoveries in anion receptor chemistry. *Chem* **2023,** *9* (11), 3045-3112.

158.   Wu, X.; Wang, P.; Lewis, W.; Jiang, Y.-B.; Gale, P. A., Measuring anion binding at biomembrane interfaces. *Nature Communications* **2022,** *13* (1), 4623.

159.   Thordarson, P. Bindfit. http://supramolecular.org (accessed 12/07/2023).

160.   Liu, Y.; Sengupta, A.; Raghavachari, K.; Flood, A. H., Anion Binding in Solution: Beyond the Electrostatic Regime. *Chem* **2017,** *3* (3), 411-427.

161.   Kubik, S., Anion recognition in water. *Chemical Society Reviews* **2010,** *39* (10), 3648-3663.

162.   Brynn Hibbert, D.; Thordarson, P., The death of the Job plot, transparency, open science and online tools, uncertainty estimation methods and other developments in supramolecular chemistry data analysis. *Chemical Communications* **2016,** *52* (87), 12792-12805.

163.   Frisch, M. J.; Trucks, G. W.; Schlegel, H. B.; Scuseria, G. E.; Robb, M. A.; Cheeseman, J. R.; Scalmani, G.; Barone, V.; Petersson, G. A.; Nakatsuji, H.; Li, X.; Caricato, M.; Marenich, A. V.; Bloino, J.; Janesko, B. G.; Gomperts, R.; Mennucci, B.; Hratchian, H.

P.; Ortiz, J. V.; Izmaylov, A. F.; Sonnenberg, J. L.; Williams; Ding, F.; Lipparini, F.; Egidi, F.; Goings, J.; Peng, B.; Petrone, A.; Henderson, T.; Ranasinghe, D.; Zakrzewski, V. G.; Gao, J.; Rega, N.; Zheng, G.; Liang, W.; Hada, M.; Ehara, M.; Toyota, K.; Fukuda, R.; Hasegawa, J.; Ishida, M.; Nakajima, T.; Honda, Y.; Kitao, O.; Nakai, H.; Vreven, T.; Throssell, K.; Montgomery Jr., J. A.; Peralta, J. E.; Ogliaro, F.; Bearpark, M. J.; Heyd, J. J.; Brothers, E. N.; Kudin, K. N.; Staroverov, V. N.; Keith, T. A.; Kobayashi, R.; Normand, J.; Raghavachari, K.; Rendell, A. P.; Burant, J. C.; Iyengar, S. S.; Tomasi, J.; Cossi, M.; Millam, J. M.; Klene, M.; Adamo, C.; Cammi, R.; Ochterski, J. W.; Martin, R. L.; Morokuma, K.; Farkas, O.; Foresman, J. B.; Fox, D. J. *Gaussian 16 Rev. C.01*, Wallingford, CT, 2016.

164.   Bryantsev, V. S.; Hay, B. P., Influence of Substituents on the Strength of Aryl C−H⋯Anion Hydrogen Bonds. *Organic Letters* **2005,** *7* (22), 5031-5034.

165.   Steiner, T., The Hydrogen Bond in the Solid State. *Angewandte Chemie International Edition* **2002,** *41* (1), 48-76.

166.   Yap, K.; Krantzman, K. D.; Lavrich, R. J., Inductive Effects on Intramolecular Hydrogen Bond Strength: An Investigation of the Effect of an Electron-Withdrawing CF3 Group Adjacent to an Alcohol Hydrogen Bond Donor. *The Journal of Physical Chemistry A* **2023,** *127* (38), 7892-7897.

167.   Lipinski, C. A., Drug-like properties and the causes of poor solubility and poor permeability. *J Pharmacol Toxicol Methods* **2000,** *44* (1), 235-49.

168.   Veber, D. F.; Johnson, S. R.; Cheng, H.-Y.; Smith, B. R.; Ward, K. W.; Kopple, K. D., Molecular Properties That Influence the Oral Bioavailability of Drug Candidates. *Journal of Medicinal Chemistry* **2002,** *45* (12), 2615-2623.

169.   Duvic, M.; Vu, J., Vorinostat in cutaneous T-cell lymphoma. *Drugs Today (Barc)* **2007,** *43* (9), 585-99.

170.   Rawling, T.; Duke, C. C.; Cui, P. H.; Murray, M., Facile and stereoselective synthesis of (Z)-15-octadecenoic acid and (Z)-16-nonadecenoic acid: monounsaturated omega-3 fatty acids. *Lipids* **2010,** *45* (2), 159-65.

171.   USEPA Methyl Iodide.

https://comptox.epa.gov/dashboard/dsstoxdb/results?search=DTXSID0024187#properties (accessed 24 September).

172.   Bowden, K.; Heilbron, I. M.; Jones, E. R. H.; Weedon, B. C. L., 13. Researches on acetylenic compounds. Part I. The preparation of acetylenic ketones by oxidation of acetylenic carbinols and glycols. *Journal of the Chemical Society (Resumed)* **1946,** (0), 39-45.

173.   Mostyn, S. N.; Rawling, T.; Mohammadi, S.; Shimmon, S.; Frangos, Z. J.; Sarker, S.; Yousuf, A.; Vetter, I.; Ryan, R. M.; Christie, M. J.; Vandenberg, R. J., Development of an N-Acyl Amino Acid That Selectively Inhibits the Glycine Transporter 2 To Produce Analgesia in a Rat Model of Chronic Pain. *Journal of medicinal chemistry* **2019,** *62* (5), 2466-2484.

174.   Elmaghrabi, Y. A.; Roseblade, A.; Rahman, K.; Rawling, T.; Murray, M., Carbon Chain Length in a Novel Anticancer Aryl-Urea Fatty Acid Modulates Mitochondrial Targeting, Reactive Oxygen Species Production and Cell Killing. *ChemMedChem* **2024,** *19* (20).

175.   York, E.; McNaughton, D. A.; Roseblade, A.; Cranfield, C. G.; Gale, P. A.; Rawling, T., Structure–Activity Relationship and Mechanistic Studies of Bisaryl Urea Anticancer Agents Indicate Mitochondrial Uncoupling by a Fatty Acid-Activated Mechanism. *ACS Chemical Biology* **2022,** *17* (8), 2065-2073.

176.   Rahman, M. K.; Umashankar, B.; Choucair, H.; Pazderka, C.; Bourget, K.; Chen, Y.; Dunstan, C. R.; Rawling, T.; Murray, M., Inclusion of the in-chain sulfur in 3-thiaCTU

increases the efficiency of mitochondrial targeting and cell killing by anticancer aryl-urea fatty acids. *European Journal of Pharmacology* **2023,** *939*, 175470.

177.   Van Der Windt, G. J. W.; Chang, C. H.; Pearce, E. L., Measuring Bioenergetics in T Cells Using a Seahorse Extracellular Flux Analyzer. *Current Protocols in Immunology* **2016,** *113* (1).

178.   Espinosa, J. A.; Pohan, G.; Arkin, M. R.; Markossian, S., Real-Time Assessment of Mitochondrial Toxicity in HepG2 Cells Using the Seahorse Extracellular Flux Analyzer. *Current Protocols* **2021,** *1* (3), e75.

179.   Natalia Romero, P. S., Andy Neilson, and Brian P. Dranka Improving Quantification of Cellular Glycolytic Rate Using Agilent Seahorse XF Technology https://www.med.upenn.edu/robertsonlab/assets/user-content/documents/seahorse-experimentation.pdf (accessed 7 June).

180.   Sakamuri, S.; Sure, V. N.; Kolli, L.; Liu, N.; Evans, W. R.; Sperling, J. A.; Busija, D. W.; Wang, X.; Lindsey, S. H.; Murfee, W. L.; Mostany, R.; Katakam, P. V. G., Glycolytic and Oxidative Phosphorylation Defects Precede the Development of Senescence in Primary Human Brain Microvascular Endothelial Cells. *Geroscience* **2022,** *44* (4), 1975-1994.

181.   Ripoll, C.; Roldan, M.; Ruedas-Rama, M. J.; Orte, A.; Martin, M., Breast Cancer Cell Subtypes Display Different Metabolic Phenotypes That Correlate with Their Clinical Classification. *Biology* **2021,** *10* (12), 1267.

182.   Kotova, E. A.; Antonenko, Y. N., Fifty Years of Research on Protonophores: Mitochondrial Uncoupling As a Basis for Therapeutic Action. *Acta Naturae* **2022,** *14* (1), 4-13.

183.   Naven, R. T.; Swiss, R.; Klug-McLeod, J.; Will, Y.; Greene, N., The development of structure-activity relationships for mitochondrial dysfunction: uncoupling of oxidative phosphorylation. *Toxicol Sci* **2013,** *131* (1), 271-8.

184.   Chen, S. Y.; Beretta, M.; Alexopoulos, S. J.; Shah, D. P.; Olzomer, E. M.; Hargett, S. R.; Childress, E. S.; Salamoun, J. M.; Aleksovska, I.; Roseblade, A.; Cranfield, C.; Rawling, T.; Quinlan, K. G. R.; Morris, M. J.; Tucker, S. P.; Santos, W. L.; Hoehn, K. L., Mitochondrial uncoupler SHC517 reverses obesity in mice without affecting food intake. *Metabolism* **2021,** *117*, 154724.

185.   Zhu, T.-T.; Zhang, Y.; Luo, X.-A.; Wang, S.-Z.; Jia, M.-Q.; Chen, Z.-X., Difference in Binding of Long- and Medium-Chain Fatty Acids with Serum Albumin: The Role of Macromolecular Crowding Effect. *Journal of Agricultural and Food Chemistry* **2018,** *66* (5), 1242-1250.

186.   Spector, A. A.; John, K.; Fletcher, J. E., Binding of long-chain fatty acids to bovine serum albumin. *J Lipid Res* **1969,** *10* (1), 56-67.

187.   Spector, A. A., Fatty acid binding to plasma albumin. *J Lipid Res* **1975,** *16* (3), 165-79.

188.   Mohamed, E. A.; Zhao, Y.; Meshali, M. M.; Remsberg, C. M.; Borg, T. M.; Foda, A. M.; Takemoto, J. K.; Sayre, C. L.; Martinez, S. E.; Davies, N. M.; Forrest, M. L., Vorinostat with sustained exposure and high solubility in poly(ethylene glycol)-b-poly(DL-lactic acid) micelle nanocarriers: characterization and effects on pharmacokinetics in rat serum and urine. *J Pharm Sci* **2012,** *101* (10), 3787-98.

189.   Duman, M.-N.; Angeloski, A.; Johnson, M. S.; Rawling, T., Aromatic long chain cations of amphiphilic ionic liquids permeabilise the inner mitochondrial membrane and induce mitochondrial dysfunction at cytotoxic concentrations. *Green Chemistry* **2023,** *25* (15), 6067-6076.

190.   Cholo, M. C.; Steel, H. C.; Fourie, P. B.; Germishuizen, W. A.; Anderson, R., Clofazimine: current status and future prospects. *J Antimicrob Chemother* **2012,** *67* (2), 290-8.

191.   Wu, X.; Wang, P.; Lewis, W.; Jiang, Y.-B.; Gale, P. A., Measuring anion binding at biomembrane interfaces. *Nature Communications* **2022,** *13* (1).

192.   Dennington, R. K., Todd A.; Millam, John M. Semichem *GaussView Version 6*, Shawnee Mission: 2016.

193.   Pinkerton, J. W.; Kim, R. Y.; Brown, A. C.; Rae, B. E.; Donovan, C.; Mayall, J. R.; Carroll, O. R.; Khadem Ali, M.; Scott, H. A.; Berthon, B. S.; Baines, K. J.; Starkey, M. R.; Kermani, N. Z.; Guo, Y. K.; Robertson, A. A. B.; O'Neill, L. A. J.; Adcock, I. M.; Cooper, M. A.; Gibson, P. G.; Wood, L. G.; Hansbro, P. M.; Horvat, J. C., Relationship between type 2 cytokine and inflammasome responses in obesity-associated asthma. *J Allergy Clin Immunol* **2022,** *149* (4), 1270-1280.